TUM

Technische Universität München
Zentrum Mathematik
M6 Mathematische Modellbildung

Spatial single cell modelling of bacterial sporulation controlled by quorum sensing

Patrick R. Stocker

I hereby declare that this thesis is my own work and that no other sources have been used except those clearly indicated and referenced.

Munich, January 31, 2019

Acknowledgements

First of all, I would like to thank Christina Kuttler, for supervising my doctorate the last years. You provided me with interesting questions when I start to work and subsequently gave me more and more room to develop and realize my own ideas. In doing so, I appreciated all the time your friendly encouragement, your positive attitude and for an always open door.

Second I want to thank Ilka Bischofs-Pfeifer, group leader of the BioQuant at the University in Heidelberg. Our meetings have been always fruitful and gave me much inspiration to develop my work.

Thank you also to Johannes Müller who was my mentor and also supervised my master thesis. Without you, I would not have felt ready to join the doctorate.

The members of the research unit M6 at the Technische Universität München deserve mentioning for a friendly and constructive atmosphere over the years.

This thesis would not be the same without my friends at the university who also did their PhD. All our coffee breaks or Mensa lunches have been a welcome change to the sometimes frustrating moments when nothing worked.

Finally, I am deeply grateful to my family and friends, especially to my girlfriend, for the encouragement and unconditional support they provided.

Zusammenfassung

Neue Forschungsergebnisse haben gezeigt, dass die Bakterien *Bacillus subtilis* eine gewisse Konzentration Pentapeptide (*PhrA*) benötigen um den Sporulationsprozess einleiten zu können. Dieses *PhrA* wird von den Bakterien selbst produziert und wirkt als Signalmolekül. Wir untersuchen unterschiedliche gewöhnliche Differentialgleichungsansätze für den Aufnahme- und Produktionsprozess des *PhrA*, wobei die Verhaltensänderung der Bakterien durch Indikatorfunktionen der rechten Seite gesteuert werden. Da wir Daten eines Schüttelkolben-Experimentes haben, wird die numerischen Lösungen an diese angepasst. Für alle verwendeten Modelle kann die Existenz als auch Eindeutigkeit einer nicht-negativen Lösung gezeigt werden. Das Modell wird um eine räumliche Komponente erweitert, sodass am Ende ein gekoppeltes PDE-ODE System entsteht. Die Existenz einer schwachen Lösung kann gezeigt werden, die Eindeutigkeit nur für einen Spezialfall. Das System wird numerisch mittels der Finiten Element Methode gelöst. Auch hierzu gibt es experimentelle Daten. Das PDE Modell kann mittels dem ODE Modell verifiziert werden. Allerdings lassen sich die experimentellen Beobachtungen mittels dem PDE-ODE System nicht vollständig reproduzieren. Dies legt nahe, dass man sowohl das räumliche Modell weiter anpassen muss als auch die umgerechneten ODE Parameter nicht unmittelbar verwenden kann.

Abstract

Recent research results have shown that the bacteria *Bacillus subtilis* need a certain concentration of pentapeptides (*PhrA*) in order to initialise the sporulation process. *PhrA* is produced by the bacteria itself and thus works as a signalling molecule. We discuss different ordinary differential model equations for the uptake and production process of *PhrA* whereas the changes in the behaviour are controlled by indicator functions on the right hand side. Then the numerically solutions are fitted to experimental data gained by shake flask experiments. For all utilized models existence and uniqueness of solutions are proven. Then we expand the model by a spatial component leading to a coupled PDE-ODE system. Existence of a weak solution can be shown, uniqueness only for a special case. The system can be solved numerically using the finite element method. Again, there are experimental data. The PDE model can be verified using the ODE model. However, the experimental observations can not be fully reproduced using the PDE-ODE system. This suggests that one must further adjust the spatial model as well as use not immediately the converted ODE parameters.

Contents

List of Figures

List of Tables

Chapter 1

Motivation

Bacillus subtilis is a very well investigated bacterium and has a wide range of industrial applications due to their ability to ferment in the acid, neutral, and alkaline pH ranges. In combination with the presence of thermophiles in the genus, this has lead to the development of a variety of new commercial enzyme products with the desired temperature, pH activity, and stability properties [25]. Additionally it is considered as a GRAS organism (**g**enerally **r**ecognized **as s**afe) and about 60% of the industrial-enzyme market are produced by species of *Bacillus subtilis* [37]. Enzymes produced by *Bacillus subtilis* are used in food industry (e.g. production of natto by solid-state fermentation of soybeans) [25], in pesticide industry (e.g. as fungicide) [14] and as cleaning agents [23][25]. However, there are still open questions as the initiation of sporulation, which is a survival mechanism if environmental condition becomes harsh. *Bischofs* stated that phosphatase regulator A (*PhrA*) acts as a quorum sensing molecule and is needed for the initiation of the sporulation process [2]. There are mathematical models describing the process of sporulation within the cell using ODE's [5][12], but no mathematical model which investigates the signalling molecule *PhrA* itself in the environment as a communication tool for bacterial microcolonies. We know by personal communication with Dr. Bischofs that some bacteria do not sporulate in specific experiments and spatial effects might be the reason. Therefore, we will develop a PDE-ODE system which describes the *Bacillus subtilis'* production and absorption process of signalling molecules diffusing through the environment serving as a communication tool between bacterial colonies controlling the sporulation initialisation. Furthermore, we obtain due to the mathematical modelling an in-depth look into the dependency of the production and absorption processes with the signalling molecule *PhrA*.

Last but not least a further nice fact: Although *Bacillus subtilis* can survive dangerous environmental conditions on earth, it can not survive at the Mars. Because of the UV flux, perchlorates becomes bacteriocidal and the sporulation process is to slow to protect the DNA [34].

Chapter 2

Basics

In this chapter, we give a background into the relevant biology in order to understand the mechanisms which will be modelled mathematically. Afterwards, some mathematical theory is given regarding the theory of second order parabolic equation as well as the finite element method.

2.1. Biological basics

A brief introduction into the mechanism of cell to cell communication and the bacterium *Bacillus subtilis* itself is given.

2.1.1. Quorum sensing

In the beginning of the 20th century, bacteria were considered as autonomous, unicellular organisms without any interaction to other bacteria of the same strain. Nevertheless it seems that a cooperative behaviour between bacteria regarding symbiosis, niche adoption or the production of secondary metabolites are advantageously [38], [39]. Bacteria produce among others pheromones which are secreted and diffuse through the environment and can be sensed by the bacteria. These pheromones are sometimes called autoinducers or signalling molecules. Of course, if the population grows then more pheromones are produced and the higher is the accumulated concentration in the environment. If this pheromone concentration reaches a certain threshold (and thus the population density as well), the bacteria change their behaviour respectively some specific action starts (e.g. luminescence in *Vibrio harveyi* [39]). The expression "Quorum Sensing" was introduced by *Fuqua et al.* [10] to describe this cell to cell communication in order to coordinate the behaviour. This term usually refers to a measurement of cell density respectively to the number of cells. There are further terms as "Diffusion Sensing" which measures the diffusibility of the surrounding space or "Compartment

Sensing" which measures the degree of compartmentalization and the possibility to distribute this information through the whole population. Both follow the same mechanism, but it has a different goal as described. In those cases bacteria sense environmental changes, e.g. temperature, pH or nutrient deprivation, rather than changes in population density [24], [39]. If bacteria do observe these environmental changes, they are able to determine their optimal survival strategy [40]. *Winzer et al.* [39] postulates four criteria a signalling molecule needs to fulfil and explains the reasons:

- The production of the signalling molecule occurs during specific stages of growth, under certain physiological conditions, or in response to changes in the environment.

- The signalling molecule accumulates extracellularly and is recognised by a specific receptor.

- Accumulation of the signalling molecule generates a concerted response, once a critical threshold concentration has been reached.

- The cellular response extends beyond physiological changes required to metabolise or detoxify the signalling molecule.

The first three criteria are fulfilled by various molecules e.g. toxic bacterial metabolites resulting in a coordinated stress action of the bacteria if a certain threshold has been reached. Henceforth, they are insufficient to define signalling molecules only. Therefore the last criterion is crucial.
On the one hand the cell-to-cell communication enables the entire population or a subpopulation to take either advantage of a rising population density or handle the problems which may arise due to this growth. On the other hand it may inform the population of environmental changes.

2.1.2. *Bacillus subtilis*, a gram-positive bacterium

Bacillus subtilis is a rod-shape Gram-positive bacterium which is well investigated especially genetically [18], [31]. There are phenotypes who can build spores in order to protect its genetic information if environmental conditions become harsh. Instead of a symmetric cell division for vegetative growth, the sporulation is an asymmetric division resulting in a mother cell and a prespore. Later on the mother cell entwine the prespore building a highly resistant coat protecting the DNA within the prespore [8], [18], [21], [22], [38]. Spores can survive for many years and germinate if environmental conditions become better again. This cycle is depicted in Figure 2.1.
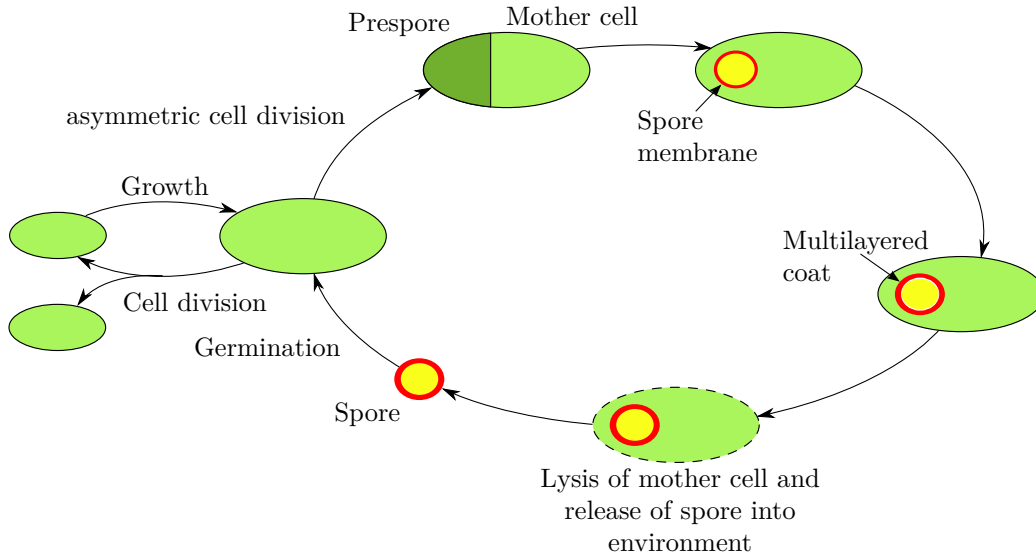
Figure 2.1.: *Scheme of sporulation process.*

There are various reasons why a bacterium starts the time- and energy expensive process, e.g. nutrient limitation, pH, temperature, diseases, production of valuable chemicals as e.g. biofuels [13], [18], [21]. The main sporulation factors of *Bacillus subtilis* are on the one hand nutrient limitation and on the other hand population growth [31]. Since the process is irreversible it is crucial to come to a right decision. Either vegetative bacteria die if they do not sporulate when environmental conditions become harsh or if the initiation of sporulation is too early, then the bacteria strain might be out-competed by another vegetative strain which keeps on dividing longer.

Gram-positive bacteria work with post-translationally modified peptides, referred as auto-inducing peptides (AIP's) as signalling molecule to couple gene expression with cell population density. *Bacillus subtilis* uses a family of isoprenylated tryptophan peptides [38], more precisely the protein *PhrA* has been postulated as a quorum sensing signal regarding the population size [6], [19]. Secreted *PhrA* can be absorbed by any other *Bacillus subtilis* cell. Within the cell, see figure 2.2, it binds to RapA inhibiting its phosphatase activity on Spo0F∼P leading to sporulation initiation [12]. There is a further process which is called competence, that is the ability to take up exogenous DNA. It is controlled by an additional autoinducing peptide [36]. The signalling molecule *PhrA* inhibits competence phosphorylation cascades but this phenomenon will be neglected in this work, we only focus on the sporulation process.

Remark 2.1.1. *We always mean the same no matter if we write "quorum sensing signalling molecule", "signalling molecule", "quorum sensing molecule" or "quorum sensing signal".*
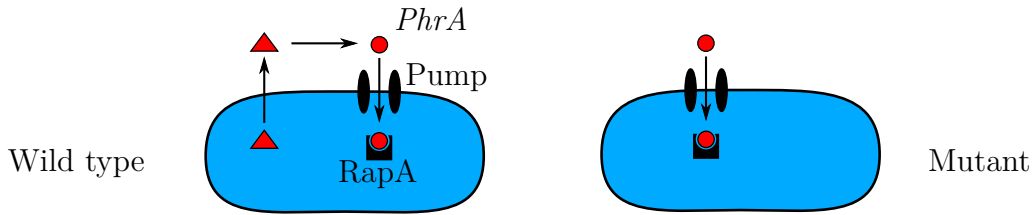
Figure 2.2.: *Scheme of dynamical processes.*

2.2. Mathematical basics

A brief introduction into some mathematical basics and notation is given which are used later in this work. Since we are interested in spatial propagation of signalling molecules, we need for the modelling part partial differential equations (PDE's), in particular second order parabolic equations. To solve such equations, the finite element method (FEM) is a common approach and will be explained afterwards.

2.2.1. Second order parabolic equation

As a guideline for this section, we follow the book of *Evans*, [9], section 7.1., which analyses a parabolic partial differential system with a homogeneous Dirichlet boundary. This boundary condition ensures that the solution is zero at the boundary which means that particles can leave the domain but not enter again. In our scenario, however, this is not realistic. We want to have conservation of mass, that is, no particle should leave the domain. Thus, we need a homogeneous Neumann boundary which means that there is no flux at the boundary. With some small adjustments, we will obtain similar results for a second order parabolic equation with a homogeneous Neumann boundary condition.

For this chapter, we assume U to be an open, bounded subset of $\mathbb{R}^n$ and $T \in \mathbb{R}_+$ be a positive fixed time. Before we introduce the parabolic equation, we introduce first the common $\mathcal{L}^p$ spaces.

Definition 2.2.1 ($\mathcal{L}^p$ spaces)**.** *Assume U is an open subset of $\mathbb{R}^n$ and $1 \leq p \leq \infty$. If $f : U \to \mathbb{R}$ is measurable, we define*

$$\|f\|_{\mathcal{L}^p(U)} := \begin{cases} \left(\int_U |f|^p \, dx \right)^{\frac{1}{p}} & \text{if } 1 \leq p < \infty \\ \operatorname*{ess\,sup}_U |f| & \text{if } p = \infty. \end{cases}$$

Remark 2.2.2. *The space $\mathcal{L}^2(U)$ is a Hilbert space with the scalar product*

$$(f, g) := \int_U fg \, dx.$$

Then a parabolic partial differential system with homogeneous Neumann boundary conditions is given by

$$
\begin{aligned}
\frac{\partial}{\partial t}u + Lu &= f & &\text{in } (0, T] \times U \\
\frac{\partial u}{\partial \boldsymbol{n}} &= 0 & &\text{on } (0, T] \times \partial U \\
u &= g & &\text{on } \{t = 0\} \times U
\end{aligned}
\tag{2.1}
$$

where $f \in \mathcal{L}^2\left((0, T] \times U\right)$ and $g \in \mathcal{L}^2(U)$ are given functions. Note that we have here a homogeneous Neumann boundary condition instead of a homogeneous Dirichlet condition compared to *Evans* book. The unknown $u = u(t, x)$ depends on two variables and $u : \overline{(0, T] \times U} \to \mathbb{R}$. L denotes a second-order partial differential operator for each time t. There is on the one hand a divergence form

$$
Lu = -\sum_{i,j=1}^{n}\left(a^{ij}(t, x)u_{x_i}\right)_{x_j} + \sum_{i=1}^{n} b^i(t, x)u_{x_i} + c(t, x)u
\tag{2.2}
$$

and on the other hand a nondivergence form

$$
Lu = -\sum_{i,j=1}^{n} a^{ij}(t, x)u_{x_i x_j} + \sum_{i=1}^{n} b^i(t, x)u_{x_i} + c(t, x)u.
\tag{2.3}
$$

We assume for now that a^{ij}, b^i, $c \in \mathcal{L}^{\infty}((0, T] \times U)$ for $i, j \in \{1, \ldots, n\}$, whereas $b^i(t, x)$ differs in (2.2) and (2.3). Additionally we suppose the symmetric condition $a^{ij} = a^{ji}$ for all i, j. For reasons of generality, both forms are quoted. If the coefficients a^{ij} $(i, j \in \{1, \ldots, n\})$ are $\mathcal{C}^1$ functions, then the divergence operator can be rewritten into the non-divergence form. Note that

$$
\sum_{i,j=1}^{n}\left(a^{ij}(t, x)u_{x_i}\right)_{x_j} = \sum_{i,j=1}^{n} a^{ij}_{x_j}(t, x)u_{x_i} + a^{ij}(t, x)u_{x_i x_j},
$$

so we have a further divergence term compared to (2.3). From that follows the definition of the types. Both are used for different approaches. The divergence form is most natural for energy methods since we use there usually integration by parts. The non-divergence form is most appropriate for maximum principle techniques. From now on we will focus only on the divergence form (2.2) since we will derive solutions by energy methods. Later in chapter 4, we choose $a^{ij}(t, x)$ to be constant, so both types coincides. If $b^i \equiv c \equiv 0$ for all i, then the operator L is equal to the well known Laplace operator $\nabla^2 u = -\sum_{i,j=1}^{n} a^{ij}(t, x)u_{x_i x_j}$ describing a diffusion process. If $b^i \equiv 0$ for all i, the system (2.1) is also known as reaction-diffusion system whereas $-c(t, x)u + f$ accounts all local reactions. Let's denote the time-dependent bilinear form by $B[u, v; t]$ which is defined as

$$B[u,v;t] := \int_U \sum_{i,j=1}^n a^{ij}(t,\cdot)u_{x_i}v_{x_j} + \sum_{i=1}^n b^i(t,\cdot)u_{x_i}v + c(t,\cdot)uv \, dx \qquad (2.4)$$

for $t \in [0,T]$ a.e. and $u,v \in \mathcal{H}^1(U)$.

The definition of an *elliptic* operator L as special case of a second-order partial differential operator, that is, time independent, is given in [9], section 6.1.1. and is defined as following:

Definition 2.2.3 (Elliptic condition)**.** *We say the partial differential operator L is (uniformly) elliptic if there exists a constant $\theta > 0$ such that*

$$\sum_{i,j=1}^n a^{ij}(t,x)\xi_i\xi_j \geq \theta|\xi|^2$$

for a.e. $x \in U$ and $\xi \in \mathbb{R}^n$.

There is also a definition when we call $\frac{\partial}{\partial t} + L$ parabolic, see [9], section 7.1.1..

Definition 2.2.4 (Parabolic condition)**.** *We say that the partial differential operator $\frac{\partial}{\partial t} + L$ is (uniformly) parabolic if there exists a constant $\theta > 0$ such that*

$$\sum_{i,j=1}^n a^{ij}(t,x)\xi_i\xi_j \geq \theta|\xi|^2$$

for a.e. $(t,x) \in (0,T] \times U$, and $\xi \in \mathbb{R}^n$.

A problem is called *well-posed* if it has in fact a solution which is unique and the solution depends continuously on the data given in the problem. Additionally we could require that this solution should be real analytical (a function that is locally given by a convergent power series) or at least infinitely differentiable. Note that analytical functions are infinitely differentiable functions but not vice versa. However, these are very strong requirements. It might be more realistic to ask for a k times continuously differentiable solution. In many cases, $k = 2$ is adequate. Then the derivatives of the PDE will exist and be continuous, although higher derivatives do not. Let's call that solution with this much smoothness, i.e. of order 2, a *classical solution* of a PDE. However, these are still strong assumptions to many PDE's with their initial and boundary conditions. That's the reason to introduce a so called *weak solution*. Therefore, some further spaces have to be introduced as well as the definition of weak partial derivatives.

Definition 2.2.5 (Local summable functions $\mathcal{L}^p_{\text{loc}}(U)$)**.** *Let U be an open subset of $\mathbb{R}^n$ and $1 \leq p \leq \infty$. If for each compact subsets V of U the function u belongs to $\mathcal{L}^p(V)$, then u is called locally p-integrable. The set of all such functions is denoted by*

$$\mathcal{L}^p_{loc}(U) := \{u : U \to \mathbb{R}^n | u \in \mathcal{L}^p(K), \; \forall K \subset U, K \; compact\}.$$

Definition 2.2.6 (Weak partial derivative). *Suppose $u, v \in \mathcal{L}^1_{loc}(\Omega)$ and $\alpha \in \mathbb{N}^N$ is a multiindex. Then, it is said that*

$$v = D^\alpha u \quad \text{in the weak sense}$$

or, equivalently, that v is the weak derivative of order α of u, if

$$\int_\Omega u D^\alpha \Phi = (-1)^{|\alpha|} \int_\Omega \Phi v \quad \text{for all } \Phi \in \mathcal{C}^\infty(\Omega).$$

Definition 2.2.7 (Sobolev space). *Let U be an open subset of $\mathbb{R}^n$, $1 \leq p \leq \infty$, k be a non-negative integer and $D^\alpha u$ exists in the weak sense. Then the Sobolev space is defined by*

$$\mathcal{W}^{k,p}(U) := \{u \in \mathcal{L}^p_{loc}(U) : D^\alpha u \in \mathcal{L}^p(U) \, \forall |\alpha| \leq k\}$$

endowed with the norm

$$\|u\|_{\mathcal{W}^{k,p}(U)} := \begin{cases} \left(\sum_{0 \leq |\alpha| \leq k} \int_U |D^\alpha u|^p \, dx \right)^{\frac{1}{p}} & \text{if } 1 \leq p < \infty \\ \sum_{0 \leq |\alpha| \leq k} \operatorname*{ess\,sup}_U |D^\alpha u| & \text{if } p = \infty. \end{cases}$$

Remark 2.2.8. *If $p = 2$, we usually write*

$$\mathcal{H}^k(U) = \mathcal{W}^{k,2}(U)$$

for all $k \in \mathbb{N}$.

To make the following definition of a weak solution plausible, we suppose that $u(t, x)$ is a smooth solution of (2.1), that is, $u \in \mathcal{C}^2([0, T] \times U)$. Then we define a new mapping

$$\boldsymbol{u} : [0, T] \to \mathcal{H}^1(U)$$

by

$$[\boldsymbol{u}(t)](x) := u(t, x) \quad \text{with } x \in U \text{ and } t \in [0, \dots, T].$$

That means we consider a mapping of $\boldsymbol{u}(t)$ into the space $\mathcal{H}^1(U)$ of functions of x. That leads to an extension of the Lebesgue spaces

Definition 2.2.9. *Let X be a real Banach space.*

(i) A function $\boldsymbol{s} : [0, T] \to X$ is called simple if it has the form

$$\boldsymbol{s}(t) = \sum_{i=1}^m \chi_{E_i}(t) u_i \quad \text{for } t \in [0, T],$$

where each E_i is a Lebesgue measurable subset of $[0, T]$ and $u_i \in X$ for $i \in \{1, \ldots, m\}$.

(ii) *A function $\boldsymbol{f} : [0, T] \to X$ is strongly measurable if there exist simple functions $\boldsymbol{s}_k : [0, T] \to X$ such that*

$$\boldsymbol{s}_k(t) \to \boldsymbol{f}(t) \quad \text{for a.e. } t \in [0, T].$$

Definition 2.2.10 (Extended $\mathcal{L}^p$). *Let X denote a real Banach space with norm $\|\cdot\|$. The space*

$$\mathcal{L}^p(0, T; X)$$

consists of all strongly measurable functions $\boldsymbol{u} : [0, T] \to X$ with

$$\|\boldsymbol{u}\|_{\mathcal{L}^p(0,T;X)} := \begin{cases} \left(\int_0^T \|\boldsymbol{u}(t)\|^p \, dt \right)^{\frac{1}{p}} < \infty & \text{for } 1 \le p < \infty \\ \operatorname*{ess\,sup}_{t \in [0,T]} \|\boldsymbol{u}(t)\| < \infty & \text{for } p = \infty. \end{cases}$$

Similarly we do the same for the right hand side:

$$\boldsymbol{f} : [0, T] \to \mathcal{L}^2(U)$$

with

$$[\boldsymbol{f}(t)] (x) := f(t, x) \quad \text{with } x \in U \text{ and } t \in [0, T].$$

Let $v \in \mathcal{H}^1(U)$. We multiply the PDE in (2.1) with v and integrate the equation over the domain U. The same is done for the initial condition as well as for the boundary condition in (2.1). Then it rewrites to

$$\begin{aligned} \int_U \frac{\mathrm{d}}{\mathrm{d}t} \boldsymbol{u} v \, dx + \int_U L\boldsymbol{u} v \, dx &= \int_U \boldsymbol{f} v \, dx \quad \text{in } (0, T] \times U \\ \int_U \frac{\mathrm{d}\boldsymbol{u}}{\mathrm{d}\boldsymbol{n}} v \, dx &= 0 \quad \text{on } (0, T] \times \partial U \\ \int_U \boldsymbol{u} v \, dx &= \int_U g v \, dx \quad \text{on } \{t = 0\} \times U \end{aligned} \tag{2.5}$$

Let's consider the first equation from above. Plug in the definition of the operator in divergence form (2.2) and integrate the first term by parts. Due to the homogeneous boundary condition in (2.5), the boundary term which arises form the partial integration vanishes then. At the end we obtain a weak formulation of the problem:

$$\int_U \frac{\mathrm{d}}{\mathrm{d}t} \boldsymbol{u} v \, dx + \int_U L\boldsymbol{u} v \, dx = \int_U \boldsymbol{f} v \, dx$$

$$\iff \int_U \frac{\partial}{\partial t} \boldsymbol{u} v \, dx - \underbrace{\left[\sum_{i,j=1}^n a^{ij}(t,x) \boldsymbol{u}_{x_i} v \right]_{\partial U}}_{=0}$$

$$+ \int_U \sum_{i,j=1}^n a^{ij}(t,x) \boldsymbol{u}_{x_i} v_{x_j} + \sum_{i=1}^n b^i(t,x) \boldsymbol{u}_{x_i} v + c(t,x) \boldsymbol{u} v \, dx = \int_U \boldsymbol{f} v \, dx$$

$$\iff \left(\frac{\mathrm{d}}{\mathrm{d}t} \boldsymbol{u}, v \right) + B[\boldsymbol{u}, v; t] = (\boldsymbol{f}, v) \tag{2.6}$$

for each $t \in [0, T]$ with $B[u, v; t]$ is the time-dependent bilinear form in (2.4). The pairing $(\cdot, \cdot)$ denotes the inner product in $\mathcal{L}^2(U)$.

With some reformulations, one can observe, that

$$\frac{\partial}{\partial t} u = g^0 + \sum_{j=1}^n g_{x_j}^j \quad \text{in } (0, T] \times U \tag{2.7}$$

whereas $g^0 := f - \sum_{i=1}^n b^i u_{x_i} - cu$ and $g^j := \sum_{i=1}^n a^{ij} u_{x_i}$ for $j \in \{1, \dots, n\}$. The coefficients of the bilinear form are in $\mathcal{L}^\infty((0, T] \times U)$ and u is assumed to be in $\mathcal{C}^2((0, T] \times U)$. Hence, $g^j \in \mathcal{L}^\infty((0, T] \times U)$ for $j \in \{0, \dots, n\}$. Note that in general it holds $\mathcal{H}^1(U) \subset \mathcal{L}^\infty(U) \subset \mathcal{L}^2(U) \simeq \mathcal{L}^{2\star} \subset \mathcal{H}^{-1}(U)$ for open sets U. $\mathcal{H}^{-1}(U)$ denotes the dual space of $\mathcal{H}^1(U)$ and is defined as following:

Definition 2.2.11 (Dual space $\mathcal{H}^{-1}$). *We denote by $\mathcal{H}^{-1}(U)$ the dual space to $\mathcal{H}^1(U)$ with norm*

$$\|f\|_{\mathcal{H}^{-1}(U)} := \sup \left\{ \langle f, v \rangle \; \middle| \; v \in \mathcal{H}^1(U), \|v\|_{\mathcal{H}^1(U)} \le 1 \right\}.$$

We will write $\langle \cdot, \cdot \rangle$ to denote the pairing between $\mathcal{H}^{-1}(U)$ and $\mathcal{H}^1(U)$.

In other words, a function $f \in \mathcal{H}^{-1}(U)$ denotes that f is a bounded linear functional on $\mathcal{H}^1(U)$.

Multiply equation (2.7) by a test function $v \in \mathcal{H}^1(U)$ with $\|v\|_{\mathcal{H}^1(U)} \le 1$ and integrate over the domain U. We obtain

$$\underbrace{\int_U u_t(t,x)v(x)\,dx}_{=\|u_t(t,\cdot)\|_{\mathcal{H}^{-1}(U)}} = \int_U \left(g^0(t,x) + \sum_{j=1}^n g^j_{x_j}(t,x) \right) v(x)\,dx$$

$$= \int_U g^0(t,x)v(x)\,dx + \underbrace{\sum_{j=1}^n g^j(t,x)v(x)\Big|_{\partial U}}_{=0 \text{ due to BC}} - \sum_{j=1}^n \int_U g^j(t,x)v_{x_j}(x)\,dx$$

$$\overset{\text{Cauchy Schwarz}}{\leq} \left\| g^0(t,\cdot) \right\|_{\mathcal{L}^2(U)} \underbrace{\|v\|_{\mathcal{L}^2(U)}}_{=\|v\|_{\mathcal{H}^2(U)} \leq 1} + \sum_{j=1}^n \left\| g^j(t,\cdot) \right\|_{\mathcal{L}^2(U)} \underbrace{\left\| v_{x_j} \right\|_{\mathcal{L}^2(U)}}_{=\|v\|_{\mathcal{H}^2(U)} \leq 1}$$

$$\leq \sum_{j=0}^n \left\| g^j(t,\cdot) \right\|_{\mathcal{L}^2(U)}$$

for a.e. time $t \in [0,T]$. Executing some standard estimates, it follows

$$\|u_t(t,\cdot)\|_{\mathcal{H}^{-1}(U)} \leq \sum_{j=0}^n \left\| f(t,\cdot) + \sum_{i=1}^n \left(a^{ij} - b^i \right) u_{x_i}(t,\cdot) - cu(t,\cdot) \right\|_{\mathcal{L}^2(U)}$$

$$\leq \|f(t,\cdot)\|_{\mathcal{L}^2(U)} + \sum_{j=1}^n \left\| \sum_{i=1}^n \left(a^{ij} - b^i \right) u_{x_i}(t,\cdot) - cu(t,\cdot) \right\|_{\mathcal{L}^2(U)}$$

$$\leq C \left(\|f(t,\cdot)\|_{\mathcal{L}^2(U)} + \|u(t,\cdot)\|_{\mathcal{H}^1(U)} \right)$$

Consequently, it might be reasonable to look for a weak solution with $\frac{\mathrm{d}}{\mathrm{d}t}(u) \in \mathcal{H}^{-1}(U)$ for a.e. time $t \in [0,T]$. We can reexpress the first term in (2.6) with $\langle \frac{\mathrm{d}}{\mathrm{d}t}\boldsymbol{u}, v \rangle$. This derivation motivates the definition of a weak solution, see [9], section 5.9.2. and 7.1.1..

Definition 2.2.12 (Weak solution of a parabolic PDE)**.** *We say a function*

$$\boldsymbol{u} \in \mathcal{L}^2\left(0,T;\mathcal{H}^1(U)\right), \ \ \text{with} \ \frac{\mathrm{d}}{\mathrm{d}t}\boldsymbol{u} \in \mathcal{L}^2\left(0,T;\mathcal{H}^{-1}(U)\right)$$

is a weak solution of the parabolic boundary problem (2.1) *provided*

(i) $\left\langle \frac{\mathrm{d}}{\mathrm{d}t}\boldsymbol{u}, v \right\rangle + B\left[\boldsymbol{u}, v; t\right] = (\boldsymbol{f}, v)$
   for each $v \in \mathcal{H}^1(U)$ *and a.e. time* $t \in [0,T]$*, and*

(ii) $\boldsymbol{u}(0) = g$.

Instead of claiming a point wise validity as for a classical solution, a weak solution can be seen as a mean integral with an arbitrary weighting function v. The same holds for the initial and boundary condition. The weak formulation of our parabolic PDE with

homogeneous Neumann boundary conditions (2.6) is similar as the weak formulation of a parabolic PDE with homogeneous Dirichlet boundary conditions. The only difference is, that our function $\boldsymbol{u}$ operates in $\mathcal{L}^2\left(0, T; \mathcal{H}^1(U)\right)$ instead of $\mathcal{L}^2(0, T; \mathcal{H}_0^1(U))$. The zero index corresponds to the homogeneous Dirichlet boundary condition. The space $\mathcal{H}_0^k(U)$ is defined as the closure of $\mathcal{C}^\infty(U)$ functions with compact support in U with respect to the norm $\mathcal{H}^k(U)$. So functions in $\mathcal{H}_0^k(U)$ can be interpreted as functions in $\mathcal{H}^k(U)$ such that "$D^\alpha u = 0$ on ∂U" for all $|\alpha| \leq k - 1$. For more details see [9] section 5.2.2.. Thus, we can use some results of this book.

To find a weak solution of the parabolic boundary problem (2.1), we use the so called *Galerkin Method*. The approach is to replace the function space by a finite-dimensional subspace and taking afterwards the limits of the approximated solution. In more detail, assume $w_k(x)$ are smooth orthogonal basis vectors of $\mathcal{L}^2(U)$ and $\mathcal{H}^1(U)$. One can normalize the basis with respect to one of the spaces and we do this with respect to the $\mathcal{L}^2(U)$ space. Remember that it is not possible to normalize the basis for both spaces. So we obtain

$$\{w_k\}_{k=1}^\infty \text{ is an orthogonal basis of } \mathcal{H}^1(U)$$

and

$$\{w_k\}_{k=1}^\infty \text{ is an orthonormal basis of } \mathcal{L}^2(U).$$

For a fixed integer m, we want to find a function $\boldsymbol{u}_m : [0, T] \to \mathcal{H}^1(U)$ of the form

$$\boldsymbol{u}_m(t) := \sum_{k=1}^m d_m^k(t) w_k. \tag{2.8}$$

Later on in section 2.2.2, we refer to the basis w_k as shape functions, since we use them to approximate the shape of the solution. Additionally, the coefficients of the approximation should satisfy

$$d_m^k(0) = \langle g, w_k \rangle \tag{2.9}$$

and it should hold

$$\left\langle \frac{\mathrm{d}}{\mathrm{d}t} \boldsymbol{u}_m, w_k \right\rangle + B\left[\boldsymbol{u}_m, w_k; t\right] = (\boldsymbol{f}, w_k). \tag{2.10}$$

One can proof that there exists for each integer m a unique function $\boldsymbol{u}_m$ of the form (2.8) satisfying (2.9) and (2.10). The proof can be found in [9], section 7.1.2..
In order to continue to send the limits to infinity, we need some uniform estimates which can be found in [9] and are slightly adjusted to our problem. The next lemma and proposition are given in [9], section 6.2.2., Theorem 2, respectively 7.1.2., Theorem 2.

Lemma 2.2.13 (Energy estimation 1)**.** *There exist constants $\alpha, \beta > 0$ and $\gamma \geq 0$ such that*

$$\beta\|u\|^2_{\mathcal{H}^1(U)} \leq B\,[u, u] + \gamma\|u\|^2_{\mathcal{L}^2(U)}.$$

Proof. Using the elliptic condition, we have

$$
\begin{aligned}
\theta \int_U |Du|^2 \, dx &\leq \int_U \sum_{i,j=1}^n a^{ij} u_{x_i} u_{x_j} \, ds \\
&= B\,[u, u] - \int_U \sum_{i=1}^n b^i u_{x_i} u + c u^2 \, dx \qquad\qquad (2.11) \\
&\leq B\,[u, u] + \sum_{i=1}^n \left\|b^i\right\|_{\mathcal{L}^\infty} \int_U |Du|\,|u| \, dx + \|c\|_{\mathcal{L}^\infty} \int_U u^2 \, dx.
\end{aligned}
$$

With Cauchy's inequality we observe for $\varepsilon > 0$

$$\int_U |Du|\,|u| \, dx \leq \varepsilon \int_U |Du|^2 \, dx + \frac{1}{4\varepsilon} \int_U u^2 \, dx.$$

We choose ε so small such that $\varepsilon \sum_{i=1}^n \left\|b^i\right\|_{\mathcal{L}^\infty} < \frac{\theta}{2}$ and insert this into (2.11). Then it holds

$$
\begin{aligned}
&\frac{\theta}{2} \int_U |Du|^2 \, dx \leq B\,[u, u] + \tilde{C} \int_U u^2 \, dx \\
\iff\quad &\frac{\theta}{2} \int_U |Du|^2 + |u|^2 \, dx \leq B\,[u, u] + \tilde{C} \int_U u^2 \, dx + \frac{\theta}{2} \int_U |u|^2 \, dx = B\,[u, u] + C \int_U u^2 \, dx
\end{aligned}
$$

for some appropriate constants $\tilde{C}$ and C. It easily follows the statement for appropriate constants $\beta > 0$, $\gamma \geq 0$. $\qquad\square$

Proposition 2.2.14 (Energy estimation 2)**.** *There exists a constant C, depending only on U, T and the coefficients of L, such that*

$$
\begin{aligned}
&\max_{t \in [0,T]} \|\boldsymbol{u}_m(t)\|_{\mathcal{L}^2(U)} + \|\boldsymbol{u}_m\|_{\mathcal{L}^2(0,T;\mathcal{H}^1(U))} + \left\|\frac{\mathrm{d}}{\mathrm{d}t}\boldsymbol{u}_m\right\|_{\mathcal{L}^2(0,T;\mathcal{H}^{-1}(U))} \\
&\qquad \leq C\left(\|\boldsymbol{f}\|_{\mathcal{L}^2(0,T;\mathcal{L}^2(U))} + \|g\|_{\mathcal{L}^2(U)}\right)
\end{aligned}
$$

for $m = 1, 2, \ldots$.

Proof. We give here only a brief summary of the proof, only parts which are important later on are more precisely. The complete proof is in [9], section 7.1.2..
By multiplying $d_m^k(t)$ to (2.10), summing up for k and recalling (2.8), we find

$$\left\langle \frac{\mathrm{d}}{\mathrm{d}t} \boldsymbol{u}_m, \boldsymbol{u}_m \right\rangle + B\left[\boldsymbol{u}_m, \boldsymbol{u}_m; t\right] = (\boldsymbol{f}, \boldsymbol{u}_m).$$

for a.e. $t \in [0, T]$. Furthermore $|(\boldsymbol{f}, \boldsymbol{u}_m)| \leq \frac{1}{2}\|\boldsymbol{f}\|^2_{\mathcal{L}^2(U)} + \frac{1}{2}\|\boldsymbol{u}_m\|^2_{\mathcal{L}^2(U)}$ and $\langle \frac{\mathrm{d}}{\mathrm{d}t}\boldsymbol{u}_m, \boldsymbol{u}_m \rangle = \frac{\mathrm{d}}{\mathrm{d}t}\left(\frac{1}{2}\|\boldsymbol{u}_m\|^2_{\mathcal{L}^2(U)}\right)$. Consequently, these equations and Lemma 2.2.13 yields

$$\frac{\mathrm{d}}{\mathrm{d}t}\left(\|\boldsymbol{u}_m\|^2_{\mathcal{L}^2(U)}\right) + 2\beta\|\boldsymbol{u}_m\|^2_{\mathcal{H}^1(U)} \leq C_1\|\boldsymbol{u}_m\|^2_{\mathcal{L}^2(U)} + C_2\|\boldsymbol{f}\|^2_{\mathcal{L}^2(U)} \tag{2.12}$$

for a.e. $t \in [0, T]$ and appropriate constants C_1 and C_2. Apply the differential form of Gronwall's inequality, that is Theorem A.2.2, to (2.12) and (2.9) yields

$$\max_{t \in [0,T]} \|\boldsymbol{u}_m(t)\|^2_{\mathcal{L}^2(U)} \leq C_3\left(\|g\|^2_{\mathcal{L}^2(U)} + \|\boldsymbol{f}\|^2_{\mathcal{L}^2(0,T;\mathcal{L}^2(U))}\right).$$

Integrate (2.12) from 0 to T and employ the inequality above to find

$$\begin{aligned} \|\boldsymbol{u}_m\|^2_{\mathcal{L}^2(0,T;\mathcal{H}^1(U))} &= \int_0^T \|\boldsymbol{u}_m\|^2_{\mathcal{H}^1(U)} dt \\ &\leq C_4\left(\|g\|^2_{\mathcal{L}^2(U)} + \|\boldsymbol{f}\|^2_{\mathcal{L}^2(0,T;\mathcal{L}^2(U))}\right). \end{aligned}$$

We choose fixed $v \in \mathcal{H}^1(U)$ with $\|v\|_{\mathcal{H}^1(U)} \leq 1$ and write $v = v^1 + v^2$, where $v^1 \in \mathrm{span}\{w_k\}_{k=1}^m$ and $\langle v^2, w_k \rangle = 0$ for all k. Note that $\{w_k\}_k^\infty$ are orthogonal in $\mathcal{H}^1(U)$, thus $\|v^1\|_{\mathcal{H}^1(U)} \leq \|v\|_{\mathcal{H}^1(U)} \leq 1$. Then this property yields with equations (2.10) and (2.8)

$$\int_0^T \left\|\frac{\mathrm{d}}{\mathrm{d}t}\boldsymbol{u}_m\right\|^2_{\mathcal{H}^{-1}(U)} dt \leq C_5\left(\|g\|^2_{\mathcal{L}^2(U)} + \|\boldsymbol{f}\|^2_{\mathcal{L}^2(0,T;\mathcal{L}^2(U))}\right).$$

$\square$

Now we take $m \to \infty$ to build a weak solution of our problem.

Theorem 2.2.15 (Existence and uniqueness)**.** *There exists an unique weak solution of* (2.1).

The following is no full proof, only a sketch of proof Theorem 2.2.15. Note that *Evans* did a proof in his book [9] for a homogeneous Dirichlet Boundary Problem. Therefore, the weak solution is in $\mathcal{L}^2\left(0, T; \mathcal{H}_0^1(U)\right)$. However, the variational formulation of our system (2.1) has the same form as the variational formulation of a homogeneous Dirichlet Boundary Problem, except that it operates in $\mathcal{L}^2\left(0, T; \mathcal{H}^1(U)\right)$. Thus, we replace in our proof $\mathcal{H}_0^1(U)$ by $\mathcal{H}^1(U)$. Equivalently, $\mathcal{H}^{-1}(U)$ denotes then the dual room of $\mathcal{H}^1(U)$. More interested readers can find details in [9], section 7.1.2, Theorem 3.

Proof. Existence: First we denote $\boldsymbol{u}_m$ as a Galerkin approximation of the problem (2.1). Then we send m to infinity and look for a subsequence that converges to a weak solution of (2.1). An estimation is used which is referred to as Energy Estimation 2, see Proposition 2.2.14. It follows that a subsequence $\boldsymbol{u}_{m_l}$ respectively $\frac{\mathrm{d}}{\mathrm{d}t}\boldsymbol{u}_{m_l}$ converges weakly in $\mathcal{L}^2(0,T;\mathcal{H}^1(U))$ respectively $\mathcal{L}^2(0,T;\mathcal{H}^{-1}(U))$. Construct a test function $\boldsymbol{v} \in \mathcal{C}^1([0,T];\mathcal{H}^1(U))$ as

$$\boldsymbol{v}(t) = \sum_{k=1}^{N} d^k(t) w_k$$

with $\{d^k\}_{k=1}^N$ are given smooth functions, w_k is a orthogonal basis of $\mathcal{H}^1(U)$ and N as a fixed integer. Functions of this form are dense in $\mathcal{L}^2(0,T;\mathcal{H}^1(U))$ and using the weak convergence of the subsequence, we obtain the weak formulation in (2.6) for each $v \in \mathcal{H}^1(U)$. Almost analogously, one obtains $\boldsymbol{u}(0) = g$.

Uniqueness: We assume two weak solutions $\boldsymbol{u_1}$ and $\boldsymbol{u_2}$ of (2.5). Taking the difference of (2.5) with $\boldsymbol{u_1}$ and $\boldsymbol{u_2}$ yield $\boldsymbol{f} \equiv 0$ and $g \equiv 0$. Let's define $\boldsymbol{u} := \boldsymbol{u_1} - \boldsymbol{u_2}$. For $\boldsymbol{v} = \boldsymbol{u}$ one obtains

$$\frac{\mathrm{d}}{\mathrm{d}t}\left(\frac{1}{2}\|\boldsymbol{u}\|_{\mathcal{L}^2(U)}^2\right) + B\left[\boldsymbol{u},\boldsymbol{u};t\right] = \left\langle \frac{\mathrm{d}}{\mathrm{d}t}\boldsymbol{u},\boldsymbol{u}\right\rangle + B\left[\boldsymbol{u},\boldsymbol{u};t\right] = 0.$$

One can find an estimation $B\left[\boldsymbol{u},\boldsymbol{u};t\right] \geq -\gamma\|\boldsymbol{u}\|_{\mathcal{L}^2(U)}^2$. That yields

$$\frac{\mathrm{d}}{\mathrm{d}t}\left(\frac{1}{2}\|\boldsymbol{u}\|_{\mathcal{L}^2(U)}^2\right) \leq \gamma\|\boldsymbol{u}\|_{\mathcal{L}^2(U)}^2.$$

Now the generalised Gronwall's inequality, Theorem A.2.3, leads to $\boldsymbol{u} \equiv 0$ because of the initial condition $g \equiv 0$. $\square$

If one assumes on the one hand stronger assumptions to the right hand side f and on the other hand to the coefficients a^{ij}, b^i, c to be smooth in U as well as the boundary itself and a^{ij} do not depend on t for all $i,j = 1,\ldots,n$, then one can find an improved regularity of the weak solution of the parabolic problem (2.1).

For the proof, we need a higher regularity of the elliptic boundary value problem. Unfortunately, we can not rewrite *Evans* proof at this point. *Solonnikov* derived a general theorem for higher regular weak solutions of elliptic problems in [30], p. 158-159. As an example, he applied it for a second boundary value problem with Neumann boundary conditions which is given here as a lemma.

Lemma 2.2.16. *Assume $a^{ij} \in \mathcal{W}_q^1(U)$, $b^i, c \in \mathcal{L}^q(U)$, $q > n$, $i,j = 1,\ldots,n$ and $\boldsymbol{f} \in \mathcal{L}^q(U)$. Suppose that $\boldsymbol{u}$ is a weak solution of the elliptic boundary-value problem*

$$Lu = f \ in \ U$$
$$\frac{\partial u}{\partial \boldsymbol{n}} = 0 \ on \ \partial U.$$

Assume finally

$$\partial U \in \mathcal{C}^2.$$

Then

$$u \in \mathcal{W}_q^2(U)$$

and we have the estimate

$$\|\boldsymbol{u}\|_{\mathcal{W}_q^2(U)} \leq C \left(\|\boldsymbol{f}\|_{\mathcal{L}^q(U)} + \|\boldsymbol{u}\|_{\mathcal{L}^q(U)} \right).$$

Using this Lemma, we can prove the regularity theorem in [9], p. 360-361, for our boundary setting.

Theorem 2.2.17 (Improved regularity for homogeneous Neumann condition)**.** *Assume* $a^{ij} \in \mathcal{H}^2(U)$, $b^i, c \in \mathcal{L}^\infty([0,T] \times U)$, $g \in \mathcal{H}^1(U)$, $\boldsymbol{f} \in \mathcal{L}^2(0,T;\mathcal{L}^2(U))$ *and* $\partial U \in \mathcal{C}^2$. *Suppose also* $\boldsymbol{u} \in \mathcal{L}^2(0,T;\mathcal{H}^1(U))$ *with* $\frac{\mathrm{d}}{\mathrm{d}t}\boldsymbol{u} \in \mathcal{L}^2(0,T;\mathcal{H}^{-1}(U))$, *is the weak solution of the parabolic problem* (2.1). *Then in fact*

$$\boldsymbol{u} \in \mathcal{L}^2(0,T;\mathcal{H}^2(U)) \cap \mathcal{L}^\infty(0,T;\mathcal{H}^1(U)), \frac{\mathrm{d}}{\mathrm{d}t}\boldsymbol{u} \in \mathcal{L}^2(0,T;\mathcal{L}^2(U)),$$

and we have the estimate

$$\operatorname*{ess\,sup}_{t \in [0,T]} \|\boldsymbol{u}(t)\|_{\mathcal{H}^1(U)} + \|\boldsymbol{u}\|_{\mathcal{L}^2(0,T;\mathcal{H}^2(U))} + \left\| \frac{\mathrm{d}}{\mathrm{d}t}\boldsymbol{u} \right\|_{\mathcal{L}^2(0,T;\mathcal{L}^2(U))}$$
$$\leq C \left(\left\| \boldsymbol{f}_{\mathcal{L}^2(0,T;\mathcal{L}^2(U))} \right\| + \|g\|_{\mathcal{H}^1(U)} \right).$$

The constant C *depends only on* U, T *and the coefficients of the Lebesgue spaces.*

Proof. Again, we will give here a brief approach of the proof given in *Evans* book [9]. Similar as in Proposition 2.2.14, we multiply equation (2.10) now by $\frac{\mathrm{d}}{\mathrm{d}t}d_m^k(t)$ for fixed m and summing up for k to discover

$$\left\langle \frac{\mathrm{d}}{\mathrm{d}t}\boldsymbol{u}_m, \frac{\mathrm{d}}{\mathrm{d}t}\boldsymbol{u}_m \right\rangle + B\left[\boldsymbol{u}_m, \frac{\mathrm{d}}{\mathrm{d}t}\boldsymbol{u}_m \right] = \left(\boldsymbol{f}, \frac{\mathrm{d}}{\mathrm{d}t}\boldsymbol{u}_m \right)$$

for a.e. $t \in [0,T]$. Recall the definition of $B\left[\boldsymbol{u}_m, \frac{\mathrm{d}}{\mathrm{d}t}\boldsymbol{u}_m \right]$, see equation (2.4),

$$B[\boldsymbol{u}_m, \frac{\mathrm{d}}{\mathrm{d}t}\boldsymbol{u}_m] = \int_U \sum_{i,j=1}^n a^{ij} \boldsymbol{u}_{m,x_i} \frac{\mathrm{d}}{\mathrm{d}t}\boldsymbol{u}_{m,x_i} \, dx + \int_U \sum_{i=1}^n b^i \boldsymbol{u}_{m,x_i} \frac{\mathrm{d}}{\mathrm{d}t}\boldsymbol{u}_m + c\boldsymbol{u}_m \frac{\mathrm{d}}{\mathrm{d}t}\boldsymbol{u}_m \, dx$$

$$=: A_1 + A_2.$$

We assumed $a^{ij} = a^{ji}$ and the coefficients do not depend on t, so one can derive

$$A_1 = \frac{\mathrm{d}}{\mathrm{d}t}\left(\frac{1}{2}A\left[\boldsymbol{u}_m, \boldsymbol{u}_m\right]\right)$$

for $A[u,v]$, $u,v \in \mathcal{H}^1(U)$, being a symmetric bilinear form. Furthermore, applying Young's Theorem, that is Theorem A.2.1,

$$|A_2| \le \frac{C}{\epsilon}\|\boldsymbol{u}_m\|^2_{\mathcal{H}^1(U)} + \epsilon\left\|\frac{\mathrm{d}}{\mathrm{d}t}\boldsymbol{u}_m\right\|^2_{\mathcal{L}^2(U)}$$

$$\left|\left(\boldsymbol{f}, \frac{\mathrm{d}}{\mathrm{d}t}\boldsymbol{u}_m\right)\right| \le \frac{C}{\epsilon}\|\boldsymbol{f}\|^2_{\mathcal{L}^2(U)} + \epsilon\left\|\frac{\mathrm{d}}{\mathrm{d}t}\boldsymbol{u}_m\right\|^2_{\mathcal{L}^2(U)}$$

for each $\epsilon > 0$ and a constant $C > 0$ depending on the coefficients b^i and c. Combining both inequalities, choosing $\epsilon = \frac{1}{4}$ and integrating, we find

$$\int_0^T \left\|\frac{\mathrm{d}}{\mathrm{d}t}\boldsymbol{u}_m\right\|^2_{\mathcal{L}^2(U)} \, dt + \sup_{t\in[0,T]} A\left[\boldsymbol{u}_m(t), \boldsymbol{u}_m(t)\right]$$

$$\le C\left(A\left[\boldsymbol{u}_m(0), \boldsymbol{u}_m(0)\right] + \int_0^T \|\boldsymbol{u}_m\|^2_{\mathcal{H}^1(U)} + \|\boldsymbol{f}\|^2_{\mathcal{L}^2(U)} \, dt\right)$$

$$\le C\left(\|g\|^2_{\mathcal{H}^1(U)} + \left\|\boldsymbol{f}^2_{\mathcal{L}^2(0,T;\mathcal{L}^2(U))}\right\|\right),$$

according to Proposition 2.2.14. Since $A[u,u] \ge \theta \int_U |Du|^2 \, dx$ for each $u \in \mathcal{H}^1(U)$, we obtain

$$\sup_{t\in[0,T]} \|\boldsymbol{u}_m(t)\|^2_{\mathcal{H}^1(U)} \le C\left(\|g\|^2_{\mathcal{H}^1(U)} + \|\boldsymbol{f}\|^2_{\mathcal{L}^2(0,T;\mathcal{L}^2(U))}\right).$$

Passing to limits as $m = m_l \to \infty$, we deduce $\boldsymbol{u} \in \mathcal{L}^\infty(0,T;\mathcal{H}^1(U))$ and $\frac{\mathrm{d}}{\mathrm{d}t}\boldsymbol{u} \in \mathcal{L}^2(0,T;\mathcal{L}^2(U))$ with the stated bounds. In particular, for a.e. t we have the identity

$$\left\langle\frac{\mathrm{d}}{\mathrm{d}t}\boldsymbol{u}, v\right\rangle + B\left[\boldsymbol{u}, v\right] = (\boldsymbol{f}, v)$$

for each $v \in \mathcal{H}^1(U)$. We rewrite this into

$$B\left[\boldsymbol{u}, v\right] = \langle\boldsymbol{h}, v\rangle$$

for $\boldsymbol{h} := \boldsymbol{f} - \frac{\mathrm{d}}{\mathrm{d}t}\boldsymbol{u}$. Since $\boldsymbol{h} \in \mathcal{L}^2(U)$ for a.e. $t \in [0, T]$, we deduce from Lemma 2.2.16 that $\boldsymbol{u}(t) \in \mathcal{H}^2(U)$ for a.e. $t \in [0, T]$, with the estimate

$$\|\boldsymbol{u}\|^2_{\mathcal{H}^2(U)} \leq C \left(\|\boldsymbol{f}\|^2_{\mathcal{L}^2(U)} + \left\| \frac{\mathrm{d}}{\mathrm{d}t}\boldsymbol{u} \right\|^2_{\mathcal{L}^2(U)} + \|\boldsymbol{u}\|^2_{\mathcal{L}^2(U)} \right).$$

Integrating and utilizing the derived estimates, we complete the proof. $\qquad\square$

Let us investigate a more complex case. We assume a nonlinearity in the right hand side of the system in (2.1), that is $f = f(u)$, but suppose simultaneously that $f(u)$ is Lipschitz continuous.

Theorem 2.2.18 (Existence and uniqueness of a nonlinear reaction diffusion system). *Let $U \subset \mathbb{R}^n$ and $u = (u^1, \ldots, u^m)$. Then there exists a unique weak solution of*

$$
\begin{aligned}
\frac{\partial}{\partial t}u + Lu &= f(u) && in\ (0, T] \times U \\
\frac{\partial u}{\partial \boldsymbol{n}} &= 0 && on\ (0, T] \times \partial U \\
u &= g && on\ \{t = 0\} \times U
\end{aligned}
\tag{2.13}
$$

with $f \in \mathcal{L}^2([0, T] \times U)$ being nonlinear but Lipschitz continuous and $g \in \mathcal{H}^1(U)$.

The following proof is an adjusted version of an example in [9] in Section 9.2.1..

Proof. Let's define an operator A to apply Banach's fixed point theorem in space $X = C([0, T], \mathcal{L}^2(U; \mathbb{R}^m))$ with norm

$$\|\boldsymbol{v}\| := \max_{t \in [0, T]} \|\boldsymbol{v}(t)\|_{\mathcal{L}^2(U; \mathbb{R}^m)}.$$

Let $\boldsymbol{u} \in X$ be a given function, then $\boldsymbol{h}(t) := \boldsymbol{f}(\boldsymbol{u}(t))$ is in $\mathcal{L}^2(0, T; \mathcal{L}^2(U, \mathbb{R}^m))$ due to the Lipschitz continuity. Consequently the linear parabolic PDE

$$
\begin{aligned}
\frac{\mathrm{d}}{\mathrm{d}t}\boldsymbol{w} + L\boldsymbol{w} &= \boldsymbol{f}(\boldsymbol{w}) && in\ (0, T] \times U \\
\frac{\partial \boldsymbol{w}}{\partial \boldsymbol{n}} &= 0 && on\ (0, T] \times \partial U \\
\boldsymbol{w} &= g && on\ \{t = 0\} \times U
\end{aligned}
$$

has a unique weak solution with

$$\boldsymbol{w} \in \mathcal{L}^2(0, T; \mathcal{H}^1(U; \mathbb{R}^m)), \text{ with } \frac{\mathrm{d}}{\mathrm{d}t}\boldsymbol{w} \in \mathcal{L}^2(0, T; \mathcal{H}^{-1}(U; \mathbb{R}^m)),$$

see Theorem 2.2.15. Thus, $\boldsymbol{w} \in X$ fulfils

$$\left\langle \frac{\mathrm{d}}{\mathrm{d}t} \boldsymbol{w}, \boldsymbol{v} \right\rangle + B\left[\boldsymbol{w}, \boldsymbol{v}; t\right] = (\boldsymbol{h}, \boldsymbol{w}) \tag{2.14}$$

for a.e. $t \in [0, T]$ and for each $\boldsymbol{v} \in \mathcal{H}^1(U; \mathbb{R}^m)$ and $\boldsymbol{w}(0) = g$. Hence we define

$$A : X \to X, \quad A\left[\boldsymbol{u}\right] = \boldsymbol{w}.$$

Next, we choose $\boldsymbol{u}, \tilde{\boldsymbol{u}} \in X$ and define $\boldsymbol{w} = A[\boldsymbol{u}]$, $\tilde{\boldsymbol{w}} = A[\tilde{\boldsymbol{u}}]$ as above. That means $\boldsymbol{w}$ verifies (2.14) for $\boldsymbol{h} = \boldsymbol{f}(\boldsymbol{u})$ respectively $\tilde{\boldsymbol{h}} = \boldsymbol{f}(\tilde{\boldsymbol{u}})$. Using the estimation (2.12) from the proof of Theorem 2.2.14, we deduce for the difference of $\boldsymbol{w} - \tilde{\boldsymbol{w}}$

$$\frac{\mathrm{d}}{\mathrm{d}t} \|\boldsymbol{w} - \tilde{\boldsymbol{w}}\|^2_{\mathcal{L}^2(U)} + 2\beta \|\boldsymbol{w} - \tilde{\boldsymbol{w}}\|^2_{\mathcal{H}^1(U)} \leq C_1 \|\boldsymbol{w} - \tilde{\boldsymbol{w}}\|^2_{\mathcal{L}^2(U)} + C_2 \left\|\boldsymbol{h} - \tilde{\boldsymbol{h}}\right\|^2_{\mathcal{L}^2(U)}$$

$$\iff \quad \frac{\mathrm{d}}{\mathrm{d}t} \|\boldsymbol{w} - \tilde{\boldsymbol{w}}\|^2_{\mathcal{L}^2(U)} \leq C_3 \|\boldsymbol{w} - \tilde{\boldsymbol{w}}\|^2_{\mathcal{L}^2(U)}$$

because of the Lipschitz continuity of $\boldsymbol{f}$. Integrate the inequality with respect to time t and we obtain

$$\|\boldsymbol{w}(s) - \tilde{\boldsymbol{w}}(\boldsymbol{s})\|^2_{\mathcal{L}^2(U)} \leq C \int_0^s \|\boldsymbol{u}(t) - \tilde{\boldsymbol{u}}(t)\|^2_{\mathcal{L}^2(U)} \, dt$$

$$\leq CT \|\boldsymbol{u} - \tilde{\boldsymbol{u}}\|^2 \tag{2.15}$$

for $s \in [0, T]$. Maximizing of the left hand side yields

$$\|\boldsymbol{w} - \tilde{\boldsymbol{w}}\|^2 \leq CT \|\boldsymbol{u} - \tilde{\boldsymbol{u}}\|^2.$$

Therefore

$$\|A[\boldsymbol{u}] - A[\tilde{\boldsymbol{u}}]\| \leq (CT)^{\frac{1}{2}} \|\boldsymbol{u} - \tilde{\boldsymbol{u}}\|$$

and if $T > 0$ is so small such that $(CT)^{\frac{1}{2}} < 1$ then operator A is a strict contraction. That means for any given $T > 0$, we select $T_1 > 0$ so small such that $(CT_1)^{\frac{1}{2}} < 1$. Then we can apply Banach's fixed point theorem (Theorem A.1.1) to find a unique weak solution $\boldsymbol{u}$ of (2.13) existing for $t \in [0, T_1]$. We can then repeat the argument to extend our solution to the interval $[T_1, 2T_1]$. Repeat this procedure and after finitely many steps, we constructed a weak solution on the full interval $[0, T]$.

In order to show uniqueness, we assume two weak solutions $\boldsymbol{u}$ and $\tilde{\boldsymbol{u}}$. Then we have $\boldsymbol{w} = \boldsymbol{u}$ and $\tilde{\boldsymbol{w}} = \tilde{\boldsymbol{u}}$ in (2.15). Thus,

$$\|\boldsymbol{u}(s) - \tilde{\boldsymbol{u}}(s)\|^2_{\mathcal{L}^2(U)} \leq C \int_0^s \|\boldsymbol{u}(t) - \tilde{\boldsymbol{u}}(s)\|^2_{\mathcal{L}^2(U)} \, dt$$

for $t \in [0, T]$. Gronwall's inequality, Theorem A.2.3 yields $\boldsymbol{u} \equiv \tilde{\boldsymbol{u}}$. $\qquad\square$

Later on in chapter 5, we will need some further results in order to proof existence and uniqueness of our adjusted parabolic equation. These are not given any more in [9]. We start to introduce a regularisation of the Heaviside function such that it becomes continuous.

Definition 2.2.19. *For $\delta > 0$, let H_δ denote the following regularisation of the Heaviside function:*

$$
H_\delta(x) = \begin{cases} 0 & x \leq 0 \\[2mm] \dfrac{x}{\delta} & 0 < x < \delta \\[4mm] 1 & x \geq \delta. \end{cases}
$$

Then $H_\delta(x) \in \mathcal{C}(\mathbb{R}) \cap \mathcal{W}^{1,\infty}(\mathbb{R})$, $H_\delta'(x) \geq 0$ a.e. and $0 \leq H_\delta(x) \leq 1$ for all $\vec{x} \in \mathbb{R}$.

The following proposition is useful to compare weak solutions of specific reaction diffusion equations.

Proposition 2.2.20 (Monotony property)**.** *Let $\Omega \subset \mathbb{R}^n$ be an open, bounded set and $T > 0$ be a fixed time point. There are two parabolic systems given:*

$$
\begin{aligned}
\frac{\partial}{\partial t} u(t, \vec{x}) =& D\nabla^2 u(t, \vec{x}) - \alpha b(t, \vec{x}) f(t, \vec{x}) u(t, \vec{x}) - \gamma u(t, \vec{x}) \\
& + \beta \Pi_\chi(h(t, \vec{x})) g(t, \vec{x}) b(t, \vec{x}) \\
u(0, \vec{x}) =& u_0(\vec{x}) \\
\frac{\partial u}{\partial \boldsymbol{n}} =& 0
\end{aligned}
\tag{2.16}
$$

and

$$
\begin{aligned}
\frac{\partial}{\partial t} v(t, \vec{x}) =& D\nabla^2 v(t, \vec{x}) - \alpha b(t, \vec{x}) F v(t, \vec{x}) + \beta \Pi G b(t, \vec{x}) - \gamma v(t, \vec{x}) \\
v(0, \vec{x}) =& v_0(\vec{x}) \\
\frac{\partial v}{\partial \boldsymbol{n}} =& 0
\end{aligned}
\tag{2.17}
$$

with

$$
\Pi_\chi(h(t, \vec{x})) := \Pi_{min} + \Delta \Pi h(t, \vec{x})
$$

and $f, g, h \in \mathcal{L}^\infty((0, T] \times \Omega)$, $u_0(\vec{x})$, $v_0(\vec{x}) \in \mathcal{H}^1(\Omega)$, $b \in \mathcal{L}^\infty((0, T] \times \Omega)$ and $D, \alpha, \beta, \gamma, \sigma, \Pi, F, G \in \mathbb{R}^+$ are non-negative constants.

We assume that there exist weak solutions $u(t, \vec{x})$ and $v(t, \vec{x})$ of (2.16) and (2.17) with $u_0(\vec{x}) \leq v_0(\vec{x})$. If $F \leq f(t, \vec{x})$, $G \geq g(t, \vec{x})$ and $\Pi \geq \Pi_\chi(h(t, \vec{x}))$, then it holds $u(t, \vec{x}) \leq v(t, \vec{x})$ for almost every $(t, \vec{x})$ in $[0, T] \times \Omega$.

Proof. Let $z := u - v$ be the difference of weak solutions of equations (2.16) and (2.17), respectively. Consequently, z solves the difference of the equations, that is,

$$
\begin{aligned}
\frac{\partial}{\partial t} z(t, \vec{x}) = {} & D \nabla^2 z(t, \vec{x}) - \alpha b(t, \vec{x}) \left[f(t, \vec{x}) u(t, \vec{x}) - F v(t, \vec{x})) \right] \\
& + \beta b(t, \vec{x}) \left[\Pi_\chi(h(t, \vec{x})) g(t, \vec{x}) - \Pi G \right] - \gamma z(t, \vec{x})
\end{aligned}
\tag{2.18}
$$

with

$$
\begin{aligned}
z(0, \vec{x}) &= u_0(\vec{x}) - v_0(\vec{x}) \\
\frac{\partial z}{\partial \mathbf{n}} &= 0.
\end{aligned}
\tag{2.19}
$$

We use Definition 2.2.19 to obtain with $\lambda > 0$

$$
\varphi(t, \vec{x}) := -e^{-\lambda t} H_\delta(z(t, \vec{x}))
$$

which we use as a test function since we can conclude that $\varphi(t, \vec{x})$ is in $\mathcal{H}^1((0, T]) \times \Omega$ because H_δ is in $\mathcal{W}^{1,\infty}$ and weak differentiability follows from the chain rule of Sobolev functions. Furthermore, the derivatives of φ with respect to t and $\vec{x}$ are in $\mathcal{L}^2$. That's because on the one hand $\partial_t z$, $\boldsymbol{\nabla} z \in \mathcal{L}^2$ since this holds each for u and v. On the other hand $\partial_t \left(-e^{-\lambda t} H_\delta(x) \right) = \lambda e^{-\lambda t} \frac{1}{\delta} \leq \frac{\lambda}{\delta}$ and $\partial_x \left(-e^{-\lambda t} H_\delta(x) \right) = \leq \frac{\lambda}{\delta}$ for all t and $\vec{x}$.

Testing equation 2.18 with $\varphi(t, \vec{x})$, applying Fubini's Theorem, we obtain

$$
-\int_\Omega \int_0^t \frac{\partial}{\partial t} z(s, \vec{x}) e^{-\lambda s} H_\delta(z(s, \vec{x})) \, ds \, d\vec{x} =
\tag{2.20}
$$

$$
- D \int_\Omega \int_0^t \nabla^2 z(s, \vec{x}) e^{-\lambda s} H_\delta(z(s, \vec{x})) \, ds \, d\vec{x}
\tag{2.21}
$$

$$
+ \int_\Omega \int_0^t \alpha b(s, \vec{x}) \left[f(s, \vec{x}) u(s, \vec{x}) - F v(s, \vec{x})) \right] e^{-\lambda s} H_\delta(z(s, \vec{x})) \, ds \, d\vec{x}
\tag{2.22}
$$

$$
- \int_\Omega \int_0^t \beta b(s, \vec{x}) \left[\Pi_\chi(h(s, \vec{x})) g(s, \vec{x}) - \Pi G \right] e^{-\lambda s} H_\delta(z(s, \vec{x})) \, ds \, d\vec{x}.
\tag{2.23}
$$

$$
+ \gamma \int_\Omega \int_0^t z(s, \vec{x}) e^{-\lambda s} H_\delta(z(s, \vec{x})) \, ds \, d\vec{x}.
\tag{2.24}
$$

We start with the left hand side (2.20). Partial integration yields

$$(2.20) = -\int_\Omega \left[z(t,\vec{x})e^{-\lambda t} H_\delta(z(t,\vec{x})) - z(0,\vec{x})H_\delta(z(0,\vec{x})) \right] d\vec{x}$$

$$+ \int_\Omega \int_0^t z(s,\vec{x}) \frac{\mathrm{d}}{\mathrm{d}s} \left[e^{-\lambda s} H_\delta(z(s,\vec{x})) \right] ds\, d\vec{x}$$

$$= -\int_\Omega z(t,\vec{x})e^{-\lambda t} H_\delta(z(t,\vec{x})) - z(0,\vec{x})H_\delta(z(0,\vec{x}))\, d\vec{x}$$

$$- \int_\Omega \int_0^t z(s,\vec{x})\lambda e^{-\lambda s} H_\delta(z(s,\vec{x}))\, ds\, d\vec{x}$$

$$+ \int_\Omega \int_0^t z(s,\vec{x})e^{-\lambda s} H_\delta'(z(s,\vec{x})) \frac{\partial}{\partial s} z(s,\vec{x})\, ds\, d\vec{x}. \qquad (2.25)$$

We focus initially on (2.25). The derivative of the regularised Heaviside function reads for a.e. $s, \vec{x}$

$$H_\delta'(z(s,\vec{x})) = \begin{cases} \dfrac{1}{\delta} & \text{for } 0 < z(s,\vec{x}) < \delta \\[2mm] 0 & \text{otherwise.} \end{cases}$$

Therefore we obtain

$$|z(s,\vec{x})H_\delta'(z(s,\vec{x}))| = z(s,\vec{x})H_\delta'(z(s,\vec{x})) \leq \delta\frac{1}{\delta} = 1 \quad \text{for a.e. } s, \vec{x}$$

and in general it holds

$$H_\delta'(z(s,\vec{x}))\chi_{(0,\delta)}(z(s,\vec{x})) = H_\delta'(z(s,\vec{x})) \quad \text{for a.e. } s, \vec{x}.$$

Using this, we can conclude for the absolute value of (2.25) the following inequality:

$$\left| \int_\Omega \int_0^t z(s,\vec{x})e^{-\lambda s} H_\delta'(z(s,\vec{x})) \frac{\partial}{\partial s} z(s,\vec{x})\, ds\, d\vec{x} \right|$$

$$= \left| \int_\Omega \int_0^t z(s,\vec{x})e^{-\lambda s} H_\delta'(z(s,\vec{x}))\chi_{(0,\delta)}(z(s,\vec{x})) \frac{\partial}{\partial s} z(s,\vec{x})\, ds\, d\vec{x} \right|$$

$$\leq \int_\Omega \int_0^t \underbrace{|z(s,\vec{x})H_\delta'(z(s,\vec{x}))|}_{\leq 1} \left| \chi_{(0,\delta)}(z(s,\vec{x})) \frac{\partial}{\partial s} z(s,\vec{x}) \right| ds\, d\vec{x}$$

$$\leq \int_\Omega \int_0^t \left| \chi_{(0,\delta)}(z(s,\vec{x})) \frac{\partial}{\partial s} z(s,\vec{x}) \right| ds\, d\vec{x}.$$

Since $\partial_t z \in \mathcal{L}^2((0,T] \times \Omega)$, we know that $\partial_t z \in \mathcal{L}^1((0,T] \times \Omega)$. That means the integrand is dominated by $\partial_t z$, an integrable function. Additionally, it holds that

$$\lim_{\delta \to 0} \chi_{(0,\delta)}(z(s,\vec{x})) \to 0$$

converges pointwise because $\bigcap_{\delta > 0}(0,\delta) = \emptyset$. Finally, we can apply the dominated convergence theorem A.4.3, yielding

$$\lim_{\delta \to 0} \int_\Omega \int_0^t \left| \chi_{(0,\delta)}(z(s,\vec{x})) \frac{\partial}{\partial s} z(s,\vec{x}) \right| ds \, d\vec{x} = 0.$$

Since $\lim_{\delta \to 0} H_\delta(z(s,\vec{x})) \to H(z(s,\vec{x}))$ converges pointwise, we obtain due to the dominated convergence theorem that (2.20) can be written finally to

$$
\begin{aligned}
-&\int_\Omega \int_0^t \frac{\partial}{\partial s} z(s,\vec{x}) e^{-\lambda s} H(z(s,\vec{x})) \, ds \, d\vec{x} \\
=& -\int_\Omega z(t,\vec{x}) e^{-\lambda t} H(z(t,\vec{x})) - z(0,\vec{x}) H(z(0,\vec{x})) \, d\vec{x} \\
& -\lambda \int_\Omega \int_0^t z(s,\vec{x}) e^{-\lambda s} H(z(s,\vec{x})) \, ds \, d\vec{x} \\
=& -e^{-\lambda t} \int_\Omega [z(t,\vec{x})]_+ \, d\vec{x} + \int_\Omega [z(0,\vec{x})]_+ \, d\vec{x} - \lambda \int_\Omega \int_0^t e^{-\lambda s} [z(s,\vec{x})]_+ \, ds \, d\vec{x}.
\end{aligned}
$$

Now we focus on the right hand side starting with the Laplace term (2.21). As in previous calculation, partial integration and Neumann boundary condition (2.19) yields

$$
\begin{aligned}
-\int_0^t \int_\Omega \nabla^2 z(s,\vec{x}) e^{-\lambda s} H_\delta(z(s,\vec{x})) \, d\vec{x} \, ds &= \\
= \int_0^t e^{-\lambda s} \int_\Omega \underbrace{\left(\nabla z(s,\vec{x}) \nabla z(s,\vec{x}) \right) H_\delta'(z(s,\vec{x}))}_{\geq 0} \, d\vec{x} \, ds &\geq 0
\end{aligned}
$$

for all $\delta > 0$.

The dominated convergence theorem A.4.3 can be applied to (2.22), (2.23) and (2.24) and allows us to replace H_δ by H. Additionally, the degradation term (2.24) can be rewritten to

$$\gamma \int_\Omega \int_0^t z(s,\vec{x}) e^{-\lambda s} H_\delta(z(s,\vec{x})) \, ds \, d\vec{x} = \gamma \int_\Omega \int_0^t e^{-\lambda s} [z(s,\vec{x})]_+ \, ds \, d\vec{x} \geq 0.$$

Summed up the results so far, we obtain

$$-e^{-\lambda t}\left\|[z(t,\cdot)]_+\right\|_{L_1(\Omega)} + \left\|[z(0,\cdot)]_+\right\|_{L_1(\Omega)} + (1-\lambda)\int_\Omega\int_0^t e^{-\lambda s}\,[z(s,\vec{x})]_+\ ds\ d\vec{x}$$

$$\geq \int_\Omega\int_0^t \alpha b(s,\vec{x})\underbrace{[f(s,\vec{x})u(s,\vec{x}) - Fv(s,\vec{x})]}_{=:M_1}H(z(s,\vec{x}))e^{-\lambda s}\ ds\ d\vec{x} \qquad (2.26)$$

$$-\int_\Omega\int_0^t \beta b(s,\vec{x})\underbrace{\left[\Pi_\chi(h(s,\vec{x}))g(s,\vec{x}) - \Pi G\right]}_{=:M_2}e^{-\lambda s}H(z(s,\vec{x}))\ ds\ d\vec{x}. \qquad (2.27)$$

We instantaneously see that $M_2 \leq 0$ due to the assumptions. That leads to

$$-\int_\Omega\int_0^t \beta b(s,\vec{x})M_2 e^{-\lambda s}H(z(s,\vec{x}))\ ds\ d\vec{x} \geq 0. \qquad (2.28)$$

The term in (2.26) is a little bit trickier. We take a first look at M_1. We can extend this expression to obtain finally

$$M_1 = \underbrace{f(s,\vec{x})u(s,\vec{x}) - f(s,\vec{x})v(s,\vec{x})}_{=f(s,\vec{x})z(s,\vec{x})}$$

$$+ \underbrace{f(s,\vec{x})v(s,\vec{x}) - Fv(s,\vec{x})}_{\geq 0 \text{ due to assumption}}.$$

Thus, the right hand side can be estimated to

$$(2.26) \geq \int_\Omega\int_0^t \alpha b(s,\vec{x})f(s,\vec{x})z(s,\vec{x})H(z(s,\vec{x}))e^{-\lambda s}\ ds\ d\vec{x}$$

$$\geq C_1\int_\Omega\int_0^t [z(s,\vec{x})]_+\,e^{-\lambda s}\ ds\ d\vec{x} \qquad (2.29)$$

with $C_1 := \alpha F \min\limits_{(s,\vec{x})\in[0,T]\times\Omega} b(s,\vec{x})|\Omega|$.

Using the estimations (2.28) and (2.29) for (2.26) and (2.27), we obtain

$$-e^{-\lambda t}\left\|[z(t,\cdot)]_+\right\|_{L_1(\Omega)} + \left\|[z(0,\cdot)]_+\right\|_{L_1(\Omega)} \geq (\lambda-1)\int_\Omega\int_0^t e^{-\lambda s}\,[z(s,\vec{x})]_+\ ds\ d\vec{x}$$
$$+ C_1\int_\Omega\int_0^t e^{-\lambda s}\,[z(s,\vec{x})]_+\ ds\ d\vec{x}. \qquad (2.30)$$

We assumed for the initial condition $u_0(\vec{x}) \leq v_0(\vec{x})$, that means $[z(0,\cdot)]_+ = 0$ almost everywhere. Thus, $\left\|[z(0,\cdot)]_+\right\|_{L_1(\Omega)} = 0$ and (2.30) simplifies to

$$-e^{-\lambda t}\left\|[z(t,\cdot)]_+\right\|_{L_1(\Omega)} \geq (\lambda - 1 + C_1) \int_\Omega \int_0^t e^{-\lambda s} \left[z(s,\vec{x})\right]_+ ds\, d\vec{x}$$
$$\geq 0, \quad \text{if } \lambda \geq C_1 - 1 \text{ is chosen.}$$

Thus, we can conclude

$$\left\|[z(t,\cdot)]_+\right\|_{\mathcal{L}^1(\Omega)} \leq 0.$$

The expression $[z]_+ = [u - v] \leq 0$ is equivalent to $u \leq v$. That means we can finally conclude that $\left\|[z(t,\cdot)]_+\right\|_{\mathcal{L}^1(\Omega)} \leq 0$ is equivalent to $u(t,\vec{x}) \leq v(t,\vec{x})$. $\qquad \square$

Corollary 2.2.21. *We assume that there exist weak solutions $u(t,\vec{x})$ and $v(t,\vec{x})$ of (2.16) and (2.17) with $u_0(\vec{x}) \geq v_0(\vec{x})$. If $F \geq f(t,\vec{x})$, $G \leq g(t,\vec{x})$ and $\Pi \leq \Pi_\chi(h(t,\vec{x}))$ then it holds $u(t,\vec{x}) \geq v(t,\vec{x})$.*

The proof is analogously since one has just to change signs and inequality signs.

The next lemma states the solution of a PDE including diffusion and degradation only.

Lemma 2.2.22. *Let $\Omega \subset \mathbb{R}^2$ and $t \in [t_0, T]$. Then the system*

$$\frac{\partial}{\partial t}\Psi(t,\vec{x}) = \nabla^2 \Psi(t,\vec{x}) - \gamma\Psi(t,\vec{x})$$
$$\Psi(t_0,\vec{x}) = e^{-\gamma t_0}\hat{\zeta}(\vec{x})$$
$$\frac{\partial\Psi(t,\vec{x})}{\partial\mathbf{n}} = 0 \quad \text{for } \vec{x} \in \partial\Omega$$

with $\gamma \in \mathbb{R}_+$ being a non-negative constant and $\Psi_{t_0}(\vec{x}) \in \mathcal{H}^1(\Omega)$ has a unique solution which reads

$$\Psi(t,\vec{x}) = e^{-\gamma t}\zeta(t,\vec{x})$$

whereas $\zeta(t,\vec{x})$ is a solution of $\frac{\partial}{\partial t}\zeta(t,\vec{x}) = \nabla^2\zeta(t,\vec{x})$ with $\zeta(t_0,\vec{x}) = \hat{\zeta}(\vec{x}) \in \mathbb{R}_+$ and $\frac{\partial\zeta(t,\vec{x})}{\partial\boldsymbol{n}} = 0$.

Proof. The existence can be proven by simply recalculating the derivatives of $\Psi(t,\vec{x})$:

$$\frac{\partial}{\partial t}\Psi(t,\vec{x}) = -\gamma e^{-\gamma t}\zeta(t,\vec{x}) + e^{-\gamma t}\frac{\partial}{\partial t}\zeta(t,\vec{x})$$
$$= -\gamma e^{-\gamma t}\zeta(t,\vec{x}) + e^{-\gamma t}\nabla^2\zeta(t,\vec{x})$$
$$\nabla\Psi(t,\vec{x}) = e^{-\gamma t}\nabla\zeta(t,\vec{x})$$
$$\nabla^2\Psi(t,\vec{x}) = e^{-\gamma t}\nabla^2\zeta(t,\vec{x}).$$

Inserting this into the PDE $\frac{\partial}{\partial t}\Psi(t,\vec{x}) = \nabla^2\Psi - \gamma\Psi$ yields

$$-\gamma e^{-\gamma t}\zeta(t,\vec{x}) + e^{-\gamma t}\nabla^2\zeta(t,\vec{x}) = e^{-\gamma t}\nabla^2\zeta(t,\vec{x}) - \gamma e^{-\gamma t}\zeta(t,\vec{x}).$$

Furthermore, the initial and boundary conditions are fulfilled, too:

$$\Psi(t_0,\vec{x}) = e^{-\gamma t_0}\zeta(t_0,\vec{x}) = e^{-\gamma t_0}\hat{\zeta}(\vec{x})$$
$$\frac{\Psi(t,\vec{x})}{(n)} = e^{-\gamma t}\frac{\zeta(t,\vec{x})}{\boldsymbol{n}} = 0.$$

To prove uniqueness, we first show that

$$\frac{\partial}{\partial t}\zeta(t,\vec{x}) = \nabla^2\zeta(t,\vec{x}) \tag{2.31}$$

has a unique solution. We assume that there exist two solutions ζ_1 and ζ_2 of (2.31). The difference of these solutions $z := \zeta_1 - \zeta_2$ solves the difference of the PDEs, that is

$$\frac{\partial}{\partial t}\zeta_1(t,\vec{x}) - \frac{\partial}{\partial t}\zeta_2(t,\vec{x}) = \nabla^2\zeta_1(t,\vec{x}) - \nabla^2\zeta_2(t,\vec{x})$$
$$\Longleftrightarrow \quad \frac{\partial}{\partial t}z(t,\vec{x}) = \nabla^2 z(t,\vec{x})$$

with

$$z(t_0,\vec{x}) = \hat{\zeta}_1(\vec{x}) - \hat{\zeta}_2(\vec{x}).$$

The equation is tested with $z(t,\vec{x})$ and integrated by t. Integration on the left and partial integration on the right hand side yields

$$\int_{t_0}^{t}\int_{\Omega}\frac{\partial}{\partial t}z(s,\vec{x})z(s,\vec{x})\,d\vec{x}\,ds = \int_{t_0}^{t}\int_{\Omega}\nabla^2 z(s,\vec{x})z(s,\vec{x})\,d\vec{x}\,ds$$
$$\Longleftrightarrow \quad \frac{1}{2}\|z(t,\cdot)\|_{\mathcal{L}^2(\Omega)}^2 + \frac{1}{2}\|z(t_0,\cdot)\|_{\mathcal{L}^2(\Omega)}^2 = -\int_{t_0}^{t}|\nabla z(s,\vec{x})|^2\,ds \leq 0.$$

Therefore, if $\zeta_1(\vec{x}) = \zeta_2(\vec{x})$ then $\frac{1}{2}\|z(t,\cdot)\|_{\mathcal{L}^2(\Omega)}^2 \leq 0$ which means that $\zeta_1(t,\vec{x}) = \zeta_2(t,\vec{x})$ due to Gronwall's inequality. Thus, the assumption was wrong leading to a unique solution.

We do the same approach for $\Psi(t,\vec{x})$. Assume that there are two solutions Ψ_1 and Ψ_2. The difference of these solutions $y(t,\vec{x}) := \Psi_1(t,\vec{x}) - \Psi_2(t,\vec{x})$ solves the difference of the corresponding PDEs, that is

$$\frac{\partial}{\partial t}y(t,\vec{x}) = \nabla^2 y(t,\vec{x}) - \gamma y(t,\vec{x})$$

with

$$y(t_0,\vec{x}) = e^{-\gamma t_0}\left(\hat{\zeta}_1(\vec{x}) - \hat{\zeta}_2(\vec{x})\right).$$

We use $y(t,\vec{x})$ as a test function to test the equation and integration by t yields

$$\int_{t_0}^t \int_\Omega \frac{\partial}{\partial t}y(s,\vec{x})y(s,\vec{x})\,d\vec{x}\,ds = \int_0^t \int_\Omega \nabla^2 y(s,\vec{x})y(s,\vec{x})\,d\vec{x}\,ds$$
$$- \gamma \int_{t_0}^t \int_\Omega y(s,\vec{x})y(s,\vec{x})\,d\vec{x}\,ds$$
$$\Longleftrightarrow \quad \frac{1}{2}\|y(t,\cdot)\|^2_{\mathcal{L}^2(\Omega)} + \frac{1}{2}\|y(t_0,\cdot)\|^2_{\mathcal{L}^2(\Omega)} \leq -\int_0^t |\nabla y(s,\vec{x})|^2\,ds - \gamma \int_0^t |y(s,\vec{x})|^2\,ds \leq 0.$$

Choosing the same initial condition, meaning $y(t_0,\vec{x}) = 0$, we obtain by Gronwall's inequality that $\Psi_1(t,\vec{x}) = \Psi_2(t,\vec{x})$ and eventually a unique solution. $\qquad\square$

2.2.2. Finite Element Method (FEM) for a parabolic PDE

As a guideline for the concept, the text book of *P. Knabner and L. Angermann* [15] is used and gives us a short introduction into application-oriented finite element method. The paragraph of Linear Elements is based on *O. C. Zienkiewicz*, see [41].

In section 2.2.1 we derived the weak formulation of a parabolic partial differential equation with homogeneous Neumann boundary condition, see Definition 2.2.12. In order to solve the PDE numerically, there are a variety of methods to do so. In this section we introduce the finite element method which is a more general approximation technique containing many finite difference schemes as special cases. Due to its geometric flexibility, practical implementation, and powerful and elegant theory, it is one of the most successful discretization methods for PDE problems. For that reasons, we concentrate on to solve the PDE with the finite element method.

One can distinguish between *full discretizations*, that is the application of so-called space-time finite element method including the time variable, too, and *semidiscretizations*. The last one includes either *the vertical method of lines*, i.e. discretization starts with respect to the spatial variable or *the horizontal method of lines*, i.e. the discretization starts with respect to the time variable, illustrated in figure 2.3. Of course, both methods need a further discretization step to obtain a fully discretized problem. The intention of a semidiscretization is to deduce intermediate problems which are well known and offer a wide variety of tools to solve. The horizontal method leads to a system of elliptic boundary problems whereas the vertical method yields a system of ordinary

differential equations. We will consider the vertical method in more detail.
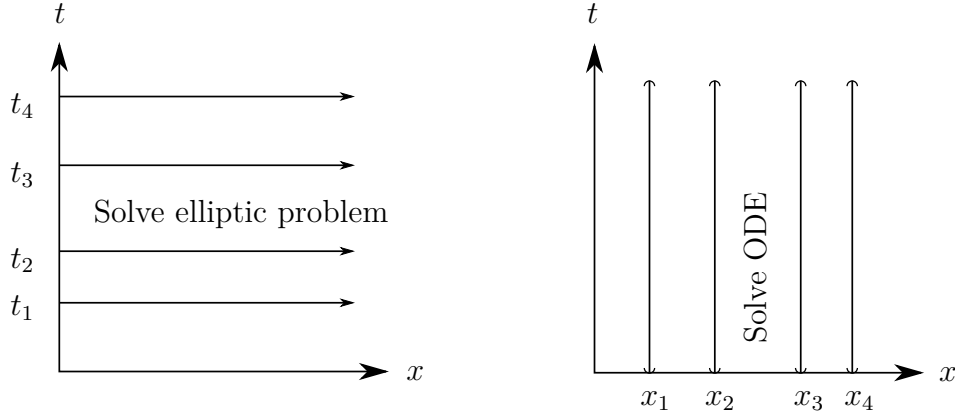
Figure 2.3.: *Scheme of the two semidiscretizations. x denotes the spatial variable, t is the time variable. The left hand side shows the horizontal method, the right hand side the vertical method.*

We use again the *Galerkin method* to discretize the equation as introduced above in section 2.2.1. We replace the function space V by a finite-dimensional subspace $V_h \subset V$ with $\dim(V_h) = N$. Later on, N corresponds to the number of nodes of our space discretisation. Then we look for a solution $u_h \in V_h$ with $t \in [0, T]$ such that

$$\left\langle \frac{\mathrm{d}}{\mathrm{d}t} \boldsymbol{u_h}, v \right\rangle + B\left[\boldsymbol{u_h}, v; t\right] = (\boldsymbol{f}, v) \tag{2.32}$$

for all $v \in V_h$ and let $\boldsymbol{u_{0h}} \in V_h$ be some approximation to $\boldsymbol{u_0}$. Let $\{\phi_i\}_{i=1}^N$ be a basis of V_h, then the approximated solution reads

$$\boldsymbol{u_h}(t) = \sum_{i=1}^N \xi_i(t)\phi_i \tag{2.33}$$

and $\boldsymbol{u_{0h}} = \sum_{i=1}^N \xi_{0i}\phi_i$. As test functions we choose $v = \phi_i$, then the discrete variational equality (2.32) is equivalent to

$$\sum_{j=1}^N \langle \phi_j, \phi_i \rangle \frac{\mathrm{d}\xi_j(t)}{\mathrm{d}t} + \sum_{j=1}^N B\left[\phi_j, \phi_i; t\right] \xi_j(t) = \langle \boldsymbol{f}, \phi_i \rangle \quad \forall i \in \{1, \ldots, N\}. \tag{2.34}$$

The ODE system (2.34) can be rewritten into a matrix form. We define the matrix $M := \langle \phi_j, \phi_i \rangle_{ij}$ which is called *mass matrix*, $K(t) := B\left[\phi_j, \phi_i; t\right]_{i,j}$ as *stiffness matrix* and $F(t) := (\boldsymbol{f}, \phi_i)_i$ is called *load vector*. The initial value is written as $\boldsymbol{\xi_{0h}} := (\xi_{0i})_i$. Then for $\boldsymbol{\xi_h} := (\xi_i(t))_i$ we obtain

$$M\frac{\mathrm{d}}{\mathrm{d}t}\boldsymbol{\xi_h}(t) + K(t)\boldsymbol{\xi_h}(t) = F(t)$$
$$\boldsymbol{\xi_h}(0) = \boldsymbol{\xi_{0h}}.$$

(2.35)

To compute the element matrices it is necessary to find some appropriate test functions respectively the so called *shape functions*. The next paragraph presents a brief instruction how we choose acceptable elements for the approximation.

Linear Elements: First of all we need to discretize the area U into a proper mesh. For reasons of simplicity as well as we don't need higher dimensional cases, we just consider a two-dimensional area $U \subseteq \mathbb{R}^2$. This dimension of area works best with either triangular elements or rectangular elements. We will focus on triangular elements since this element form is very flexible for geometrically challenging boundaries. A triangulation should satisfy following properties which are stated in [15], section 2.2.

Definition 2.2.23. *Let $\mathcal{T}$ be a partition of U into closed triangles K, including the boundary ∂U. We call T a triangulation if*

(1) $\bar{U} = \bigcup_{K \in \mathcal{T}} K$

(2) For $K, K' \in \mathcal{T}$, $K \neq K'$,

$$\mathring{K} \cap \mathring{K'} = \emptyset,$$

where $\mathring{K}$ denotes the open triangle (without the boundary ∂K).

If additionally holds

(3) If $K \neq K'$ but $K \cap K' \neq \emptyset$, then $K \cap K'$ is either a point or a common edge of K and K'.

then $\mathcal{T}$ is called a conforming triangulation.

<center>confirm   non confirm</center>
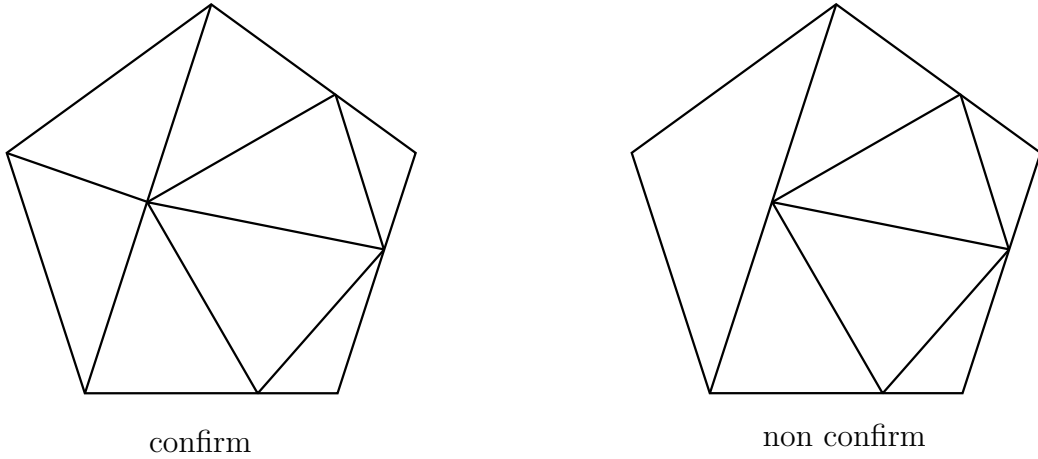
Figure 2.4.: *Scheme of a confirm and non confirm triangulation.*

Usually one considers only conforming triangulation, e.g. see figure 2.4 and so do we in this thesis. The vertices of a triangle are also called *nodes*. For linear finite elements, the ansatz space V_h is defined as

$$V_h := \left\{ u \in \mathcal{C}(\bar{U}) : \ u|_K \in \mathcal{P}_1(K) \ \forall K \in \mathcal{T} \right\}.$$

$\mathcal{P}_1(K)$ denotes the set of linear polynomials in 2 variables on K. Using Cartesian coordinates x and y, a suitable approximation $\hat{u}$ for the unknown u for one triangle element can be written as

$$\hat{u}(x, y) = a_1 + a_2 x + a_3 y \tag{2.36}$$

with constant parameters a_i. That means at vertices of the triangle we require

$$u_1 = a_1 + a_2 x_1 + a_3 y_1$$
$$u_2 = a_1 + a_2 x_2 + a_3 y_2$$
$$u_3 = a_1 + a_2 x_3 + a_3 y_3$$

respectively written in matrix form

$$\begin{pmatrix} u_1 \\ u_2 \\ u_3 \end{pmatrix} = \underbrace{\begin{pmatrix} 1 & x_1 & y_1 \\ 1 & x_2 & y_2 \\ 1 & x_3 & y_3 \end{pmatrix}}_{=:\Lambda} \begin{pmatrix} a_1 \\ a_2 \\ a_3 \end{pmatrix}.$$

where u_i is the approximated value at a node i, i.e. $u_i = \hat{u}_i(x_i, y_i)$. Matrix Λ can be inverted such that we obtain a solution for the parameters a_i given by

$$
\begin{pmatrix} a_1 \\ a_2 \\ a_3 \end{pmatrix} = \frac{1}{2A_\triangle} \begin{pmatrix} x_2 y_3 - x_3 y_2 & x_3 y_1 - x_1 y_3 & x_1 y_2 - x_2 y_1 \\ y_2 - y_3 & y_3 - y_1 & y_1 - y_2 \\ x_3 - x_2 & x_1 - x_3 & x_2 - x_1 \end{pmatrix} \begin{pmatrix} u_1 \\ u_2 \\ u_3 \end{pmatrix}.
$$

The symbol $A_\triangle$ denotes the area of the corresponding triangle and can be written as

$$
A_\triangle = \frac{1}{2} \left(x_1 \left(y_2 - y_3 \right) + x_2 \left(y_3 - y_1 \right) + x_3 \left(y_1 - y_2 \right) \right).
$$

Inserting the parameters a_i into equation (2.36) and rearranging yields

$$
\hat{u}(x, y) = \phi_1(x, y) u_1 + \phi_2(x, y) u_2 + \phi_3(x, y) u_3
$$

with ϕ_i being test functions defined as

$$
\phi_1(x, y) := \frac{1}{2A_\triangle} \left[(x_2 y_3 - x_3 y_2) + (y_2 - y_3)x + (x_3 - x_2)y \right]
$$

$$
\phi_2(x, y) := \frac{1}{2A_\triangle} \left[(x_3 y_1 - x_1 y_3) + (y_3 - y_1)x + (x_1 - x_3)y \right]
$$

$$
\phi_3(x, y) := \frac{1}{2A_\triangle} \left[(x_1 y_2 - x_2 y_1) + (y_1 - y_2)x + (x_2 - x_1)y \right].
$$

So each approximated solution on a triangle element is given by its nodal values u_i. Note that the derivatives may not be continuous between elements such that the solution provides only $\mathcal{C}_0$. Furthermore it typically holds the local properties of a shape function:

Let e be the set of edges of one triangle. Then it holds

$$
\phi_i(\vec{x}_j) = \delta_{ij}
$$

for i, j building an edge in e.

Additionally, the shape functions satisfy the following condition

$$
\sum_i \phi_i(x) = 1, \qquad \forall x \in e.
$$

The derivatives of $\phi_i(x, y)$ can be easily written down and read

$$\frac{\partial \phi}{\partial x} = \begin{pmatrix} \frac{\partial \phi_1}{\partial x} \\ \frac{\partial \phi_2}{\partial x} \\ \frac{\partial \phi_3}{\partial x} \end{pmatrix} = \frac{1}{2A_\triangle} \begin{pmatrix} y_2 - y_3 \\ y_3 - y_1 \\ y_1 - y_2 \end{pmatrix} \quad \text{and} \quad \frac{\partial \phi}{\partial y} = \frac{1}{2A_\triangle} \begin{pmatrix} x_3 - x_2 \\ x_1 - x_3 \\ x_2 - x_1 \end{pmatrix}. \tag{2.37}$$

Chapter 3

ODE model

The probably most common way to model physical, chemical or biological processes in time can be realized simplest by ordinary differential equations (ODEs). In order to understand the processes, one can study the model analytically or simulate it numerically to learn something about it. Even prediction of the behaviour is then possible. Note that an ODE system usually does not consider spatial effects. A compartmental approach could be used to describe a spatial structure and thus staying in the ODE context, but would not be sufficient do describe this system including precise diffusion processes. For that reason we use partial differential equations (PDEs) which will be modelled in chapter 4 and analysed in chapter 5. Henceforth the variables of the ODEs are often concentrations and densities. According to this, it seems reasonable to model the quorum sensing process of *Bacillus subtilis* in form of ODEs as a first attempt to get a first understanding of the process. The laboratory μCats of the BioQuant in Heidelberg with their group leader Dr. Ilka Bischofs provided experimental data for so called "wild type" bacteria which produce and absorb signalling molecules and "mutant" bacteria which absorb signalling molecules only. After we have derived a suitable model, we start to investigate the ordinary differential equations first analytically. Then we try to fit the parameters with the given data of the experiments and if needed we change the model equations to obtain a better result. All details of the best fit algorithm and calculation confidence intervals are given in appendix B.

A review of ordinary differential equations will be not given here but can be found e.g. in [32] or [35].

The upcoming informations, experimental approaches and data in section 3.1 and 3.2 are given by personal communication with Dr. Ilka Bischofs. The corresponding manuscript is not submitted yet.

3.1. Experimental approach

The research group of Dr. Ilka Bischofs in the BioQuant laboratory in Heidelberg developed a bimolecular sensor which can report on *PhrA*-signalling in *Bacillus subtilis* in more detail, a FRET reporter strain. It is necessary that *PhrA* reaches a certain concentration such that the sporulation process of *Bacillus subtilis* can start. Without *PhrA*, *Bacillus subtilis* do not sporulate. The part "FRET" of the reporter means "Förster resonance energy transfer" and describes a physical process of energy transfer from one chromophore molecule, the "donor", to a neighbouring chromophore, the "acceptor" [3]. As donor, they use the fluorophores protein CFP which is fused to RapA and as acceptor a fluorophores protein YFP which is fused to Spo0F. There have been independent measurements from at least four biological replicates executed by the μCats laboratory, seeing the results in figure 3.1. Fluorescence increases up to 30% if YFP-CFP fusion protein is on the same promoter, see last bar in figure 3.1. A strain with a YFP-CFP fusion protein serves as a positive control since a significantly amount of FRET will occur in the YFP-CFP fusion protein highlighted as fluorescence of YFP. If both proteins are separately on a strain, no FRET occurs meaning no bar in the figure and one sees only the fluorescence of CFP. This will be used as a negative control. The BioQuant laboratory concluded that the RapA and Spo0F fusion proteins interact and form a FRET-complex in the cell whereas the fluorescence increases up to 11%. This corresponds to the top bar in figure 3.1.
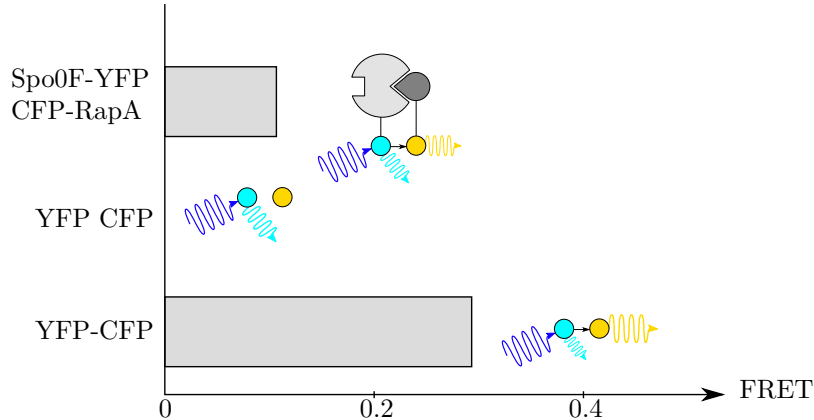
Figure 3.1.: *Bar-plot of the average FRET in the mutant cells for different configurations of YFP and CFP.*

The most important fact is that *PhrA* stimulated cells perturb the interaction of YFP-CFP, thereby decreasing FRET. This is schematically depicted in figure 3.2.
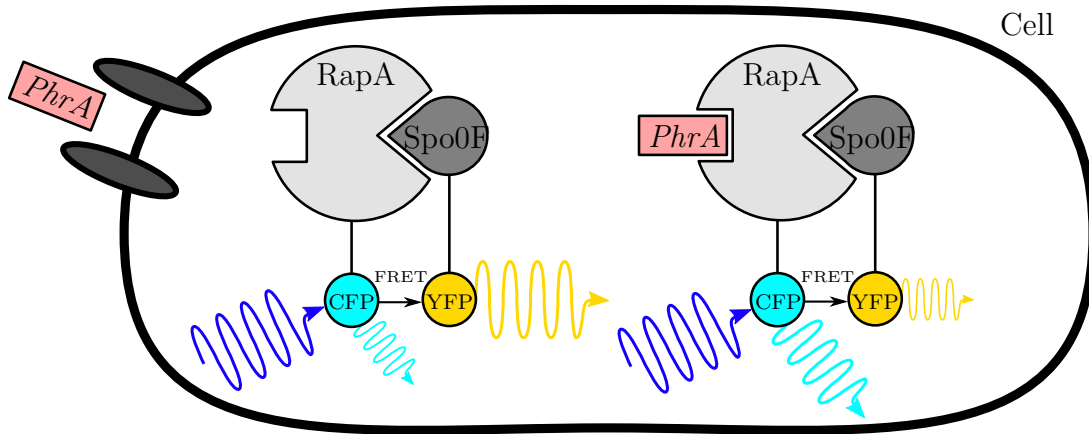
Figure 3.2.: *Scheme of the FRET process within a mutant cell.*

Let's briefly describe the experimental set-up to measure this perturbation. A dense layer of induced cells is on a agarose gel pad illuminated permanently by a specific blue light. After 60 seconds the YFP-acceptor is bleached for 20 seconds and abolishes FRET, resulting in a higher emission of CFP fluorescence. The CFP fluorescence will be measured by a photomultipler tube over time. The amount of FRET is quantified as the ratio of CFP emissions before (CFP_{pre}) and after the photobleaching (CFP_{post}). A typical fluorescence trajectory form the Spo0F-RapA reporter strain is given in figure 3.3. There we see that the CFP emissions of unbleached cells are about 11% lower than that of bleached cells.
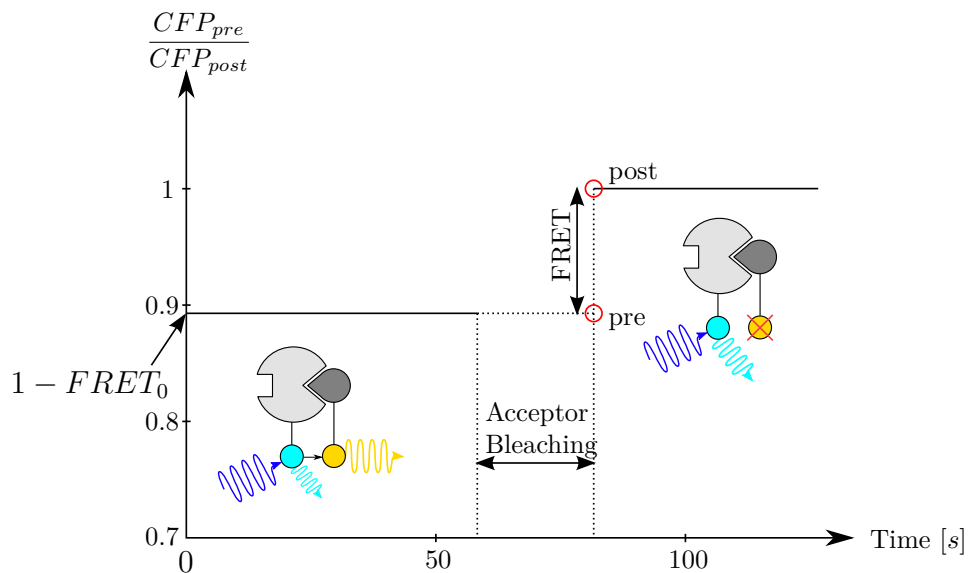
Figure 3.3.: *FRET between CFP-RapA and Spo0F-YFP of unstimulated mutant cells.*

The next step of the biologists was to find out how much the reporter cells respond

to RapA stimulated by signalling peptide *PhrA*. They incubated $10\frac{\mu mol}{l}$ *PhrA* for 5 minutes into the shake flask, washed the cells and measured the FRET by acceptor-photobleaching. A drop to about 4% FRET in *PhrA* stimulated cells compared to the 11% of unstimulated cells have been observed, see figure 3.4. Thus, their FRET reporter is a suitable tool to quantitatively study *PhrA* signalling in *Bacillus subtilis.*
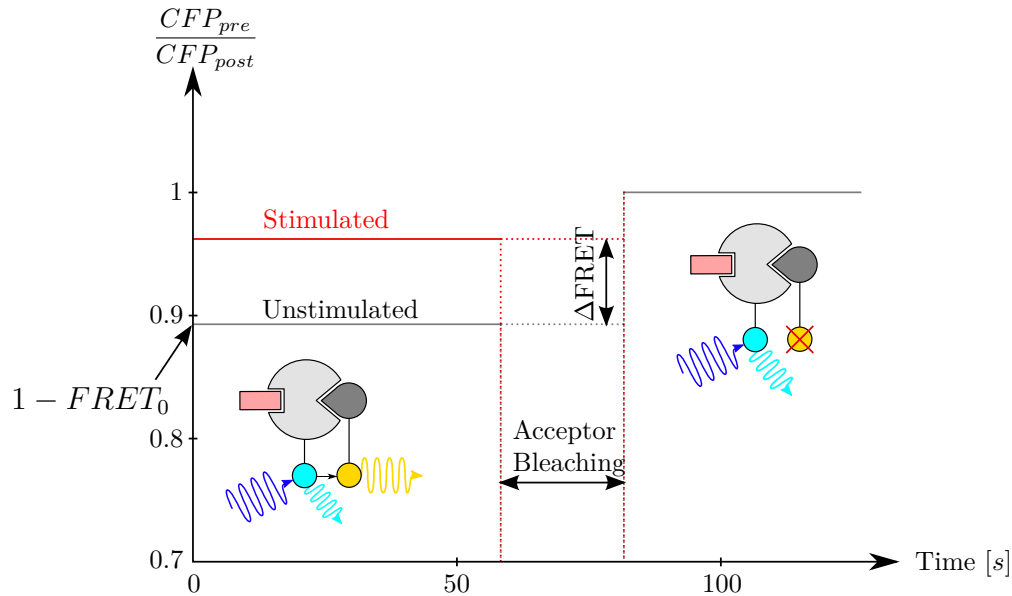
Figure 3.4.: *FRET between CFP-RapA and Spo0F-YFP of $10\frac{nmol}{l}$ PhrA stimulated mutant cells (red line) compared to the prior case of unstimulated mutant cells (grey line).*

   The BioQuant laboratory did three different experiments in order to obtain FRET data sets. Let's briefly describe these experiments.

In the first experiment, the uptake of synthetic *PhrA* signalling molecules by mutants only is investigated and measured. We refer this part of the experiment as intracellular FRET kinetics. The experiments length of time was 20 minutes. The cell density of mutants can be measured by Spectrophotometry. The optical density (OD) is directly proportional to the biomass in the cell suspension, but only for a specific range depending on the cell type [16]. In our case, we can assume that the given range of OD of *Bacillus subitilis* is proportional to the cell density. Mutants were cultured to $OD_{600nm} = 1.6$, whereas $OD_{600nm} = 1$ corresponds to $1.19 \cdot 10^8 \frac{cells}{ml}$, and concentrated 10-fold by centrifuging. This corresponds to $OD_{600nm} = 16$. Then $50\mu l$ were taken of that, this corresponds to $9.52 \cdot 10^7$ cells, and incubated into a reaction tube of a growth medium volume of $500\mu l$. They stimulated the mutants with $10\frac{nmol}{l}$ of

synthetic signalling molecules at time $t = 0$. To measure the FRET at some time $t \in \{0, 1, 2, 3, 6, 11, 21\}$ in minutes, the reaction mixture is centrifuged for one minute in order to obtain on the one hand the mutants only and on the other hand a mutant free supernatant. These mutants were bleached as described above and in that way the intracellular FRET kinetics is determined at time point t. Into the mutant free supernatant, we insert 50 μl of a $OD_{600nm} = 16$ suspension of unstimulated mutants. After 5 minutes, the mixture is centrifuged for one minute and the mutants were bleached again. The FRET of these mutants is referred as extracellular FRET kinetics at time point t. The μCats did 20 test series at all for the intracellular FRET kinetics and measured 14 times the extracellular FRET kinetics. The resulting data as well as the mean and standard deviation are given in figure 3.5.

(a)

(b)
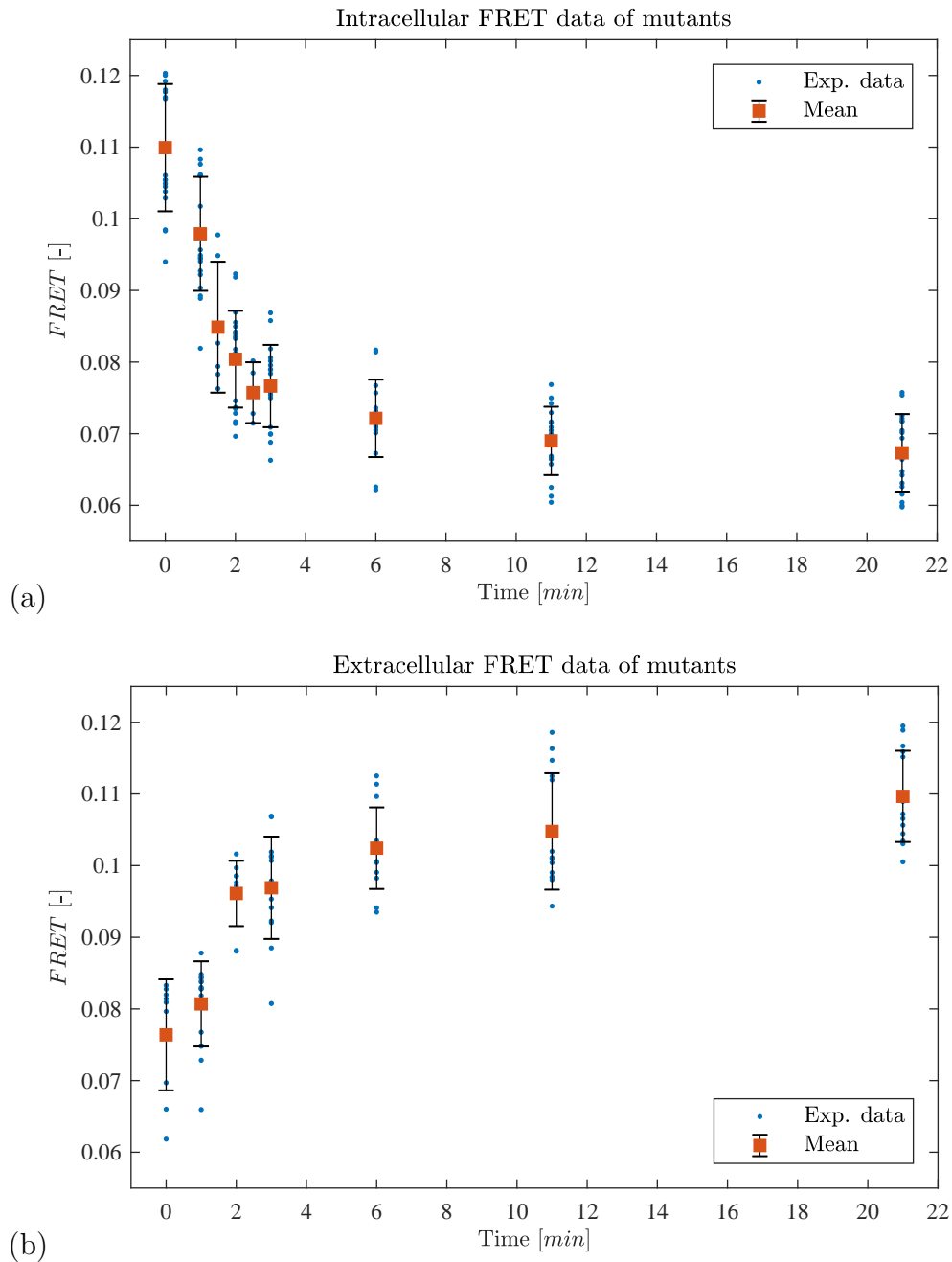
Figure 3.5.: *All data sets are from the μCats laboratory; (a): Experimental data of intracellular FRET of mutants; (b): Experimental data of extracellular FRET of mutants;*

The second mutant experiment was a dose response experiment. The synthetic signalling molecule stimulus varies logarithmically from $0\frac{nmol}{l}$ to $100\frac{nmol}{l}$ at time $t = 0$. The incubation time takes 6 minutes inclusively the time for centrifugation. The total number of mutants and the external volume are the same as for the first experiment.

The data and the mean with standard deviation are given in figure 3.6.
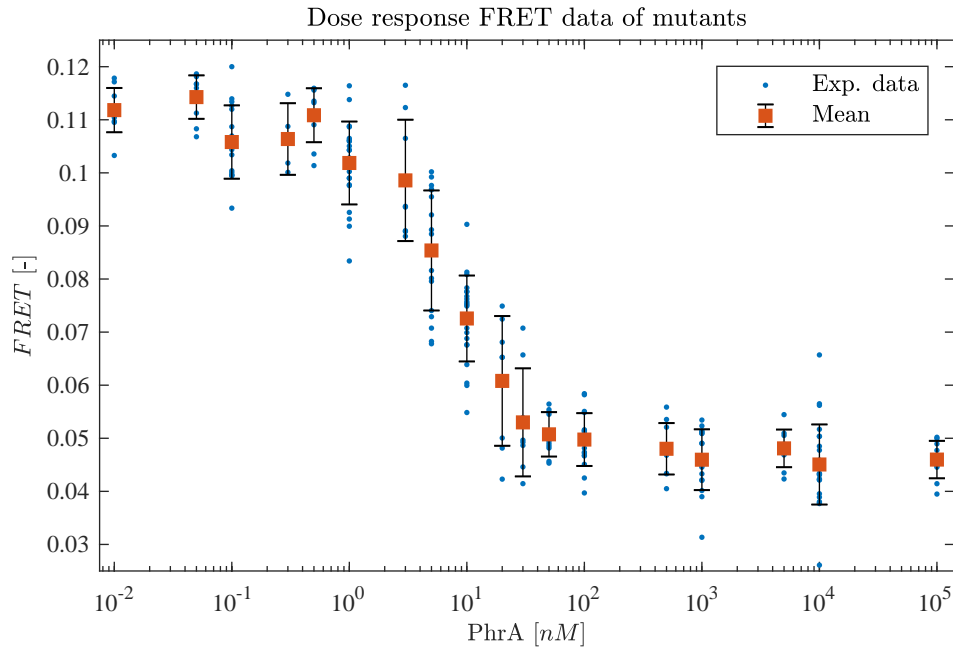
Figure 3.6.: *Data set is from the μCats laboratory; Experimental data of dose response experiment of mutants;*

The last experiment was performed with wild types in an initially signalling free environment regarding the accumulation of extracellular *PhrA* during sporulation. Besides the extracellular FRET, also the bacterial optical density was measured in time. Henceforth wild types were cultured up to $OD_{600nm} = 0.6$ and suspended into a shake flask with 100ml growth medium. Since the wild types are always cultured under the same requirements, the intracellular concentration of signalling molecules is basically equal. We shift this value to zero to work initially with a signalling molecule free cell. Of course the extracellular signalling molecule concentration is zero initially. Within the first two hours, they measured the FRET each 15 minutes, after that each 30 minutes. This was done until the experiment lasts 6 hours. The procedure of measuring extracellular FRET is similar as for experiment 1. Mutants were concentrated to $OD_{600nm} = 16$. Then $50\mu l$ of that were mixed with $1950\mu l$ of wild type free supernatant, incubated for 20 minutes, centrifuged for one minute and bleached to determine the extracellular FRET kinetics of wild types. Additionally the OD of the filtrated bacteria was measured to obtain bacterial growth data. The results are given in figure 3.7.

(a)

(b)
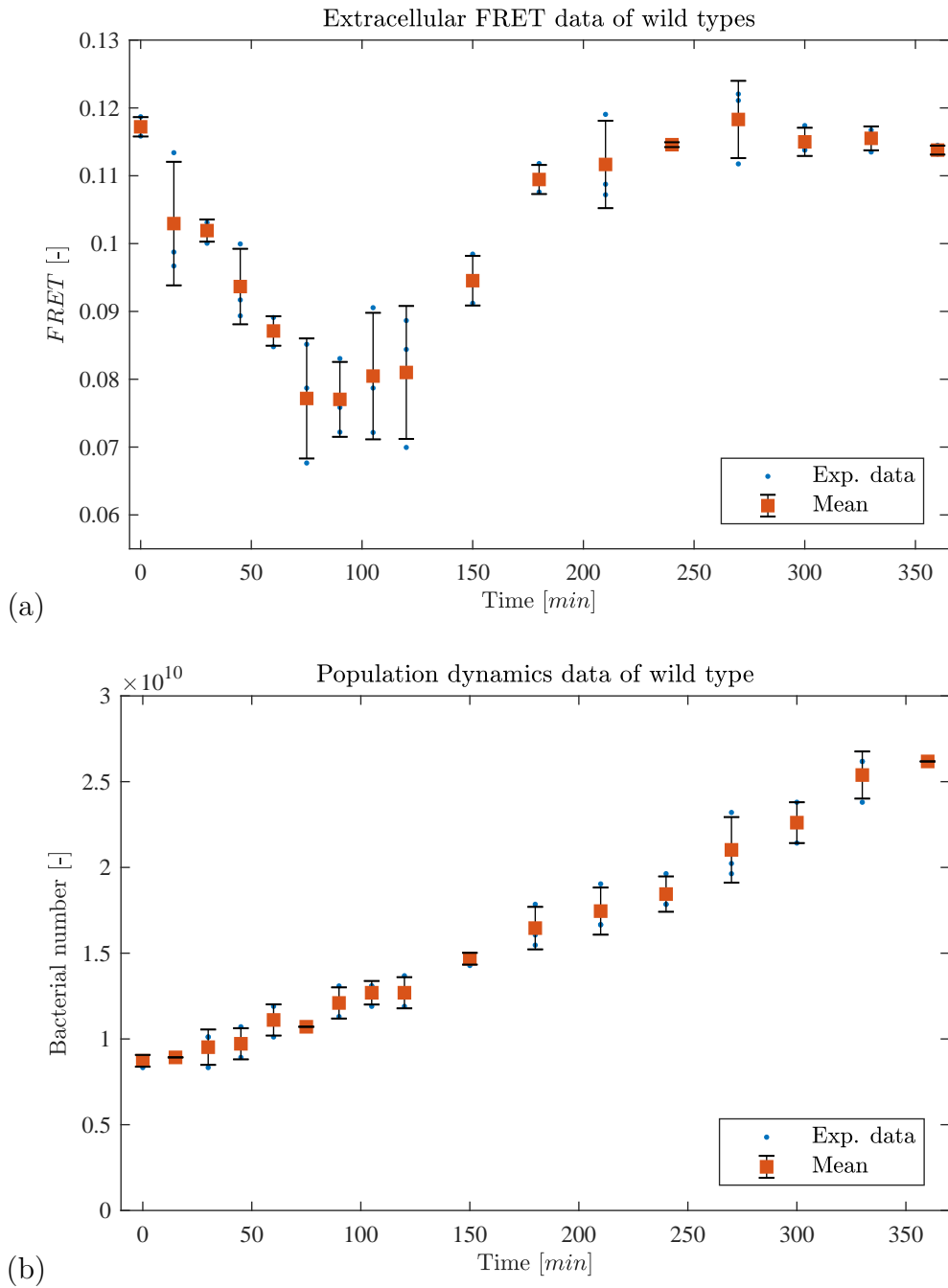
Figure 3.7.: *All data sets are from the µCats laboratory; (a): Experimental data of extracellular FRET of wild types; (b): Experimental growth data of wild types;*

3.2. Model equation of FRET response

So far we know that the intracellular quorum sensing signalling molecule concentration in mutants, that is $C_{i,m}$ alters negatively the FRET response. That means the more signalling molecules *PhrA* are in the mutant cell, the less is the FRET response including a saturation, see figure 3.5(a). Henceforth, the FRET curve could be modelled as

$$FRET(t) = FRET_0 - \Delta FRET \frac{C_{i,m}(t)}{\xi + C_{i,m}(t)}. \tag{3.1}$$

$FRET_0$ denotes the amount of FRET when there is no signalling molecule within the mutant cell. The parameter $\Delta FRET$ corresponds to the decrease when signalling molecules bind to RapA and alters FRET negatively. However, it does not decrease permanently, only to some level which can be seen in the dose response data in figure 3.6. Thus, we need a parameter which controls the decline of FRET. This one is denoted as ξ and describes the intracellular concentration where the half-maximal response occurs.

In order to evaluate the FRET data of all experiments with equation (3.1), regardless of whether intracellular or extracellular FRET, we need the intracellular and extracellular signalling molecule kinetics of the mutants and wild types.

3.3. Dynamic of biological processes

After the description of the experimental approach, we describe the dynamic of biological process of peptide uptake and absorption of *Bacillus subtilis* mutants and wild types and their consequences by introducing the relevant variables and parameters. Note that **all parameters are strictly positive** in order to describe a biological feasible behaviour **unless we state it explicitly otherwise**. Figure 3.8 is a graphical illustration of the following dynamical description.
All three experiments are performed with a **shake flask** where we have a growth medium within the flask for the bacteria. We denote the **volume** of the growth medium as $\boldsymbol{V_e}$. The use of such a shake flask ensures homogeneously distributed signalling molecules and bacteria and justify the approach of ordinary differential equations.
Experiment 1 and 2 concern only the mutant population and their uptake of **extracellular quorum sensing signalling molecule concentration $\boldsymbol{C_e(t)}$** with rate $\boldsymbol{\sigma_m}$ per bacterium. This becomes to an **intracellular signalling molecule concentration** within a bacterium and is denoted by $\boldsymbol{C_{i,m}(t)}$. Most likely, we have **natural degradation rates** for the extracellular as well as for the intracellular signalling molecule concentration. These rates are denoted with $\boldsymbol{\gamma_e}$ and $\boldsymbol{\gamma_i}$ and are non-negative. In the upcoming discussion, we will then distinguish between strictly positive and zero values. The time duration of the experiment is short compared to the generation time of *Bacillus subtilis*. Thus, we assume a **constant number of mutant bacteria** denoted by

N_c in order to simplify calculations.

Experiment 3 concerns only the kinetics of a wild type population. The dynamic is the same as for the mutants adding additionally a production term per cell of a prototype of signalling molecule *PhrA* Pentapeptide. The experiment lasts six hours such that we can't neglect bacterial growth. We assume that the number of **wild type bacteria**, denoted by $b_w(t)$, are homogeneously distributed within the shake flask as well. We have to add a further ODE for the bacterial growth, e.g. logistic growth. This equation is independent on the extracellular and intracellular signalling molecules.
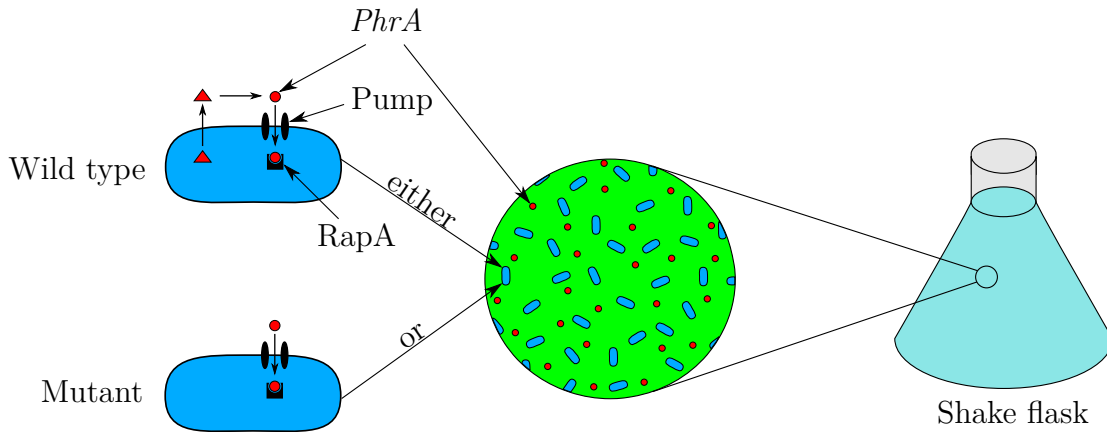
Figure 3.8.: *Scheme of the bacterial process and described dynamic.*

A consequence of absorbing extracellular signalling molecules is that the intracellular signalling molecule concentration increases. If the intracellular quorum sensing molecule concentration reaches some certain **threshold ξ** we say that the necessary condition is fulfilled. Then the bacterium changes its behaviour, e.g. production of signalling molecules stops. In order to realize such a mechanism we introduce for the moment the indicator function.

Definition 3.3.1 (Indicator function)**.** *Let A be a subset of a set X, then an indicator function $\chi_A : X \to \{0, 1\}$ is defined as*

$$\chi_A(x) := \begin{cases} 1 & \text{if } x \in A \\ 0 & \text{if } x \notin A. \end{cases}$$

Note that we want to have this switch in the bacteria's behaviour only once in their lifetime. Therefore, the indicator function has to be adjusted.

Definition 3.3.2 (Time-dependent indicator function)**.** *Let A be a subset of a set X, then a time-dependent indicator function $\hat{\chi}_{A \times t^*} : X \times \mathbb{R}_+ \to \{0, 1\}$ is defined as*

$$\hat{\chi}_{A \times t^*}(x(t), t) := \begin{cases} 1 & \text{if } t < t^* \\ \\ 0 & \text{if } t \geq t^* \end{cases}$$

with

$$t^* = \inf \left\{ t \in \mathbb{R}_+ : \chi_A(x(t)) = 0 \right\}.$$

In the next few sections we will investigate some hypotheses regarding the absorption and production process.

3.4. Mutant model: Negative feedback regarding absorption

First we derive model equations for the mutant experiments for the intracellular peptide uptake. In this section, we want to check the following hypothesis:

HM 1 When the intracellular concentration $C_{i,m}$ has reached the threshold ξ then we have a negative feedback regarding the absorption, that is, absorption of signalling molecules stops.

In the next section, we formulate a suitable model for this hypothesis HM 1.

3.4.1. Model equations

Let's briefly describe how we derive the ODEs for the extracellular quorum sensing signalling molecule concentration $C_e(t)$ and the intracellular signalling molecule concentration $C_{i,m}(t)$ for the mutants. We deduce a negative change of quorum sensing molecules due to the absorption of signalling molecules with rate σ_m by mutant bacteria of number N_c. The units of the rate is given per time and per cell. At that point, we have to be aware that we work here with concentrations. As a result of signalling molecule flux into the bacterium, the extracellular and intracellular quorum sensing molecule concentration change in inverse proportion to the volume of the growth medium V_e and the total volume of mutant bacteria $V_{i,m}$. Thus, the absorption rate σ_m has to be divided by V_e modelling the extracellular signalling molecule concentration. In unison, the intracellular concentration of signalling molecule $C_{i,m}(t)$ increases for mutants with a rate $\frac{\sigma_m}{V_{i,m}}$ per bacterium. The total volume of mutant type bacteria is given by $V_{i,m} = N_c V_{bac}$. The parameter V_{bac} describes the volume of a single bacterium. Furthermore, we assume a natural degradation for the extracellular and intracellular quorum sensing molecules. The extracellular degradation rate is given as

γ_e, the intracellular degradation rate is denoted as γ_i. The ODE for the extracellular quorum sensing molecule is given in (3.3), the ODE for the intracellular quorum sensing molecule in (3.4). As long as the intracellular concentration does not reach its threshold, that is,

$$t < t_F := \inf\{t \in \mathbb{R}_+ : \xi = C_{i,m}(t)\}, \tag{3.2}$$

the time-dependent indicator function is 1. Otherwise, it is zero and the uptake function vanishes due to the hypothesis HM 1. The initial amount of the extracellular respectively intracellular signalling molecule concentration in the shake flask is denoted as a constant $C_{e,0}$ and $C_{i,m,0}$ respectively, see (3.5) and (3.6). Gathering all differential equations, we obtain

$$\frac{\mathrm{d}}{\mathrm{d}t} C_e(t) = -\hat{\chi}_{[0,\xi] \times t_F}(C_{i,m}(t), t) \, N_c \frac{\sigma_m}{V_e} C_e(t) - \gamma_e \, C_e(t) \tag{3.3}$$

$$\frac{\mathrm{d}}{\mathrm{d}t} C_{i,m}(t) = \hat{\chi}_{[0,\xi] \times t_F}(C_{i,m}(t), t) \, N_c \frac{\sigma_m}{V_{i,m}} C_e(t) - \gamma_i C_{i,m}(t)$$

$$= \hat{\chi}_{[0,\xi] \times t_F}(C_{i,m}(t), t) \, \frac{\sigma_m}{V_{bac}} C_e(t) - \gamma_i C_{i,m}(t) \tag{3.4}$$

with initial conditions

$$C_e(0) = C_{e,0} \tag{3.5}$$

$$C_{i,m}(0) = C_{i,m,0}. \tag{3.6}$$

We used here freely selectable initial conditions in order to obtain a very general model such that the following analysis becomes as general as possible. When we need better suited initial conditions, especially for the intracellular signalling molecule concentration since it is zero in experiment 1 and 2, we note that explicitly.

3.4.2. Analysis

Since the right hand sides of (3.3) and (3.4) are not continuous due to the time-dependent indicator function, we can not apply the Picard-Lindelöf theorem, see Theorem A.3.1. However, the right hand sides are piecewise continuous. Let's briefly describe the approach how we show existence and uniqueness for solutions of equations (3.3) and (3.4) in $[0, \infty)$. Let's consider the non-trivial case, that is, we assume ξ to be sufficiently big such that the mutants do not reach the threshold initially, that is, $C_{i,m}(t_0) < \xi$. It means in effect that there is at least a small time interval such that the time-dependent indicator function $\hat{\chi}$ is 1 until the necessary condition is fulfilled. It might be the case that the threshold is never reached by $C_{i,m}(t)$ in $t \in [0, \infty)$, then the time-dependent

indicator function is always 1 and Picard-Lindelöf can be applied. Otherwise we already know the time point such that the necessary condition is fulfilled, that is, t_F, see (3.2). So we can apply the Picard-Lindelöf theorem to show existence and uniqueness of equations (3.3) and (3.4) for $t \in [0, t_F)$. We can even solve the equations explicitly within that time interval. We then consider the "activated" system for $t \in [t_F, \infty)$, regardless if some term is added or neglected. It just describes the fact that the necessary condition is fulfilled. Consequently, the time-dependent indicator function is zero then and the initial values become $C_e(t_F) = \hat{C}_e(t_F)$, $C_{i,m}(t_F) = \hat{C}_{i,m}(t_F)$, with $\hat{\ }$ being the solutions for $t \in [0, t_F)$. For the activated system with $t \in (t_F, \infty)$, the Picard-Lindelöf theorem can be applied again. At the end, we stick the solutions together and obtain for each ODE a unique, piecewise continuous differentiable solution in $[0, \infty)$. All derived interim results are registered as a lemma.

We consider the case $C_{i,m}(t_0) \leq \xi$ as stated, that is, the necessary condition is not fulfilled yet and the time-dependent indicator function is equal 1. That leads to a auxiliary model with following result.

Lemma 3.4.1. *Let's consider following system*

$$\frac{\mathrm{d}}{\mathrm{d}t}C_e(t) = -\left(\frac{\sigma_m}{V_e}N_c + \gamma_e\right)C_e(t) \tag{3.7}$$

$$\frac{\mathrm{d}}{\mathrm{d}t}C_{i,m}(t) = \frac{\sigma_m}{V_{bac}}C_e(t) - \gamma_i\,C_{i,m}(t) \tag{3.8}$$

with

$$C_e(t_0) = C_{e,0} \tag{3.9}$$

$$C_{i,m}(t_0) = C_{i,m,0} \tag{3.10}$$

for $t \in [0, \infty)$. Then there exists a unique and differentiable solution which reads

$$C_e(t) = C_{e,0} e^{(t_0 - t)\beta} \tag{3.11}$$

$$C_{i,m}(t) = \begin{cases} C_{i,m,0} - \dfrac{\sigma_m}{V_{bac}\beta} C_{e,0}\left(e^{(t_0-t)\beta} - 1\right) \\[1em] \quad \text{for } \gamma_i = 0 \\[1.5em] C_{i,m,0} e^{-\gamma_i(t-t_0)} + \dfrac{\sigma_m}{V_{bac}} C_{e,0}(t-t_0)e^{-\gamma_i(t-t_0)} \\[1em] \quad \text{for } \gamma_i > 0 \text{ and } \gamma_i = \beta \\[1.5em] e^{-\gamma_i(t-t_0)}\left(C_{i,m,0} - \dfrac{\sigma_m C_{e,0}\beta}{V_{bac}\beta(\gamma_i - \beta)}\right) + \dfrac{\sigma_m C_{e,0}\beta}{V_{bac}\beta(\gamma_i - \beta)}e^{-\beta(t-t_0)} \\[1em] \quad \text{for } \gamma_i > 0 \text{ and } \gamma_i \neq \beta \end{cases}$$

$$\tag{3.12}$$

with $\beta := \dfrac{\sigma_m}{V_e} N_c + \gamma_e$.

Proof. The right hand sides of (3.7) and (3.8) are linear functions in C_e and $C_{i,m}$ and thus globally Lipschitz continuous. Henceforth the Picard-Lindelöf theorem A.3.1 yields existence and uniqueness for all $t \in [0, \infty)$. Furthermore, we can calculate solutions explicitly. Equation (3.7) with initial condition (3.9) can be solved e.g. by an exponential ansatz yielding

$$\begin{aligned} C_e(t) &= C_{e,0}\, e^{-\int_{t_0}^t \frac{\sigma_m}{V_e} N_c + \gamma_e \, d\tilde{t}} \\ &= C_{e,0}\, e^{(t_0 - t)\beta} \end{aligned}$$

with $\beta := \frac{\sigma_m}{V_e} N_c + \gamma_e$. Now we are able to calculate the solution of the intracellular quorum sensing molecule concentrations in equation (3.8). We first deal with the case of no internal degradation of quorum sensing molecules, that is $\gamma_i = 0$. Integration of the ODE leads to

$$C_{i,m}(t) = C_{i,m,0} + \frac{\sigma_m}{V_{bac}} \int_{t_0}^t C_e(s) \, ds.$$

The integral on the right hand side can be solved explicitly using (3.11):

$$\begin{aligned} \int_{t_0}^t C_e(s) \, ds &= \int_{t_0}^t C_{e,0} e^{(t_0 - s)\beta} \, ds \\ &= -\frac{C_{e,0}}{\beta}\left(e^{(t_0 - t)\beta} - 1\right). \end{aligned}$$

Altogether, the solution reads

$$C_{i,m}(t) = C_{i,m,0} - \frac{\sigma_m C_{e,0}}{V_{bac}\beta}\left(e^{(t_0 - t)\beta} - 1\right).$$

In case of $\gamma_i > 0$ the variation of constants yields

$$C_{i,m}(t) = e^{-\gamma_i(t - t_0)}\left(\frac{\sigma_m}{V_{bac}}\int_{t_0}^{t} C_e(\tilde{t})e^{\gamma_i(\tilde{t} - t_0)}\, d\tilde{t} + C_{i,m,0}\right). \tag{3.13}$$

The integral in (3.13) can be solved by using (3.11):

$$\int_{t_0}^{t} C_e(\tilde{t})e^{\gamma_i(\tilde{t} - t_0)}\, d\tilde{t} = C_{e,0}\int_{t_0}^{t} e^{(\gamma_i - \beta)(s - t_0)}\, ds. \tag{3.14}$$

At that point we have to do a case differentiation. If and only if $\gamma_i = \beta$, then the second integral of the right hand side becomes one. Otherwise it can be solved and $\gamma_i - \beta$ being a denominator.

Let's continue first with the case $\gamma_i = \beta$. Then the integral on the left hand side is equal $C_{e,0}(t - t_0)$ resulting to

$$C_{i,m}(t) = \left(C_{i,m,0} + \frac{\sigma_m}{V_{bac}}C_{e,0}(t - t_0)\right)e^{-\gamma_i(t - t_0)}.$$

Now we consider the other case $\gamma_i \neq \beta$. The integral on the right hand side of equation (3.14) can be solved and reads

$$\int_{t_0}^{t} C_e(\tilde{t})e^{\gamma_i(\tilde{t} - t_0)}\, d\tilde{t} = \frac{C_{e,0}\beta}{\beta(\gamma_i - \beta)}\left(e^{(\gamma_i - \beta)(t - t_0)} - 1\right). \tag{3.15}$$

Then (3.15) is inserted in (3.13) and altogether, the solution of equation (3.8) for $\gamma_i > 0$ and $\gamma_i \neq \beta$ reads

$$\begin{aligned} C_{i,m}(t) =& e^{-\gamma_i(t - t_0)}\left(C_{i,m,0} - \frac{\sigma_m}{V_{bac}}\left(\frac{C_{e,0}\beta}{\beta(\gamma_i - \beta)}\right)\right) \\ &+ \frac{\sigma_m}{V_{bac}}\left(\frac{C_{e,0}\beta}{\beta(\gamma_i - \beta)}\right)e^{-\beta(t - t_0)}. \end{aligned}$$

$\square$

As long as the necessary condition is not fulfilled, that means there exists no t_F, the quorum sensing molecule concentration C_e as well as the intracellular concentration $C_{i,m}$ may tend to steady states. The stability of those can be investigated by the eigenvalues λ of the Jacobian. The steady states are locally asymptotically stable if and only if the real parts of the eigenvalues λ of the Jacobian are negative, that is, $\mathrm{Re}\{\lambda\} < 0$ for all eigenvalues λ.

Lemma 3.4.2. *For $\gamma_i > 0$, there exists an asymptotically stable steady state $(\bar{C}_e, \bar{C}_{i,w})$ of system* (3.7) *-* (3.10) *for $t \in [0, \infty)$ with*

$$\bar{C}_e = 0$$
$$\bar{C}_{i,m} = 0.$$

For $\gamma_i = 0$, there exists a stable line of steady states which reads

$$(\bar{C}_e, \bar{C}_{i,m}) = (0, C)$$

with $C \in \mathbb{R}$ being a positive constant.

Proof. We start with the simpler case $\gamma_i > 0$. In order to calculate the steady states we set the right hand side of the ODE equations (3.7) and (3.8) equal zero. The steady state of the external quorum sensing concentration reads

$$0 = -\bar{C}_e \left(\frac{\sigma_m}{V_e} N_c + \gamma_e \right) = -\bar{C}_e \beta$$
$$\Longleftrightarrow \quad \bar{C}_e = 0.$$

The steady state of the intracellular quorum sensing concentration of the mutant is given by

$$0 = \frac{\sigma_m}{V_{bac}} \bar{C}_e - \gamma_i \, \bar{C}_{i,m}$$
$$\Longleftrightarrow \quad \bar{C}_{i,w} = 0.$$

The stability can be derived by the Jacobian of $\begin{pmatrix} (3.7) \\ (3.8) \end{pmatrix}$ and reads

$$J(C_e, C_{i,m}) = \begin{pmatrix} -\dfrac{\sigma_m}{V_e} N_c - \gamma_e & 0 \\[2ex] \dfrac{\sigma_m}{V_{bac}} & -\gamma_i \end{pmatrix}.$$

It is independent of the steady states and all eigenvalues are negative due to the positivity of all parameters. That means the steady states $\bar{C}_e$ and $\bar{C}_{i,m}$ are locally asymptotically stable and the solutions of the system tend to these points if we start close to these steady states.

For $\gamma_i = 0$, the steady state $\bar{C}_e = 0$ remains and is asymptotically stable. The equation (3.7) for $\gamma_i = 0$ reads

$$\frac{\mathrm{d}}{\mathrm{d}t}C_{i,m}(t) = \frac{\sigma_m}{V_{bac}}C_e(t) \overset{!}{=} 0.$$

This equation is only fulfilled if C_e tends to its steady state $\bar{C}_e = 0$. That means we obtain a line of steady states which is stable. It reads

$$(\bar{C}_e, \bar{C}_{i,m}) = (0, C)$$

with $C \in \mathbb{R}$ being a positive constant depending on the initial value $C_{i,m,0}$. $\qquad \square$

Yet we don't know when and even if the necessary condition will be ever fulfilled. Thus, we investigate if there exists an intersection of $C_{i,m}(t) = \xi$ for all three different cases in (3.12). This time point is denoted as t_F and denotes the moment when the necessary condition is fulfilled.

In order to simplify things, we assume $C_{i,m}(0) = C_{i,m,0} = 0$ which means that the cells are initially empty which corresponds also the experimental approach. That leads to following lemma:

Lemma 3.4.3. *Assume the following initial conditions for (3.7) and (3.8):*

$$C_e(0) = C_{e,0} > 0$$
$$C_{i,m}(0) = 0.$$

For $\gamma_i = 0$ there exists a unique feasible solution $t_F = -\dfrac{1}{\beta}\ln\left(1 - \dfrac{\xi V_{bac}\beta}{C_{e,0}\sigma_m}\right)$ if and only if $C_{e,0} \geq \dfrac{\xi V_{bac}\beta}{\sigma_m}$.

For $\gamma_i > 0$ and $\gamma_i = \beta > 0$ there exists a unique feasible solution t_F if and only if $C_{e,0} \geq \dfrac{\xi V_{bac}\gamma_i e}{\sigma_m}$.

For $\gamma_i > 0$ and $\gamma_i \neq \beta$ there exists a unique feasible solution t_F if and only if $C_{e,0} \geq \dfrac{\xi V_{bac}\beta}{\sigma_m}\left(\dfrac{\beta}{\gamma_i}\right)^{\frac{\gamma_i}{\beta - \gamma_i}}.$

Proof. For $\gamma_i = 0$, we set the solution (3.12) with initial conditions $C_e(0) = C_{e,0} > 0$ and $C_{i,m}(0) = C_{i,m,0} = 0$ equal ξ, that is,

$$\xi \overset{!}{=} C_{e,0} \frac{\sigma_m}{V_{bac}\beta} - C_{e,0} \frac{\sigma_m}{V_{bac}\beta} e^{-t\beta}$$

$$\Longleftrightarrow \quad 1 - \frac{\xi V_{bac}\beta}{C_{e,0}\sigma_m} \overset{!}{=} e^{-t\beta}.$$

The right hand side is strictly monotonously decreasing from 1 but remains positive. That means the left hand side must satisfy following inequality chain:

$$1 \geq 1 - \frac{\xi V_{bac}\beta}{C_{e,0}\sigma_m} > 0$$

$$\Longleftrightarrow \quad C_{e,0} \geq \frac{\xi V_{bac}\beta}{\sigma_m} > 0.$$

So there exists a unique solution t_F if and only if $C_{e,0} \geq \frac{\xi V_{bac}\beta}{\sigma_m}$ and reads

$$t_F = -\frac{1}{\beta} \ln\left(1 - \frac{\xi V_{bac}\beta}{C_{e,0}\sigma_m}\right).$$

For $\gamma_i > 0$, $\gamma_i = \beta$ and the corresponding initial conditions, we obtain

$$\xi \overset{!}{=} \frac{\sigma_m}{V_{bac}} C_{e,0} t e^{-\gamma_i t}$$

$$\Longleftrightarrow \quad \frac{\xi v_{bac}}{\sigma_m C_{e,0}} \overset{!}{=} t e^{-\gamma_i t} =: g(t).$$

We briefly do curve sketching for $g(t)$. The first derivative reads $\frac{\mathrm{d}}{\mathrm{d}t} g(t) = e^{-\gamma_i t}(1 - \gamma_i t)$ which has it root at $\bar{t} = \frac{1}{\gamma_i}$ and its maximum reads $g(\bar{t}) = \frac{1}{e\gamma_i}$. So in order to obtain at least one solution it must hold

$$\frac{\xi v_{bac}}{\sigma_m C_{e,0}} \leq \frac{1}{e\gamma_i}$$

$$\Longleftrightarrow \quad C_{e,0} \geq \frac{\xi V_{bac}\gamma_i e}{\sigma_m}.$$

For equality, we have only one solution t_F otherwise there exist two solutions $t_{F,1}$ and $t_{F,2}$. The minimum of both is the relevant solution, that is, $t_F = \min\{t_{F,1}, t_{F,2}\}$.

Finally we consider the last case, that is, the solution (3.12) for $\gamma_i > 0$ and $\gamma_i \neq \beta$ with the new suited initial conditions must be equal ξ. We get

$$\xi \overset{!}{=} \frac{\sigma_m}{V_{bac}} \left(\frac{C_{e,0}\beta}{\beta(\gamma_i - \beta)} \right) \left(e^{-\beta t} - e^{-\gamma_i t} \right)$$

$$\Longleftrightarrow \quad \frac{\xi V_{bac}\beta(\gamma_i - \beta)}{\sigma_m \beta C_{e,0}} \overset{!}{=} e^{-\beta t} - e^{-\gamma_i t} =: h(t).$$

If $\gamma_i > \beta$, then both sides are positive, otherwise they are negative. As above, we do again a brief curve sketching of the right hand side which is denoted as $h(t)$. The root of the derivative $\frac{d}{dt}h(t) = -\beta e^{-\beta t} + \gamma_i e^{-\gamma_i t}$ reads

$$\bar{t} = \frac{\ln\left(\dfrac{\beta}{\gamma_i} \right)}{\beta - \gamma_i}.$$

If $\gamma_i > \beta$, then we have a maximum at $\bar{t}$ with

$$h(\bar{t}) = \left(\frac{\beta}{\gamma_i} \right)^{-\frac{\beta}{\beta - \gamma_i}} - \left(\frac{\beta}{\gamma_i} \right)^{-\frac{\gamma_i}{\beta - \gamma_i}} = \left(\frac{\beta}{\gamma_i} \right)^{-\frac{\gamma_i}{\beta - \gamma_i}} \left(\frac{\gamma_i}{\beta} - 1 \right).$$

If $\gamma_i < \beta$, then $h(\bar{t})$ is a minimum. Additionally it holds $h(0) = 0 = \lim\limits_{t \to \infty} h(t)$. For an intersection in case of $\gamma_i > \beta$, we require

$$\frac{\xi V_{bac}\beta(\gamma_i - \beta)}{\sigma_m \beta C_{e,0}} \leq \left(\frac{\beta}{\gamma_i} \right)^{-\frac{\gamma_i}{\beta - \gamma_i}} \left(\frac{\gamma_i}{\beta} - 1 \right)$$

$$\Longleftrightarrow \quad C_{e,0} \geq \frac{\xi V_{bac}\beta}{\sigma_m} \left(\frac{\beta}{\gamma_i} \right)^{\frac{\gamma_i}{\beta - \gamma_i}}.$$

Analogously, we obtain the same condition for $\gamma_i < \beta$. Similar as above, we obtain up to two roots denoted as $t_{F,1}$ and $t_{F,2}$. The relevant one is the smaller one, that is, $t_F = \min\{t_{F,1}, t_{F,2}\}$. $\qquad\square$

We have shown that there exists for specific parameter values a time point t_F such that the necessary condition is fulfilled. That means the time-dependent indicator function in (3.3) and (3.4) is no longer 1. So the system equation changes and the initial conditions have to be adjusted. The new solution for $t \in [t_F, \infty)$ should start where the solution for $t \in [0, t_F)$ ends. Let's denote the solutions of Lemma 3.4.1 with $\hat{\cdot}$ for the time period $t \in [0, t_F)$. Before we derive the solution of equations (3.3) and (3.4) with initial condition (3.5) and (3.5) we need a further intermediate result.

Lemma 3.4.4. *Consider following system:*

$$\frac{\mathrm{d}}{\mathrm{d}t}C_e(t) = -\gamma_e\,C_e(t) \tag{3.16}$$

$$\frac{\mathrm{d}}{\mathrm{d}t}C_{i,m}(t) = -\gamma_i\,C_e(t) \tag{3.17}$$

with initial conditions

$$C_e(t_F) = \hat{C}_e(t_F)$$
$$C_{i,m}(t_F) = \hat{C}_{i,m}(t_F).$$

Then there exist unique solutions which read

$$C_e(t) = \hat{C}_e(t_{t_F})e^{\gamma_e(t_F - t)}$$
$$C_{i,m}(t) = \hat{C}_{i,m}(t_F)e^{\gamma_i(t_F - t)}.$$

Proof. Since the right hand sides of (3.16) and (3.17) are Lipschitz continuous, we obtain immediately existence and uniqueness of a solution by applying the Picard-Lindelöf theorem. The solutions can be easily calculated by e.g. the exponential ansatz and read as stated. $\qquad\square$

Remark 3.4.5. *Note that the system in Lemma 3.4.4 and so do its results correspond to the case when $C_{i,m}(t_0) > \xi$. This was stated as the trivial case.*

Now we have all tools to conclude the following result:

Theorem 3.4.6. *Let's consider the ODE system (3.3) and (3.4), that is,*

$$\frac{\mathrm{d}}{\mathrm{d}t}C_e(t) = -\hat{\chi}_{[0,\xi]\times t_F}(C_{i,m}(t),t)\,N_c\frac{\sigma_m}{V_e}C_e(t) - \gamma_e C_e(t)$$

$$\frac{\mathrm{d}}{\mathrm{d}t}C_{i,m}(t) = \hat{\chi}_{[0,\xi]\times t_F}(C_{i,m}(t),t)\,\frac{\sigma_m}{V_{bac}}C_e(t) - \gamma_i C_{i,m}(t)$$

with initial conditions

$$C_e(0) = C_{e,0}$$
$$C_{i,m}(0) = 0.$$

Then there exist unique and piecewise continuous differentiable solutions which read:

If $\gamma_i = 0$ and $C_{e,0} \geq \dfrac{\xi V_{bac}\beta}{\sigma_m}$ then

$$C_e(t) = \begin{cases} C_{e,0}e^{-t\beta} & \text{for } t \in [0, t_F) \\[2mm] C_e(t_F)e^{\gamma_e(t_F - t)} & \text{for } t \in [t_F, \infty) \end{cases}$$

$$C_{i,m}(t) = \begin{cases} -\dfrac{\sigma_m}{V_{bac}\beta}C_{e,0}\left(e^{-t\beta} - 1\right) & \text{for } t \in [0, t_F) \\[2mm] C_{i,m}(t_F)e^{\gamma_i(t_F - t)} & \text{for } t \in [t_F, \infty) \end{cases}$$

else

$$C_e(t) = C_{e,0}e^{-t\beta}$$
$$C_{i,m}(t) = -\frac{\sigma_m}{V_{bac}\beta}C_{e,0}\left(e^{-t\beta} - 1\right)$$

for $t \in [0, \infty)$.

If $\gamma_i > 0$, $\beta = \gamma_i$ and $C_{e,0} \geq \dfrac{\xi V_{bac}\gamma_i e}{\sigma_m}$ then

$$C_e(t) = \begin{cases} C_{e,0}e^{-t\beta} & \text{for } t \in [0, t_F) \\[2mm] C_e(t_F)e^{\gamma_e(t_F - t)} & \text{for } t \in [t_F, \infty) \end{cases}$$

$$C_{i,m}(t) = \begin{cases} -\dfrac{\sigma_m}{V_{bac}}C_{e,0}te^{-t\gamma_i} & \text{for } t \in [0, t_F) \\[2mm] C_{i,m}(t_F)e^{\gamma_i(t_F - t)} & \text{for } t \in [t_F, \infty) \end{cases}$$

else

$$C_e(t) = C_{e,0}e^{-t\beta}$$
$$C_{i,m}(t) = -\frac{\sigma_m}{V_{bac}}C_{e,0}te^{-t\gamma_i}$$

for $t \in [0, \infty)$.

If $\gamma_i > 0$, $\beta \neq \gamma_i$ and $C_{e,0} \geq \dfrac{\xi V_{bac}\beta}{\sigma_m}\left(\dfrac{\beta}{\gamma_i}\right)^{\frac{\gamma_i}{\beta - \gamma_i}}$ then

$$C_e(t) = \begin{cases} C_{e,0}e^{-t\beta} & \text{for } t \in [0, t_F) \\ C_e(t_F)e^{\gamma_e(t_F - t)} & \text{for } t \in [t_F, \infty) \end{cases}$$

$$C_{i,m}(t) = \begin{cases} \dfrac{\sigma_m C_{e,0}\beta}{V_{bac}\beta(\gamma_i - \beta)}e^{-t\beta} - e^{-t\gamma_i}\left(\dfrac{\sigma_m C_{e,0}\beta}{V_{bac}\beta(\gamma_i - \beta)}\right) & \text{for } t \in [0, t_F) \\ C_{i,m}(t_F)e^{\gamma_i(t_F - t)} & \text{for } t \in [t_F, \infty) \end{cases}$$

else

$$C_e(t) = C_{e,0}e^{-t\beta}$$

$$C_{i,m}(t) = \frac{\sigma_m C_{e,0}\beta}{V_{bac}\beta(\gamma_i - \beta)}e^{-t\beta} - e^{-t\gamma_i}\left(\frac{\sigma_m C_{e,0}\beta}{V_{bac}\beta(\gamma_i - \beta)}\right)$$

for $t \in [0, \infty)$.

Proof. Using Lemma 3.4.1, Lemma 3.4.2, Lemma 3.4.3 and Lemma 3.4.4, we obtain on the one hand the unique existence of a solution and on the other hand an explicit formula. $\qquad\square$

We see, there exists a unique solution, but we don't know yet, if it is biologically feasible, that is, the solution has to be non-negative.

Lemma 3.4.7 (Non-negativity)**.** *Trajectories of* (3.3) *and* (3.4) *with initial conditions* (3.5) *and* (3.6) *are non-negative for $t \in [0, \infty)$.*

Proof. We use Theorem A.3.2 to prove non-negativity of (3.3) and (3.4) with (3.5) and (3.6). In Theorem 3.4.6 we have shown that there exists a unique solution. Furthermore it holds

$$\frac{\mathrm{d}}{\mathrm{d}t}C_e(t)\Big|_{C_e(t)=0} = 0$$

$$\frac{\mathrm{d}}{\mathrm{d}t}C_{i,m}(t)\Big|_{C_{i,m}(t)=0} = \hat{\chi}_{[0,\xi]\times t_F}(C_{i,m}(t), t)\,\frac{\sigma_m}{V_{bac}}C_e(t) \geq 0 \quad \text{for } C_e(t) \geq 0.$$

which means the vector field points inwards to the axis. Thus, we have fulfilled the requirements of Theorem A.3.2 which yields non-negativity. $\qquad\square$

Next, we solve the equations numerically by MATLAB and perform a best fit simulation. Although we have an analytical solution, we solve the equations numerically because it will be very tedious to implement all different cases. Additionally, some part of the code can be used later, especially for the PDE-ODE approach in section 6.3.

3.4.3. Best fit simulation

We choose the experimental parameters as described in section 3.1, that is, the volume of the growth medium $V_e = 500 \mu l$ and the number of cell $N_c = 9.53 \cdot 10^7$. Additionally, the μCats laboratory extracted from the images the length and diameter of a *Bacillus subtilis* cell. Modeling a cylindrical cell with hemispheres on both ends yields for the cell volume $V_b = 0.973 fl$. This value was given by personal communication. The initial conditions are $C_e(0) = 10\frac{nmol}{l}$ and $C_{i,m}(0) = 0\frac{\mu mol}{l}$. The remaining parameters of ODE system (3.3) and (3.4) and FRET equation (3.1) have to be fitted, that is,

$$\sigma_m, \ \xi, \ FRET_0, \ \Delta FRET, \ \gamma_i, \ \text{and} \ \gamma_e.$$

The solver algorithm we use is described in appendix B as mentioned in the beginning of this chapter and yields as best fit:

Parameter	Lower bound	Best fit	Upper bound
$\sigma_m \ [pl/min]$	$4.1 \cdot 10^{-7}$	2.27	3.74
$\xi \ [\mu mol/l]$	0.36	113.85	147.77
$FRET_0 \ [-]$	0.105	0.110	0.114
$\Delta FRET \ [-]$	0.109	0.122	0.135
$\gamma_i \ [1/min]$	$2.4 \cdot 10^{-9}$	$2.6 \cdot 10^{-9}$	0.036
$\gamma_e \ [1/min]$	$8.1 \cdot 10^{-8}$	$3.0 \cdot 10^{-4}$	0.683

Table 3.1.: Parameter confidence interval estimation of fit of model equations (3.3) and (3.4).

The lower and upper bounds in table 3.1 correspond to the parameter confidence interval estimation. The best fit of the intracellular degradation rate γ_i is very small. Furthermore, experiments of the μCats laboratory have shown, that there is no intracellular degradation within two hours. Thus, one can assume that there is no natural intracellular degradation and neglect this parameter in future. We plot the best fit solutions together with the mean values of the data sets. The results are given in figure 3.9(a), 3.9(b) and 3.10.

(a)

(b)

Figure 3.9.: *Best fit solutions of model equations (3.3) and (3.4) with best fit parameters given in table 3.1; (a): Intracellular FRET kinetics of mutants; (b): Extracellular FRET kinetics of mutants;*
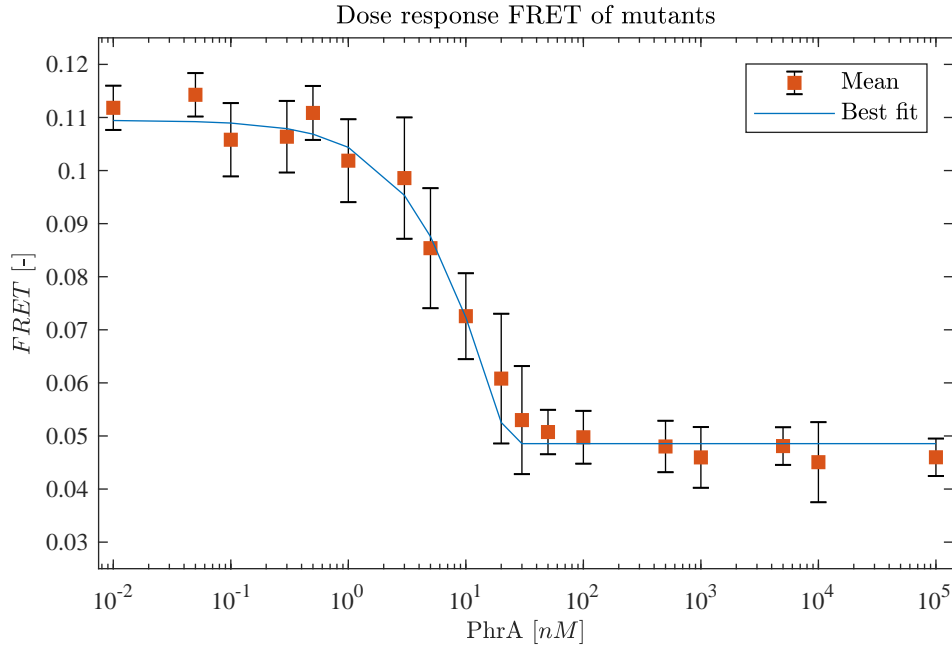
Figure 3.10.: *Best fit solution of FRET concerning the dose response data by using model equations (3.3) and (3.4) with best fit parameters given in table 3.1.*

Figure 3.9(a) represents the best fit for the intracellular kinetics. Due to the absorption of signalling molecules, the FRET is altered which reflects the fact that the curve decreases. Figure 3.9(b) behaves vice versa. In the beginning of the experiment, there is a high amount of signalling molecule in the supernatant after the centrifugation. Thus, the new empty mutant absorbs the signalling molecules which alters the FRET negatively. The amount of signalling molecules in the supernatant becomes less and less which results in an increase of FRET since the signalling molecules *PhrA* do not perturb the interaction. In figure 3.10, we see that the higher the stimulus of signalling molecules becomes the less becomes the FRET. However it does not undercut the level 0.05. All best fit solutions fit the data very well verified by a small sum of squared residuals $SSR = 3.74 \cdot 10^{-4}$, see equation (B.2.1), too. However, there is a further test series of experiment 1 which investigates the uptake dynamics. Only the initial amount of synthetic peptide was changed to $100\frac{nmol}{l}$. That means the initial condition (3.5) reads $C_e(0) = 100\frac{nmol}{l}$. So we use the parameters given in table 3.1 and evaluate our model with this new initial data. We see that the fit for the intracellular kinetics, figure 3.11(a), is reasonable. It only decreases too fast which is a hint that the absorption rate σ_m is too high or it may depend on the extracellular signalling molecule concentration such that it is not a constant rate, rather a term with a sigmoid behaviour. The fit for the extracellular kinetics, figure 3.11(b), is very bad. The best fit is just a horizontal line and does not increase at all. The reason for that is our hypothesis HM 1. A negative feedback regarding the absorption was assumed which means that when the intracellular concentration has reached ξ, the mutants stop to absorb and a high concentration of extracellular peptides remains in the supernatant. This concentration is

so high, such that the empty mutant cells, which where added into the cell free supernatant, reach their threshold ξ again very fast and do not lower the extracellular level significantly. Thus, the extracellular FRET curve is basically a horizontal line. So we can conclude that when the extracellular concentration decreases, the FRET curve in figure 3.11(b) increases. So the hypothesis HM 1 is at least not sufficient to explain the observed behaviour and we reject it. In the next section, we will state a new hypothesis.

(a)

(b)
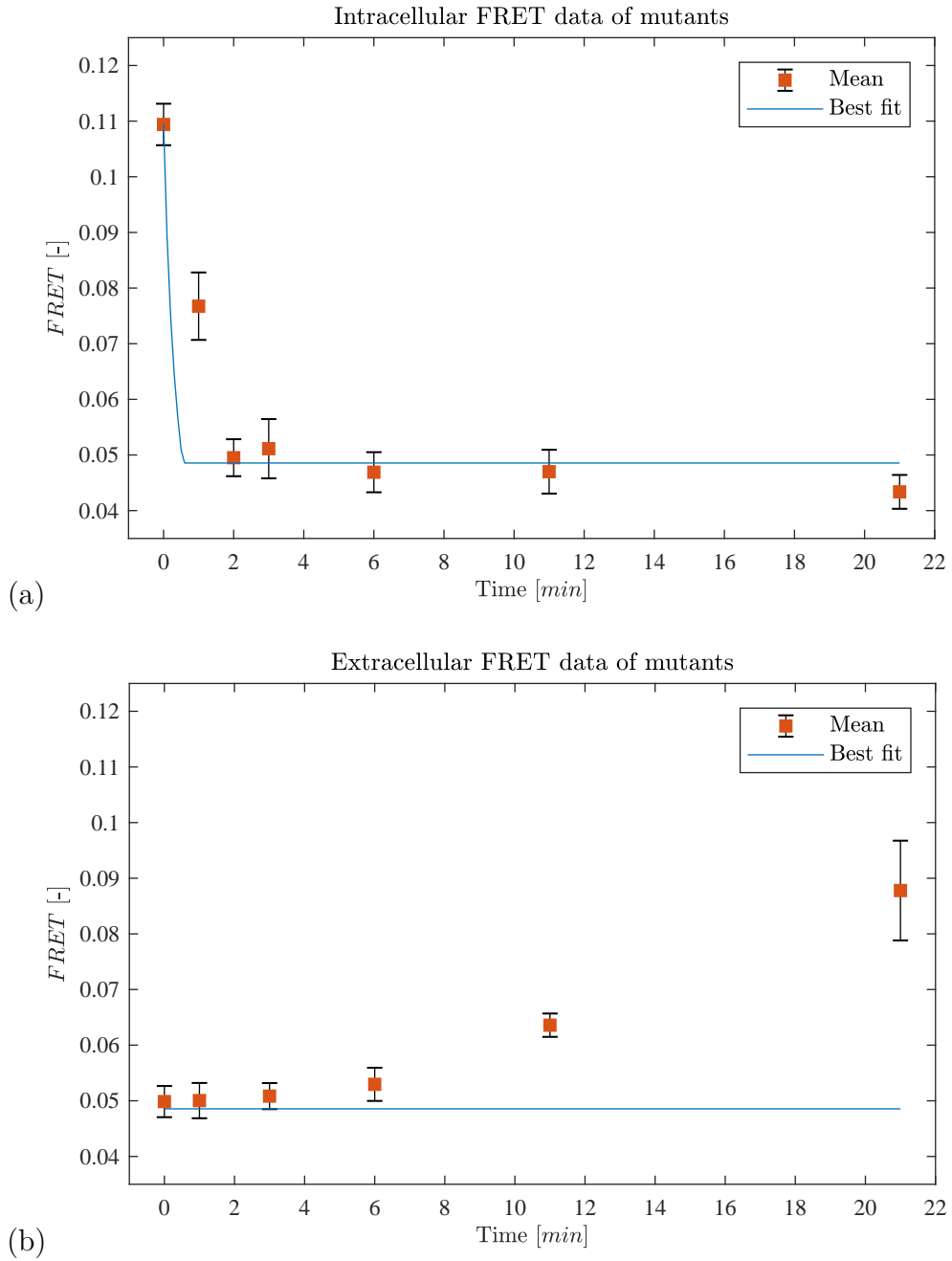
Figure 3.11.: *Best fit solutions of model equations (3.3) and (3.4) with best fit parameters given in table 3.1. In contrast to figure 3.9, we changed the initial condition (3.5) to $C_e(0) = 100\frac{nmol}{l}$; (a): Intracellular FRET kinetics of mutants; (b): Extracellular FRET kinetics of mutants.*

3.5. Mutant model: No feedback regarding absorption

The result of the previous section was to scrap hypothesis HM 1. Thus, we formulate a new one which reads:

HM 2 There is no feedback regarding the absorption. That means absorption of signalling molecules is continuous over time.

As in the previous chapter, we state a rectified model and analyse it afterwards. At the end, a best fit procedure is performed.

3.5.1. Model equations

The descriptions of the model terms are the same as in section 3.4.1, except we neglect the time-dependent indicator function which corresponds to the new hypothesis HM 2. So the rectified system reads

$$\frac{\mathrm{d}}{\mathrm{d}t}C_e(t) = - N_c \frac{\sigma_m}{V_e} C_e(t) - \gamma_e \, C_e(t) \tag{3.18}$$

$$\frac{\mathrm{d}}{\mathrm{d}t}C_{i,m}(t) = \frac{\sigma_m}{V_{bac}} C_e(t) - \gamma_i C_{i,m}(t) \tag{3.19}$$

with unaltered initial conditions

$$C_e(0) = C_{e,0} \tag{3.20}$$

$$C_{i,m}(0) = C_{i,m,0}. \tag{3.21}$$

3.5.2. Analysis

The model equations of this section coincide with the model equations in section 3.4.1 when the auxiliary model was considered. Thus, we can conclude from Lemma 3.4.1 existence and uniqueness of a solution.

Corollary 3.5.1. *There exists a unique and differentiable solution of system* (3.18) *and* (3.19) *with initial conditions* (3.20) *and* (3.21). *The solutions are given in* (3.11) *and* (3.12).

In order to obtain a biologically feasible solution, we can prove the non-negativity of the system as before.

Lemma 3.5.2 (Non-negativity). *Trajectories of* (3.18) *and* (3.19) *with initial conditions* (3.20) *and* (3.21) *are non-negative for* $t \in [0, \infty)$.

Proof. The approach is analogously as in the previous section 3.4.2. Uniqueness of a solution follows from Corollary 3.5.1. The vector field on the axis reads

$$\frac{\mathrm{d}}{\mathrm{d}t}C_e(t)\Big|_{C_e(t)=0} = 0$$

$$\frac{\mathrm{d}}{\mathrm{d}t}C_{i,m}(t)\Big|_{C_{i,m}(t)=0} = \frac{\sigma_m}{V_{bac}}C_e(t) \geq 0 \quad \text{for } C_e(t) \geq 0.$$

Henceforth, the solutions are non-negative. $\square$

3.5.3. Best fit simulation

The experimental parameters as well as the initial conditions are the same as in section 3.4.3. That means $V_e = 500\mu l$, $N_c = 9.53 \cdot 10^7$, $V_b = 0.973 fl$, $C_e(0) = 10\frac{nmol}{l}$ and $C_{i,m}(0) = 0\frac{\mu mol}{l}$. Again we want to fit parameters σ_m, ξ, $FRET_0$, $\Delta FRET$, γ_i, and γ_e. The results of the solver algorithm are given in table 3.2.

Parameter	Lower bound	Best fit	Upper bound
σ_m $[pl/min]$	$1.9 \cdot 10^{-4}$	2.34	4.07
ξ $[\mu mol/l]$	$1.3 \cdot 10^{-6}$	38.93	56.20
$FRET_0$ $[-]$	0.106	0.111	0.116
$\Delta FRET$ $[-]$	0.059	0.066	0.074
γ_i $[1/min]$	$4.7 \cdot 10^{-7}$	$5.1 \cdot 10^{-7}$	0.01
γ_e $[1/min]$	$2.0 \cdot 10^{-8}$	0.005	1.0

Table 3.2.: Parameter confidence interval estimation of fit of model equations (3.18) and (3.19).

As in section 3.4.3, we obtain a good fit for the data with initially $10\frac{nmol}{l}$ of stimulus, see figure 3.12 and 3.13. The SSR is a bit bigger with $4.16 \cdot 10^{-4}$ as in section 3.4.3, where we had $3.74 \cdot 10^{-4}$, but still in the same order.
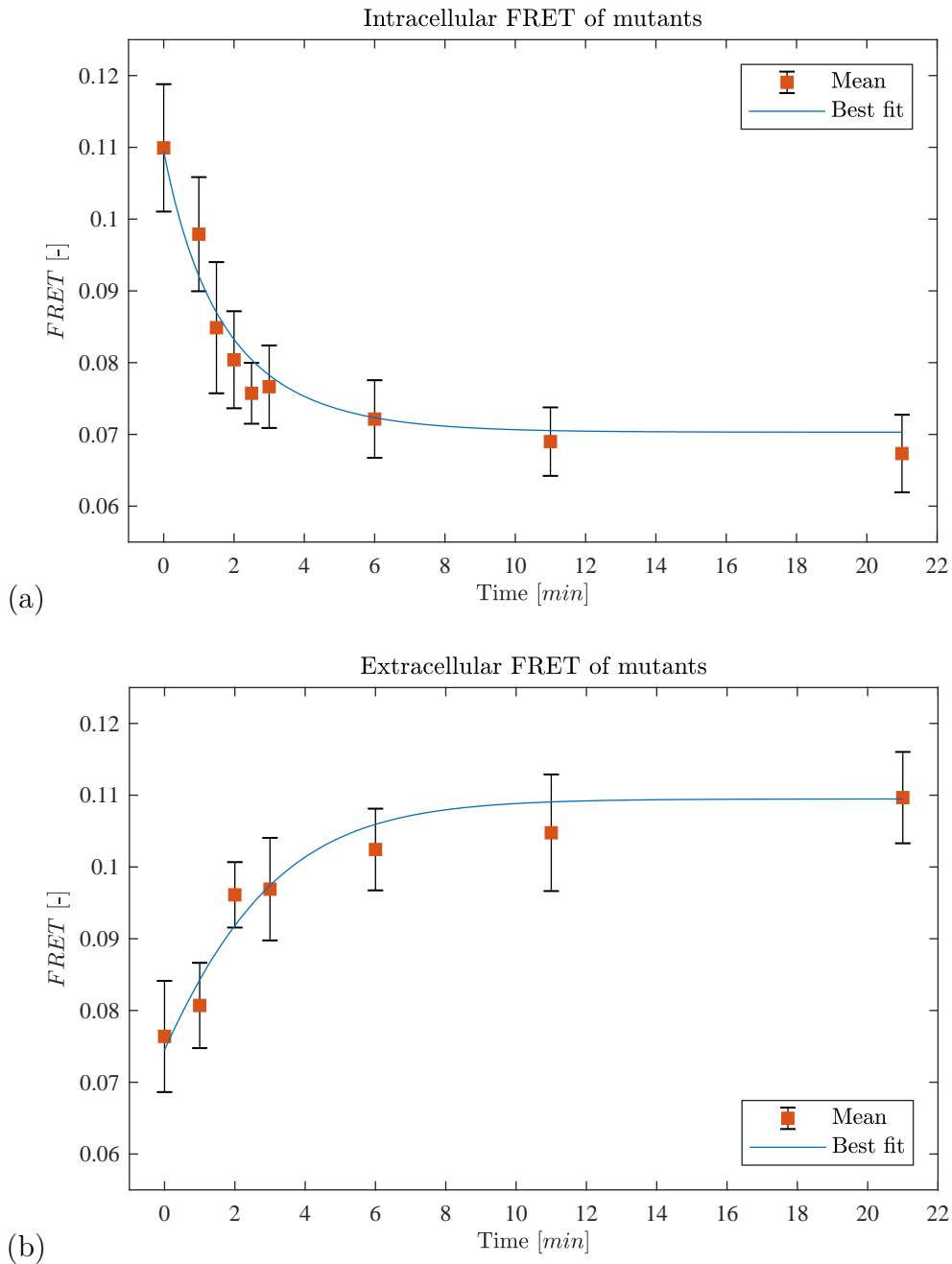
(a)

(b)
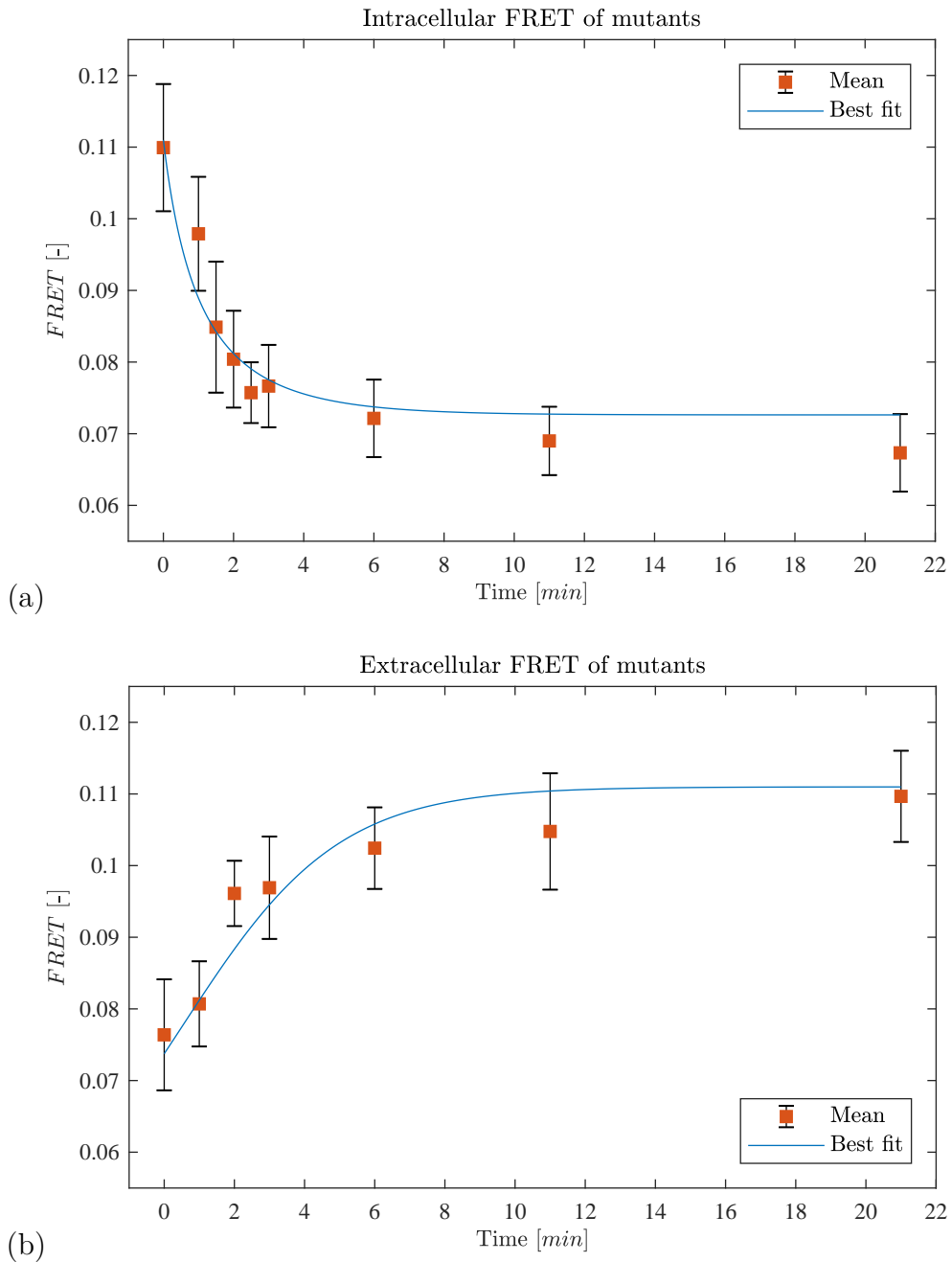
Figure 3.12.: *Best fit solutions of model equations* (3.18) *and* (3.19) *with best fit parameters given in table 3.2; (a): Intracellular FRET kinetics; (b): Extracellular FRET kinetics;*
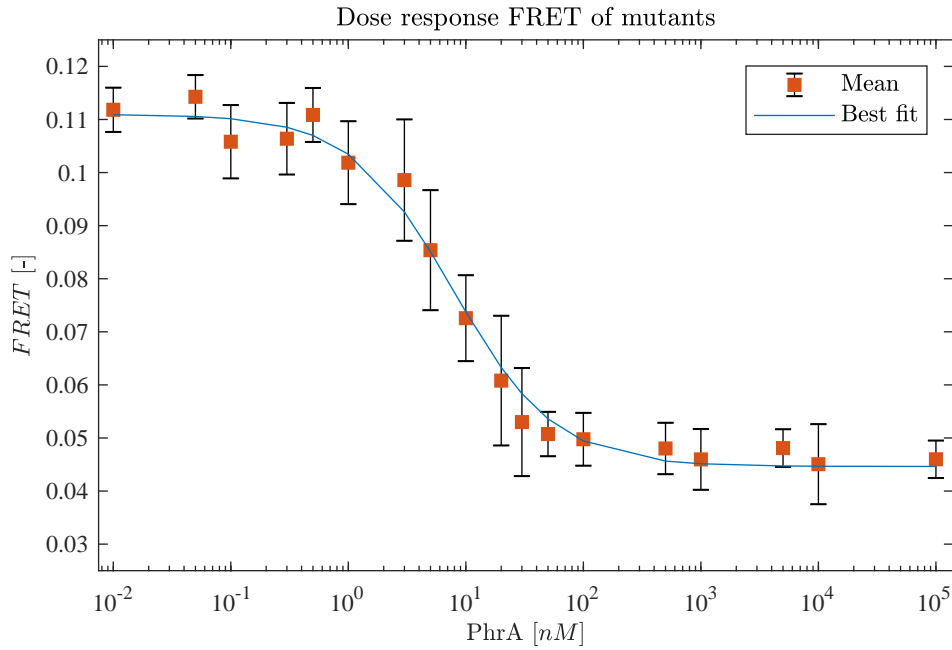
Figure 3.13.: *Best fit solution of FRET concerning the dose response data by model equations* (3.18) *and* (3.19) *with best fit parameters given in table 3.2.*

The problem with the model regarding hypothesis HM 1 was the evaluation of the model with $C_e(0) = 100\frac{nmol}{l}$. So we test the model with the new hypothesis HM 2, using the parameters in table 3.2. The fit for the intracellular kinetics in figure 3.14(a) is again satisfying. One can note that the fit of the FRET for the extracellular kinetics in figure 3.14(b) is now better but still not acceptable. The FRET curve finally increases compared to figure 3.11(b) but it increases way too fast. Furthermore the FRET curve reaches a level of approximately 0.11 at time $t = 21$ minutes which is significantly higher than the FRET data point with approximately 0.09 at $t = 21$ minutes. Nevertheless we can conclude that the model with hypothesis HM 2 is better than the model with hypothesis HM 1. On the one hand it fits the data for $C_e(0) = 10\frac{nmol}{l}$ well and on the other hand the fit regarding the $100nM$ stimulus is more realistic. However we have to restrict our model to a low concentration of extracellular signalling molecules.

(a)

(b)
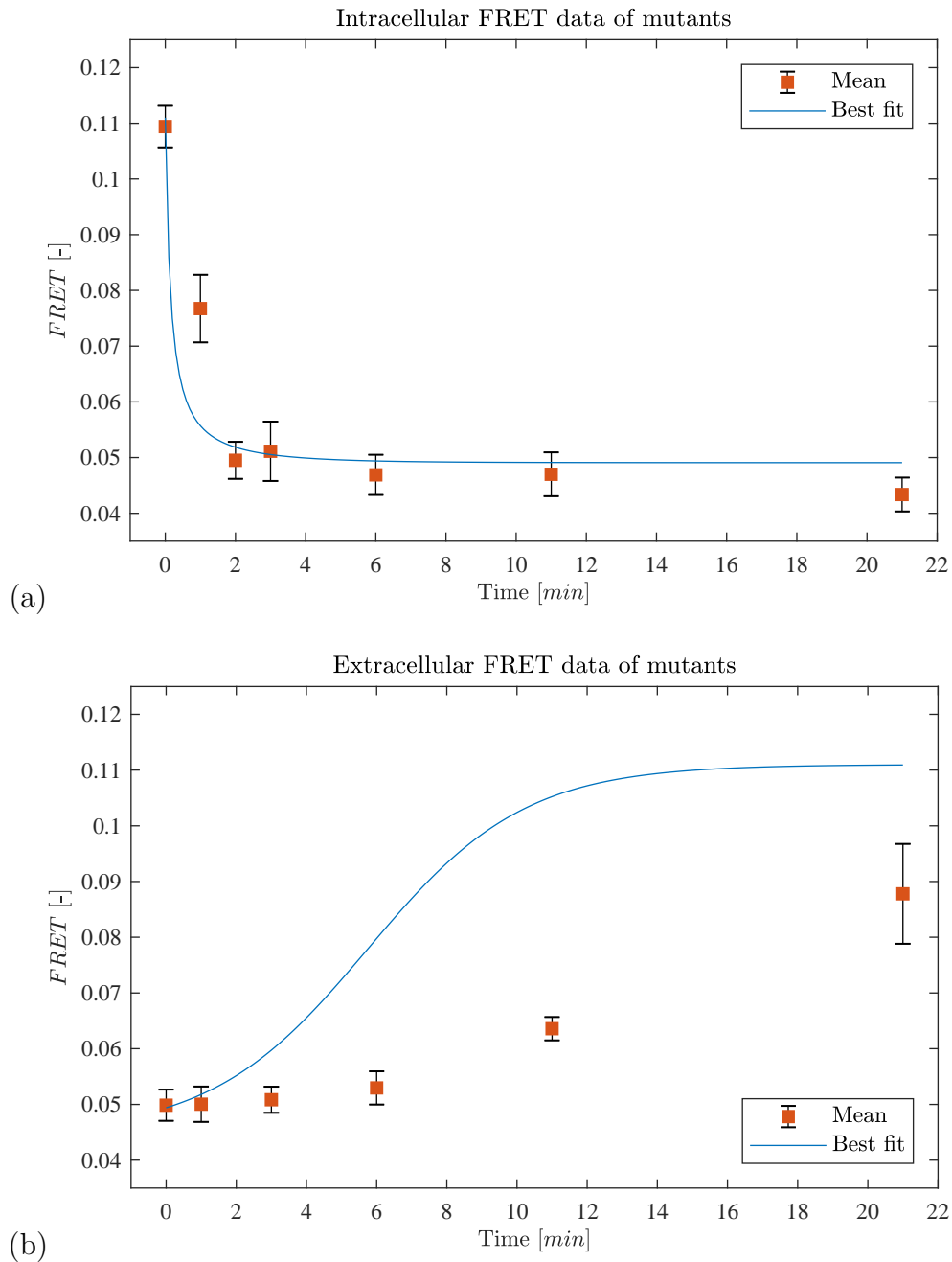
Figure 3.14.: *Best fit solutions of model equations* (3.18) *and* (3.19) *with best fit parameters given in table 3.2. In contrast to figure 3.12, we changed the initial condition* (3.20) *to* $C_e(0) = 100\frac{nmol}{l}$; *(a): Intracellular FRET kinetics; (b): Extracellular FRET kinetics;*

Finally, we do a bootstrap in order to find the confidence interval of the fitted curves. The procedure is briefly described in appendix B. The results of the bootstrapping procedure are given in figures 3.15 and 3.16. In both figures, we can see that the range of

the solutions is narrow and fits to the mean values and standard deviation well.

(a)

(b)
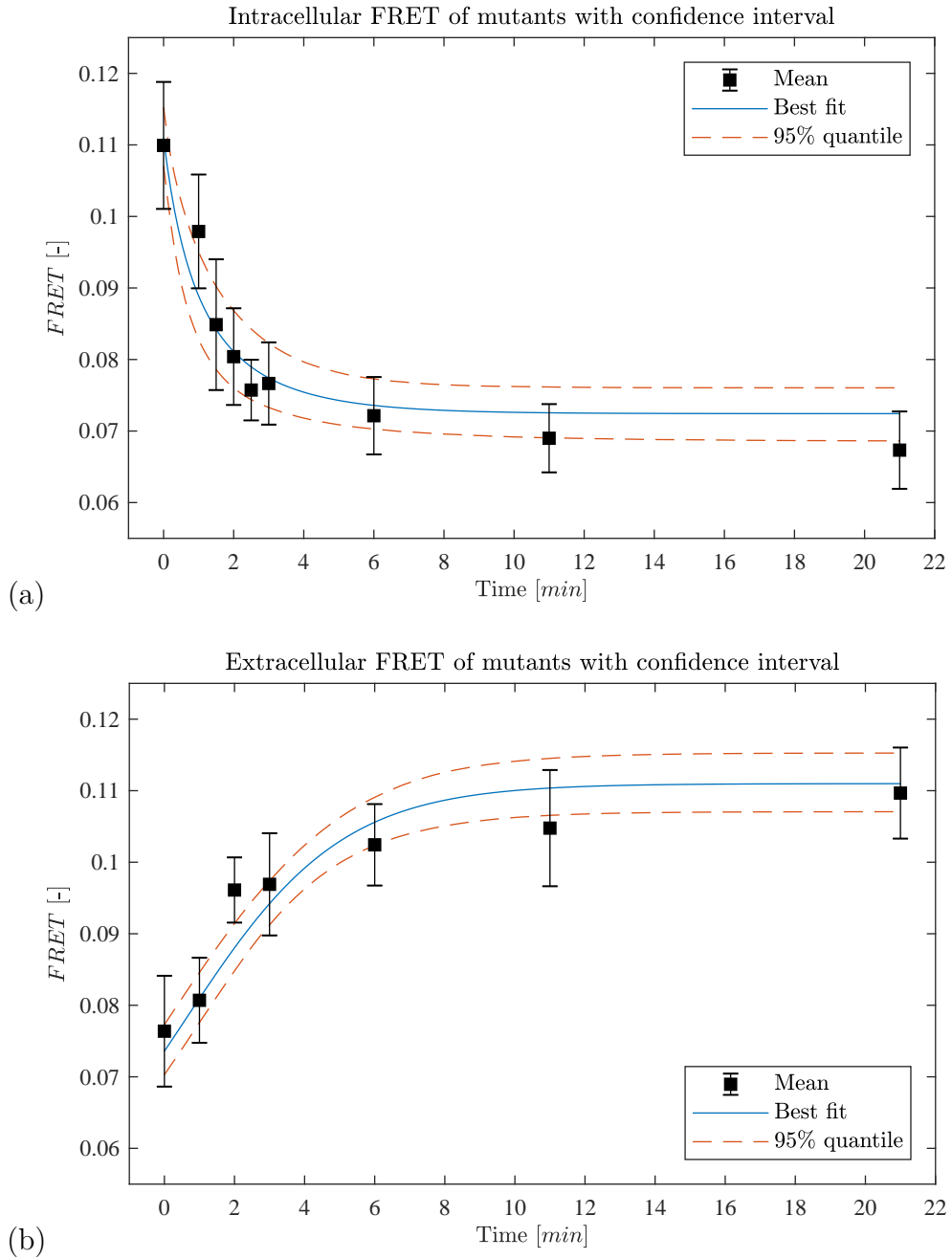
Figure 3.15.: *Best fit solutions model equations* (3.18) *and* (3.19) *depicted as solid blue line. Confidence interval of the fitted curve depicted as dashed red line; (a): Intracellular FRET kinetics; (b): Extracellular FRET kinetics;*
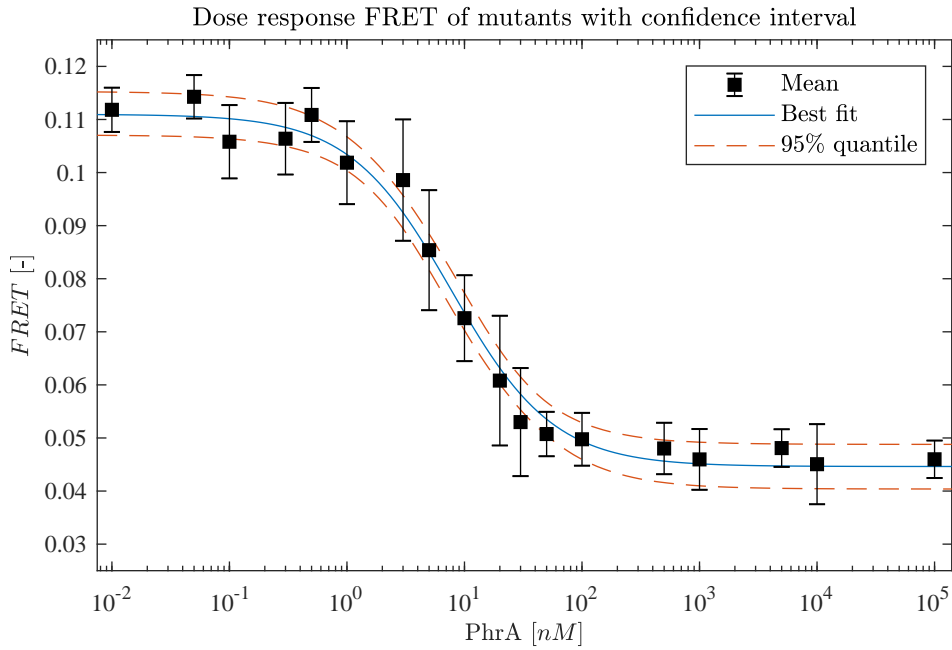
Figure 3.16.: *Best fit solution of FRET concerning the dose response data by model equations* (3.18) *and* (3.19) *depicted as solid blue line. Confidence interval of the fitted curve depicted as dashed red line.*

Both degradation rates are very small, especially for the intracellular degradation. Thus, we set both degradation rates equal zero, that is $\gamma_i = \gamma_e = 0$ and run a best fit simulation. The best fit parameter values and their bounds are given in table 3.3. Furthermore, we obtain a sum of squared residuals of $4.17 \cdot 10^{-4}$ which is slightly bigger than with degradation rates. Additionally, we see that the results of the bootstrapping and also for the best are equal, see figures 3.17 and 3.18. Therefore, we use this set of parameter values for the next calculations in order to reduce the complexity.

Parameter	Lower bound	Best fit	Upper bound
$\sigma_m \ [pl/min]$	1.34	2.23	3.65
$\xi \ [\mu mol/l]$	27.30	38.10	52.85
$FRET_0 \ [-]$	0.107	0.111	0.116
$\Delta FRET \ [-]$	0.060	0.066	0.073

Table 3.3.: Parameter confidence interval estimation of fit of model equations (3.18) and (3.19) with $\gamma_i = \gamma_e = 0$.

(a)

(b)
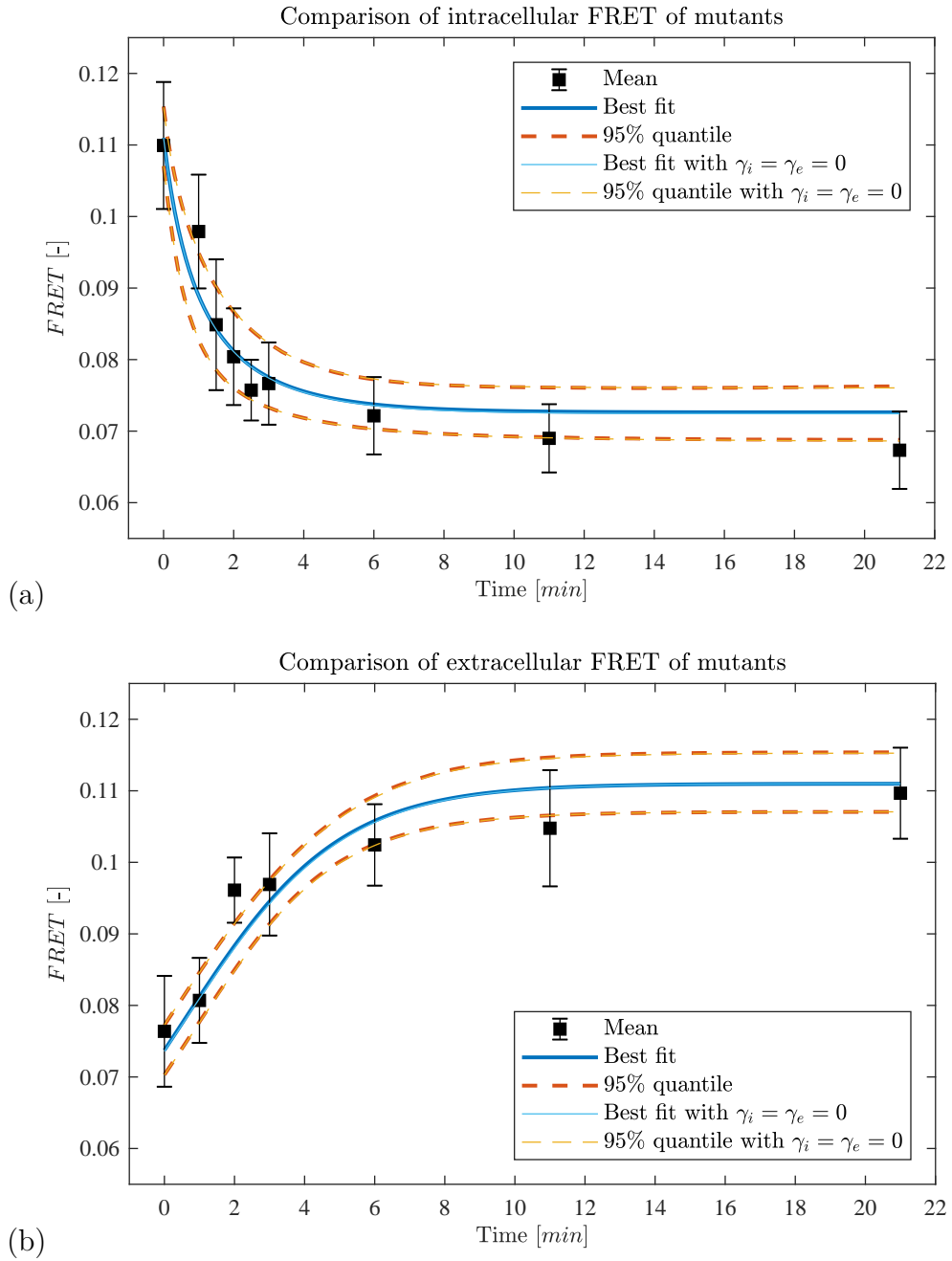
Figure 3.17.: *Comparison of bootstrapping with degradation rates and without degradation rates; (a): Intracellular FRET kinetics; (b): Extracellular FRET kinetics;*
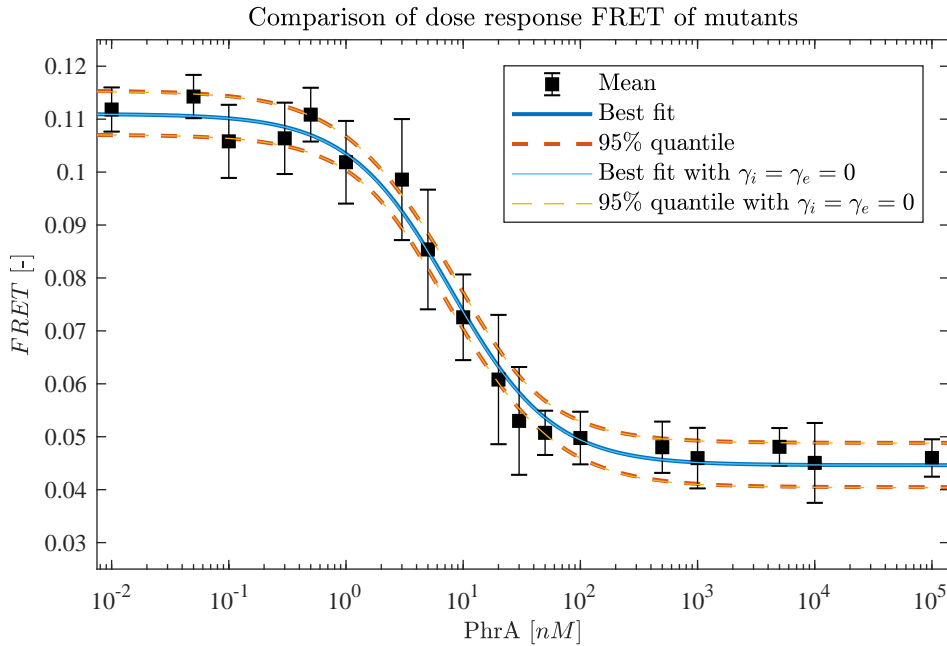
Figure 3.18.: *Comparison of bootstrapping with respect to the dose response data with degradation rates and without degradation rates*

3.6. Conclusion for mutant type

The key result of the mutant experiments 1 and 2 is to reject hypothesis HM 1, which means that the mutants absorb signalling molecules over time. We also see that a constant exponential absorption rate fits the data well. In a manuscript of *I. Bischofs*, received personally, the data were fitted by a model with a sigmoidal absorption depending on the extracellular signalling molecule concentration and without degradation rates. The results are similar except for the evaluation test with the $100\frac{nmol}{l}$ stimulus. In this case, they provided a better fit for the extracellular kinetics which means that they were able to fit the first four data points well in contrast to our fit, see figure 3.14(b). Afterwards the FRET curve increases as well quite fast and reaches the same level as our fit, that is 0.11. The last data point, however, has its level at approximately 0.08. One reason to stop the increasing of FRET is that the absorption stops at some point such that the intracellular concentration remains constant in time and so do the FRET curve. For the bacterium, it makes no sense to absorb forever signalling molecules. One simple reason could be that the cell is just full of signalling molecules. Another reason might be that it is to expansive in context of energy to absorb signalling molecules over a very long time. Or the absorption is described by another time-dependant function. However to test such a hypothesis, one needs more data points at the end to figure out in what kind of way the FRET curve increases. So we can infer that for a low extracellular concentration of signalling molecules a constant exponential absorption rate is an appropriate assumption. Additionally, we saw that

the model with degradation rates and without degradation rate, that are figures 3.17 and 3.18, yields the same results of the bootstrap method. We can conclude eventually, that the degradation rates can be neglected in order to simplify the analysis of the models.

3.7. Wild type model: No feedback regarding production

We adapt the key result of the mutant experiment 1 and 2 to the wild type experiment 3, that is, we have no feedback regarding the absorption. So the wild type do absorb signalling molecules over the entire time. In contrast to mutants, wild types can produce signalling molecules. As a first attempt, we assume that the production of signalling molecules also does not stop reaching the intracellular concentration ξ. Formulated as a hypothesis of the wild type it reads:

HW 1 There is no feedback at all regarding the absorption and production of signalling molecules.

3.7.1. Model equations

A part of the description of the model equations of the wild types is equivalent to the description of the model equations (3.18) and (3.19) of the mutant in section 3.5.1. So we only elaborate the difference of the model in the following passage.

Due to the longer experimental time duration, the bacterial growth can not be neglected. Therefore, the **number of wild type bacteria** is denoted as a time dependent variable $\boldsymbol{b_w(t)}$. Since the data yields no crucial hint regarding a dependency to the intracellular signalling molecule concentration, we assume that the bacterial growth is not coupled with the intracellular signalling molecule concentration. Since bacteria generally can't grow to infinity due to the limit of food respectively of space, bacterial growth is assumed to be logistic. Thus, the **exponential growth rate** is denoted as $\boldsymbol{\alpha}$ and the **carrying capacity** as $\boldsymbol{\kappa}$. Bacteria reproduce by cell division, the intracellular concentration decreases with the same rate as the bacteria divides. This rate is denoted as $f(b_w(t))$ and corresponds to the exponential growth rate of the wild type. The last and main important difference it that the **wild types produce signalling molecules** with a rate $\boldsymbol{\Pi}$ per bacterium with a unit given per volume and per time. So we have a positive change of external signalling molecules $C_e(t)$. Then the model for wild type bacteria respectively experiment 3 reads

$$\frac{\mathrm{d}}{\mathrm{d}t}C_e(t) = b_w(t)\mathbf{\Pi} - \left(\frac{\sigma_w}{V_e}b_w(t) + \gamma_e\right)C_e(t) \tag{3.22}$$

$$\frac{\mathrm{d}}{\mathrm{d}t}C_{i,w}(t) = \frac{\sigma_w}{V_{bac}}C_e(t) - \left(\gamma_i + f(b_w(t))\right)\,C_{i,w}(t) \tag{3.23}$$

$$\frac{\mathrm{d}}{\mathrm{d}t}b_w(t) = \alpha b_w(t)\left(1 - \frac{b_w(t)}{\kappa}\right) =: b_w(t)f(b_w(t)) \tag{3.24}$$

with initial conditions

$$C_e(0) = C_{e,0} \tag{3.25}$$

$$C_{i,w}(0) = C_{i,w,0} \tag{3.26}$$

$$b_w(0) = b_{w0}. \tag{3.27}$$

3.7.2. Analysis

There are no time-dependent indicator functions in the right hand sides of (3.22) - (3.24). Therefore we can show existence and uniqueness at once for $t \in [0, \infty)$ in contrast to the mutant models in section 3.4 or 3.5. However, the integrals which arise here are way more complicated to calculate. Hence, we do not derive here explicit solution formulas for all ODEs. Afterwards, one can show again the non-negativity of solutions.

Theorem 3.7.1. *There exist unique solutions of* (3.22) - (3.24) *with initial conditions* (3.25) - (3.27).

Proof. The ODE with respect to the bacterial growth, (3.24), is uncoupled to the two other equations and can be analysed for that reason separately. With the so called "trick of Riccati" one can solve the ODE, see [17]. The solution reads

$$b_w(t) = \frac{b_{w0}\kappa}{e^{-\alpha t}\left(\kappa - b_{w0}\right) + b_{w0}} \tag{3.28}$$

and is bounded for all $t \in [0, \infty)$. With the solution for the bacterial number we can continue with (3.22) and (3.23).

Let $t_1 \in (0, \infty)$. First we prove that there exists a unique local solution in the compact interval $[0, t_1]$. The right hand sides of (3.22) and (3.23) are continuous differentiable in C_e respectively $C_{i,w}$ and thus Lipschitz continuous for $t \in [0, t_1]$. Applying the Picard-Lindelöf Theorem A.3.1 yields the existence of unique solutions in $t \in [0, t_1]$. Integrating both sides of (3.22) over time we find following estimate:

$$C_e(t) = \underbrace{C_{e,0} + \int_0^{t_1} \Pi b_w(s)\,ds}_{=:g(t)} - \int_0^{t_1} \underbrace{\left(\frac{\sigma_w}{V_e}b_w(s) + \gamma_e\right)}_{=:h(s)} C_e(s)\,ds$$

$$\leq g(t) + \int_0^{t_1} |h(s)| C_e(s)\,ds.$$

Note that $g(t)$ is strictly increasing. Then we can apply the generalized Gronwall inequality, that is Theorem A.2.3, and obtain that the solution $C_e(s)$ is bounded in $t \in [0, t_1]$. One can show analogously the same for $C_{i,w}(t)$. After that, we consider the next time interval $[t_1, t_2]$ with $t_2 \in (t_1, \infty)$ arbitrary. Since the solutions in $[0, t_1]$ are bounded, we have feasible initial values for the new time interval. Thus, we obtain iteratively a unique solution for $t \in [0, \infty)$. $\qquad\square$

Lemma 3.7.2 (Non-negativity)**.** *Trajectories of* (3.22) - (3.24) *with initial conditions* (3.25) - (3.27) *are non-negative for* $t \in [0, \infty)$.

Proof. The approach is analogous as in the previous sections for the mutant cases. We use again Theorem A.3.2 to show non-negativity. From Theorem 3.7.1 we obtain uniqueness of solutions. Then we can show

$$\frac{\mathrm{d}}{\mathrm{d}t}C_e(t)\Big|_{C_e(t)=0} = b_w(t)\Pi > 0$$

$$\frac{\mathrm{d}}{\mathrm{d}t}C_{i,w}(t)\Big|_{C_{i,w}(t)=0} = \frac{\sigma_w}{V_{bac}}C_e(t) \geq 0 \quad \text{for } C_e(t) \geq 0$$

$$\frac{\mathrm{d}}{\mathrm{d}t}b_w(t)\Big|_{b_w(t)=0} = 0.$$

Consequently, the solutions are non-negativity. $\qquad\square$

Let's check if the system (3.22) - (3.24) may tend to steady states. Their stability can be investigated by the eigenvalues λ of the Jacobian. The steady states are asymptotically stable if and only if the real part of all eigenvalues λ of the Jacobian are negative, that is, $\mathrm{Re}\{\lambda\} < 0$.

Proposition 3.7.3. *For* $\gamma_i > 0$, *there exists an asymptotically stable steady state* $\left(\bar{C}_e, \bar{C}_{i,w}, \bar{b}_w\right)$ *of system* (3.22) - (3.24) *for* $t \in [0, \infty)$ *with*

$$\bar{C}_e = \frac{\Pi \kappa V_e}{\sigma_w \kappa + V_e \gamma_e}$$

$$\bar{C}_{i,w} = \frac{\sigma_w \Pi \kappa V_e}{\gamma_i V_{bac}(\sigma_w \kappa + V_e \gamma_e)}$$

$$\bar{b}_w = \kappa$$

and an unstable steady state

$$\bar{C}_e = 0$$
$$\bar{C}_{i,w} = 0$$
$$\bar{b}_w = 0.$$

For $\gamma_i = 0$, the system has no steady state.

Proof. In order to calculate the steady states we set the right hand side of the ODE equations (3.22) - (3.24) equal zero. Since (3.24) is completely decoupled from (3.22) and (3.23), we take a first glance of this equation.

$$0 = \alpha \bar{b}_w \left(1 - \frac{\bar{b}_w}{\kappa} \right)$$
$$\Longleftrightarrow \quad \bar{b}_w = 0 \ \vee \ \bar{b}_w = \kappa$$

Thus, the steady state of the bacterial number reads $\bar{b}_{w,1} = 0$ and $\bar{b}_{w,2} = \kappa$. The steady state of the extracellular signalling molecule concentration reads

$$0 = \Pi \bar{b}_w - \bar{C}_e \left(\frac{\sigma_w}{V_e} \bar{b}_w + \gamma_e \right)$$
$$\Longleftrightarrow \quad \bar{C}_e = \frac{\Pi \bar{b}_w V_e}{\sigma_w \bar{b}_w + V_e \gamma_e}.$$

Hence $\bar{C}_{e,1} = 0$ for $\bar{b}_{w,1}$ or $\bar{C}_{e,2} = \frac{\Pi \kappa_w V_e}{\sigma_w \kappa_w + V_e \gamma_e}$ for $\bar{b}_{w,2}$.

The steady state of the intracellular signalling molecule concentration is given by

$$0 = \frac{\sigma_w}{V_{bac}} \bar{C}_e - \bar{C}_{i,w} \left(\gamma_i + f(\bar{b}_w) \right)$$
$$\Longleftrightarrow \quad \bar{C}_{i,w} = \frac{\sigma_w \Pi \bar{b}_w V_e}{\left(\gamma_i + f(\bar{b}_w) \right) V_{bac} (\sigma_w \bar{b}_w + V_e \gamma_e)}.$$

For $\bar{b}_{w,1}$, we obtain $\bar{C}_{i,w,1} = 0$. Otherwise for $\bar{b}_{w,2}$ and $\gamma_i > 0$ the steady state reads $\bar{C}_{i,w,2} = \frac{\sigma_w \Pi \kappa V_e}{\gamma_i V_{bac} (\sigma_w \kappa + V_e \gamma_e)}$. If $\gamma_i = 0$ there exists no steady state. Summed up, we have only two steady states which read $(\bar{C}_{e,1}, \bar{C}_{i,w,1}, \bar{b}_{w,1})$ and $(\bar{C}_{e,2}, \bar{C}_{i,w,2}, \bar{b}_{w,2})$.

The stability can be derived by the Jacobian of $((3.22), (3.23), (3.24))^T$ and reads

$$J(C_e, C_{i,w}, b_w) = \begin{pmatrix} -\dfrac{\sigma_w}{V_e}\bar{b}_w - \gamma_e & 0 & 0 \\[2em] \dfrac{\sigma_w}{V_{bac}} & -\gamma_i & 0 \\[2em] 0 & 0 & \alpha - 2\alpha\dfrac{b_w}{\kappa} \end{pmatrix}.$$

Thus, the trivial steady state $(\bar{C}_{e,1}, \bar{C}_{i,w,1}, \bar{b}_{w,1})$ is not stable since $\alpha - 2\alpha\frac{\bar{b}_{w,1}}{\kappa} = \alpha$ is positive and the non-trivial steady states $(\bar{C}_{e,2}, \bar{C}_{i,w,2}, \bar{b}_{w,2})$ is asymptotically stable since $\alpha - 2\alpha\frac{\bar{b}_{w,2}}{\kappa} = -\alpha$ is negative. The solution of the system tends to this point. $\quad\square$

3.7.3. Best fit simulation

The data of bacterial growth given in figure 3.7(b) and is fitted first since we need solution function $b_w(t)$ in order to fit $C_e(t)$ and $C_{i,w}(t)$. We will fit following parameters:

$$b_{w0}, \; \alpha, \; \text{and} \; \kappa.$$

The results of the best fit simulation is given in table 3.4 and the plot of the best fit inclusive the estimated confidence interval of a fitted solution can be seen in figure 3.19. The SSR of the logistic approach reads 0.0180.

Parameter	Lower bound	Best fit	Upper bound
$b_{w0} \; [-]$	$7.93 \cdot 10^9$	$8.55 \cdot 10^9$	$9.13 \cdot 10^9$
$\alpha \; [10^{-3}/min]$	3.01	4.30	5.67
$\kappa \; [-]$	$3.84 \cdot 10^{10}$	$6.17 \cdot 10^{10}$	$7.03 \cdot 10^{23}$

Table 3.4.: Parameter confidence interval estimation of fit of model equation (3.24).
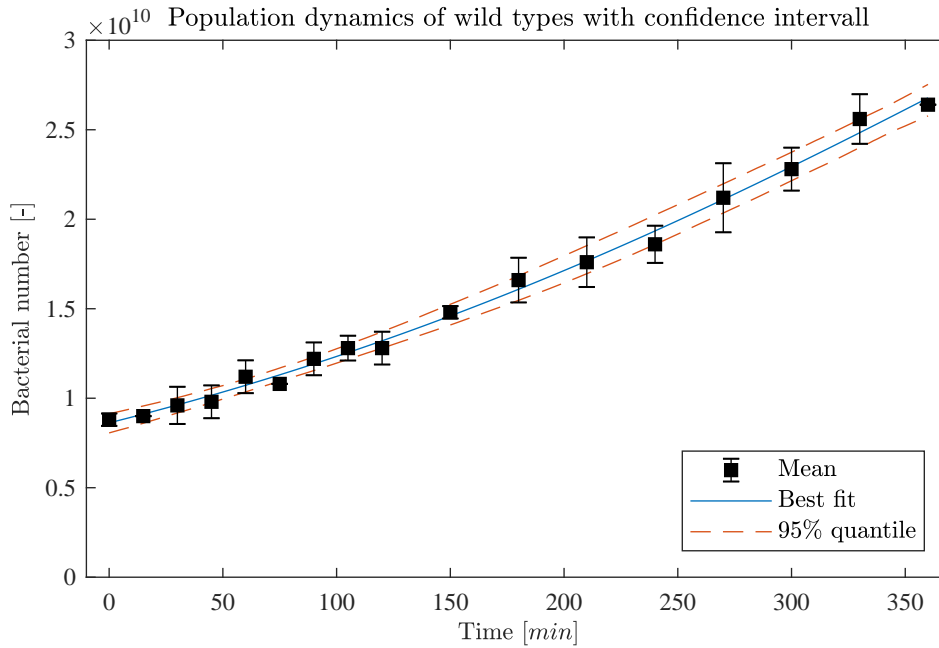
Figure 3.19.: *Best fit of bacterial growth model equation (3.24) depicted as solid blue line. Confidence interval of the fitted curve depicted as dashed red line.*

Remark 3.7.4. *Further data fits with an exponential and linear approach yield a bigger SSR. The one of the exponential approach was 0.0289, the one of the linear approach was 0.0511. Thus, the assumption of a logistic growth is confirmed.*

Now we can start to fit the FRET data of the wild type experiment 3. The experimental parameter V_e changes in this experiment to $100ml$ and the initial values reads $C_e(0) = 0\frac{\mu mol}{l}$, $C_{i,w}(0) = 0\frac{\mu mol}{l}$ and from above we obtained $b_w(0) = 8.55 \cdot 10^9$ cells. After a while, we insert the mutants, in total $16 \cdot OD_{600nm} \cdot 50\mu l = 16 \cdot 1.2 \cdot 10^8 \frac{cells}{ml} \cdot 50\mu l = 9.6 \cdot 10^7$ cells, into the cell free supernatant of size $V_e = 1950 \cdot 10^{-6}l$. As a first attempt, we assume that the wild type bacteria has the same parameter values as the mutants which are given in table 3.3. The only parameter which is left to fit is the production rate Π.

Running the program code of the best fit simulation, we obtain the best fit values in table 3.5 and the FRET curve is depicted in figure 3.20 which is not acceptable. One can detect three problems considering the fit. First, for $t = 0$, the FRET curve does not match the first data point and starts with a lower intercept. The consequence being that we will also never reach the last five data points even if we change the hypothesises. Second, the FRET curve does not decrease enough to reach the smallest mean data points. Third, the FRET curves tend to a steady state and do not increase after 120 minutes in contrast to the data. Let's discuss how these problems might be solved. The first problem can be easily solved by shifting the parameter value $FRET_0$. However it is not sure if this is unison with the biology. But after personal communication with

Ilka Bischofs, we can do this shift since they also detected this phenomenon in their experiments. It seems that the $FRET_0$ depends on the way how the mutant types are cultured. The parameter value $\Delta FRET$ is not affected by this coincidence.

From a mathematical point of view, it is obvious why the second problem arises, that is, the extracellular signalling molecule concentration is (almost) constant after half an hour, see figure 3.21, with a relative small amount of signalling molecules. But we need more extracellular signalling molecules to lower the FRET curve in figure 3.20. One possibility could be to increase the production rate. But that would also result in a steeper slope of the FRET curve and the curve would never match the points at $t = 100$. That's why the best fit algorithm did not do that. However, there is a further possibility to increase the level of signalling molecules: to reduce the absorption rate. We assumed in the beginning that the absorption rate σ_w of the wild type is the same as for the mutants. In the mutant experiments 1 and 2 only synthetic signalling molecules were added into the environment. However, the wild types produce also further molecules which are transported into the cell by the same oligopermease transporters, as we know by personal communication with Dr. Bischofs. We can call this competition effect. Thus, the net absorption rate of *PhrA* molecules is smaller. Luckily, these molecules have no effect to the FRET reporter strain within the cell such that we can neglect them in the model equations.

After that, it is obvious what we have to do such that the FRET curve increases: the production has to stop in order to ensure the increase of FRET. So we will change the hypothesis HW 1 appropriately and formulate a new hypothesis.

Parameter	Lower bound	Best fit	Upper bound
Π [$zmol/(l \cdot min)$]	2.82	10.53	20.83

Table 3.5.: Parameter confidence interval estimation of fit of model equations (3.22) and (3.23).

Figure 3.20.: *Best fit solution of extracellular FRET kinetics by model equations* (3.22) *and* (3.23) *with best fit parameters of the mutants given in table 3.3, the bacterial growth given in table 3.4 and wild types given in table 3.5.*
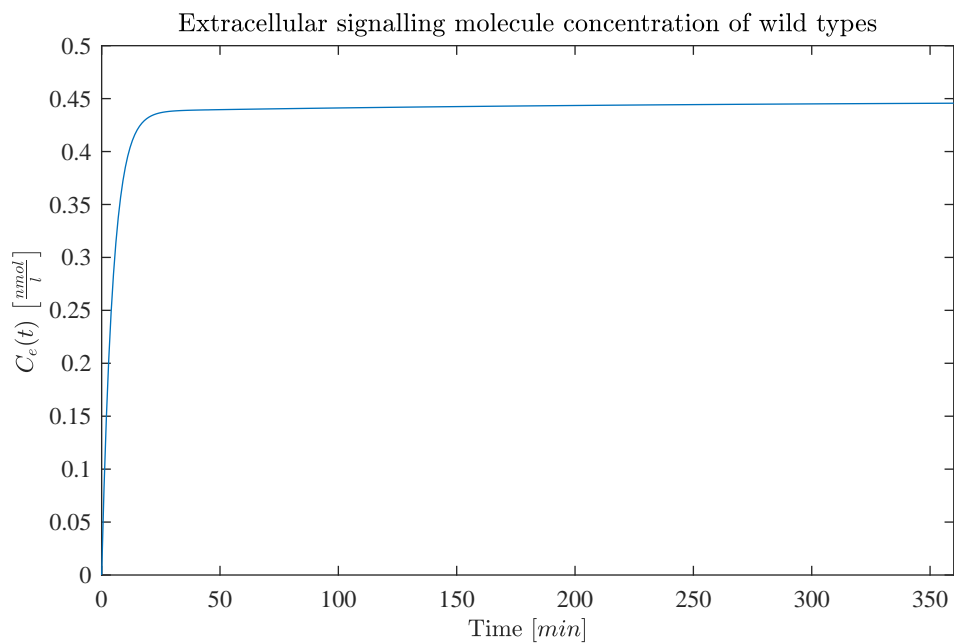
Figure 3.21.: *Solution of* (3.22) *with best fit parameters given in table 3.3, 3.4 and 3.5.*

3.8. Wild type model: Negative feedback regarding production

We concluded to reject hypothesis HW 1 since we need an increase of extracellular FRET. Hence the new formulation reads:

HW 2 When the intracellular concentration $C_{i,w}$ has reached the threshold ξ_n, then there is a negative feedback regarding the production, but no feedback regarding the absorption of signalling molecules at all.

Note that the threshold ξ_n is a different one as the threshold ξ of the mutant.

3.8.1. Model equations

Compared to the model equations (3.22) - (3.24) in section 3.7.1, we only add an time-dependent indicator function to the production term. Then the system reads

$$\frac{\mathrm{d}}{\mathrm{d}t}C_e(t) = \hat{\chi}_{[0,\xi_n] \times t_n}(C_{i,w}(t), t) \, b_w(t)\Pi - \left(\frac{\sigma_w}{V_e}b_w(t) + \gamma_{e,w}\right) \, C_e(t) \tag{3.29}$$

$$\frac{\mathrm{d}}{\mathrm{d}t}C_{i,w}(t) = \frac{\sigma_w}{V_{bac}}C_e(t) - (\gamma_{i,w} + f(b_w(t))) \, C_{i,w}(t) \tag{3.30}$$

$$\frac{\mathrm{d}}{\mathrm{d}t}b_w(t) = \alpha b_w(t)\left(1 - \frac{b_w(t)}{\kappa}\right) =: b_w(t)f(b_w(t)) \tag{3.31}$$

with initial conditions

$$C_e(t_0) = C_{e,0} \tag{3.32}$$
$$C_{i,w}(t_0) = C_{i,w,0} \tag{3.33}$$
$$b_w(t_0) = b_{w0} \tag{3.34}$$

and

$$t_n := \inf\{t \in \mathbb{R}_+ : \xi_n = C_i(t)\}.$$

3.8.2. Analysis

The approach to show existence and uniqueness of a solution is similar as in section 3.4. In case of $C_{i,w} \geq \xi_n$, the wild type model almost coincides with the mutant model in section 3.5. The difference is the population dynamics for the wild types. Thus, the ODE of the intracellular concentration is different and we can not use Lemma 3.4.1 immediately, but after a small change. If $C_{i,w} < \xi_n$, that means the time-dependent

indicator function is one, the model coincides with the wild type model in the previous section 3.7. One just has to know when the necessary condition is fulfilled and this is nothing else than the intersection of $C_{i,w}(t) = \xi_n$ yielding t_n. However, to calculate the solution of $C_{i,w}(t)$ respectively $C_e(t)$ explicitly is a difficult task to undertake. So in the upcoming Corollary, we will have no requirements such that the necessary condition is fulfilled.

Corollary 3.8.1. *There exist unique and piecewise continuous differentiable solutions of* (3.29) - (3.31) *with initial conditions* (3.32) - (3.34). *The solutions are non-negative.*

Proof. If $C_{i,w}(t_0) < \xi_n$ then the model coincides with the model in section 3.7.1 for at least a small time interval $[t_0, t_1]$. Theorem 3.7.1 yields existence and uniqueness for that time interval. If there exists a $t_s \in [t_0, t_1]$ such that $C_{i,w}(t_s) \geq \xi_n$ then Theorem 3.7.1 yields again existence and uniqueness for $t \in [t_0, t_s)$. The solutions for this time interval are denoted as $\hat{}$. As mentioned above, the model almost coincides with the mutant system in section 3.5 and the existence and uniqueness of a solution can be obtain by and adjusted proof of Lemma 3.4.1. One just has to replace in the ODE γ_i by $\gamma_{i,w} + f(b_w(t))$. The new ODE can be solved by variation of constants for both cases $\gamma_{i,w} = 0$ and $\gamma_{i,w} \neq 0$. The resulting integral exists since $b_w(t) \in \mathcal{L}^\infty$ and so is $f(b_w(t)) \in \mathcal{L}^\infty$. Henceforth, we obtain for $t \in [t_s, \infty)$ existence and uniqueness of a solution for given adjusted initial conditions $C_e(t_s) = \hat{C}_e(t_s)$, $C_{i,w}(t_s) = \hat{C}_{i,w}(t_s)$ and $b_w(t_s) = \hat{b}_w(t_s)$. Joint together, there exists a unique and piecewise continuous differentiable solution in $t \in [t_0, \infty)$. If there exists no $t_s \in [t_0, t_1]$, we consider a further interval $[t_1, t_2]$ and check again if there exist a t_s. This can be done iteratively until we obtain a at least piecewise continuous differentiable solution in $t \in [t_0, \infty)$.

If $C_{i,w}(t_0) > \xi_n$ then the model coincides with the model in section 3.5.1 for at least a small time interval $[t_0, t_1]$. Then the approach is analogous to above. Since it holds

$$\frac{\mathrm{d}}{\mathrm{d}t}C_e(t)\Big|_{C_e(t)=0} = \hat{\chi}_{[0,\xi_n]\times t_n}(C_{i,w}(t),t)\, b_w(t)\Pi \geq 0$$

$$\frac{\mathrm{d}}{\mathrm{d}t}C_{i,m}(t)\Big|_{C_{i,m}(t)=0} = \frac{\sigma_w}{V_{bac}}C_e(t) \geq 0 \quad \text{for } C_e(t) \geq 0,$$

the system is non-negative because of Theorem A.3.2. $\qquad\square$

3.8.3. Best fit simulation

In the best fit simulation, the experimental parameters as well as the initial conditions are the same as in the previous section 3.7. For the bacterial parameters, we use the best fit data from table 3.19. For the mutants, we use the parameters given in table 3.3 except for $FRET_0$ as discussed above. Instead, we use the mean value of the data which is given by 0.117. We have concluded that the absorption rate of the wild type should

be smaller than that of a mutant, hence σ_w is beside the production rate Π a parameter which has to be fitted. In addition, we test for wild types if there are degradation rates of the signalling molecules as the "natural" signalling molecule might behave different as "synthetic" signalling molecules. Summed up we will fit five parameters which read

$$\Pi, \; \sigma_w, \; \xi_n, \; \gamma_{i,w} \text{ and } \gamma_{e,w}.$$

The results of the best fit simulation are given in table 3.6. As predicted, the absorption rate σ_w of a wild type is smaller than that of a mutant, see table 3.3. Again, the absorption rates $\gamma_{i,w}$ and $\gamma_{e,w}$ are very small such that one can neglect them in the wild type model as well. The SSR is of size $1.99 \cdot 10^{-4}$ which is quite small.

Parameter	Lower bound	Best fit	Upper bound
$\Pi \; [zmol/(l \cdot min)]$	2.08	5.06	58.31
$\sigma_w \; [pl/min]$	$9.0 \cdot 10^{-7}$	0.18	0.28
$\xi_n \; [\mu mol/l]$	10.47	28.60	68.98
$\gamma_{i,w} \; [1/min]$	$1.3 \cdot 10^{-9}$	$1.3 \cdot 10^{-9}$	$3.2 \cdot 10^{-5}$
$\gamma_{e,w} \; [1/min]$	$1.6 \cdot 10^{-8}$	$1.7 \cdot 10^{-6}$	0.005

Table 3.6.: Parameter confidence interval estimation of fit of model equations (3.29) and (3.30).

The best fit in figure 3.22 seems very nice but can be still improved. On the one hand, we do not really match the first data points, the curve decreases to fast. However, if we lower the production rate by hand, then the curve would not reach the minimum. So it seems that the production rate Π is time dependent. On the other hand, we have a sharp angle when the initiation of sporulation starts and production of signalling molecules stops. However, it is not realistic that all bacteria stop simultaneously. Each bacterium is not identical to each other, there are small diversities from a biological point of view. In the next chapter, we will implement these ideas to the model.
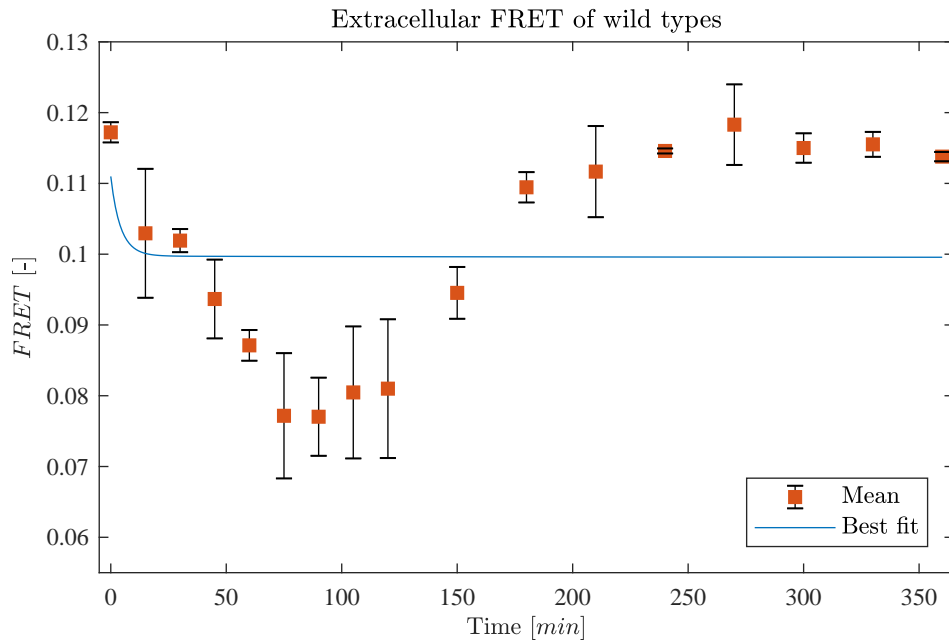
Figure 3.22.: *Best fit solution of extracellular FRET kinetics by model equations* (3.29) *and* (3.30) *with best fit parameters table 3.3, 3.4 and 3.6.*

3.9. Extended wild type model: Negative feedback regarding time dependent production

We do not reject hypothesis HW 2, instead we extend the model as described above. In place of a constant production rate Π we will deduce a production rate depending on the intracellular signalling molecule concentration which itself depends on time. So in the beginning when we have a low intracellular signalling molecule concentration, the production rate should be low, too. If the intracellular signalling molecule concentration increases, the production rate do so as well and tend to a constant value. Such a behaviour can be described by a sigmoid function

$$\Pi_s(C_{i,w}) = \frac{\Pi_{max}C_{i,w}^m}{K^m + C_{i,w}^m}$$

with Π_{max} as the maximal production rate of extracellular signalling molecules, n being the curvature index and K is the "half-max-velocity constant", that is the value of $C_{i,w}$ when $\Pi_s = \frac{1}{2}\Pi_{max}$. Since the intracellular concentration is usually zero in the beginning, we have to add a minimal production rate Π_{min} such that the production of signalling molecules starts. Summed up, a suitable function reads

$$\Pi_S(C_{i,w}) := \Pi_{min} + \frac{\Pi_{max}C_{i,w}^m}{K^m + C_{i,w}^m}.$$

Since we have small diversities in each bacterial cell, we assume a noise in the sporulation threshold. That means we will consider subpopulations $j \in W$ and due to the diversity, each subpopulation has a different sporulation threshold $\xi_{n,j}$. The set $\{w_1, \ldots, w_n\} =: W$ denotes the n wild type subpopulations. We assume that the noise is normally distributed. The new extended hypothesis reads

HW 3 When the intracellular concentration $C_{i,j}$ of subpopulation j has reached the threshold $\xi_{n,j}$, then there is a negative feedback regarding the production but no feedback regarding the absorption of signalling molecules at all.

Additionally, we concluded that the degradation rates $\gamma_{i,w}$ and $\gamma_{e,w}$ are very small. Thus, we neglect them in the extended model.

3.9.1. Model equations

The description of the model parameters as well as the dynamic can be found in the previous chapter 3.7.1. Here, we implement the new ideas from above.

$$\frac{\mathrm{d}}{\mathrm{d}t}C_e(t) = \sum_{j=w_1}^{w_n} \hat{\chi}_{[0,\xi_{n,j}]\times t_{n,j}}(C_{i,j}(t), t)\, b_j(t)\Pi_S\left(C_{i,j}(t)\right) - \sum_{j=w_1}^{w_n} b_j(t)\frac{\sigma_w}{V_e}C_e(t) \qquad (3.35)$$

$$\frac{\mathrm{d}}{\mathrm{d}t}C_{i,j}(t) = \frac{\sigma_w}{V_{bac}}C_e(t) - f(b_j(t))C_{i,j}(t) \qquad \text{for } j \in W \qquad (3.36)$$

$$\frac{\mathrm{d}}{\mathrm{d}t}b_j(t) = \alpha b_j(t)\left(1 - \frac{b_j(t)}{\kappa}\right) =: b_j(t)f(b_j(t)) \qquad \text{for } j \in W \qquad (3.37)$$

with initial conditions

$$C_e(t_0) = C_{e,0} \qquad (3.38)$$
$$C_{i,j}(t_0) = C_{i,j,0} \qquad \text{for } j \in W \qquad (3.39)$$
$$b_j(t_0) = b_{j0} \qquad \text{for } j \in W. \qquad (3.40)$$

The thresholds $\xi_{n,j}$ should vary slightly from ξ_n. So it can be seen as a perturbed parameter with a normal distributed perturbation. We could assume that the threshold $\xi_{n,j}$ varies up to around 20% of ξ_n. This can be achieved by $\xi_{n,j} = \xi_n + 0.2 \cdot \xi_n \nu_j$ with $\nu_j \sim \mathcal{N}(0,1)$. The time point $t_{n,j}$ is defined as

$$t_{n,j} := \inf\{t \in \mathbb{R}_+ : \xi_{n,j} = C_{i,j}(t)\}$$

for all $j \in W$.

3.9.2. Analysis

The approach to show existence and uniqueness of solutions of equations (3.35)-(3.37) in $t \in [t_0, \infty)$ is a combination of the proofs of Theorem 3.7.1 and Corollary 3.8.1.

Theorem 3.9.1. *There exist unique and piecewise continuously differentiable solutions of* (3.35) - (3.37) *with initial conditions* (3.38) - (3.40). *The solutions are non-negative.*

Proof. The equations for the bacterial growth (3.37) are uncoupled to the other equations (3.35) and (3.36). As in the proof of Theorem 3.7.1, there exist unique bounded solutions of (3.37) in $t \in [t_0, \infty)$ for all $j \in W$.

We assume that $C_{i,j}(t_0) < \xi_{n,j}$ for all $j \in W$. That means there exists a small time interval $[t_0, t_1]$ such that all time-dependent indicator functions are one and the right hand sides are continuously differentiable. This implies Lipschitz continuity and henceforth existence and uniqueness of solutions by the Picard-Lindelöf Theorem. The generalized Gronwall inequality yields boundedness of the solutions C_e and $C_{i,w}$. If there exists a time point $t_{n,k} \in [t_0, t_1]$ such that the intracellular signalling molecule concentration of a subpopulation k reaches its threshold $\xi_{n,k}$ with $k \in W$, then one has to consider an adjusted system for $[t_{n,k}, t_1]$. That means we do not sum over subpopulation k in the production term and the initial values have to be adapted, that is, the solution evaluated at $t_{n,k}$. Since the solutions in $[t_0, t_1]$ are bounded, we have feasible initial values for the new time interval. With the same approach, we can show existence and uniqueness for $[t_{n,k}, t_1]$. Afterwards, we consider the next time interval $[t_1, t_2]$ with $t_2 \in (t_1, \infty)$ arbitrary. The approach for that interval is analogous. Henceforth, we yield iteratively a unique and continuous piecewise differentiable solution for $t \in [0, \infty)$.

If there exists a $j \in W$ such that $C_{i,j}(t_0) > \xi_{n,j}$, then we do not sum over all subpopulations in $[t_0, t_1]$. The approach, however, is analogous to above.

The non-negativity can be shown as always with Theorem A.3.2. The trajectories are non-negative since it holds

$$\frac{\mathrm{d}}{\mathrm{d}t} C_e(t) \Big|_{C_e(t)=0} = \sum_{j=w_1}^{w_n} \hat{\chi}_{[0,\xi_{n,j}] \times t_{n,j}} (C_{i,j}(t), t) \, b_j(t) \Pi_S (C_{i,j}(t)) \geq 0$$

$$\frac{\mathrm{d}}{\mathrm{d}t} C_{i,j}(t) \Big|_{C_{i,j}(t)=0} = \frac{\sigma_w}{V_{bac}} C_e(t) \geq 0 \qquad \text{for } C_e(t) \geq 0, \ j \in W$$

$$\frac{\mathrm{d}}{\mathrm{d}t} b_j(t) \Big|_{b_j(t)=0} = 0 \qquad \text{for } j \in W.$$

$\square$

3.9.3. Best fit simulation

The experimental parameters V_e, V_b and the initial conditions are given in section 3.7 and the best fit parameters for the mutant can be found in table 3.3. We assume $n = 10$ subpopulations, that is $W = \{w_1, \ldots, w_{10}\}$ of equal size in the simulation. Then the

solution of a subpopulation (3.37) is given by the solution of the logistic function given (3.28) divided by the number of supopulation. The noise $\nu = (\nu_{w_1}, \ldots, \nu_{w_{10}})$ of the threshold is given with $\nu = (-0.82, -1.58, 0.51, 0.28, 0.03, -1.33, 1.13, 0.35, -0.30, 0.023)$. The remaining parameters will be fitted, that is,

$$\Pi_{min}, \ \Pi_{max}, \ K, \ \sigma_w, \ m \text{ and } \xi_n.$$

The parameters of the best fit algorithm are given in table 3.7 and the corresponding plot is depicted in figure 3.23. Now the solution fits the first data points better which reflects also in a better SSR of $7.11 \cdot 10^{-5}$. The sharp angle vanishes as predicted fitting the minimal points also very good.

$\Pi_{min} = 3.59 \ [zmol/(l \cdot min)]$	$\Pi_{max} = 5.10 \ [zmol/(l \cdot min)]$	$K = 4.90 \ [\mu mol/l]]$
$\sigma_w = 0.22 \ [pl/min]$	$m = 16.70 \ [-]$	$\xi_n = 37.31 \ [\mu mol/l]$

Table 3.7.: Parameter choice of model equations (3.35) and (3.30) which yields a good result.
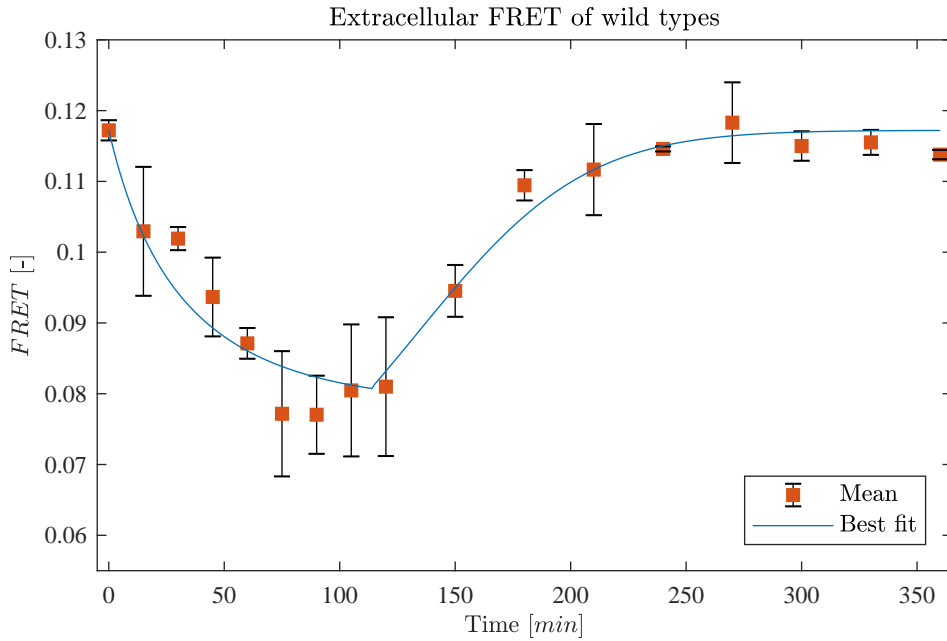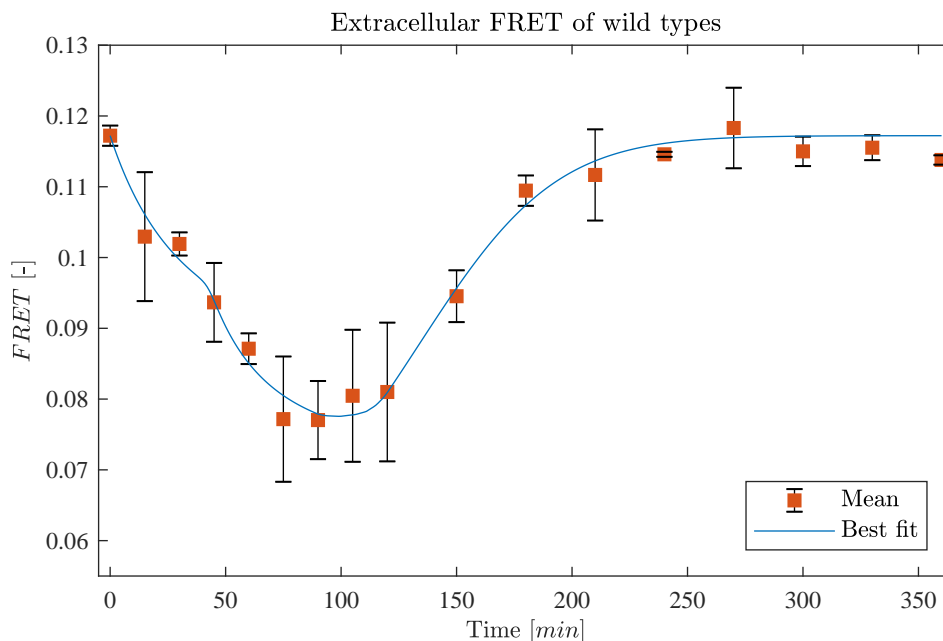

Figure 3.23.: *Best fit solution of extracellular FRET kinetics by model equations* (3.35) *and* (3.36) *with best fit parameters given in table 3.3, table 3.4 and table 3.7.*

However the estimation of parameter confidence intervals yields frequently warnings of singular matrices solving the ODE system. Then we obtain finally the warning, that

the next step can not be chosen smaller than machine precision and the calculations stops. Compared to the previous model in section 3.8, we changed only two things: the number of equations and the production term. The change in number of equations can not be the reason since the ODE's are mostly decoupled. So it has to be the production term. Plotting the sigmoid function $\Pi_S\left(C_{i,j}(t)\right)$ using the best fit parameters in table 3.7 for an arbitrary $j \in W$, see figure 3.24, reveals the problem: the slope of the function is already very steep for the best fit solution. So running the algorithm to estimate confidence intervals of the parameters by maximizing/minimizing them leads probably to a even steeper slope such that numerical integration has problems to integrate the function when calculating a solution. The idea to avoid these warnings is to replace the sigmoidal production term $\Pi_S\left(C_{i,j}(t)\right)$ with a step function which is a sum of time-dependent indicator functions. This is done in the next section.

Figure 3.24.: *Best fit solution of extracellular FRET kinetics by model equations* (3.22) *and* (3.30) *with best fit parameters of the mutants given in table 3.3, the bacterial growth given in table 3.4 and the wild types given table 3.6.*

3.10. Extended wild type model: Positive and negative feedback regarding time dependent production

In this section we only replace the sigmoidal production term with a step function. So in the beginning, the production rate of signalling molecules is low and constant. This is also called the basal phase. Then when the intracellular signalling molecule concentration has reached a certain threshold $\xi_{p,j}$, the production rate jumps to a higher constant rate. This is modelled with a time-dependent indicator function. That also leads to a change in the hypothesis.

HW 4 When the intracellular concentration $C_{i,j}$ has reached the threshold $\xi_{p,j}$, then there is a positive feedback regarding the production, but if it has reached the threshold $\xi_{n,j}$, then there is a negative feedback regarding the production. We have no feedback regarding the absorption of signalling molecules at all.

3.10.1. Model equations

The description of the model parameters as well as the dynamic can be found in the previous chapter 3.9. Here, we only implement the new production term. This can be realized by

$$\Pi_{\hat{\chi}}\left(C_{i,j}(t)\right) := \Pi_{min} + \hat{\chi}_{(\xi_{p,j},\infty)\times t_{p,j}}(C_{i,j}(t),t)\Delta\Pi \tag{3.41}$$

with

$$t_{p,j} := \inf\{t \in \mathbb{R}_+ : \xi_{p,j} = C_{i,j}(t)\}$$

for all $j \in W$. So the final improved model reads

$$\frac{\mathrm{d}}{\mathrm{d}t}C_e(t) = \sum_{j=w_1}^{w_n} \hat{\chi}_{[0,\xi_{n,j}]\times t_{n,j}}(C_{i,j}(t),t)\Pi_{\hat{\chi}}\left(C_{i,j}(t)\right)b_j(t) - \sum_{j=w_1}^{w_n} b_j(t)\frac{\sigma_w}{V_e}C_e(t) \tag{3.42}$$

$$\frac{\mathrm{d}}{\mathrm{d}t}C_{i,j}(t) = \frac{\sigma_w}{V_{bac}}C_e(t) - f(b_j(t))C_{i,j}(t) \qquad \text{for } j \in W \tag{3.43}$$

$$\frac{\mathrm{d}}{\mathrm{d}t}b_j(t) = \alpha b_j(t)\left(1 - \frac{b_j(t)}{\kappa}\right) =: b_j(t)f(b_j(t)) \qquad \text{for } j \in W \tag{3.44}$$

with initial conditions

$$C_e(t_0) = C_{e,0} \tag{3.45}$$

$$C_{i,j}(t_0) = C_{i,j,0} \qquad \text{for } j \in W \tag{3.46}$$

$$b_j(t_0) = b_{j0} \qquad \text{for } j \in W. \tag{3.47}$$

3.10.2. Analysis

The additional time-dependent indicator function in (3.42) leads to a more tedious analysis. The approach is the same as for the proof of Theorem 3.9.1. Consequently, we can conclude:

Corollary 3.10.1. *There exist unique and piecewise continuous differentiable solutions of* (3.42) - (3.44) *with initial conditions* (3.45) - (3.47). *The solutions are non-negative.*

3.10.3. Best fit simulation

The setting is the same as in section 3.9.3, only the fitted parameters change to

$$\Pi_{min}, \; \Delta\Pi, \; \xi_{p,j}, \; \sigma_w \text{ and } \; \xi_n.$$

Now, the solver performs without any warning and yields reasonable results. The parameters Π_{min} and $\Delta\Pi$ corresponds to the plateaus in in figure 3.24. The absorption rate σ_w is still in the same range as in the other cases as well as the two thresholds. We also have the same least squared residual of $7.1 \cdot 10^{-5}$ as in section 3.9.3. All best parameter fits and their estimated confidence intervals are given in table 3.8. A plot of the best fit extracellular FRET can be seen in figure 3.25. Note that it is similar to figure 3.23.

Parameter	Lower bound	Best fit	Upper bound
$\Pi_{min} \; [zmol/(l \cdot min)]$	1.98	3.83	5.72
$\Delta\Pi \; [zmol/(l \cdot min)]$	0.87	5.39	13.51
$\xi_{p,j} \; [\mu mol/l]$	0.26	6.31	14.83
$\sigma_w \; [pl/min]$	0.15	0.22	0.27
$\xi_n \; [\mu mol/l]$	0.09	37.64	69.42

Table 3.8.: Parameter confidence interval estimation of fit of model equations (3.42) and (3.43).
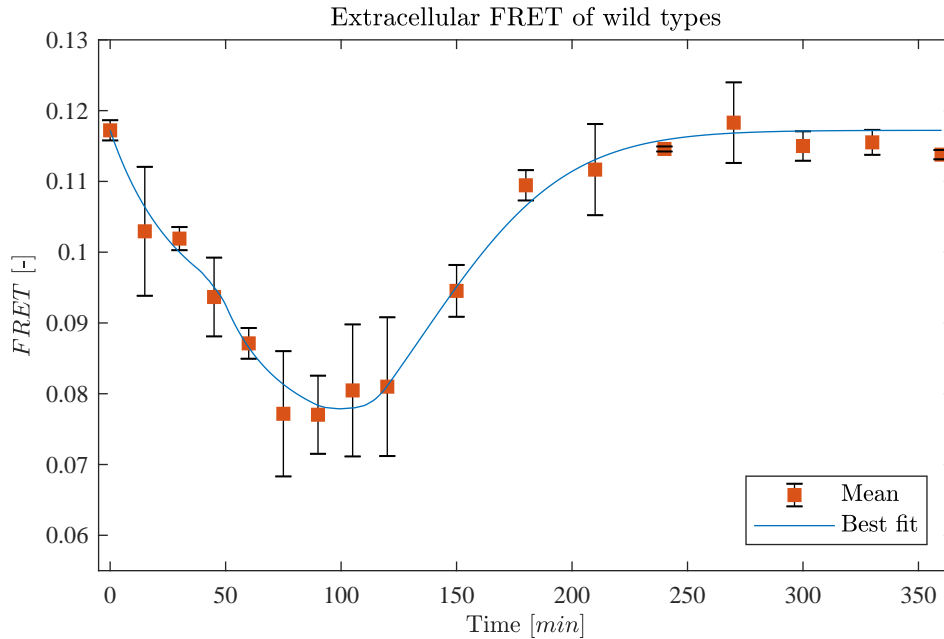
Figure 3.25.: *Best fit solution of extracellular FRET kinetics by model equations* (3.42) *and* (3.43) *with best fit parameters of the mutants given in table 3.3, the bacterial growth given in table 3.4 and of the wild types given in table 3.8.*

At last, we run a bootstrap in order to find the confidence interval of the fitted curves as in section 3.5.3. The result is given in figure 3.26. Within the narrow band lie all mean values and most of the standard deviations. Note that the band at the end is quite big which means that there are parameter constellations such that there are signalling molecules left in the supernatant meaning a subpopulation still produces signalling molecules. However, the production is then too little and due to the cell division, the intracellular concentration increases very slowly or even decreases. That means the threshold ξ_n can not be reached, at least not in the time interval we considered.
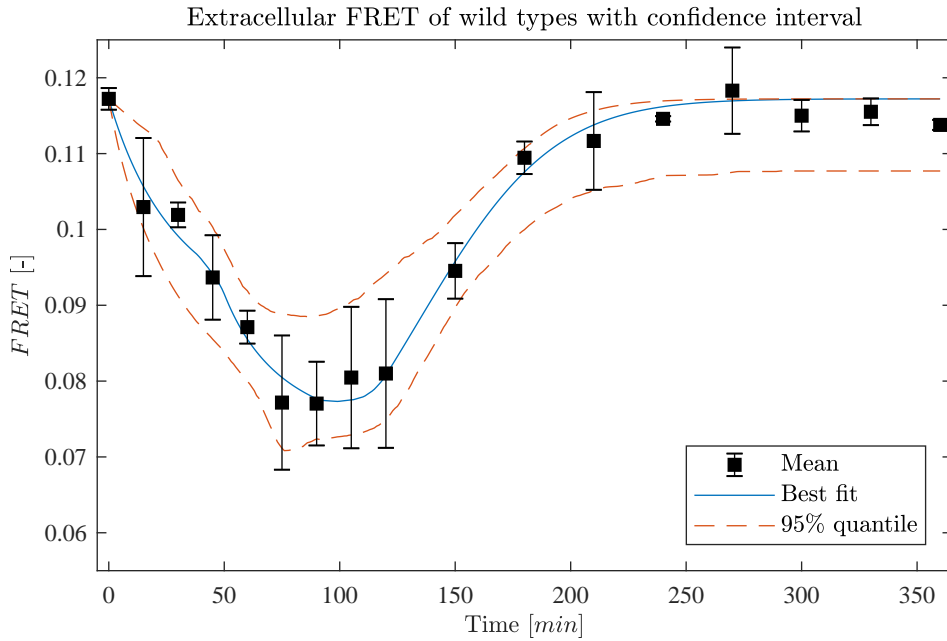
Figure 3.26.: *Best fit solution of extracellular FRET kinetics by model equations* (3.42) *and* (3.43) *depicted as solid blue line. Confidence interval of the fitted curve depicted as dashed red line.*

3.11. Consequences of competition effect

In section 3.7.3, we concluded for the wild type a competition effect regarding the absorption rate σ_w since the rate was a factor of 10 smaller than the absorption rate of the mutant σ_m. Then we improved the best fit step by step coming to the final result in 3.10. What we did not consider is a competition effect of the mutants absorption rate! That might be possible after consultation with *Bischofs*. So we perform a further best fit with positive and negative feedback regarding the time dependent production of signalling molecules but now choosing the mutants absorption rate as an additional fitting parameter. The best fit parameters inclusively their estimated parameter confidence interval is given in table 3.9, the graphical solution is given in figure 3.27. We can see, that we can fit the data points as well and the confidence interval of fitted curve is narrow and matches the standard deviation well. The parameter values of the production as well as the thresholds for the feedbacks increase about the factor 5.

Parameter	Lower bound	Best fit	Upper bound
$\Pi_{min}\ [zmol/(l \cdot min)]$	2.83	19.00	19.12
$\Delta\Pi\ [zmol/(l \cdot min)]$	$2 \cdot 10^{-7}$	26.9	31.32
$\xi_{p,j}\ [\mu mol/l]$	0.03	29.99	32.13
$\sigma_w\ [pl/min]$	0.10	0.21	0.40
$\sigma_m\ [pl/min]$	0.12	0.18	0.31
$\xi_n\ [\mu mol/l]$	1.90	179.99	233.15

Table 3.9.: Parameter confidence interval estimation of fit of model equations (3.42) and (3.43) with σ_m as additional fitting parameter.
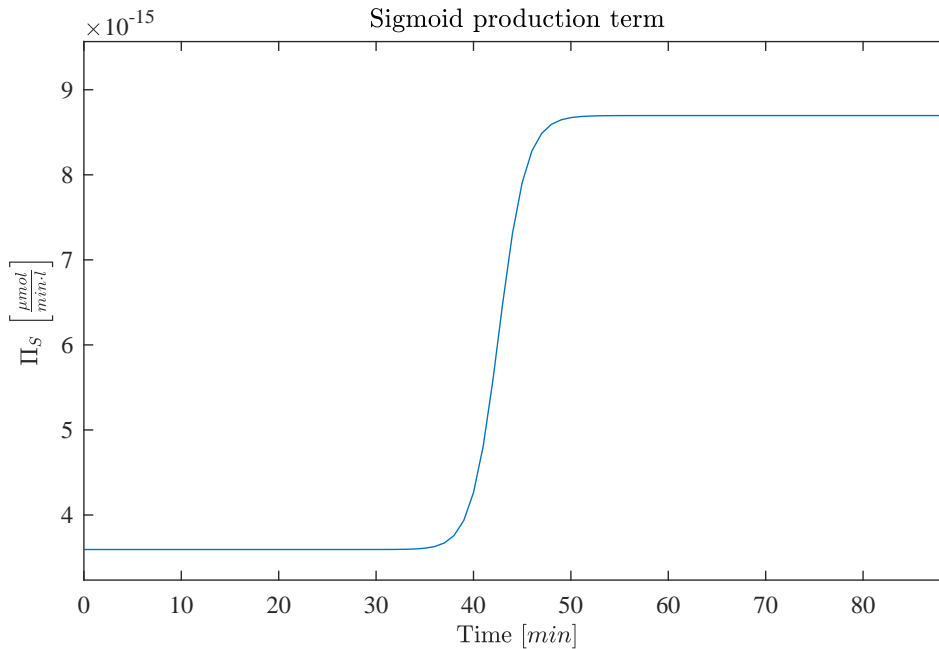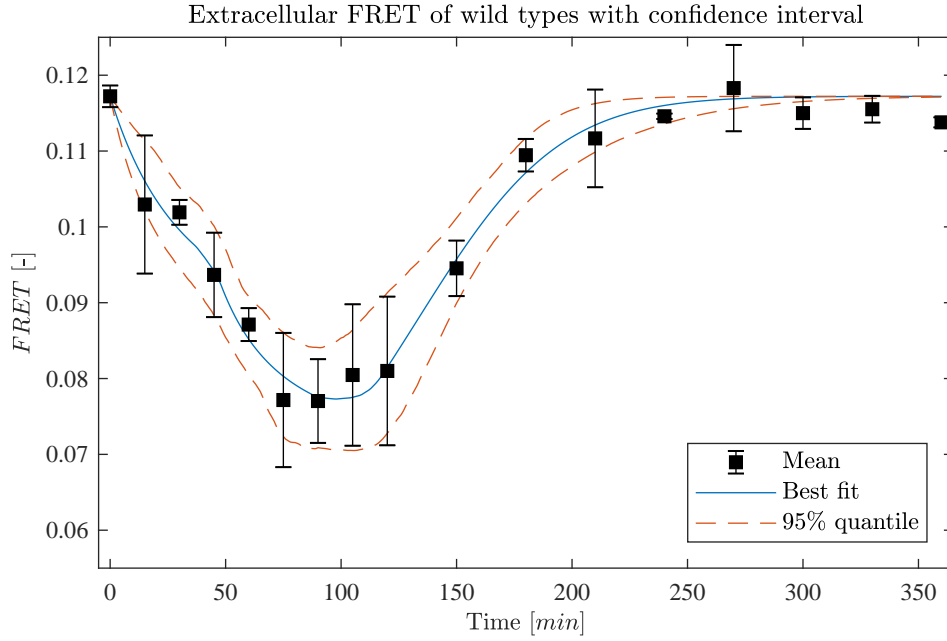

Figure 3.27.: *Best fit solution depicted as solid blue line of extracellular FRET kinetics by model equations (3.42) and (3.43) with best fit parameters of the mutants given in table 3.3, except for the absorption rate σ_m, the bacterial growth given in table 3.4 and of the wild types inclusively the mutant absorption rate given in table 3.9. Confidence interval of the fitted curve depicted as dashed red line.*

3.12. Conclusion for wild type

At the end, we can conclude three main results regarding production and absorption process of *Bacillus subtilis.*

We found that the production of signalling molecules had to stop in order to ensure an increase of extracellular FRET. With that data, we also can prove that it is important, that *Bacillus subtilis* absorb (at least for our cases) signalling molecules over time. But it is reasonable, that *Bacillus subtilis* stops some time the absorption of signalling molecules. This new hypothesis needs further experimental data to confirm or exclude it.

After that, we saw that the production period is separated in two stages. In the first stage, the production rate is constant, but low. After we have reached a certain intracellular signalling molecule concentration, the production rate jumps to a higher rate which is still constant.

Last but not least, there might be a competition effect regarding the absorption of signalling molecules. At first, the best fit absorption rate of the mutants was ten times higher than of the wild types. We suggested that the reason might be the further molecules the wild types produce and absorb together with the signalling molecule *PhrA*. That means the net rate of *PhrA* decreases and so do the absorption rate. But we didn't apply that assumption for the mutants immediately. When we did so, we were able to find a best fit solution but with higher parameter values in production rates and feedback thresholds. So the data is not consistent in order to determine the parameters of the production process. One needs further experiments to confirm or exclude competition effects of the absorption process. Since the μCats laboratory rather supports the idea of a competition effect, we will use the parameters in table 3.9 together with hypothesis HW 4 for further computations.

Chapter 4

PDE model

In chapter 3, we introduced a system of ordinary differential equations to model on the one hand the uptake process and on the other hand the production process of signalling molecule *PhrA* of *Bacillus subtilis*. We assumed homogeneously distributed bacteria within the shake flask as well as for the extracellular signalling molecule concentration. Biological experiments on a pad, however, showed up a small sporulation delay of mutant bacteria. Since mutants do not produce any signalling molecules, they have to wait until signalling molecules produced by wild types reaches them. This motivates to consider a spatial model of the signalling molecule uptake which is necessary to initiate the sporulation process.

In this chapter, we only introduce the experimental approach and results, the dynamic and the model equations. In contrast to the ODE case, the analysis of the PDE system is done in a separate chapter, see chapter 5.

4.1. Experimental approach and results

The diameter of the pad is $9mm$ and the biologists put $4 \cdot 10^4$ cells on it. Each cell forms then a microcolony. Then they performed two different experiments.
In the first experiment, they placed either only wild types on the pad and counted the spores for 80 hours or they placed mutants on the pad stimulating them with different concentrations of signalling molecule *PhrA* and counting spores again.
The second experiment is a wild type-mutant ratio experiment. Both types are placed on the pad of different population ratios and spores were counted for 80 hours again.
In figure 4.1, we can see the results which we can use later in order to compare it with the simulation results. Note that the experimental output is not the total number of spores, it is the number of spores per cell.

(a)

(b)
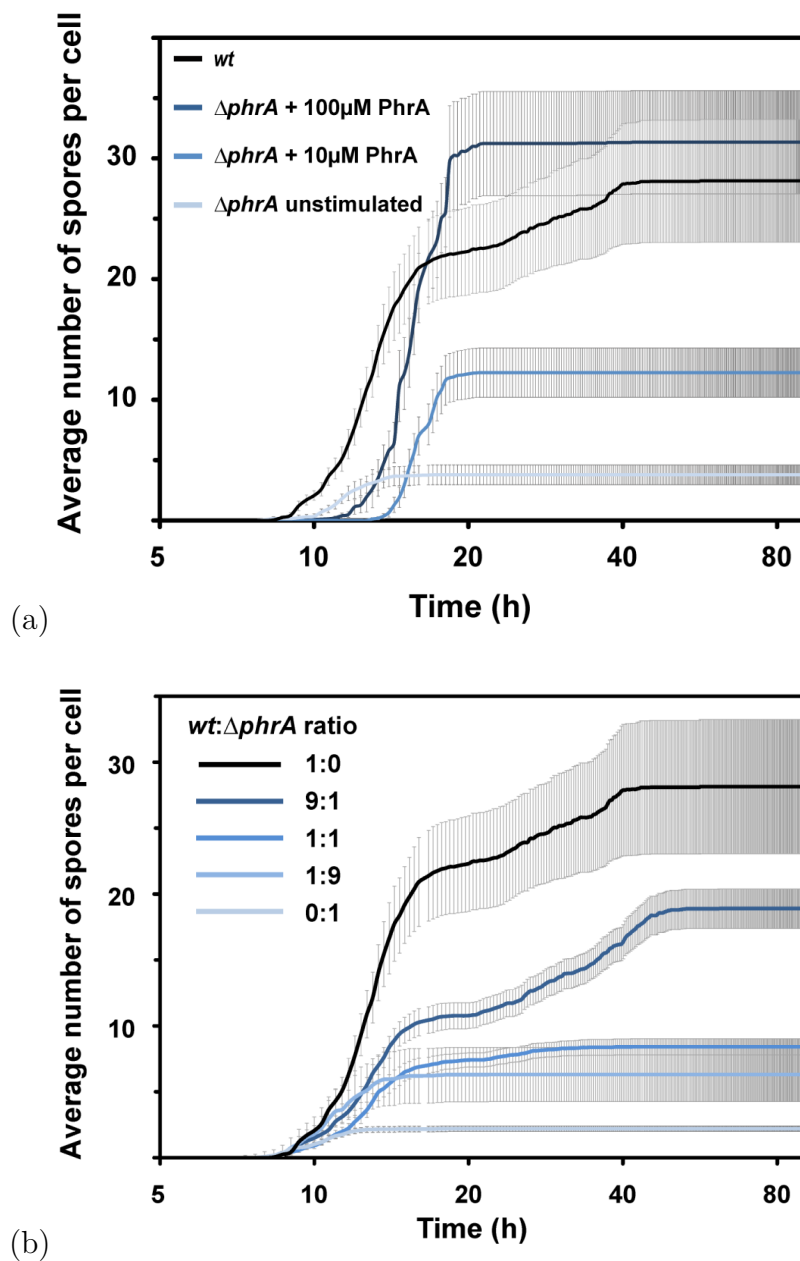
Figure 4.1.: *(a): Number of spores per cell of the stimulation experiment; wt corresponds to wild types and ΔphrA corresponds to mutants; (b): Number of spores per cell for different wild type-mutant ratios; These data sets and plots are from the μCats laboratory;*

Additionally, they counted the number of cells of a microcolony such that we can approximate the bacterial growth on the pad, see figure 4.2.
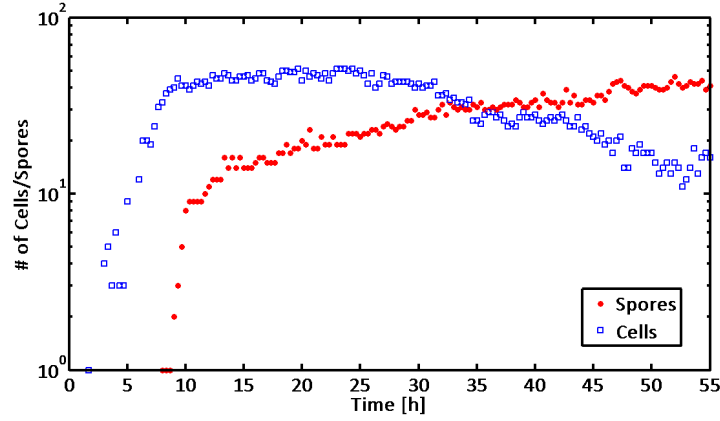
Figure 4.2.: *Bacterial growth of a microcolony; This data set and plot is from the μCats laboratory;*

4.2. Dynamic and model equations

As for the ODE system in chapter 3, the dynamic for the PDE system is similar and illustrated in figure 4.3. We just have to include spatial effects on the **pad** $\boldsymbol{\Omega} \subset \mathbb{R}^2_+$ of size $\boldsymbol{A}$. On the pad, there is a thin agarose layer of hight h. Henceforth the volume of the growth medium reads $V_e := \Omega \times h$. A consequence of the experimental approach is that we consider now bacterial colonies within V_e and each colony exists of only one type, that is either a wild type or a mutant. The colonies arise due to the cell division and the assumption, that spontaneous mutations are very rare. That's why we have separated, not mixed colonies. The **total number of wild type colonies** is given by $\boldsymbol{W_{max}}$, for **mutant colonies** by $\boldsymbol{M_{max}}$. The volume covered by *Bacillus* is denoted as $\boldsymbol{V_w}$ (wild types) resp. $\boldsymbol{V_m}$ (mutants) with $w \in W := \{W_1, \ldots, W_{max}\}$ and $m \in M := \{M_1, \ldots, M_{max}\}$. Obviously it holds $V_w, V_m \subset V_e$ for all $w \in W$ and $m \in M$. The density of **wild type bacteria** is denoted by $\boldsymbol{b_w(t, \vec{x})}$ for $\vec{x} := (x, y, z) \in V_w$ and **mutant bacteria** by $\boldsymbol{b_m(t, \vec{x})}$ for $\vec{x} \in V_m$ for $w \in W$ and $m \in M$. That means, $b(t, \vec{x}) = 0$ for $\vec{x} \in V_e \setminus V_w \cup V_m$ for all $w \in W$ and $m \in M$. Thus, the **bacterial density** is denoted by

$$
b(t, \vec{x}) := \begin{cases} b_w(t, \vec{x}) & \text{for } \vec{x} \in V_w \\[2ex] b_m(t, \vec{x}) & \text{for } \vec{x} \in V_m \\[2ex] 0 & \text{for } \vec{x} \in V_e \setminus V_w \cup V_m \end{cases}
$$

for all $w \in W$ and $m \in M$. The signalling molecule can be **absorbed** from both types with rate $\boldsymbol{\sigma}$. We denote this **intracellular signalling molecule concentration** again

by $C_i(t, \vec{x})$. As for the ODE model in chapter 3, we assume that hypothesis HW 4 holds. That means only wild type bacteria produce *PhrA* Pentapeptide with basal rate $\mathbf{\Pi_{min}}$ and a supplement rate $\mathbf{\Delta\Pi}$ and will be then transported outside the cell, becoming the **extracellular signalling molecule $C_e(t, \vec{x})$**. The transition from basal to maximal production rate $\Pi_{min} + \Delta\Pi$ is controlled by C_i. If it reaches the intracellular threshold $\boldsymbol{\xi_p(\vec{x})}$ per bacterium, then the change to the maximal production rate is initiated. The intracellular **threshold** such that the production of signalling molecules by the wild type stops is denoted by $\boldsymbol{\xi_n(\vec{x})}$ per bacterium. By deriving a suitable ODE model, we had the suspicion, that at some time the absorption of signalling molecules stops which is a contradiction to hypothesis HM 2. However, the ODE mutant experiments last only 20 minutes (plus one minute for centrifugation), the experiments regarding the PDE model takes much longer, though. Thus, we introduce for reasons of generality an intracellular threshold $\boldsymbol{\xi_a(\vec{x})}$ per bacterium such that the bacterium stops absorbing signalling molecules. We assume again, that $C_e(t, \vec{x})$ is **degraded** outside the cell with rate $\boldsymbol{\gamma_e}$. As in chapter 3, a logistic growth of bacteria is assumed with **exponential growth rate $\boldsymbol{\alpha}$,carrying capacity $\boldsymbol{\kappa}$** and independence of the intracellular signalling molecule concentration. Additionally we assume a non-moving boundary of the bacterial colony in the *x-y* plane, so we have only a movement induced by growth in *z* direction. Of course this is a rough simplification but it simplifies the manageability a lot. Last but not least, the most important term is missing, that is, the diffusion term of the signalling molecules. Usually, the thickness of the layer is small compared to the diameter of the entire pad. Thus, we assume that there is no gradient in *z* direction which means we only have movement of the signalling molecule concentration in *x-y* plane. This **diffusion** is constant with rate $\boldsymbol{D}$. However, the signalling molecules can't diffuse through the solid boundary of the pad, so they do not leave the reaction volume.
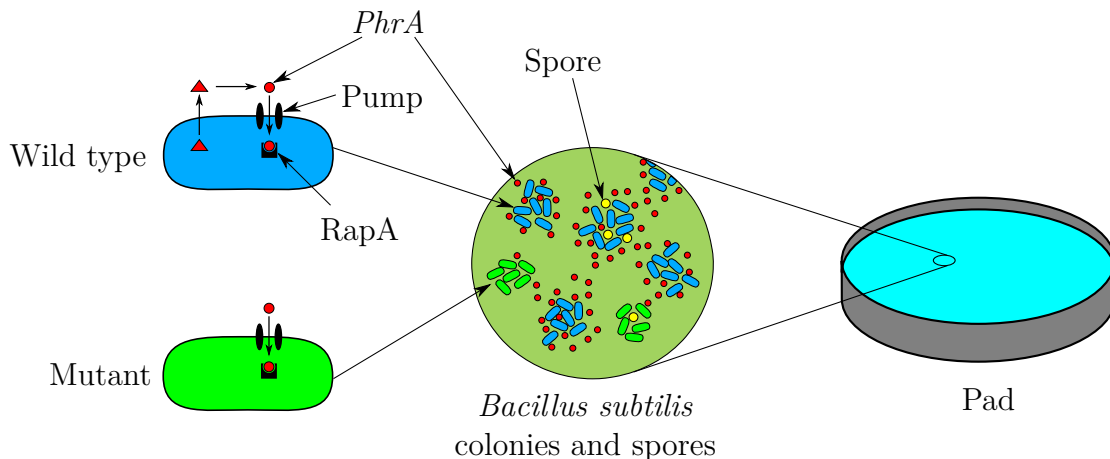
Figure 4.3.: *Scheme of the bacterial process and explained dynamic. Instead of homogeneous distributed bacteria, we have here colonies.*

As announced above, we consider now spatial effects for the extracellular signalling molecule concentration $C_e(t, \vec{x})$, leading to a PDE which is also known as Reaction-

Diffusion equation. The intracellular signalling molecule concentration $C_i(t, \vec{x})$ is described by an ordinary differential equation for each $\vec{x} \in V_w \cup V_m$ for all w, m. This is sufficient, since we are not interested in the cascade transition. Both equations are coupled which makes it difficult to solve. Since we assume only signalling molecules as a trigger for sporulation, the bacterial growth is independent of it. Thus, the equation for bacterial growth is decoupled from the PDE-ODE system. Let's explain the equations briefly.

We start to model the PDE. The propagation of quorum sensing signalling molecules, or better known as diffusion, can be modelled with the Laplace Operator. The reaction process contains on the one hand the production process, the plus term, and on the other hand the absorption process, the minus term, of signalling molecules. Note that only for wild type bacteria we have a production term of signalling molecules at $\vec{x} \in \Omega_w$. The hypothesis HW 4 from section 3.10 yields on the one hand two production phases whereas the switch is controlled by threshold $\bar{\xi}_p \in \mathbb{R}_+$. On the other hand, the cells stop to produce signalling molecules which are controlled by the threshold $\bar{\xi}_n \in \mathbb{R}_+$ and stop to absorb signalling molecules controlled by the threshold $\bar{\xi}_a \in \mathbb{R}_+$. We assume, that the thresholds are not constant in x-y plane. That means there is a noise for the thresholds to model the diversity of bacterial individuals. The noise varies only in the x-y plane yielding $\xi_n(\vec{x}) = \left| \bar{\xi}_n + 0.2 \cdot \bar{\xi}_n \nu(x, y) \right|$ with $\nu \sim \mathcal{N}\left(\begin{pmatrix} 0 \\ 0 \end{pmatrix}, \begin{pmatrix} 1 & 0 \\ 0 & 1 \end{pmatrix} \right)$, is chosen initially and then fixed for the whole simulation. We choose the perturbation in a way, such that 68.27% of the thresholds vary up to around 20% of the mean value. The same approach holds for the other thresholds $\xi_p(\vec{x})$ and $\xi_a(\vec{x})$, too. The switches in the right hand side can be expressed by indicator functions, see Definition 3.3.1, and should switch exactly once for each $\vec{x}$. Here, the corresponding set of the indicator function is of interest as well as the argument $C_i(t, \vec{x})$. Since the thresholds are given per bacterium, we have to multiply the thresholds with the bacterial density, e.g. $\xi_a(\vec{x}) b\left(t(\vec{x}), \vec{x} \right) =: \eta_a\left(t(\vec{x}), \vec{x} \right)$. Due to this fact, the indicator set changes in time caused by the bacterial growth. In this case, the set reads then $[0, \eta_a(t(\vec{x}), \vec{x})]$. So we have only switches if

$$C_i(t_a(\vec{x}), \vec{x}) = \eta_a(t_a(\vec{x}), \vec{x})$$

for $t_a(\vec{x}) \in [0, T]$ and $\vec{x} \in V_w \cup V_m$. For our application, we are again only interested in the first point in time when the switch arise. We use the same idea as for the ODE models in chapter 3. Note that the solution of (4.2) for $t \in [0, t_a(\vec{x})]$ reads

$$C_i(t, \vec{x}) = \int_0^t \sigma C_e(s, \vec{x}) b(s, \vec{x}) \, ds(\vec{x}).$$

Thus, $t_a(\vec{x})$ is defined implicitly by

$$t_a(\vec{x}) := \inf \left\{ t(\vec{x}) \in \mathbb{R}_+ : \int_0^{t(\vec{x})} \sigma C_e(s(\vec{x}), \vec{x}) b(s(\vec{x}), \vec{x}) \, ds(\vec{x}) = \eta_a(t(\vec{x}), \vec{x}) \right\}.$$

Note that $\inf\{\emptyset\} = \infty$. The terms $\eta_p(t, \vec{x})$ and $\eta_n(t, \vec{x})$ as well as $t_p(\vec{x})$ and $t_n(\vec{x})$ are defined analogously. Last but not least, we assume that degradation takes place all over the pad and is modelled as a negative term. The entire PDE for C_e is given in (4.1). Naturally, the ODE contains the same absorption part of the PDE, but with a changed sign. When the intracellular concentration reach threshold $\eta_a(t, \vec{x})$, absorption of signalling molecules stops. In contrast to the ODE model equations in chapter 3, we have no negative term caused by bacterial growth. There, we modelled the intracellular concentration for a single cell and had to include the bacterial growth. Now, we consider the intracellular concentration at a point $\vec{x}$ which is regardless of bacteria. Since we consider no propagation of the internal quorum sensing molecules, we obtain an ODE which is given in (4.2).

The bacteria grows according to the logistic equation and is given in (4.3) with the corresponding initial condition (4.6). Note that the logistic equation is decoupled from the other two equations.

Since signalling molecules can't leave the pad, we assume homogeneous Neumann boundary conditions, see (4.5). As initial condition, it is reasonable to assume no signalling molecules in the dish and bacteria, which has no peptides consumed. That leads to (4.4). Finally, for $t \in [0, T]$ and $\vec{x} \in V_e$ the system reads

$$
\begin{aligned}
\frac{\partial}{\partial t} C_e(t, \vec{x}) =& \nabla \left(\begin{pmatrix} D & 0 & 0 \\ 0 & D & 0 \\ 0 & 0 & 0 \end{pmatrix} \nabla C_e(t, \vec{x}) \right) - \gamma_e C_e(t, \vec{x}) \\
& - \chi_{[0, \eta_a(t_a(\vec{x}), \vec{x})]}(C_i(t, \vec{x})) \sigma C_e(t, \vec{x}) b(t, \vec{x}) \\
& + \sum_{w=W_1}^{W_{max}} \chi_{V_w}(\vec{x}) \chi_{[0, \eta_n(t_n(\vec{x}), \vec{x})]}(C_i(t, \vec{x})) \Pi_\chi \left(C_i(t, \vec{x}) \right) b(t, \vec{x})
\end{aligned}
\tag{4.1}
$$

$$
\frac{\partial}{\partial t} C_i(t, \vec{x}) = \chi_{[0, \eta_a(t_a(\vec{x}), \vec{x})]}(C_i(t, \vec{x})) \sigma C_e(t, \vec{x}) b(t, \vec{x})
\tag{4.2}
$$

$$
\frac{\partial}{\partial t} b(t, \vec{x}) = \alpha b(t, \vec{x}) \left(1 - \frac{b(t, \vec{x})}{\kappa} \right)
\tag{4.3}
$$

with

$$
C_e(0, \vec{x}) = C_i(0, \vec{x}) = 0
\tag{4.4}
$$

$$
\frac{\partial C_e}{\partial \boldsymbol{n}} = 0 \quad \text{for } \vec{x} \in \partial V_e
\tag{4.5}
$$

$$
b(0, \vec{x}) = \begin{cases} b_w(0, \vec{x}) = b_{w0}(\vec{x}) > 0 & \text{for } \vec{x} \in V_w \\[2mm] b_m(0, \vec{x}) = b_{m0}(\vec{x}) > 0 & \text{for } \vec{x} \in V_m \\[4mm] 0 & \text{for } \vec{x} \in V_e \setminus V_w \cup V_m \end{cases}
\tag{4.6}
$$

for all $w \in W$ and $m \in M$. $\boldsymbol{n}$ is the outer normal of ∂V_e and the production term

$$\Pi_\chi\left(C_i(t, \vec{x})\right) := \Pi_{min} + \chi_{(\eta_p(t_p(\vec{x}),\vec{x}),\infty)}(C_i(t,\vec{x}))\Delta\Pi$$

is similar to the one in the ODE model, see (3.41).

We stated the model equations for $\vec{x} = (x, y, z) \in \mathbb{R}^3$ but without movement in z direction and thus, no change due to the thin layer assumption. So instead of considering concentrations in $\mathbb{R}^3$, we want to work with surface densities in the x-y plane in $\mathbb{R}^2$, more specifically, in the pad Ω. This can be realized if we multiply the variables and initial conditions by the agarose layer height h, that is,

$$C_e(t, (x, y)) = h \cdot C_e(t, (x, y, z))$$
$$C_i(t, (x, y)) = h \cdot C_i(t, (x, y, z))$$
$$b(t, (x, y)) = h \cdot b(t, (x, y, z)).$$

Consequently, we denote the covered area of bacteria on the pad as Ω_w with $w \in W$ for wild types and Ω_m with $m \in M$ for mutants. Then for $t \in [0, T]$ and $\vec{x} = (x, y) \in \Omega$, the model equations simplify to

$$
\begin{aligned}
\frac{\partial}{\partial t}C_e(t, \vec{x}) =\ & D\nabla^2 C_e(t, \vec{x}) - \gamma_e C_e(t, \vec{x}) \\
& - \chi_{[0,\eta_a(t_a(\vec{x}),\vec{x})]}(C_i(t, \vec{x}))\frac{\sigma}{h}C_e(t, \vec{x})b(t, \vec{x}) \\
& + \sum_{w=W_1}^{W_{max}} \chi_{\Omega_w}(\vec{x})\chi_{[0,\eta_n(t_n(\vec{x}),\vec{x})]}(C_i(t, \vec{x}))\Pi_\chi\left(C_i(t, \vec{x})\right)b(t, \vec{x})
\end{aligned}
\tag{4.7}
$$

$$\frac{\partial}{\partial t}C_i(t, \vec{x}) = \chi_{[0,\eta_a(t_a(\vec{x}),\vec{x})]}(C_i(t, \vec{x}))\frac{\sigma}{h}C_e(t, \vec{x})b(t, \vec{x}) \tag{4.8}$$

$$\frac{\partial}{\partial t}b(t, \vec{x}) = \alpha b(t, \vec{x})\left(1 - \frac{b(t, \vec{x})}{h\kappa}\right) \tag{4.9}$$

with

$$C_e(0, \vec{x}) = C_i(0, \vec{x}) = 0 \tag{4.10}$$

$$\frac{\partial C_e}{\partial \boldsymbol{n}} = 0 \quad \text{for } \vec{x} \in \partial\Omega \tag{4.11}$$

$$b(0, \vec{x}) = \begin{cases} b_w(0, \vec{x}) = b_{w0}(\vec{x}) > 0 & \text{for } \vec{x} \in \Omega_{W_1} \cup \ldots \cup \Omega_{W_{max}} =: \Omega_W \\ b_m(0, \vec{x}) = b_{m0}(\vec{x}) > 0 & \text{for } \vec{x} \in \Omega_{M_1} \cup \ldots \cup \Omega_{M_{max}} =: \Omega_M \\ 0 & \text{for } \vec{x} \in \Omega \setminus \{\Omega_W \cup \Omega_M\} \end{cases} \qquad (4.12)$$

and

$$\Pi_\chi \left(C_i(t, \vec{x}) \right) := \Pi_{min} + \chi_{(\eta_p(t_p(\vec{x}), \vec{x}), \infty)}(C_i(t, \vec{x})) \Delta \Pi. \qquad (4.13)$$

Additionally, the first time point of the switches have to be rescaled to, that is e.g.

$$t_a(\vec{x}) := \inf \left\{ t(\vec{x}) \in \mathbb{R}_+ : \int_0^{t(\vec{x})} \frac{\sigma}{h} C_e(s(\vec{x}), \vec{x}) b(s(\vec{x}), \vec{x}) \, ds(\vec{x}) = \eta_a(t(\vec{x}), \vec{x}) \right\}$$

with

$$\eta_a(t, \vec{x}) = \xi_a(\vec{x}) b(t, \vec{x}).$$

The approach is analogous for $t_p(\vec{x})$ and $t_n(\vec{x})$.

Chapter 5

Analysis of the PDE-ODE system

After we have formulated the PDE-ODE system in chapter 4, we analyse the resulting equations mathematically. We'll be able to show the existence of a weak solution but the uniqueness can be only shown for a time constant population, that means $b(t, \vec{x}) = b(\vec{x})$. However, if we mollify the discontinuity then we can show besides the existence also the uniqueness of a weak solution for time dependent populations.

5.1. PDE-ODE system

We know that the coupled PDE-ODE system in (4.7) and (4.8) describing the quorum sensing process is decoupled of the bacterial growth in (4.9). In section 3.7, we calculated a solution of the logistic growth for the ODE, see equation (3.28). Using this approach, the solution of (4.9) holds for each $\vec{x} \in \Omega$ and tends to its steady state $h\kappa$ for all initial conditions, whether or not it is smaller or bigger than $h\kappa$. That means the bacterial growth solution $b(t, \vec{x})$ is positive and bounded, meaning that $b(t, \vec{x}) \in \mathcal{L}^\infty((0, T] \times \Omega) \subset \mathcal{L}^2((0, T] \times \Omega)$. Henceforth it is sufficient to consider only the reduced system (4.7) and (4.8) with its initial condition (4.10) and boundary condition (4.11) by using the solution $b(t, \vec{x})$. We show first that weak solutions of that system exist and that they are non-negative for almost every $\vec{x} \in \Omega$. Note that we have an indicator function in the right hand side, therefore there exists no "classical" or "strong" solution.

The existence of weak solutions can be shown by using Schauder's fixed point theorem, that is Theorem A.1.3.

Theorem 5.1.1 (Existence of weak solutions)**.** *There exists a non-negative weak solution of the coupled PDE-ODE system* (4.7) *and* (4.8) *with initial condition* (4.10) *and homogeneous Neumann boundary condition* (4.11)*.*

Proof. We transform the model equations (4.7), (4.8) into a fixpoint equation in order to apply Schauder's Fixed Point Theorem A.1.3. Choose $C_e(t, \vec{x}) = z(t, \vec{x}) \in \mathcal{L}^2((0, T] \times \Omega)$ arbitrary but fixed and consider the ODE

$$\frac{\partial}{\partial t} C_i(t, \vec{x}) = \chi_{[0, \eta_a(t_a(\vec{x}), \vec{x})]}(C_i(t, \vec{x})) \frac{\sigma}{h} z(t, \vec{x}) b(t, \vec{x}).$$

Integration by time yields

$$C_i(t, \vec{x}) = \underbrace{C_i(0, \vec{x})}_{=0} + \int_0^t \chi_{[0, \eta_a(t_a(\vec{x}), \vec{x})]}(C_i(t, \vec{x})) \frac{\sigma}{h} z(s, \vec{x}) b(s, \vec{x}) \, ds. \qquad (5.1)$$

The solution $b(t, \vec{x})$ and the indicator function χ are Lebesgue integrable. Thus, the integral in (5.1) exists and is also unique. If the indicator functions reach their jump discontinuities, then the value at $\vec{x}$ does not change any more in time which means the solution stay constant from that time point on. Note that this solution depends also on $z(t, \vec{x})$. Thus, we denote the solution of (5.1) from now on as $C_i(z(t, \vec{x}), t, \vec{x})$.

Now we insert solution $C_i(z(t, \vec{x}), t, \vec{x})$ into equation (4.7) leading to

$$\left.\begin{aligned}
\frac{\partial}{\partial t} C_e(t, \vec{x}) &= D\nabla^2 C_e(t, \vec{x}) - \gamma_e C_e(t, \vec{x}) \\
&\quad - \chi_{[0, \eta_a(t_a(\vec{x}), \vec{x})]}(C_i(z(t, \vec{x}), t, \vec{x})) \frac{\sigma}{h} C_e(t, \vec{x}) b(t, \vec{x}) \\
&\quad + \sum_{w=W_1}^{W_{max}} \chi_{\Omega_w}(\vec{x}) \chi_{[0, \eta_n(t_n(\vec{x}), \vec{x})]}(C_i(z(t, \vec{x}), t, \vec{x})) \Pi_\chi \left(C_i(z(t, \vec{x}), t, \vec{x}) \right) b(t, \vec{x}).
\end{aligned}\right\} P(z)$$

We apply the existence and uniqueness Theorem 2.2.15 on $P(z)$ and obtain the unique weak solution $C_e^* \in \mathcal{L}^2((0, T]; \mathcal{H}^1(\Omega))$. We prove now that this solution is non-negative:

Let's consider an auxiliary PDE system, given by

$$\begin{aligned}
\frac{\partial}{\partial t} v(t, \vec{x}) &= D\nabla^2 v(t, \vec{x}) - \frac{\sigma}{h} b(t, \vec{x}) - \gamma_e v(t, \vec{x}) \\
v(0, \vec{x}) &= 0 \\
\frac{\partial v}{\partial \boldsymbol{n}} &= 0.
\end{aligned}$$

This system is solved by the trivial weak solution $v(t, \vec{x}) = 0$. Using Corollary 2.2.21, we obtain that the weak solution C_e^* of $P(z)$ is a.e. non-negative for all $\vec{x} \in \Omega$. Using this fact, it is obvious that the ODE solution (5.1) is non-negative, too.

Since $z(t, \vec{x})$ was chosen arbitrarily we define a map

$$\Phi : \mathcal{L}^2_+((0, T]; \mathcal{H}^1(\Omega)) \to \mathcal{L}^2_+((0, T]; \mathcal{H}^1(\Omega))$$
$$z \mapsto C_e^*.$$

whereas the subscript $_+$ declares functions spaces considering only non-negative functions, e.g. $\mathcal{L}^2_+ := \{f \in \mathcal{L}^2 : f \geq 0 \text{ almost everywhere}\}$ endowed with the norm of $\mathcal{L}^2$. Consequently the function C_e^* is a non-negative weak solution of (4.7) if and only if C_e^* is a unique non-negative weak solution of $P(z)$, that is $\Phi(C_e^*) = C_e^*$ which means C_e^* is a fixed point of Φ. So we have to solve a fixed point equation. We will do this with the second version of Schauder's Theorem, see Theorem A.1.3.

As a first step, we have to find a convex, closed set and show that our defined operator is invariant. In the first instance we derive the weak formulation for (4.7) with C_e^* as a test function. This reads

$$\underbrace{\int_\Omega \frac{\partial}{\partial t} C_e^*(t, \vec{x}) C_e^*(t, \vec{x}) \, d\vec{x}}_{(1)} = \underbrace{D \int_\Omega \nabla^2 C_e^*(t, \vec{x}) C_e^*(t, \vec{x}) \, d\vec{x}}_{(2)}$$

$$- \underbrace{\int_\Omega \gamma_e C_e^*(t, \vec{x}) C_e^*(t, \vec{x}) \, d\vec{x}}_{(3)}$$

$$+ \underbrace{\int_\Omega -\chi_{[0, \eta_a(t_a(\vec{x}), \vec{x})]}(C_i(t, \vec{x})) \frac{\sigma}{h} C_e^*(t, \vec{x}) b(t, \vec{x}) C_e^*(t, \vec{x}) \, d\vec{x}}_{(4)} \tag{5.2}$$

$$+ \underbrace{\int_\Omega \sum_{w=W_1}^{W_{max}} \chi_{\Omega_w}(\vec{x}) \chi_{[0, \eta_n(t_n(\vec{x}), \vec{x})]}(C_i(t, \vec{x})) \Pi_\chi (C_i(t, \vec{x})) \, b(t, \vec{x}) C_e^*(t, \vec{x}) \, d\vec{x}}_{(5)}.$$

The terms (1), (2) and (3) can be reformulated to

$$(1) \Leftrightarrow \int_\Omega \frac{\partial}{\partial t} \frac{1}{2} \left(C_e^*(t, \vec{x})\right)^2 \, d\vec{x}$$

$$(2) \underset{\text{p. I.}}{\Leftrightarrow} \underbrace{[D\nabla C_e^*(t, \vec{x}) C_e^*(t, \vec{x})]_{\partial\Omega}}_{=0} - \int_\Omega D\nabla C_e^*(t, \vec{x}) \nabla C_e^*(t, \vec{x}) \, d\vec{x}$$

$$= -D\|\nabla C_e^*(t, \vec{x})\|^2_{\mathcal{L}^2(\Omega)}$$

$$(3) \Leftrightarrow \gamma\|C_e^*(t, \cdot)\|^2_{\mathcal{L}^2(\Omega)}.$$

Integrate the weak formulation (5.2) with respect to t. Since $C_e^*(t, \vec{x}) \in \mathcal{L}^2((0, T] \times \Omega)$ we can apply Fubini's Theorem A.4.1 and obtain

$$(1) \Leftrightarrow \quad \frac{1}{2}\left\|C_e^*(\bar{t},\cdot)\right\|_{\mathcal{L}^2(\Omega)}^2 + \underbrace{\frac{1}{2}\|C_e^*(0,\cdot)\|_{\mathcal{L}^2(\Omega)}^2}_{=0}$$

$$(2) \Leftrightarrow \quad \int_0^{\bar{t}} -D\|\nabla C_e^*(t,\cdot)\|_{\mathcal{L}^2(\Omega)}^2 \, dt$$

$$(3) \Leftrightarrow \quad \int_0^{\bar{t}} \gamma_e \|C_e^*(t,\cdot)\|_{\mathcal{L}^2(\Omega)}^2 \, dt$$

$$(4) \Leftrightarrow \quad \int_0^{\bar{t}} \int_\Omega -\chi_{[0,\eta_a(t_a(\vec{x}),\vec{x})]}(C_i(t,\vec{x}))\frac{\sigma}{h}C_e^{*2}(t,\vec{x})b(t,\vec{x}) \, d\vec{x} \, dt$$

$$(5) \Leftrightarrow \quad \int_0^{\bar{t}} \int_\Omega \sum_{w=W_1}^{W_{max}} \chi_{\Omega_w}(\vec{x})\chi_{[0,\eta_n(t_n(\vec{x}),\vec{x})]}(C_i(t,\vec{x}))\Pi_\chi\left(C_i(t,\vec{x})\right)b(t,\vec{x})C_e^*(t,\vec{x}) \, d\vec{x} \, dt.$$

We can find an upper estimation of the weak formulation of the PDE by neglecting (4) due to the negative integrand. This leads to

$$\frac{1}{2}\left\|C_e^*(\bar{t},\cdot)\right\|_{\mathcal{L}^2(\Omega)}^2 + \int_0^{\bar{t}} D\|\nabla C_e^*(t,\cdot)\|_{\mathcal{L}^2(\Omega)}^2 \, dt + \int_0^{\bar{t}} \gamma_e\|C_e^*(t,\cdot)\|_{\mathcal{L}^2(\Omega)}^2 \, dt$$

$$\leq \int_0^{\bar{t}} \int_\Omega \sum_{w=W_1}^{W_{max}} \chi_{\Omega_w}(\vec{x})\chi_{[0,\eta_n(t_n(\vec{x}),\vec{x})]}(C_i(t,\vec{x}))\Pi_\chi\left(C_i(t,\vec{x})\right)b(t,\vec{x})C_e^*(t,\vec{x}) \, d\vec{x} \, dt.$$

$$(5.3)$$

Young's inequality A.2.1 yields a further estimation for the right hand side of (5.3). Assume $\epsilon_w > 0 \; \forall w \in [W_1,\ldots,W_{max}]$, then

$$\int_0^{\bar{t}} \int_\Omega \sum_{w=W_1}^{W_{max}} \chi_{\Omega_w}(\vec{x})\chi_{[0,\eta_n(t_n(\vec{x}),\vec{x})]}(C_i(t,\vec{x}))\Pi_\chi\left(C_i(t,\vec{x})\right)b(t,\vec{x})C_e^*(t,\vec{x}) \, d\vec{x} \, dt$$

$$\leq \int_0^{\bar{t}} \int_\Omega \sum_{w=W_1}^{W_{max}} \chi_{\Omega_w}(\vec{x})\chi_{[0,\eta_n(t_n(\vec{x}),\vec{x})]}(C_i(t,\vec{x}))\epsilon_w C_e^{*2} + \frac{(2\epsilon_w)^{1-2}}{2}\left(b(t,\vec{x})\Pi_\chi\left(C_i(t,\vec{x})\right)\right)^2 \, d\vec{x} \, dt$$

$$\leq \int_0^{\bar{t}} \epsilon_{max}\|C_e^*(t,\cdot)\|_{\mathcal{L}^2(\Omega)}^2 + \int_0^{\bar{t}} \frac{(2\epsilon_{max})^{-\frac{1}{2}}\Pi_{max}^2}{2}\|b(t,\cdot)\|_{\mathcal{L}^2(\Omega)}^2 \, dt$$

for $\epsilon_{max} := \max\limits_{w\in[W_1,W_{max}]} \epsilon_w$ and $\Pi_{max} := \Pi_{min} + \Delta\Pi$. Using this estimation, equation (5.3) can be rewritten to

$$\int_0^{\bar{t}} (\gamma_e - \epsilon_{max})\|C_e^*(t,\cdot)\|_{\mathcal{L}^2(\Omega)}^2 \, dt \leq \int_0^{\bar{t}} \frac{(2\epsilon_{max})^{-\frac{1}{2}}\Pi_{max}^2}{2}\|b(t,\cdot)\|_{\mathcal{L}^2(\Omega)}^2 \, dt$$

$$- \frac{1}{2}\left\|C_e^*(\bar{t},\cdot)\right\|_{\mathcal{L}^2(\Omega)}^2 - \int_0^{\bar{t}} D\|\nabla C_e^*(t,\cdot)\|_{\mathcal{L}^2(\Omega)}^2 \, dt$$

$$\leq \tilde{Q}\bar{t}$$

with

$$\tilde{Q} := \int_0^{\bar{t}} \frac{(2\epsilon_{max})^{-\frac{1}{2}} \Pi_{max}^2}{2} \|b\|_{\mathcal{L}^\infty((0,T]\times\Omega)}^2 \, dt.$$

That is, if we choose $\epsilon_{max} \in (0, \gamma_e)$ we obtain

$$\int_0^{\bar{t}} \|C_e^*(t,\cdot)\|_{\mathcal{L}^2(\Omega)}^2 \, dt \leq Q\bar{t}$$

whereas $Q := \dfrac{\tilde{Q}}{\gamma_e - \epsilon_{max}}$. We immediately see, that

$$\int_0^{\bar{t}} \|C_e^*(t,\cdot)\|_{\mathcal{L}^2(\Omega)}^2 \, dt = \|C_e^*(t,\cdot)\|_{\mathcal{L}^2((0,\bar{t}]\times\Omega)}^2 = \|\Phi(z)\|_{\mathcal{L}^2((0,\bar{t}]\times\Omega)}^2.$$

So we choose $\bar{t} \leq \frac{1}{Q}$ such that $\|\Phi(z)\|_{\mathcal{L}^2((0,\bar{t}]\times\Omega)}^2 \leq 1$. That means the operator Φ maps $B_1(0)$ into itself. That corresponds to a non-empty, convex, bounded and closed set. That's an assumption in order to apply Schauder's second version, see Theorem A.1.3. Note, that the solution can be continuously extended to the whole interval $(0, T]$ by changing the integrals bounds first and repeat the approach analogously.

The second step is to show the compactness of Φ. Therefore one has to show that Φ maps bounded subsets to relatively compact subsets and that Φ is continuous. We start to proof the relative compactness. Since the right hand side, that is, $f := -(3) + (4) + (5)$ is in $\mathcal{L}^2((0,T] \times U)$, the weak solution $C_e^*(t, \vec{x})$ is in $\mathcal{H}^1((0,T] \times \Omega)$, see Theorem 2.2.17. Then we apply the Rellich-Kondrachov Theorem, see Theorem A.4.2. That means $\mathcal{W}^{1,2}((0,T] \times \Omega) = \mathcal{H}^1((0,T] \times \Omega)$ embedded continuously in $\mathcal{L}^6((0,T] \times \Omega)$ and embedded compactly in $\mathcal{L}^q((0,T] \times \Omega)$ with $1 \leq q \leq 6$, especially in $\mathcal{L}^2((0,T] \times \Omega)$. That is, C_e^* is in a function space, which can be embedded compactly in $\mathcal{L}^2((0,T] \times \Omega)$. Altogether, there is an operator $J^* : \mathcal{L}^2((0,T] \times \Omega) \to \mathcal{H}^1((0,T] \times \Omega)$. This operator is bounded due to the improved regularity of the weak solution C_e^*, see Theorem 2.2.17. Moreover, $\mathcal{H}^1((0,T] \times \Omega)$ can be embedded compactly into $\mathcal{L}^2((0,T] \times \Omega)$, i.e. the identity operator $id : \mathcal{H}^1((0,T] \times \Omega) \to \mathcal{L}^2((0,T] \times \Omega)$ is compact. By definition, this operator maps bounded subsets of $\mathcal{H}^1((0,T] \times \Omega)$ into relatively compact subsets of $\mathcal{L}^2((0,T] \times \Omega)$. That is, $J := id \circ J^*$ maps bounded subsets of $\mathcal{L}^2((0,T] \times \Omega)$ relatively compact into $\mathcal{L}^2((0,T] \times \Omega)$ respectively $J : \mathcal{L}_+^2((0,T] \times \Omega) \to \mathcal{L}_+^2((0,T] \times \Omega)$. Now we show the continuity of J by definition in terms of limits of sequences. Let $z_n \in \mathcal{L}^2((0,T] \times \Omega)$ with $z_n \to z \in \mathcal{L}^2((0,T] \times \Omega)$. First and foremost we check convergence of the ODE solution $C_i(z, t, \vec{x})$. W.l.o.g. we assume $C_i(z_n, t, \vec{x}) > C_i(z, t, \vec{x})$ for a $\vec{x} \in \Omega$. Then it holds

$$0 < C_i(z_n, t, \vec{x}) - C_i(z, t, \vec{x}) =$$

$$= \int_0^t \frac{\sigma}{h} b(t, \vec{x}) \chi_{[0, \eta_a(t_a(\vec{x}), \vec{x})]}(C_i(z_n, s, \vec{x})) z_n(s, \vec{x}) \, ds$$

$$- \int_0^t \frac{\sigma}{h} b(t, \vec{x}) \chi_{[0, \eta_a(t_a(\vec{x}), \vec{x})]}(C_i(z, s, \vec{x})) z(s, \vec{x}) \, ds$$

$$= \int_0^t \frac{\sigma}{h} b(t, \vec{x}) \underbrace{\left(\chi_{[0, \eta_a(t_a(\vec{x}), \vec{x})]}(C_i(z_n, s, \vec{x})) z_n(s, \vec{x}) - \chi_{[0, \eta_a(t_a(\vec{x}), \vec{x})]}(C_i(z_n, s, \vec{x})) z(s, \vec{x}) \right)}_{\to 0 \text{ for } z_n \to z}$$

$$+ \chi_{[0, \eta_a(t_a(\vec{x}), \vec{x})]}(C_i(z_n, s, \vec{x})) z(s, \vec{x}) - \chi_{[0, \eta_a(t_a(\vec{x}), \vec{x})]}(C_i(z, s, \vec{x})) z(s, \vec{x}) \Big) \, ds$$

$$= \int_0^t \underbrace{\frac{\sigma}{h} b(t, \vec{x})}_{>0} \quad \underbrace{\left(\chi_{[0, \eta_a(t_a(\vec{x}), \vec{x})]}(C_i(z_n, s, \vec{x})) z(s, \vec{x}) - \chi_{[0, \eta_a(t_a(\vec{x}), \vec{x})]}(C_i(z, s, \vec{x})) z(s, \vec{x}) \right)} \quad ds$$

$$\to \begin{cases} 0 \quad \lightning \quad \text{if } C_i(z_n, t, \vec{x}), C_i(z, t, \vec{x}) \in [0, \eta_a(t_a(\vec{x}), \vec{x})] \\[2mm] -1 \quad \lightning \quad \text{if } C_i(z_n, t, \vec{x}) \notin [0, \eta_a(t_a(\vec{x}), \vec{x})], \ C_i(z, t, \vec{x}) \in [0, \eta_a(t_a(\vec{x}), \vec{x})] \\[2mm] \qquad\qquad \Leftrightarrow C_i(z_n, t, \vec{x}) > C_i(z, t, \vec{x}) \\[2mm] 1 \qquad \text{if } C_i(z_n, t, \vec{x}) \in [0, \eta_a(t_a(\vec{x}), \vec{x})], \ C_i(z, t, \vec{x}) \notin [0, \eta_a(t_a(\vec{x}), \vec{x})] \\[2mm] \qquad\qquad \Leftrightarrow C_i(z_n, t, \vec{x}) < C_i(z, t, \vec{x}). \quad \lightning \end{cases}$$

Altogether, that is a contradiction, hence the assumption was wrong and $C_i(z_n, t, \vec{x})$ converges strongly against $C_i(z, t, \vec{x})$ in $\mathcal{L}^2((0, T] \times \Omega)$ for $z_n \to z$ strong in $\mathcal{L}^2((0, T] \times \Omega)$. Now we can check convergence of $(C_e^*)_n \to C_e^*$ for $n \to \infty$ respectively $(C_e^*)_n - C_e^* \to 0$ for $n \to \infty$. The sequence $C_i(z_n(t, \vec{x}), t, \vec{x})$ is bounded, hence the right hand side f as well. Thus, the solution $C_e^*(t, \vec{x})$ is bounded in $\mathcal{H}^1((0, T] \times \Omega)$ due to the same argument as before, that is, bounded subsets are embedded on relatively compact subsets. $\mathcal{H}^1((0, T] \times \Omega)$ embedded compactly in $\mathcal{L}^2((0, T] \times \Omega)$ (Theorem of Rellich-Kondrachov), that is, one can find one strong convergent subsequence $(C_e^*)_{n_k}$ in $\mathcal{L}^2((0, T] \times \Omega)$ with limit $\bar{C}_e$. The approach for the weak formulation of $(C_e^*)_{n_k} - C_e^*$ is analogously as in (5.2) and (5.3). Then we obtain the following estimation

$$\lim_{k \to \infty} \frac{1}{2} \|(C_e^*)_{n_k} - C_e^*\|_{\mathcal{L}^2(\Omega)} \le$$

$$\int_0^{\bar{t}} \int_\Omega \sum_{w=W_1}^{W_{max}} \Big\{ \chi_{\Omega_w}(\vec{x}) \chi_{[0,\eta_n(t_n(\vec{x}),\vec{x})]}(C_i(z_{n_k},t,\vec{x})) \left[\Pi_\chi \left(C_i(z_{n_k}t,\vec{x}) \right) b(t,\vec{x}) \right]$$

$$- \chi_{[0,\eta_a(t_a(\vec{x}),\vec{x})]}(C_i(z_{n_k},t,\vec{x})) \frac{\sigma}{h} (C_e^*)_{n_k} b(t,\vec{x})$$

$$- \chi_{\Omega_w}(\vec{x}) \chi_{[0,\eta_n(t_n(\vec{x}),\vec{x})]}(C_i(z,t,\vec{x})) \left[\Pi_\chi \left(C_i(z,t,\vec{x}) \right) b(t,\vec{x}) \right]$$

$$- \chi_{[0,\eta_a(t_a(\vec{x}),\vec{x})]}(C_i(z,t,\vec{x})) \frac{\sigma}{h} C_e^* b(t,\vec{x}) \Big\} \left((C_e^*)_{n_k} - C_e^* \right) \, d\vec{x} \, dt$$

$$\iff \left\| \bar{C}_e - C_e^* \right\|^2_{\mathcal{L}^2((0,T] \times \Omega)} \le \int_0^{\bar{t}} \chi_{[0,\eta_a(t_s(\vec{x}),\vec{x})]}(C_i(z,t,\vec{x})) \frac{\sigma}{h} b(t,\vec{x})(C_e^* - \bar{C}_e)(\bar{C}_e - C_e^*) \, d\vec{x} \, dt$$

$$\le 0$$

Thus, we can conclude $\bar{C}_e \to C_e^*$ for $k \to \infty$. This construction works for every arbitrary subsequence z_n, especially z_{n_k}. Hence, every subsequence of $(C_e)_n^*$ has a subsequence $(C_e^*)_{n_k}$ that converges against C_e^*. As a consequence, $(C_e^*)_n$ converges strongly against C_e^*, which corresponds to the continuity of operator J.
Finally, we can apply the second version of Schauder's fixed point theorem, i.e. Theorem A.1.3, which states the existence of at least one fixed point. $\qquad \square$

Let's consider a reduced system using the same arguments as for $P(z)$. Note that we can neglect the indicator function of the integral in (5.1) since all indicator functions of the PDE need the ODE solution only for $t \in [0, t_a(\vec{x})]$ because all switches have been done and the PDE is then independent of the ODE solution. Then the reformulated PDE equation reads

$$\frac{\partial}{\partial t} C_e(t,\vec{x}) = D \nabla^2 C_e(t,\vec{x}) - \gamma_e C_e(t,\vec{x})$$

$$- \chi_{[0,\eta_a(t_a(\vec{x}),\vec{x})]} \left(m_{C_e}(t,\vec{x}) \right) \frac{\sigma}{h} C_e(t,\vec{x}) b(\vec{x}) \tag{5.4}$$

$$+ \sum_{j=W_1}^{W_{max}} \chi_{\Omega_j}(\vec{x}) \chi_{[0,\eta_n(t_n(\vec{x}),\vec{x})]} \left(m_{C_e}(t,\vec{x}) \right) \Pi_\chi \left(m_{C_e}(t,\vec{x}) \right) b(\vec{x})$$

with

$$m_{C_e}(t,\vec{x}) := \int_0^t \frac{\sigma}{h} b(\vec{x}) C_e(s,\vec{x}) \, ds$$

allowing for a shorter notation.

We see, there exist a non-negative weak solution. But we don't know yet, if this weak solution of (4.7) and (4.8) is unique. Unfortunately, there is no proof of the uniqueness of the coupled PDE-ODE system (4.7) and (4.8) with non constant function $b(t, \vec{x})$ in time t. However, one can show that the PDE-ODE system has a solution for a constant function $b(\vec{x})$ in time.

Theorem 5.1.2 (Uniqueness of weak solutions for constant b)**.** *Let $supp(b(0, \vec{x})) \subset \Omega$, $b(0, \vec{x}) \in \mathcal{L}^{\infty}(\Omega)$ and $\frac{\partial}{\partial t} b(t, \vec{x}) = 0$. Then the weak solution of the coupled PDE-ODE system (4.7) and (4.8) with initial condition (4.10) and homogeneous Neumann boundary condition (4.11) is unique.*

Proof. Let's consider again the reformulated PDE (5.4). Since there is no bacterial growth, we can write $\eta(t_i(\vec{x}), \vec{x}) = \eta(\vec{x})$ for $i = a, n, p$ and obtain

$$
\begin{aligned}
\frac{\partial}{\partial t} C_e(t, \vec{x}) = & D\nabla^2 C_e(t, \vec{x}) - \gamma_e C_e(t, \vec{x}) \\
& - \chi_{[0, \eta_a(\vec{x})]} \left(m_{C_e}(t, \vec{x}) \right) \frac{\sigma}{h} C_e(t, \vec{x}) b(\vec{x}) \\
& + \sum_{j=W_1}^{W_{max}} \chi_{\Omega_j}(\vec{x}) \chi_{[0, \eta_n(\vec{x})]} \left(m_{C_e}(t, \vec{x}) \right) \Pi_\chi \left(m_{C_e}(t, \vec{x}) \right) b(\vec{x})
\end{aligned}
$$

with

$$
m_{C_e}(t, \vec{x}) = \int_0^t \frac{\sigma}{h} b(\vec{x}) C_e(s, \vec{x}) \, ds.
$$

When we have shown the uniqueness of the reformulated PDE solution, then we can easily follow the uniqueness of the ODE equation (4.8).

Note that the production term Π_χ is bounded since it was constructed as a step function. So we can conclude that there exist constants $K_1, K_2, M_1, M_2 > 0$ such that we obtain for all t and $\vec{x} \in \Omega_W \cup \Omega_M$

$$
K_1 \leq b(\vec{x}) \leq K_2 \tag{5.5}
$$

$$
M_1 \leq \Pi_\chi(m_{C_e}(t, \vec{x})) \leq M_2. \tag{5.6}
$$

We assume that there exist two weak solutions of the PDE (5.4) called y_1 and y_2. We define the difference of these solutions as $z := y_1 - y_2$ yielding

$$\frac{\partial}{\partial t} z(t, \vec{x}) = D\nabla^2 z(t, \vec{x}) - \gamma_e z(t, \vec{x}) - \Big[\chi_{[0,\eta_a(\vec{x})]} \left(m_{y_1}(t, \vec{x}) \right) y_1(t, \vec{x})$$

$$- \chi_{[0,\eta_a(\vec{x})]} \left(m_{y_2}(t, \vec{x}) \right) y_2(t, \vec{x}) \Big] \frac{\sigma}{h} b(\vec{x})$$

$$+ \sum_{j=W_1}^{W_{max}} \chi_{\Omega_j}(\vec{x}) \Big[\chi_{[0,\eta_n(\vec{x})]} \left(m_{y_1}(t, \vec{x}) \right) \Pi_\chi \left(m_{y_1}(t, \vec{x}) \right) \tag{5.7}$$

$$- \chi_{[0,\eta_n(\vec{x})]} \left(m_{y_2}(t, \vec{x}) \right) \Pi_\chi \left(m_{y_2}(t, \vec{x}) \right) \Big] b(\vec{x})$$

with

$$m_{y_1}(t, \vec{x}) = \int_0^t \frac{\sigma}{h} b(\vec{x}) y_1(s, \vec{x}) \, ds$$

$$m_{y_2}(t, \vec{x}) = \int_0^t \frac{\sigma}{h} b(\vec{x}) y_2(s, \vec{x}) \, ds.$$

Note that (5.7) has to be interpreted in the weak sense. Next, as a suitable test function, we choose a regularisation of the signum function such that we obtain a Lipschitz continuous function. We already did the same in the proof of Proposition 2.2.20 for the Heaviside function, see Definition 2.2.19. Analogously, we obtain for $\delta > 0$ following regularisation of the signum function:

$$\text{sign}_\delta(z) = \begin{cases} -1 & z < -\delta \\[2mm] \dfrac{z}{\delta} & -\delta \le z \le \delta \\[2mm] 1 & z > \delta. \end{cases}$$

Then the weak formulation of (5.7) reads

$$\int_\Omega \frac{\partial}{\partial s} z(t, \vec{x}) \, \text{sign}_\delta(z) \, d\vec{x} = D \int_\Omega \boldsymbol{\nabla}^2 z(t, \vec{x}) \, \text{sign}_\delta(z) \, d\vec{x} \tag{5.8}$$

$$- \gamma_e \int_\Omega z(t, \vec{x}) \, \text{sign}_\delta(z) \, d\vec{x} \tag{5.9}$$

$$- \int_\Omega \Big[\chi_{[0,\eta_a(\vec{x})]} \left(m_{y_1}(t, \vec{x}) \right) y_1(t, \vec{x})$$

$$- \chi_{[0,\eta_a(,\vec{x})]} \left(m_{y_2}(t, \vec{x}) \right) y_2(t, \vec{x}) \Big] \frac{\sigma}{h} b(\vec{x}) \, \text{sign}_\delta(z) \, d\vec{x} \tag{5.10}$$

$$+ \int_\Omega \sum_{j=W_1}^{W_{max}} \chi_{\Omega_j}(\vec{x}) \Big[\chi_{[0,\eta_n(\vec{x})]} \left(m_{y_1}(t, \vec{x}) \right) \Pi_\chi \left(m_{y_1}(t, \vec{x}) \right)$$

$$- \chi_{[0,\eta_n(\vec{x})]} \left(m_{y_2}(t, \vec{x}) \right) \Pi_\chi \left(m_{y_2}(t, \vec{x}) \right) \Big] b(\vec{x}) \, \text{sign}_\delta(z) \, d\vec{x}. \tag{5.11}$$

The main goal is to find a suitable estimation to apply Gronwall's inequality A.2.3 in order to show uniqueness. We consider first the Laplacian term in (5.8). Partial integration and chain rule leads to

$$
D \int_\Omega \boldsymbol{\nabla}^2 z(t,\vec{x}) z \, \mathrm{sign}_\delta(z) \, d\vec{x} = D \left(\underbrace{[\nabla z(t,\vec{x}) \, \mathrm{sign}_\delta(z)]_{\partial\Omega}}_{=0} - \int_\Omega \nabla z(t,\vec{x}) \nabla (\, \mathrm{sign}_\delta(z)) \, d\vec{x} \right)
$$

$$
= -D \int_\Omega (\nabla z(t,\vec{x}))^2 \underbrace{\frac{\mathrm{d}}{\mathrm{d}z} \, \mathrm{sign}_\delta(z)}_{\geq 0} \, d\vec{x} \leq 0.
$$

As a consequence, we can neglect this term and find an upper estimation of the right hand side of the PDE. Then, we can replace eventually the regularisation by the actual signum function due to the dominated convergence theorem, as we did in the proof of Proposition 2.2.20. Integrating the left hand side of (5.8), (5.9), (5.10) and (5.11) with respect to the time t we obtain

$$
\int_0^t \int_\Omega \frac{\partial}{\partial s} z(s,\vec{x}) \, \mathrm{sign}\,(z) \, d\vec{x}\, ds \leq -\gamma_e \int_0^t \int_\Omega z(s,\vec{x}) \, \mathrm{sign}\,(z) \, d\vec{x}\, ds \tag{5.12}
$$

$$
- \int_0^t \int_\Omega \Big[\chi_{[0,\eta_a(\vec{x})]}\,(m_{y_1}(s,\vec{x}))\, y_1(s,\vec{x}) \tag{5.13}
$$

$$
- \chi_{[0,\eta_a(\vec{x})]}\,(m_{y_2}(s,\vec{x}))\, y_2(s,\vec{x}) \Big] \frac{\sigma}{h} b(\vec{x}) \, \mathrm{sign}\,(z) \, d\vec{x}\, ds
$$

$$
+ \int_0^t \int_\Omega \sum_{j=W_1}^{W_{max}} \chi_{\Omega_j}(\vec{x}) \Big[\chi_{[0,\eta_n(\vec{x})]}\,(m_{y_1}(s,\vec{x}))\, \Pi_\chi\,(m_{y_1}(s,\vec{x})) \tag{5.14}
$$

$$
- \chi_{[0,\eta_n(\vec{x})]}\,(m_{y_2}(s,\vec{x}))\, \Pi_\chi\,(m_{y_2}(s,\vec{x})) \Big] b(\vec{x}) \, \mathrm{sign}\,(z) \, d\vec{x}\, ds.
$$

We can simplify the integral on the left hand side of (5.12) leading to

$$
\int_0^t \int_\Omega \frac{\partial}{\partial s} z(s,\vec{x}) \, \mathrm{sign}\,(z) \, d\vec{x}\, ds = \int_0^t \int_\Omega \frac{\partial}{\partial s} |z(s,\vec{x})| \, d\vec{x}\, ds
$$

$$
= \int_\Omega |z(t,\vec{x})| \, d\vec{x} - \int_\Omega |z(0,\vec{x})| \, d\vec{x}
$$

$$
= \|z(t,\cdot)\|_{L_1(\Omega)} - \|z(0,\cdot)\|_{L_1(\Omega)}. \tag{5.15}
$$

The term on the right hand side of (5.12) can be estimated upwards to

$$
-\gamma_e \int_0^t \int_\Omega z(s,\vec{x}) \, \mathrm{sign}\,(z) \, d\vec{x}\, ds = -\gamma_e \int_0^t \int_\Omega |z(s,\vec{x})| \, d\vec{x}\, ds \leq 0. \tag{5.16}
$$

The terms (5.13) and (5.14) are much more complicated to estimate. Nevertheless, it is possible after some tedious work. Note that the integrals are only non-zero where

we have some bacteria, that is, $\vec{x} \in \Omega_W \cup \Omega_M$. Otherwise the integrand becomes zero and the integral vanishes eventually. We start with (5.13) and take the absolute value of the term as well as use (5.5) in order to estimate the term upwards. Then it holds

$$|(5.13)| \leq \frac{\sigma}{h} K_2 \int_0^t \int_\Omega \Big| \Big[\chi_{[0,\eta_a(\vec{x})]} \left(m_{y_1}(s,\vec{x}) \right) y_1(s,\vec{x}) \tag{5.17}$$
$$- \chi_{[0,\eta_a(\vec{x})]} \left(m_{y_2}(s,\vec{x}) \right) y_2(s,\vec{x}) \Big] \Big| \, d\vec{x} \, ds.$$

The main part of this proof is to find a proper estimation of (5.17) regarding the applicability of Gronwall's Lemma. For this purpose, we try to find a suitable approximation of the integrand. The term in the bracket $[\ldots]$ in (5.17) can be rewritten to

$$[\ldots] = \underbrace{\chi_{[0,\eta_a(\vec{x})]} \left(m_{y_1}(s,\vec{x}) \right) y_1(s,\vec{x}) - \chi_{[0,\eta_a(\vec{x})]} \left(m_{y_1}(s,\vec{x}) \right) y_2(s,\vec{x})}_{=\chi_{[0,\eta_a(\vec{x})]} \left(m_{y_1}(s,\vec{x}) \right) z(s,\vec{x})}$$
$$+ \underbrace{\chi_{[0,\eta_a(\vec{x})]} \left(m_{y_1}(s,\vec{x}) \right) y_2(s,\vec{x}) - \chi_{[0,\eta_a(\vec{x})]} \left(m_{y_2}(s,\vec{x}) \right) y_2(s,\vec{x})}_{=y_2(s,\vec{x}) \left[\chi_{[0,\eta_a(\vec{x})]} \left(m_{y_1}(s,\vec{x}) \right) - \chi_{[0,\eta_a(\vec{x})]} \left(m_{y_2}(s,\vec{x}) \right) \right]}.$$

We can show that the absolute value of a solution y_1 resp. y_2 is bounded by a constant. Let $v(t)$ be the solution of $\dot{v}(t) = M_2$ with $v(0) = 0$ using the maximal production rate, see (5.6). Since an indicator function is an element of $\mathcal{L}^\infty$, we can apply Proposition 2.2.20 and conclude eventually that $y_2(s,\vec{x}) \leq v(s)$ for all $s \in [0,T]$ and $\vec{x} \in \Omega$. This solution $v(s)$ also solves $\frac{\partial}{\partial v}(t,\vec{x}) = \nabla^2 v(t,\vec{x}) + M_2$ with $\frac{\partial v(t,\vec{x})}{\partial \boldsymbol{n}} = 0$ since $v(s)$ is constant in $\vec{x}$. Then we can conclude that $v(s) \leq v(0) + M_2 s$ leads to $y_2(s,\vec{x}) \leq M_2 s$ for all $(s,\vec{x}) \in (0,T] \times \Omega$. Since $s \in [0,T]$, we obtain $y_2(s,\vec{x}) \leq C$ with $M_2 T =: C \in \mathbb{R}_+$ is constant. Using this result, (5.17) can be estimated to

$$(5.17) \leq \frac{\sigma}{h} K_2 \int_0^t \int_\Omega \underbrace{\left| \chi_{[0,\eta_a(\vec{x})]} \left(m_{y_1}(s,\vec{x}) \right) z(s,\vec{x}) \right|}_{\leq |z(s,\vec{x})|} \, d\vec{x} \, ds$$
$$+ C \int_0^t \int_\Omega \left| \chi_{[0,\eta_a(\vec{x})]} \left(m_{y_1}(s,\vec{x}) \right) - \chi_{[0,\eta_a(\vec{x})]} \left(m_{y_2}(s,\vec{x}) \right) \right| \, d\vec{x} \, ds. \tag{5.18}$$

The last integral (5.18) is now of interest. In order to estimate it in a proper way, we define the time points when the indicator functions become zero pointwise for all $\vec{x}$, that is,

$$m_{y_1}(t_1(\vec{x}),\vec{x}) = \int_0^{t_1(\vec{x})} \frac{\sigma}{h} b(\vec{x}) y_1(s,\vec{x}) \, ds = \eta_a(\vec{x}) \tag{5.19}$$

$$m_{y_2}(t_2(\vec{x}),\vec{x}) = \int_0^{t_2(\vec{x})} \frac{\sigma}{h} b(\vec{x}) y_2(s,\vec{x}) \, ds = \eta_a(\vec{x}). \tag{5.20}$$

Then we have to distinguish the cases which of the indicator functions become first zero.

Case 1: $t_1(\vec{x}) \leq t_2(\vec{x})$

The absolute value of (5.18) can be estimated to

$$\left| \chi_{[0,\eta_a(\vec{x})]}\left(m_{y_1}(s,\vec{x})\right) - \chi_{[0,\eta_a(\vec{x})]}\left(m_{y_2}(s,\vec{x})\right) \right| \leq \chi_{[t_1(\vec{x}),t_2(\vec{x})]}(s).$$

If $t \leq t_1(\vec{x}) \leq t_2(\vec{x})$ then for (5.18) it holds

$$C \int_0^t \left| \chi_{[0,\eta_a(\vec{x})]}\left(m_{y_1}(t,\vec{x})\right) - \chi_{[0,\eta_a(\vec{x})]}\left(m_{y_2}(t,\vec{x})\right) \right| ds \leq C \int_0^t \chi_{[t_1(\vec{x}),t_2(\vec{x})]}(s) \, ds$$
$$= 0.$$

For $t_1(\vec{x}) \leq t \leq t_2(\vec{x})$ the integral is non-zero. Since we integrate over a indicator function, the integral is nothing else than the Lebesgue measure of the corresponding domain, that is,

$$\int_0^t \int_{\Omega_A} \left| \chi_{[0,\eta_a(\vec{x})]}\left(m_{y_1}(t,\vec{x})\right) - \chi_{[0,\eta_a(\vec{x})]}\left(m_{y_2}(t,\vec{x})\right) \right| d\vec{x} \, ds$$
$$\leq \int_0^t \int_{\Omega_A} \chi_{[t_1(\vec{x}),t_2(\vec{x})]}(s) \, d\vec{x} \, ds$$
$$= \lambda \left(\underbrace{\{(\vec{x},s) \in \Omega \times [0,t] : t_1(\vec{x}) \leq s \leq t_2(\vec{x})\}}_{=:A(t)} \right).$$

Due to the definition in (5.19) and (5.20) we obtain

$$0 \geq \int_0^{\min\{t,t_2(\vec{x})\}} \frac{\sigma}{h} b(\vec{x}) y_2(s,\vec{x}) \, ds - \int_0^{t_1(\vec{x})} \frac{\sigma}{h} b(\vec{x}) y_1(s,\vec{x}) \, ds$$
$$= \int_{t_1(\vec{x})}^{\min\{t,t_2(\vec{x})\}} \frac{\sigma}{h} b(\vec{x}) y_2(s,\vec{x}) \, ds + \int_0^{t_1(\vec{x})} \frac{\sigma}{h} b(\vec{x}) \left[y_2(s,\vec{x}) - y_1(s,\vec{x}) \right] \, ds.$$

The first integral can be estimated downwards by using Corollary 2.2.21. The solution $y_2(s,\vec{x})$ can be compared with the solution of $\frac{\partial}{\partial t}\Psi(t,\vec{x}) = \nabla^2\Psi(t,\vec{x}) - K_2\frac{\sigma}{h}\Psi(t,\vec{x}) - \gamma_e\Psi(t,\vec{x})$.

Lemma 2.2.22 yields a solution to that system. The second integral can be estimated downwards by using (5.5) and the fact $x - y \geq -|x - y|$. Altogether, we obtain

$$0 \geq \int_{t_1(\vec{x})}^{\min\{t,t_2(\vec{x})\}} \frac{\sigma}{h} K_1 \Psi(s,\vec{x}) \, ds - \frac{\sigma}{h} K_2 \int_0^t |y_1(s,\vec{x}) - y_2(s,\vec{x})| \, ds \qquad (5.21)$$

with $\Psi(s, \vec{x}) := e^{-\left(K_2\frac{\sigma}{h} + \gamma_e\right)s}\zeta(s, \vec{x})$. The function $\zeta(s, \vec{x})$ solves $\frac{\partial}{\partial s}\zeta(s, \vec{x}) = \nabla^2\zeta(s, \vec{x})$ with $\zeta(s_0, \vec{x}) = y_2(s_0, \vec{x})$ and $s_0 \in (0, t^*)$. The solution Ψ needs to be non-zero, thus, we show that $\zeta(s, \vec{x})$ is a non-zero solution.

We have already shown that $y_2(s, \vec{x}) \leq M_2s$ for all $(s, \vec{x}) \in (0, T] \times \Omega$. That means the right hand side of the original PDE (5.4) performs no jumps as long as it holds

$$\int_0^t b(\vec{x})y_2(s, \vec{x})\,ds \leq \int_0^t b(\vec{x})M_2s\,ds$$
$$\leq \int_0^t K_2M_2s\,ds \stackrel{!}{\leq} \min_{x \in \Omega_W \cup \Omega_M}\eta_a(\vec{x}). \tag{5.22}$$

The left hand side of (5.22) is monotonously increasing. That means there exists a $t^* > 0$ which solves the equality of (5.22). This time point is the earliest time point when changes in the right hand side of (5.4) appear. Until that, the reaction term is non-zero and so is the solution $y_2(t, \vec{x})$ for $(t, \vec{x}) \in (0, t^*)_W \cup \Omega_M$. We choose $s_0 \in (0, t^*)$ such that the initial value $\zeta(s_0, \vec{x}) = y_2(s_0, \vec{x})$ is non-zero for all $\vec{x} \in \Omega_W \cup \Omega_M$.

Let's assume that $\zeta(t_1, \vec{x}_1) = 0$ for $(t_1, \vec{x}_1) \in (s_0, T] \times \Omega$. Since $\zeta(s_0, \vec{x})$ is non-zero for $\vec{x} \in \Omega_w \cup \Omega_M$ and we have homogeneous Neumann boundary conditions, it is obvious that $\zeta(s, \vec{x}) \geq 0$ for $(t, \vec{x}) \in (s_0, T) \times \Omega$. Thus, we have a minimum at $(t_1, \vec{x}_1)$. Then the strong maximum principle of Laplace, Theorem A.5.1, yields $\zeta(t, \vec{x}) = 0$ on $(s_0, t_1] \times \Omega$. That's a contradiction to $\zeta(s, \vec{x}) > 0$ for $(t, \vec{x}) \in (s_0, T) \times \Omega_W \cup \Omega_M$. Thus, the solution $\zeta(t, \vec{x})$ is non-zero in $(s_0, T] \times \Omega$. Since $\mathrm{supp}(b(0, \vec{x})) \subset \Omega$, it is sufficient that we have this conclusion only for the inner of Ω. Then we choose a compact set $K := \mathrm{supp}(b(0, \vec{x})$ such that

$$\min_{(s, \vec{x}) \in (t^*, T) \times K}\zeta(s, \vec{x}) =: \theta > 0 \tag{5.23}$$

because of the continuity of $\zeta(s, \vec{x})$.

Case 2: $t_1(\vec{x}) \geq t_2(\vec{x})$

The approach of case 2 is similar to case 1. The absolute value of (5.18) can be estimated again to

$$\left|\chi_{[0,\eta_a(\vec{x})]}\left(m_{y_1}(s, \vec{x})\right) - \chi_{[0,\eta_a(\vec{x})]}\left(m_{y_2}(s, \vec{x})\right)\right| \leq \chi_{[t_2(\vec{x}), t_1(\vec{x})]}(s).$$

If $t \leq t_2(\vec{x}) \leq t_1(\vec{x})$ then (5.18) leads to

$$C\int_0^t\int_\Omega\left|\chi_{[0,\eta_a(\vec{x})]}\left(m_{y_1}(t, \vec{x})\right) - \chi_{[0,\eta_a(\vec{x})]}\left(m_{y_2}(t, \vec{x})\right)\right|\,d\vec{x}\,ds \leq 0.$$

For $t_2(\vec{x}) \leq t \leq t_1(\vec{x})$ we obtain the Lebesgue measure of the domain, that is,

$$\int_0^t \int_\Omega \left| \chi_{[0,\eta_a(\vec{x})]}\left(m_{y_1}(t,\vec{x})\right) - \chi_{[0,\eta_a(\vec{x})]}\left(m_{y_2}(t,\vec{x})\right) \right| d\vec{x}\, ds$$

$$\leq \lambda \left(\underbrace{\{(\vec{x},s) \in \Omega \times [0,t] : t_2(\vec{x}) \leq s \leq t_1(\vec{x})\}}_{=:B(t)} \right).$$

Again, the definition in (5.19) and (5.20) yields

$$0 \geq \int_0^{\min\{t,t_1(\vec{x})\}} \frac{\sigma}{h} b(\vec{x}) y_1(s,\vec{x})\, ds - \int_0^{t_2(\vec{x})} \frac{\sigma}{h} b(\vec{x}) y_2(s,\vec{x})\, ds$$

$$= \int_{t_2(\vec{x})}^{\min\{t,t_1(\vec{x})\}} \frac{\sigma}{h} b(\vec{x}) y_1(s,\vec{x})\, ds + \int_0^{t_2(\vec{x})} \frac{\sigma}{h} b(\vec{x}) \left[y_1(s,\vec{x}) - y_2(s,\vec{x}) \right]\, ds.$$

Using the same arguments as for case 1, we obtain

$$0 \geq \int_{t_2(\vec{x})}^{\min\{t,t_1(\vec{x})\}} \frac{\sigma}{h} K_1 \Psi(s,\vec{x})\, ds - \frac{\sigma}{h} K_2 \int_0^t |y_2(s,\vec{x}) - y_1(s,\vec{x})|\, ds \qquad (5.24)$$

with $\Psi(s,\vec{x}) := e^{-\left(K_2 \frac{\sigma}{h} + \gamma_e\right)s} \zeta(s,\vec{x})$ and $\zeta(s,\vec{x})$ solves $\frac{\partial}{\partial s}\zeta(s,\vec{x}) = \nabla^2\zeta(s,\vec{x})$ with $\zeta(s_0,\vec{x}) = y_1(s_0,\vec{x}) \neq 0$.

Adding (5.21) and (5.24) we obtain an estimation for (5.18) for all $t \in [0,T]$ and pointwise for almost all $\vec{x} \in \Omega$.

$$0 \geq \int_{t_1(\vec{x})}^{\min\{t,t_2(\vec{x})\}} K_1 \Psi(s,\vec{x})\, ds + \int_{t_2(\vec{x})}^{\min\{t,t_1(\vec{x})\}} K_1 \Psi(s,\vec{x})\, ds$$

$$- 2K_2 \int_0^t |y_1(s,\vec{x}) - y_2(s,\vec{x})|\, ds. \qquad (5.25)$$

Furthermore it holds

$$\Psi(t,\vec{x}) = e^{-\left(K_2 \frac{\sigma}{h} + \gamma_e\right)s} \zeta(s,\vec{x}) \geq e^{-\left(K_2 \frac{\sigma}{h} + \gamma_e\right)s} \theta.$$

Then we can conclude

$$\int_{t_1(\vec{x})}^{\min\{t,t_2(\vec{x})\}} K_1 \Psi(s,\vec{x})\, ds \geq \int_{t_1(\vec{x})}^{\min\{t,t_2(\vec{x})\}} K_1 \theta e^{-\left(K \frac{\sigma}{h} + \gamma_e\right)s}\, ds$$

$$\geq \underbrace{\min_{s \in [0,T]} K_1 \theta e^{-\left(K \frac{\sigma}{h} + \gamma_e\right)s}}_{=:\beta} |\min\{t,t_2(\vec{x})\} - t_1(\vec{x})|.$$

Analogously,

$$\int_{t_2(\vec{x})}^{\min\{t,t_1(\vec{x})\}} K_1 \Psi(s,\vec{x}) \, ds \geq \beta |\min\{t, t_1(\vec{x})\} - t_2(\vec{x})|.$$

Using these two inequalities, inequality (5.25) estimates to

$$
\begin{aligned}
0 \geq &\beta|\min\{t, t_2(\vec{x})\} - t_1(\vec{x})| + \beta|\min\{t, t_1(\vec{x})\} - t_2(\vec{x})| \\
&- 2K_2 \int_0^t |y_1(s,\vec{x}) - y_2(s,\vec{x})| \, ds.
\end{aligned}
$$

Integration over the domain Ω leads to

$$\frac{K_2}{\beta} \underbrace{\int_\Omega \int_0^t |y_1(s,\vec{x}) - y_2(s,\vec{x})| \, ds \, d\vec{x}}_{\|z\|_{L_1(\Omega \times [0,T])}} \geq \underbrace{\int_\Omega |\min\{t, t_2(\vec{x})\} - t_1(\vec{x})| \, d\vec{x}}_{=\lambda(A(t))}$$

$$+ \underbrace{\int_\Omega |\min\{t, t_1(\vec{x})\} - t_2(\vec{x})| \, d\vec{x}}_{=\lambda(B(t))}.$$

Finally we obtain a suitable estimation for (5.18)

$$
\begin{aligned}
C \int_0^t \int_\Omega \left| \chi_{[0,\eta_a(\vec{x})]} \left(m_{y_1}(t,\vec{x})\right) - \chi_{[0,\eta_a(\vec{x})]} \left(m_{y_2}(t,\vec{x})\right) \right| d\vec{x} \, ds &\leq C(\lambda(A(t)) + \lambda(B(t))) \\
&\leq \frac{CK_2}{\beta} \|z\|_{L_1(\Omega \times [0,t])} \quad (5.26)
\end{aligned}
$$

and thus, using (5.17), (5.18) and (5.26), we find a proper upper estimation for (5.13):

$$
\begin{aligned}
- \int_0^t \int_\Omega &\Big[\chi_{[0,\eta_a(\vec{x})]} \left(m_{y_1}(s,\vec{x})\right) y_1(s,\vec{x}) \\
&- \chi_{[0,\eta_a(\vec{x})]} \left(m_{y_2}(s,\vec{x})\right) y_2(s,\vec{x}) \Big] \frac{\sigma}{h} b(\vec{x}) \operatorname{sign}(z) \, d\vec{x} \, ds \\
\leq &- \frac{\sigma}{h} K_2 \|z\|_{L_1(\Omega \times [0,t])} + \frac{CK_2}{\beta} \|z\|_{L_1(\Omega \times [0,t])}.
\end{aligned}
\quad (5.27)
$$

Last but not least, the production term (5.14) has to be estimated upwards. Taking the absolute value and using the upper bound of $b(\vec{x})$, see inequality (5.5), we obtain

$$
\begin{aligned}
|(5.14)| \leq K_2 \int_0^t \int_\Omega &\big| \chi_{[0,\eta_n(\vec{x})]} \left(m_{y_1}(s,\vec{x})\right) \Pi_\chi \left(m_{y_1}(s,\vec{x})\right) \\
&- \chi_{[0,\eta_n(\vec{x})]} \left(m_{y_2}(s,\vec{x})\right) \Pi_\chi \left(m_{y_2}(s,\vec{x})\right) \big| \, d\vec{x} \, ds.
\end{aligned}
\quad (5.28)
$$

The argument of the absolute value in (5.28) can be added with terms summing up to zero. Then we can use the triangular inequality to estimate the absolute value upwards:

$$
\begin{aligned}
&\left| \chi_{[0,\eta_n(\vec{x})]}\left(m_{y_1}(t,\vec{x})\right) \Pi_\chi\left(m_{y_1}(t,\vec{x})\right) - \chi_{[0,\eta_n(\vec{x})]}\left(m_{y_2}(t,\vec{x})\right) \Pi_\chi\left(m_{y_2}(t,\vec{x})\right) \right| \\
&= \left| \chi_{[0,\eta_n(\vec{x})]}\left(m_{y_1}(t,\vec{x})\right) \Pi_\chi\left(m_{y_1}(t,\vec{x})\right) - \chi_{[0,\eta_n(\vec{x})]}\left(m_{y_2}(t,\vec{x})\right) \Pi_\chi\left(m_{y_1}(t,\vec{x})\right) \right. \\
&\quad \left. + \chi_{[0,\eta_n(\vec{x})]}\left(m_{y_2}(t,\vec{x})\right) \Pi_\chi\left(m_{y_1}(t,\vec{x})\right) - \chi_{[0,\eta_n(\vec{x})]}\left(m_{y_2}(t,\vec{x})\right) \Pi_\chi\left(m_{y_2}(t,\vec{x})\right) \right| \\
&\leq \left| \Pi_\chi\left(m_{y_1}(t,\vec{x})\right) \left[\chi_{[0,\eta_n(\vec{x})]}\left(m_{y_1}(t,\vec{x})\right) - \chi_{[0,\eta_n(\vec{x})]}\left(m_{y_2}(t,\vec{x})\right) \right] \right| && (5.29) \\
&\quad + \left| \chi_{[0,\eta_n(\vec{x})]}\left(m_{y_2}(t,\vec{x})\right) \left[\Pi_\chi\left(m_{y_1}(t,\vec{x})\right) - \Pi_\chi\left(m_{y_2}(t,\vec{x})\right) \right] \right|. && (5.30)
\end{aligned}
$$

The function Π_χ is bounded due to its construction:

$$
0 \leq |\Pi_\chi| \leq \Pi_{min} + \Delta\Pi := \Pi_{max}.
$$

Additionally, the difference of functions Π_χ reads

$$
\Pi_\chi\left(m_{y_1}(t,\vec{x})\right) - \Pi_\chi\left(m_{y_2}(t,\vec{x})\right) = \Delta\Pi \left[\chi_{[\eta_p(\vec{x}),\infty]}\left(m_{y_1}(t,\vec{x})\right) - \chi_{[\eta_p(\vec{x}),\infty]}\left(m_{y_2}(t,\vec{x})\right) \right].
$$

Henceforth, the terms in (5.29) and (5.30) can be estimated to

$$
\begin{aligned}
(5.29) &\leq \Pi_{max} \left| \chi_{[0,\eta_n(\vec{x})]}\left(m_{y_1}(t,\vec{x})\right) - \chi_{[0,\eta_n(\vec{x})]}\left(m_{y_2}(t,\vec{x})\right) \right| \\
(5.30) &\leq \Delta\Pi \left| \chi_{[\eta_p(\vec{x}),\infty]}\left(m_{y_1}(t,\vec{x})\right) - \chi_{[\eta_p(\vec{x}),\infty]}\left(m_{y_2}(t,\vec{x})\right) \right|.
\end{aligned}
$$

Using this estimations, inequality (5.28) becomes

$$
\begin{aligned}
(5.28) &\leq K_2 \int_0^t \int_\Omega \Pi_{max} \left| \chi_{[0,\eta_n(\vec{x})]}\left(m_{y_1}(t,\vec{x})\right) - \chi_{[0,\eta_n(\vec{x})]}\left(m_{y_2}(t,\vec{x})\right) \right| d\vec{x}\, ds \\
&\quad + K_2 \int_0^t \int_\Omega \Delta\Pi \left| \chi_{[\eta_p(\vec{x}),\infty]}\left(m_{y_1}(t,\vec{x})\right) - \chi_{[\eta_p(\vec{x}),\infty]}\left(m_{y_2}(t,\vec{x})\right) \right| d\vec{x}\, ds.
\end{aligned} \tag{5.31}
$$

Both integrals are equivalent to (5.18) and for that integral, we have already a suitable estimation. Therefore, we can estimate (5.31) upwards to

$$
\begin{aligned}
(5.31) &\leq K_2 \left(\frac{K_2^2 \Pi_{max}}{\beta} \|z\|_{L_1(\Omega \times [0,t])} + \frac{K_2^2 \Delta\Pi}{\beta} \|z\|_{L_1(\Omega \times [0,t])} \right) \\
&= \tilde{C} \|z\|_{L_1(\Omega \times [0,t])}
\end{aligned} \tag{5.32}
$$

with $\tilde{C} = \frac{K_2^2}{\beta}\left(\Pi_{max} + \Delta\Pi\right)$.

Summing up all estimations (5.15), (5.16), (5.27), (5.32), the weak formulation in (5.12) to (5.14) can be estimated to

$$\|z(t,\cdot)\|_{L_1(\Omega)} \le \|z(0,\cdot)\|_{L_1(\Omega)} + \left(\tilde{C} + \frac{CK}{\beta}\right)\int_0^t \|z(s,\cdot)\|_{L_1(\Omega)}$$

for all $t \in [0,T]$. Then the Generalized Gronwall's inequality A.2.3 leads to

$$\|z(t,\cdot)\|_{L_1(\Omega)} \le \|z(0,\cdot)\|_{L_1(\Omega)} e^{\left(\tilde{C} + \frac{CK}{\beta}\right)T}. \tag{5.33}$$

If we assume that the solutions y_1 and y_2 have the same initial condition, then $z(0,\cdot) = 0$ a.e. such that we can conclude due to (5.33) that $z(t,\cdot) = 0$ a.e. which means that (5.4) has a unique weak solution.

To proof uniqueness for the ODE (4.8), we assume again two solutions y_1 and y_2. Denote the difference as $z := y_1 - y_2$ and the corresponding ODE for each $\vec{x} \in \Omega$ reads

$$\begin{aligned}
\frac{\partial}{\partial t} z(t,\vec{x}) &= \int_0^t \chi_{[0,\eta_a(t,\vec{x})]}\left(m_{C_e}(t,\vec{x})\right)\frac{\sigma}{h}b(t,\vec{x})C_e(t,\vec{x}) \\
&\quad - \int_0^t \chi_{[0,\eta_a(t,\vec{x})]}\left(m_{C_e}(t,\vec{x})\right)\frac{\sigma}{h}b(t,\vec{x})C_e(t,\vec{x}) \\
&= 0.
\end{aligned}$$

Hence we can conclude $y_1 = y_2$ meaning we have a unique ODE solution.

Altogether, this shows uniqueness for the whole system for the special case of a time constant population $b(\vec{x})$. $\qquad\square$

So far, we have only shown uniqueness for a special case and this was much work. The difficulty of the the proof of existence and uniqueness of a weak solution of our system is caused by the non continuous right hand side which arises due to the indicator function, e.g. $\chi_{[0,\eta_n(t,\vec{x})]}(C_i(t,\vec{x}))$. We were not able to use other theorems as Banach's fixpoint theorem which proofs existence and uniqueness of a fixed point. Many other theorems require some continuity of the right hand side. For that reason we want to find a function looking similarly as the indicator function and in addition continuous. That means the switch from 1 to 0 of $\chi_{[0,\eta_n(t,\vec{x})]}(C_i(t,\vec{x}))$ has to be sufficiently steep.

5.2. PDE-ODE system with mollified right hand side

Let's replace the indicator function, which corresponds to the feedbacks regarding production of signalling molecules by bacteria, with a continuous function $\psi(t,\vec{x})$ as announced in the previous section. This can be realized by so called mollifiers. We will introduce such functions as next and use as a guideline [28], section 2.1.1.

Definition 5.2.1 (Mollifiers)**.** *For each $\varepsilon > 0$, let $\phi_\varepsilon \in \mathcal{C}\infty_0\left(\mathbb{R}^n\right)$ be given with the properties*

(i) $\varphi_\varepsilon(x) \geq 0$

(ii) $supp(\varphi_\varepsilon) \subset \{x \in \mathbb{R}^n : |x| \leq \varepsilon\}$

(iii) $\int_{\mathbb{R}^n} \varphi_\varepsilon(x)dx = 1.$

An appropriate mollifier function for $0 < \varepsilon \leq 1$ is given by

$$\varphi_\varepsilon(x) = \begin{cases} c \exp\left(-\frac{1}{\varepsilon^2 - \|x\|^2}\right) & \text{for } \|x\| < \epsilon \\ \\ 0 & \text{for } \|x\| \geq \epsilon \end{cases}$$

with $c \in \mathbb{R}_+$ being a proper constant to normalize the integral to 1, e.g.

$$c = \left(\int_{-\varepsilon}^{\varepsilon} \exp\left(-\frac{1}{\varepsilon^2 - \|s\|^2}\right)ds\right)^{-1}.$$

Let $f \in \mathcal{L}1(G)$ and $G \subset \mathbb{R}^n$ be an open subset. Suppose $supp(f)$ is compact and $supp(f) \subset G$. Furthermore, we extend f to zero on the complement of G. Then a mollified function f_ε is the convolution of functions f and φ_ε, that is,

$$f_\varepsilon(x) := f \star \varphi_\varepsilon = \int_{\mathbb{R}^n} f(x - y)\varphi_\varepsilon(y)dy.$$

Proposition 5.2.2. *If $f \in C_0(G)$, then $f_\varepsilon \to f$ uniformly on G as $\varepsilon \to 0$. If $f \in \mathcal{L}p(G)$, $1 \leq p < \infty$, then $\|f_\varepsilon\|_{\mathcal{L}p(G)} \leq \|f\|_{\mathcal{L}p(G)}$ and $f_\varepsilon \to f$ in $\mathcal{L}p(G)$ as $\varepsilon \to 0$.*

This Proposition corresponds to Lemma 1.2 in [28]. Interested readers find the proof there.

Since the bacterial growth is independent of the signalling molecules, it is sufficient to consider only (4.7) and (4.8). In order to avoid the discontinuity of the right hand side, we identify $f = \chi_{[0,\eta_n(t,\vec{x})]}(C_i(t,\vec{x}))$ and obtain a Lipschitz continuous function

$$\psi_\varepsilon(t, \vec{x}, C_i) := \int_{\mathbb{R}} \chi_{[0,b(t,\vec{x})\hat{\xi}_n(\vec{x})]}(C_i(t,\vec{x}) - \vec{y})\varphi_\varepsilon(\vec{y})d\vec{y}$$

with $\varepsilon > 0$ sufficiently small. The model equations rewrite then to

$$\frac{\partial}{\partial t}C_e(t, \vec{x}) = D\nabla^2 C_e(t, \vec{x}) - \gamma_e C_e(t, \vec{x}) - \sigma_w C_e(t, \vec{x})b(t, \vec{x})$$
$$+ \sum_{w=W_1}^{W_{max}} \chi_{\Omega_w}(\vec{x})\psi_\varepsilon(t, \vec{x}, C_i)(\Pi_\chi\left(C_i(t, \vec{x})\right)b(t, \vec{x})) \tag{5.34}$$

$$\frac{\partial}{\partial t}C_i(t, \vec{x}) = \sigma_w C_e(t, \vec{x})b(t, \vec{x})\psi_\varepsilon(t, \vec{x}, C_i) - \gamma_i C_i(t, \vec{x})\psi_\varepsilon(t, \vec{x}, C_i) \tag{5.35}$$

with

$$C_e(0, \vec{x}) = C_i(0, \vec{x}) = 0 \tag{5.36}$$

$$\frac{\partial C_e}{\partial \boldsymbol{n}} = 0 \quad \text{for } \vec{x} \in \partial\Omega. \tag{5.37}$$

With the same arguments as in the proof of Theorem 5.1.1 showing non-negativity of solution C_e^*, we can conclude following statement:

Corollary 5.2.3 (Non-negativity). *The solution of* (5.34) *and* (5.35) *with initial condition* (5.36) *and boundary condition* (5.37) *remains non-negative for all* $t \in [0, T]$ *and* $\vec{x} \in \Omega$.

Due to the Lipschitz continuity of ψ_ε in C_i, we can use some standard theorems to show existence and even uniqueness of system (5.34) to (5.37).

Theorem 5.2.4 (Existence and uniqueness of a weak solution). *There exists a unique weak solution of our system* (5.34) *to* (5.37).

Proof. First of all, we consider the ODE (5.35) only. The theorem of Picard-Lindelöf, see A.3.1, shows the existence and uniqueness of a solution in $t \in [0, T]$, since the right hand side is now Lipschitz continuous in C_i. Thus, we find a solution $C_i(C_e(t, \vec{x}), t, \vec{x})$ depending on function $C_e(t, \vec{x})$. Insert this function into (5.34). Then we have decoupled the system and can apply Theorem 2.2.18 which yields a unique weak solution of the PDE. $\square$

Chapter 6

Numerical approach

One of the main goals is to solve the system equations (4.7) to (4.9) with their corresponding initial and boundary conditions given in (4.10), (4.12) and (4.11). We decided to solve the corresponding PDE with the finite element method (FEM). This method can be implemented in MATLAB. The main issue is the discontinuous right hand side caused by the indicator functions. First of all, a suitable grid is needed. After we have derived that, we implement the FEM for the PDE (4.7). As for the simulation results of the ODE model in section 3, we use a self-adjusted version of the *ode15s* solver to solve the entire system, not only the PDE. A very steep slope of the mollified function will cause problems in the step size control, because near the sporulation we will be unable to meet integration tolerances without reducing the step size below the smallest value allowed by the step size control.

6.1. Grid generation

First of all the domain Ω has to be discretized. We require a fine-mesh in Ω_M and Ω_W, outside of the bacterial colony, the mesh can be coarser. We use the mesh generator of Persson in [20]. The generator uses *signed distance functions* to decide if a node resp. mesh point is inside the geometric boundary or outside. With these functions one can create more complex objects. An appropriate force-displacement function is used to move the nodes and a Delaunay triangulation algorithm adjusts the topology to obtain a well shaped, high quality mesh with confirm triangulations. For more details, especially the code itself, see [20]. *Persson* offers a website (http://persson.berkeley.edu/distmesh/) where one can download the code and some further useful functions e.g. some functions to construct complex distance functions. We use these functions to construct first a mesh with holes for the bacteria. Afterwards we build meshes for each bacterial colony and merged the grids. Now we would obtain double nodes and edges at the boundary of the bacterial colony. So we remove these nodes and adjust the triangulation matrix

such that we obtain finally a $N \times 2$ node matrix with N nodes and a $T \times 3$ triangulation matrix with T triangles. An example of a conform triangulation is given in figure 6.1.
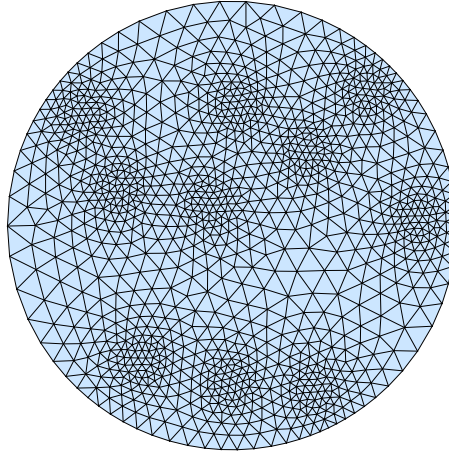
Figure 6.1.: *Grid of test area with ten randomly distributed bacterial colonies.*

6.2. Numerical implementation of FEM

In order to solve the PDE, we use the FEM, which results into a system of ODEs. As in (2.5), we multiply the partial differential equation (4.7) with the linear test function $\phi_i(\vec{x})$ as introduced in paragraph "Linear Elements" in section 2.2.2 and integrate over the domain Ω. We assume that an approximated solution $\hat{C}_e(t, \vec{x})$ of $C_e(t, \vec{x})$ reads

$$\hat{C}_e(t, \vec{x}) := \sum_{j=1}^{N} \phi_j(\vec{x}) c_j(t),$$

see (2.33), and insert this as well into (4.7). Altogether, we obtain

$$\int_\Omega \frac{\partial}{\partial t} \sum_{j=1}^{N} \phi_j(\vec{x}) c_j(t) \phi_i(\vec{x}) \, d\vec{x} =$$

$$D \underbrace{\int_\Omega \nabla^2 \sum_{j=1}^{N} \phi_j(\vec{x}) c_j(t) \phi_i(\vec{x}) \, d\vec{x}}_{(\star)} - \int_\Omega \gamma_e \sum_{j=1}^{N} \phi_j(\vec{x}) c_j(t) \phi_i(\vec{x}) \, d\vec{x}$$

$$- \frac{\sigma}{h} \int_\Omega \sum_{j=1}^{N} \chi_{[0,\eta_a(t_a(\vec{x}),\vec{x})]}(C_i(t,\vec{x})) \phi_j(\vec{x}) c_j(t) b(t,\vec{x}) \phi_i(\vec{x}) \, d\vec{x}$$

$$+ \int_\Omega \sum_{w=W_1}^{W_{max}} \chi_{\Omega_w}(\vec{x}) \chi_{[0,\eta_n(t_n(\vec{x}),\vec{x})]}(C_i(t,\vec{x})) \Pi_\chi(C_i(t,\vec{x})) b(t,\vec{x}) \phi_i(\vec{x}) \, d\vec{x}$$

for all $i \in \{1, \ldots, N\}$. Assembly the terms in order to obtain a system of ODE's as in equation (2.35). Note that partial integration for $(\star)$ is applied again. For $i \in \{1, \ldots, N\}$, this yields

$$\sum_{j=1}^{N} \int_\Omega \phi_j(\vec{x}) \phi_i(\vec{x}) \, d\vec{x} \, \frac{\partial}{\partial t} c_j(t) = \tag{6.1}$$

$$\left. \begin{aligned} &- D \sum_{j=1}^{N} \left(\int_\Omega \nabla \phi_j(\vec{x}) \nabla \phi_i(\vec{x}) + \gamma_e \phi_j(\vec{x}) \phi_i(\vec{x}) \, d\vec{x} \right) c_j(t) \\ &- \frac{\sigma}{h} \sum_{j=1}^{N} \left(\int_\Omega \chi_{[0,\eta_a(t_a(\vec{x}),\vec{x})]}(C_i(t,\vec{x})) b(t,\vec{x}) \phi_j(\vec{x}) \phi_i(\vec{x}) \, d\vec{x} \right) c_j(t) \end{aligned} \right\} \tag{6.2}$$

$$+ \int_\Omega \sum_{w=W_1}^{W_{max}} \chi_{\Omega_w}(\vec{x}) \chi_{[0,\eta_n(t,\vec{x})]}(C_i(t,\vec{x})) \Pi_\chi(C_i(t,\vec{x})) b(t,\vec{x}) \phi_i(\vec{x}) \, d\vec{x}. \tag{6.3}$$

Since the area Ω is discretized by a triangulation, we approximate the integral by the sum of integrals over each triangles, that means

$$\int_\Omega \cdot \; d\vec{x} = \sum_{m=1}^{T} \int_{\Delta_m} \cdot \; d\vec{x}.$$

Insert this discretization into the terms (6.1) to (6.3) and then solve one integral over a triangle after another. In case we do not know an analytical solution, we use the Gaussian quadrature for a triangle to approximate an integral. The approach can be found in [15], section 3.5.2, and [41], section 6.8.3, and is given by

$$\int_\Delta f(\vec{x}) d\vec{x} \approx 2 A_\Delta \sum_{i=1}^{N_g} W_i f(\vec{\vec{x}}_i)$$

where N_g are the number of quadrature points, $\vec{x}_i$ are quadrature points located inside the triangle and $W_i > 0$ are the weights. The standard method is to use three quadrature points to obtain a symmetrical Gaussian quadrature of degree 2, which solves polynomials of degree 2 exactly. That means our integrals are solved exactly, since we use linear elements. The weights have the value $W_i = \frac{1}{6}$ for all $i = \{1,\ 2,\ 3\}$ and the quadrature points are a linear combination of the vertices $\{(x_1, y_1),\ (x_2, y_2),\ (x_3, y_3)\}$, that is

$$
\begin{pmatrix} \bar{x}_1 & \bar{y}_1 \\ \bar{x}_2 & \bar{y}_2 \\ \bar{x}_3 & \bar{y}_3 \end{pmatrix} = L \begin{pmatrix} x_1 & y_1 \\ x_2 & y_2 \\ x_3 & y_3 \end{pmatrix}
$$

with

$$
L = \begin{pmatrix} 0.5 & 0.5 & 0 \\ 0 & 0.5 & 0.5 \\ 0.5 & 0 & 0.5 \end{pmatrix}.
$$

Starting with (6.1), we have to solve the integral $\int_\Delta \phi_j(\vec{x})\phi_i(\vec{x})d\vec{x}$. In the book of *Zienkiewicz*, [41], an analytical solution is given by

$$
\int_\Delta \phi_i^a(\vec{x})\phi_j^b(\vec{x})\phi_k^c(\vec{x})\ d\vec{x} = \frac{a!b!c!}{(a+b+c+2)!}2|A_\Delta|
$$

where A_Δ is the area of a triangle Δ. That means e.g.

$$
\int_\Delta \phi_i(\vec{x})\phi_j\ d\vec{x} = \frac{1!1!0!}{(1+1+0+2)!}2|A_\Delta| = \frac{1}{12}|A_\Delta|
$$

$$
\int_\Delta \phi_i^2(\vec{x})\ d\vec{x} = \frac{2!0!0!}{(2+0+0+2)!}2|A_\Delta| = \frac{1}{6}|A_\Delta|.
$$

The property $\phi_i(\vec{x}_j) = \delta_{ij}$ leads to a sparse symmetrical and nearly diagonal matrix. This result corresponds to the mass matrix in (2.35) and thus reads $M := \langle \phi_j, \phi_i \rangle_{i,j}$ while $\langle \cdot, \cdot \rangle$ is the inner product in $\mathcal{L}^2(\Omega)$.

We will skip term (6.2) for the moment and handle these terms at last. Hence, we continue with (6.3). In case the indicator functions χ are equally one, the integral has to be calculated. Otherwise the integral is equally zero. Applying Gaussian quadrature of degree 2 for triangles, equation (6.3) rewrites to

$$
(6.3) \iff \sum_{w=W_1}^{W_{max}} \sum_{m=1}^{T} \int_{\Delta_m} \chi_{\Omega_w}(\vec{x})\chi_{[0,\eta_n(t,\vec{x})]}(C_i(t,\vec{x}))\Pi_\chi(C_i(t,\vec{x}))2\Delta_m \sum_{l=1}^{3} W_l b(t,\vec{x}_l)\phi_i(\vec{x}_l)\ d\vec{x}.
$$

This expression generates the load vector $F(t)$. If there is no bacterium located on a node, the entry of the vector is zero.

Now we can concern ourselves with the terms in (6.2). Note that the part of the integral with respect to the gradient of the shape functions can be computed by pencil and paper. Calculate the derivative of ϕ with respect to $\vec{x}$, see equation (2.37). It follows

$$
\begin{aligned}
\int_{A_{\Delta_m}} \nabla\phi_j(\vec{x})\nabla\phi_i(\vec{x})d\vec{x} &= \int_{A_{\Delta_m}} \frac{\partial\phi_j}{\partial x}\frac{\partial\phi_i}{\partial x} + \frac{\partial\phi_j}{\partial y}\frac{\partial\phi_i}{\partial y} \, dx \, dy \\
&= \int_{A_{\Delta_m}} \frac{(y_j - y_l)(y_l - y_i)}{4A_{\Delta_m}^2} + \frac{(x_l - x_j)(x_i - x_l)}{4A_{\Delta_m}^2} \, d\vec{x} \\
&= \frac{1}{4A_{\Delta_m}}\left((y_j - y_l)(y_l - y_i) + (x_j - x_l)(x_l - x_i)\right).
\end{aligned}
$$

The rest is done analogously to the two previous calculations. This leads to a matrix $K(t)$ which is known as the stiffness matrix.

All in all the discretized ODE system reads

$$
M\frac{\mathrm{d}}{\mathrm{d}t}\boldsymbol{c}(t) + K(t)\boldsymbol{c}(t) = F(t)
$$
$$
\boldsymbol{c}(0) = \boldsymbol{c_0}
$$

with $\boldsymbol{c_0}$ as the initial value. The variables in **bold** are vectors with N entries because we have N nodes. The stiffness matrix and the load vector change in time. On the one hand it is caused by the bacterial growth, on the other hand, if we reach one of the thresholds, let's say the negative feedback, then we have also a change in the load vector. The process was described by the indicator function $\chi_{[0,\eta_n(t_n(\vec{x}),\vec{x})]}(C_i(t,\vec{x}))$. So if node l sporulates, the indicator function becomes zero and thus the entrie in the l'th row in vector $F(t)$.

6.3. The solver algorithm

Three equations have to be solved, that is the PDE (4.7) for the extracellular signalling molecule equation, the ODE (4.8) for the intracellular signalling molecule concentration and the bacterial growth ODE (4.9) using their initial conditions (4.10),(4.12) and boundary condition (4.11). The ODE for bacterial growth can be considered point-wise for each $x \in \Omega_w \cup \Omega_m$. As for the ODE model in chapter 3, the ODE of the bacterial growth is solved first since it neither depends on the PDE (4.7) nor on the ODE (4.7). Using the solution of the ODE given in (3.28), a point-wise solution for each $x \in \Omega_w \cup \Omega_m$ reads

$$b(t, \vec{x}) = \frac{b_0(\vec{x}) h \kappa}{\exp(-\alpha\, t)\, (h\kappa - b_0(\vec{x})) + b_0(\vec{x})} \quad \text{for } \vec{x} \in \Omega_w \cup \Omega_m.$$

The PDE (4.7) is coupled with the ODE (4.8) only with respect to the indicator function. That means that C_i itself do not affect the solution of C_e, it just determines when some terms in the right hand side vanish, that is when one of the thresholds are reached. In contrast to that, the solution C_e of the PDE does affect the solution C_i of ODE (4.8) directly. This basically means that we solve first the PDE for a certain time interval $[t_n, t_{n+1}] \in [0, T]$ and then we solve the ODE for that interval $[t_n, t_{n+1}]$. After that, we check the feedback condition, e.g. $C_i(t, \vec{x}) \leq \eta_n(t, \vec{x})$ for all $t \in [t_n, t_{n+1}]$. This corresponds to the so called "event driven method", see appendix B or [7] for more details. If the inequality holds, we can continue to calculate the solution for the next time interval $[t_{n+1}, t_{n+2}]$. Otherwise, we determine the time-point $t_F \in [t_n, t_{n+1}]$ such that $C_i(t_F, \vec{x}) > \eta_n(t_F, \vec{x})$. Then we recalculate the solution of $C_e(t, \vec{x})$ for $t \in [t_n, t_F]$ and the corresponding stiffness matrix or right hand side of the PDE (4.7) has to be adjusted. That's the idea how the algorithm works. Let's go into more detail how we solve the equations numerically.

As a basis for our solver, we use the stiff MATLAB solver *ode15s*. More details regarding the solver can be found in appendix B. Such a solver can solve ODE systems, which arises from the FEM for PDE's. In section 6.2, we have used the FEM to discretize the space variable of PDE (4.7), leading to system of ODEs with variable $\boldsymbol{c}$. Note that the number of these ODEs corresponds to the number of nodes in the grid. Our new solver is called *Bacillus_solver* and solves the derived ODE system $\boldsymbol{c}$ coupled with the C_i ODE. Note that this ODE will be solved for each $\vec{x} \in \Omega_W \cup \Omega_M$ respectively for each node in that area. Our solver needs the mass matrix M as well as a right hand side of the derived ODE system, that is $-K(t)\boldsymbol{c}(t) + F(t)$. Then it solves the system for a given interval in time, in our case $[0, T]$.

Let's assume we calculated so far the solutions $\boldsymbol{c}_k$ and $(C_i)_k$ for $k \in \{0, 1, \ldots, n\}$ time steps. Then the solver derives a new, successful time-step $t_{n+1} \leq T$ with a new solution $\boldsymbol{c}_{n+1}$. Successful just means that the estimated error is smaller than 10^3. At that point it follows the main adjustment, that is the query of feedback. For this, we calculate a solution of the C_i ODEs by using a linear approximation between $\boldsymbol{c}_n$ and $\boldsymbol{c}_{n+1}$. A suitable solver to solve such an ODE is *ode45* solver. When we have this new value $(C_i)_{n+1}$, we check if we reach one of the thresholds, that is, the indicator functions from above with $C_i(t_{n+1}, \vec{x})$ as its argument. If it becomes zero, we have to adjust the stiffness matrix or load vector to obtain $K((t_{n+1}))$ resp. $F(t_{n+1})$. One has to be careful here to change the entries in the right manner. That's because one affected node affects all other integrals using this node as a vertex of their domain of integration. After that, the algorithm starts over again using this adjusted matrix resp. vector using $\boldsymbol{c}_{n+1}$ and $C_i(t_{n+1}, \vec{x})$ as new initial conditions.

6.4. Convert ODE parameters to PDE parameters

In chapter 3, we discussed the absorption process of the mutants and the production/absorption process of wild types. As a result, we obtained best fit parameters, see table 3.3 and table 3.9. However, these parameters can not be used immediately for the coupled PDE-ODE model in (4.7) and (4.8). We have to convert them to suitable PDE parameter values.

In the coupled PDE-ODE model, we projected the entire mass to the x-y plane, see figure 6.2. Thus, the units of surface densities C_e and C_i are given with respect to m^2, that is, $\frac{\mu mol}{m^2}$ in contrast to the pure ODE model in chapter 3 where it was given as $\frac{\mu mol}{l}$. For the units of bacteria it is similar. In the ODE, we modelled the number of bacteria, in the PDE case, it is a surface density with unit $\left[\frac{cells}{m^2}\right]$. To distinguish the variables and parameters of both models, we denote these ones corresponding to the PDE equations with $\tilde{\cdot}$. The following parameters of the ODE model are going to be converted: the production rates Π_{min} and $\Delta\Pi$, the absorption rate σ and the thresholds $\xi_{p,j}$ and $\xi_{n,j}$. Remember that the units of the ODE parameters read

$$[\Pi_{min}] = [\Delta\Pi] = \frac{\mu mol}{l \cdot min \cdot cells}, \ [\sigma] = \frac{l}{min \cdot cells} \text{ and } [\xi_{p,j}] = [\xi_{n,j}] = \frac{\mu mol}{l \cdot cells}$$

and for the PDE parameters, we need

$$[\tilde{\Pi}_{min}] = [\Delta\tilde{\Pi}] = \frac{\mu mol}{min \cdot cells}, \ [\tilde{\sigma}] = \frac{m^3}{min \cdot cells} \text{ and } [\tilde{\xi}_{p,j}] = [\tilde{\xi}_{n,j}] = \frac{\mu mol}{cells}$$
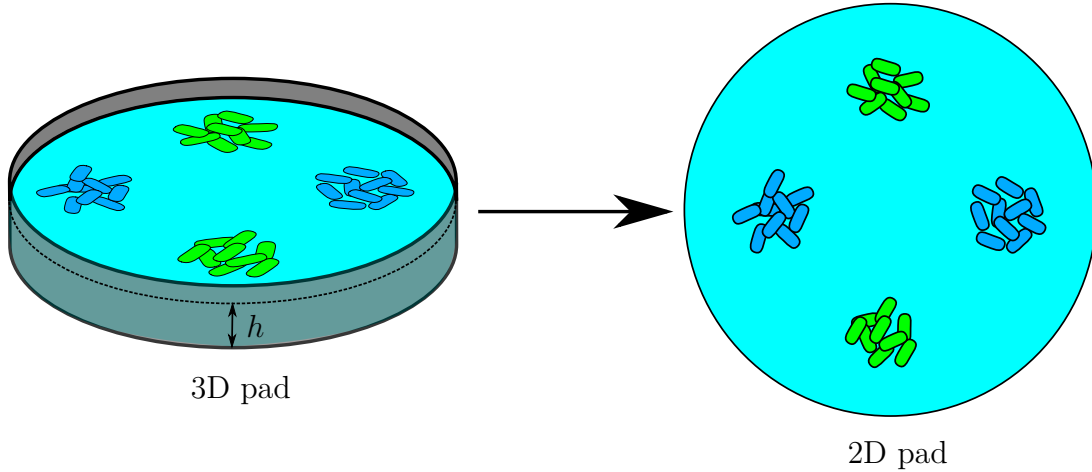
to be consistent.

Figure 6.2.: *Scheme of 3D to 2D conversion.*

The approach to find suitable parameter values for the PDE based on the ODE parameters is following. For the ODE and PDE case each, we consider one bacterium in

the corresponding environment and calculate the number of signalling molecules produced or absorbed in a small time interval $[0, \varepsilon]$ with $\varepsilon > 0$. Since we consider a very small time interval, we can assume that the number of bacteria as well as the number of signalling molecules in the environment are constant in time. Then the number of signalling molecules of each case should be equal after time ε. Then we can conclude eventually the recalculation for the PDE parameter in terms of the ODE parameter.

Let's start to recalculate the production rate Π_{min}. We consider only the production process of signalling molecules in an initially signalling molecule free environment. Then for the ODE model, the number of signalling molecules SM within the shake flask with volume V_e reads

$$C_e(t) = C_e(0) + \int_0^\varepsilon \Pi_{min} b(t) \, dt$$

$$\Longrightarrow SM = C_e(t) V_e = V_e \left(C_e(0) + \int_0^\varepsilon \Pi_{min} \underbrace{b(t)}_{=1} \, dt \right)$$

$$= \Pi_{min} V_e \varepsilon.$$

In the PDE case the population is usually not homogeneously distributed, instead bacteria are gathered in colonies. Therefore, a bacterium is located at $\Omega_{bac} \subset \Omega$ and the density $\tilde{b}(t, \vec{x})$ is zero at $\vec{x} \in \Omega \setminus \Omega_{bac}$. Again we assume that the bacteria density, and thus the number is constant in time. So we obtain

$$\int_\Omega \tilde{b}(t, \vec{x}) \, dA = 1.$$

We know that diffusion with homogeneous boundary conditions do not change the total mass. That means we can neglect the diffusion term in our consideration. Then the total number of signalling molecules SM in an initially signalling molecule free environment Ω reads

$$SM = \int_\Omega \tilde{C}_e(\varepsilon, \vec{x}) \, dA = \int_\Omega \int_0^\varepsilon \tilde{\Pi}_{min} \tilde{b}(t, \vec{x}) \, dt \, dA$$

$$= \int_0^\varepsilon \tilde{\Pi}_{min} \underbrace{\int_\Omega \tilde{b}(t, \vec{x}) \, dA}_{=1} \, dt$$

$$= \tilde{\Pi}_{min} \varepsilon.$$

The two relations yield

$$\Pi_{min} V_e \varepsilon = \tilde{\Pi}_{min} \varepsilon$$

$$\Longleftrightarrow \quad \tilde{\Pi}_{min} = V_e \Pi_{min}.$$

The approach for $\Delta\tilde{\Pi}$ is analogously. We obtain

$$\Delta\tilde{\Pi} = \Delta\Pi V_e.$$

The approach for the absorption rate is slightly different. First, we start to calculate the number of signalling molecules for the ODE. The concentration of signalling molecule concentration reads $C_e(t)$ and we consider still only one bacterium within the shake flask of volume V_e. Both variables do not change in time due to the small time interval. Thus, the constant signalling molecule concentration reads C. For the ODE case we obtain

$$SM = V_e C_e(\varepsilon) = V_e \int_0^\varepsilon \frac{\sigma}{V_e} \underbrace{b(t)}_{=1} \underbrace{C_e(t)}_{=C} \, dt$$

$$= \sigma C \varepsilon.$$

The signalling molecule surface density reads $\hat{C}(t, \vec{x})$ which is again constant C because of the small time interval considered as well as for the number of bacteria, that means $\int_{\hat{V}_e} \hat{b}(t, \vec{x}) \, dV = 1$. This leads to following result:

$$SM = \int_{\hat{V}_e} \hat{C}_e(\varepsilon, \vec{x}) dV = \int_{\hat{V}_e} \int_0^\varepsilon \hat{\sigma} \hat{b}(t, \vec{x}) C_e(t, \vec{x}) \, dt \, dV$$

$$= \int_0^\varepsilon \hat{\sigma} C \underbrace{\int_{\hat{V}_e} \hat{b}(t, \vec{x}) \, dV}_{=1} \, dt$$

$$= \hat{\sigma} C \varepsilon.$$

Both relations yield

$$\hat{\sigma} = \sigma.$$

The initial number of signalling molecule concentration reads SM_0 and we consider again only one bacterium on the pad. Both variables still do not change in time due to the small time interval $[0, \varepsilon]$. For the 3D case, the signalling molecule concentration reads $\frac{SM_0}{\hat{V}_e}$ and we obtain

$$SM = \int_{\hat{V}_e} C_e(\varepsilon, \vec{x}) \, dV = \int_{\hat{V}_e} \int_0^\varepsilon \hat{\sigma} \hat{b}(t, \vec{x}) \frac{SM_0}{\hat{V}_e} \, dt \, dV$$

$$= \int_0^\varepsilon \hat{\sigma} \frac{SM_0}{\hat{V}_e} \underbrace{\int_{\hat{V}_e} \hat{b}(t, \vec{x}) \, dV}_{=1} \, dt$$

$$= \hat{\sigma} \frac{SM_0}{\hat{V}_e} \varepsilon.$$

The situation for the 2D case is similar. Note that the reaction volume of the 3D case reads $\hat{V}_e = \Omega \times h$ and thus the size is $A \cdot h$. The variables and parameters of the 2D PDE case are denoted with $\tilde{\cdot}$ as usual. We assume again an initial number of quorum sensing molecules of SM_0 which means, that the surface density reads $\tilde{C}_e(t, \vec{x}) = \frac{SM_0}{A}$. The number of bacteria is still one, that means $\int_\Omega \tilde{b}(t, \vec{x}) \, dA = 1$. Neither the signalling molecule density nor the bacterial density changes. This leads to following equation:

$$
\begin{aligned}
SM &= \int_\Omega \tilde{C}_e(\varepsilon, \vec{x}) dA = \int_\Omega \int_0^\varepsilon \frac{\tilde{\sigma}}{h} \tilde{b}(t, \vec{x}) \frac{SM_0}{A} \, dt \, dA \\
&= \int_0^\varepsilon \frac{\tilde{\sigma}}{h} \frac{SM_0}{A} \underbrace{\int_\Omega \tilde{b}(t, \vec{x}) \, dA}_{=1} \, dt \\
&= \frac{\tilde{\sigma}}{h} \frac{SM_0}{A} \varepsilon.
\end{aligned}
$$

Thus, both relations yield

$$
\tilde{\sigma} = \hat{\sigma} \frac{Ah}{\hat{V}_e} = \hat{\sigma} = \sigma.
$$

Last but not least, we have to adjust the feedback thresholds. For the ODE case, the thresholds are given per cell and we also considered the intracellular concentration with respect to the bacterial volume V_{bac}. So the total number of signalling molecules within a cell reads $\xi_{p,j} V_{bac}$ respectively $\xi_{n,j} V_{bac}$. This is also the threshold for the PDE since the coupled ODE measures the concentration of intracellular signalling molecules at a given point $\vec{x} \in \Omega$ with respect to the bacterial density. That means

$$
\tilde{\xi}_{p,j} = \xi_{p,j} V_{bac} \quad \text{and} \quad \tilde{\xi}_{n,j} = \xi_{n,j} V_{bac}.
$$

Chapter 7

Simulation results of PDE model

Before we try to reproduce the experimental pad results of the BioQuant laboratory described in chapter 4 and depicted in figure 4.1 by our model, we first verify the PDE-ODE system (4.7), (4.8), (4.10), and (4.11) as well as the conversion of parameters from the ODE results. This works since a high diffusion rate diminishes spatial effects. Then we vary the diffusion rate as well as the extracellular degradation of signalling molecules and interpret the results. Since we simulate the behaviour of microcolonies, we will check finally, if we see some new phenomena for bigger colony sizes. Remind, that we add to the PDE-ODE system a further threshold $\bar{\xi}_a \in \mathbb{R}_+$ which is responsible for the stop of absorption. Taking this value to infinity, $t_a(\vec{x}) = \infty$, too, leading to an indicator function which is equal to one. Thus, this part of the model dynamic coincides with the assumptions regarding the ODE system in chapter 3. Note that this holds for all simulations in chapter 7.

In section 4.1, we stated that on a pad of diameter $9mm$, leading to a area of approximately $63.6 \ mm^2$, there are $4 \cdot 10^4$ cells initially. The height h of the agarose gel is $1mm$. We, however, simulate only a small segment of the pad. On our segment Ω, we consider 10 colonies and each colony consist initially of only one bacterium as we know from data of the BioQuant laboratory, see figure 4.2. Henceforth, we can determine the radius r_p of our simulated pad as follows:

$$\frac{\text{\# initial population}}{\text{area of pad}} = \frac{\text{\# bacterial colonies} \cdot \text{colony size}}{\text{area of } \Omega}$$

$$\iff \frac{4 \cdot 10^4}{(4.5 \ mm)^2 \pi} = \frac{10 \cdot 1}{r_p^2 \pi}$$

$$\implies r_p = \sqrt{\frac{10}{4 \cdot 10^4} \cdot (4.5 \ mm)^2} \approx 71 \mu m.$$

Furthermore, we need the spatial size of a colony. In our model, we consider a fixed radius of the colony Ω_w and Ω_m for all w, m. In figure 4.2, the population growth of a microcolony is given and we see that there are maximal 50 bacteria in one colony. For that reason we assume very harshly that colony size in the simulations corresponds to a size of a colony with an average of 25 bacteria. The size of a *Bacillus subtilis* cell was given by personal communication from Dr. Ilka Bischofs and reads approximately 4.3μ times $0.8\mu m$. Thus, one bacterium covers an area of $3.44\mu m^2$. Then we can conclude that the colony radius r_{col} reads

$$r_{col} = \sqrt{\frac{25 \cdot 3.44\mu m^2}{\pi}} \approx 5.23\mu m.$$

These are always the geometric values of our simulated pad Ω as long as nothing else is mentioned in the simulation results.

Yet, the μCats laboratory haven't measured the diffusion of signalling molecules in the pad. However, the diffusion of the signalling molecule in the agarose gel is comparable with a pentapeptide in water due to the similar molecular weight. In [11], one can find the diffusion coefficient of a pentapeptide in Leu-enkephalin which is like water due to similar molecular weight. Consequently, we choose

$$D = 24.6 \cdot 10^{-9} \; \frac{m^2}{min}$$

as arranged with the μCats laboratory, too. Similar as above, as long as nothing else is noted, we use this diffusion rate for the simulations.

7.1. Evaluation of the PDE model

As mentioned, we check first if the model equations as well as recalculated parameter values yield feasible solutions. Necessary to that end is to perform the shake flask experiments in section 3.1 now with the coupled PDE-ODE model equations (4.7) and (4.8) with its corresponding boundary condition (4.11). The high diffusivity ensures that the signalling molecule is almost equally distributed in our pad and thus the results should be very similar. Additionally, we will test on the one hand the influence of different diffusion and extracellular degradation rates and on the other hand the change of geometrical parameters as the radii of the pad and colony to the simulated solutions.

7.1.1. Reproduction of ODE results

We start with the evaluation of the mutant experiment using Hypothesis HM 2 which states that there is no feedback regarding the absorption. For those mutant simulations,

we assumed a constant number of bacteria with respect to time. Then the corresponding PDE model reads

$$\frac{\partial}{\partial t}C_e(t,\vec{x}) = D\nabla^2 C_e(t,\vec{x}) - \frac{\sigma_m}{h}C_e(t,\vec{x})b(\vec{x}) - \gamma_e C_e(t,\vec{x})$$

$$\frac{\partial}{\partial t}C_i(t,\vec{x}) = \frac{\sigma_m}{h}C_e(t,\vec{x})b(\vec{x})$$

with

$$C_e(0,\vec{x}) = C_i(0,\vec{x}) = 0$$

$$\frac{\partial C_e}{\partial \boldsymbol{n}} = 0 \quad \text{for } \vec{x} \in \partial\Omega$$

$$b(\vec{x}) = \begin{cases} b_{m0} > 0 & \text{for } \vec{x} \in \Omega_m \\ \\ 0 & \text{for } \vec{x} \in \Omega \setminus \Omega_m. \end{cases}$$

The shake flask had a reaction volume of $V_{ode} := 500ml$ and the experiments were performed with a total number of $b_{ode} := 9.52 \cdot 10^7$ mutants. So we need for each colony in our simulated pad a cell number of

$$b_{col} := \frac{1}{10}b_{ode}\frac{A \cdot h}{V_{ode}} \approx 252.$$

That means the initial surface density for each colony reads

$$b_{m0} = \frac{b_{col}}{A_{col}}$$

with A_{col} being the geometrical size of one colony on the pad.

We use the approach in section 6.4 and the parameter values in table 3.3 to find the corresponding PDE parameter values yielding

$$\sigma_m = 2.23 \cdot 10^{-12}\frac{l}{min} = 2.23 \cdot 10^{-15}\frac{m^3}{min}$$

$$\gamma_e = 0\frac{1}{min}.$$

When we have solved the system for the given time interval $[0, 21]$ minutes, we take then the mean values of the intra- and extracellular concentrations, that is,

$$C_i(t) = \frac{1}{A}\int_\Omega C_i(t,\vec{x})\,d\vec{x} \quad \text{resp.} \quad C_e(t) = \frac{1}{A}\int_\Omega C_e(t,\vec{x})\,d\vec{x}$$

in order to evaluate the FRET function (3.1) and compare it with the best fit FRET solutions in section 3.5.3.

To evaluate the intracellular FRET, we can not use the FRET function immediately because the FRET function (3.1) was build for the intracellular concentration in one bacterium. We, however, calculate the intracellular surface density of all bacterial with respect to the simulated surface area A. Henceforth, the adjusted FRET function for the PDE case reads

$$FRET\left(C(t)\right) = FRET_0 - \Delta FRET \frac{C(t)\dfrac{A}{10 \cdot b_{col}V_{bac}}}{E + C(t)\dfrac{A}{10 \cdot b_{col}V_{bac}}}$$

with $C(t)$ being the intracellular signalling molecule concentration.
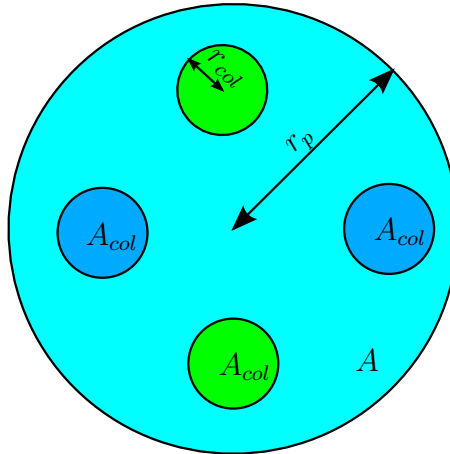
Figure 7.1.: *Scheme to declare geometrical parameters.*

Let's briefly repeat how we obtain the extracellular FRET, see section 3.1: We stimulate new, "empty" mutants with the extracellular signalling molecule concentration $C_e(t)$ after the centrifugation process. To calculate the extracellular FRET, we use the ODE model approach of section 3.4 and section 3.5. If we would use here again the PDE model, we somehow measure the spatial effects of the wild types (which we want) and additionally the spatial effects mutants (which we do not want). Thus, we use the ODE approach to obtain the intracellular signalling molecule concentration $C_i^e(t)$. This concentration can immediately be used to evaluate the FRET function (3.1) in order to obtain the extracellular FRET for the mutants of the PDE case.

Description	Parameter	Value	Unite
Radius of simulated pad	r_p	71	μm
Area of simulated pad	A	$r_p^2 \pi$	μm^2
Area of a single colony	A_{col}	$r_{col}^2 \pi$	μm^2
Height of pad	h	1	mm
Volume of single cell	V_{bac}	$0.973 \cdot 10^{-15}$	l
Radius of single colony	r_{col}	5.23	μm
Diffusion rate	D	$24.6 \cdot 10^{-9}$	$\frac{m^2}{min}$
Volume of shake flask in ODE experiment (mutant/wild type)	V_{ode}	500/100	ml
Number of cells in ODE experiment (mutant/wild type)	b_{ode}	$9.52 \cdot 10^7 / 8.55 \cdot 10^9$	$cells$

Table 7.1.: Standard parameter values for simulations.

The corresponding results of the simulation with the derived parameter values are given in figure 7.2. There we see that the intracellular FRET regarding the PDE model is virtually identical to the intracellular and extracellular FRET regarding the ODE. Due to the high diffusion, signalling molecules are transported from the surrounding very fast to the bacteria and thus, spatial effects can be neglected. So we can conclude that the PDE model and the chosen parameter values describe the uptake of signalling molecules very well.

Comparison of intracellular FRET of mutants

(a)

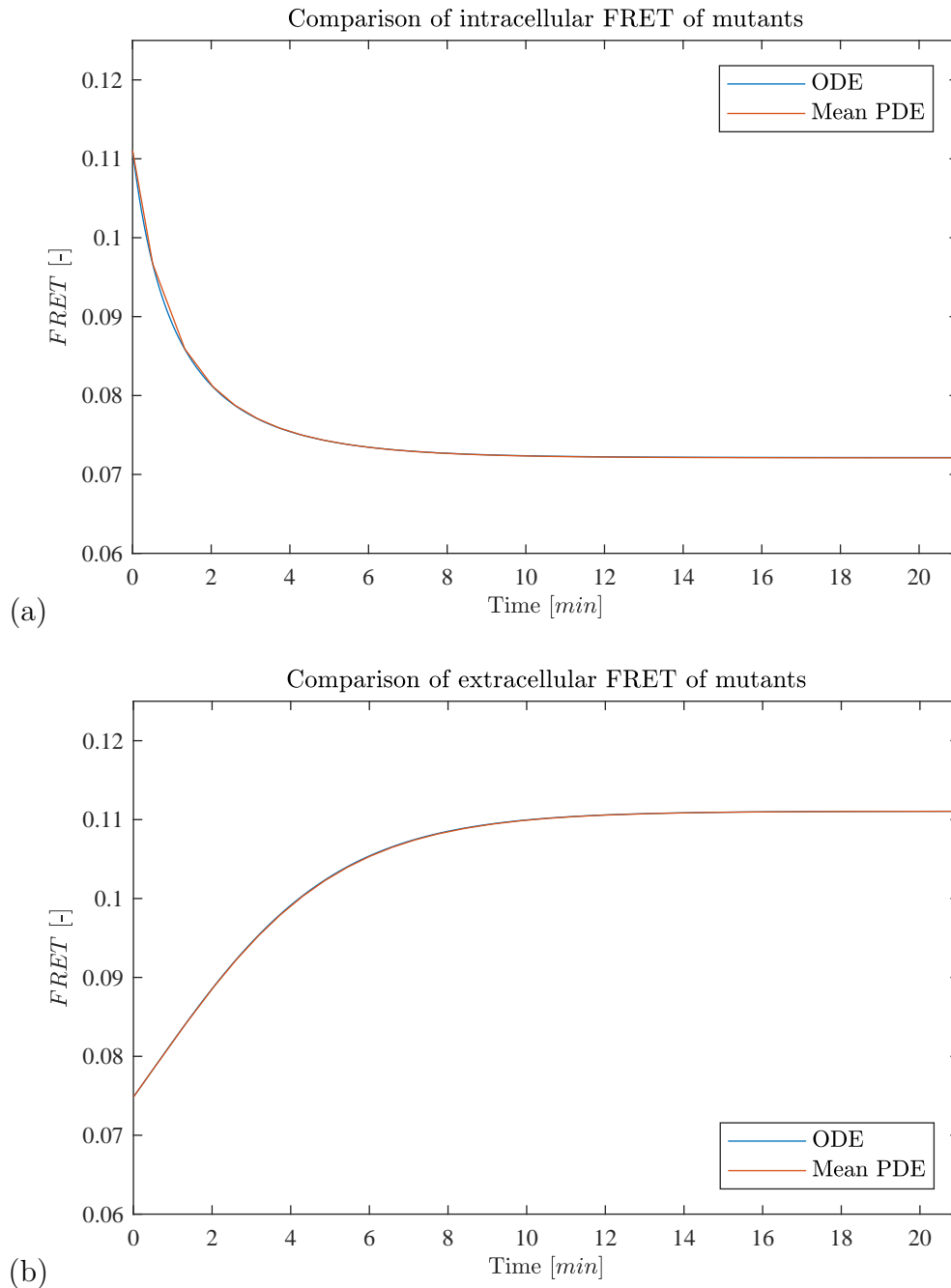Comparison of extracellular FRET of mutants

(b)

Figure 7.2.: *Comparison of mutant FRET for shake flask experiments, that is the ODE, and PDE model, using ODE setting; (a) Intracellular FRET kinetics; (b): Extracellular FRET kinetics;*

The same procedure is realized for the wild type model using hypothesis HW 4 and competition effects among the peptides regarding the uptake. The corresponding PDE model reads

$$\frac{\partial}{\partial t}C_e(t,\vec{x}) = D\nabla^2 C_e(t,\vec{x}) - \gamma_e C_e(t,\vec{x})$$
$$- \frac{\sigma_w}{h}C_e(t,\vec{x})b(t,\vec{x})$$
$$+ \sum_{w=W_1}^{W_{10}} \chi_{\Omega_w}(\vec{x})\chi_{[0,\eta_n(t_n(\vec{x}),\vec{x})]}(C_i(t,\vec{x}))\Pi_\chi(C_i(t,\vec{x}))\,b(t,\vec{x})$$
$$\frac{\partial}{\partial t}C_i(t,\vec{x}) = \frac{\sigma_w}{h}C_e(t)b(t,\vec{x})$$
$$\frac{\partial}{\partial t}b(t,\vec{x}) = \alpha b(t,\vec{x})\left(1 - \frac{b(t,\vec{x})}{\kappa h}\right)$$

with initial and boundary conditions

$$C_e(0,\vec{x}) = C_i(0,\vec{x}) = 0$$
$$\frac{\partial C_e}{\partial \boldsymbol{n}} = 0 \quad \text{for } \vec{x} \in \partial\Omega$$
$$b(0,\vec{x}) = \begin{cases} b_{w0} > 0 & \text{for } \vec{x} \in \Omega_{W_1} \cup \ldots \cup \Omega_{W_{10}} := \Omega_W \\[2mm] 0 & \text{for } \vec{x} \in \Omega \setminus \Omega_W. \end{cases}$$

Since the bacterial growth equation can be solved explicitly, we consider the corresponding parameters first. The values are given in table 3.4. The size of the shake flask was $V_{ode} := 0.1l$ and we had initially $b_{ode} := 8.55 \cdot 10^9$ cells in the flask using the ODE fit of b_{w0}. That means the number of bacteria in each of the 10 bacterial colony reads

$$b_{col} = \frac{1}{10}b_{ode}\frac{A \cdot h}{V_{ode}} \approx 113.4.$$

So the initial surface density of a colony of spatial size A_{col} is given by

$$b_{w0} = \frac{b_{col}}{A_{col}}.$$

The parameter value of the exponential growth rate can be used for the PDE without any changes. Only the carrying capacity κ_{ode} has to be adjusted. Since this parameter depends on the environmental conditions, we have to adjust it to the new reaction volume and that they are gathered in colonies. We obtain

$$\frac{\kappa \cdot A_{col} \cdot h}{A \cdot h} = \frac{\kappa_{ode}}{V_{ode}}$$
$$\implies \kappa = \kappa_{ode}\frac{A \cdot h}{V_{ode} \cdot A_{col} \cdot h} \approx 9.52 \cdot 10^{13}.$$

For the other parameters, we use the values in table 3.9 and recalculate them with the approach in section 6.4. Then one obtains

$$\sigma_w = 0.21 \cdot 10^{-12} \frac{l}{min} = 0.21 \cdot 10^{-15} \frac{m^3}{min}$$

$$\sigma_m = 0.18 \cdot 10^{-12} \frac{l}{min} = 0.18 \cdot 10^{-15} \frac{m^3}{min}$$

$$\Pi_{min} = 1.9 \cdot 10^{-14} \frac{\mu mol}{l \cdot min} \cdot V_{ode} = 1.9 \cdot 10^{-15} \frac{\mu mol}{min}$$

$$\Delta\Pi = 2.7 \cdot 10^{-14} \frac{\mu mol}{l \cdot min} \cdot V_{ode} = 2.7 \cdot 10^{-15} \frac{\mu mol}{min}$$

$$\xi_p = 29.99 \frac{\mu mol}{l} \cdot V_{bac} = 2.92 \cdot 10^{-14} \mu mol$$

$$\xi_n = 179.99 \frac{\mu mol}{l} \cdot V_{bac} = 1.75 \cdot 10^{-13} \mu mol$$

$$\gamma_e = 0 \frac{1}{min}.$$

We solve the system for $[0, 360]$ minutes and take the mean of the extracellular concentration $C_e(t, \vec{x})$, that is

$$C_e(t) = \frac{1}{A} \int_\Omega C_e(t, \vec{x}) \, d\vec{x}.$$

Then for each $t \in [0, 360]$ we use this concentration to stimulate new and empty mutant cells by using the ODE approach as we did for the mutants above. We yield their intracellular concentration denoted as $C_i^e(t)$ and insert this into the FRET equation 3.1.

The comparison of the ODE result and PDE result using the derived parameter values can be seen in figure 7.3. Note that we distinguish for the moment between some noise in the threshold (a) and no noise (b). Usually, we consider always some noise in the threshold and consider therefore initially the results with noise, that is, figure 7.3(a). We see that the extracellular FRET curves are almost identically for the first 115 minutes. Then the PDE FRET curve increases more slowly and also reaches a lower end stage. That's caused by the noise or put it another way, some bacteria did not reach the negative feedback and still produce signalling molecules leading to a higher concentration of signalling molecules and thus a lower stage of the FRET curve. This can be proven by figure 7.3(b) where we see the FRET curve without any noise. There, the FRET curve tends to the same level as the FRET regarding the ODE. However, the FRET curve regarding the PDE model without noise decreases further and leading finally to a sharp peak. The reason for the further decreasing is that signalling molecules diffuses away form the bacterial colony and is not absorbed everywhere on the pad. Thus, the concentration of signalling molecules is higher than in

the ODE case. The peak in the curve symbolises the simultaneous stop of production of signalling molecules for almost all bacteria. For all that, the PDE model and adjusted parameter values yields reasonable results.
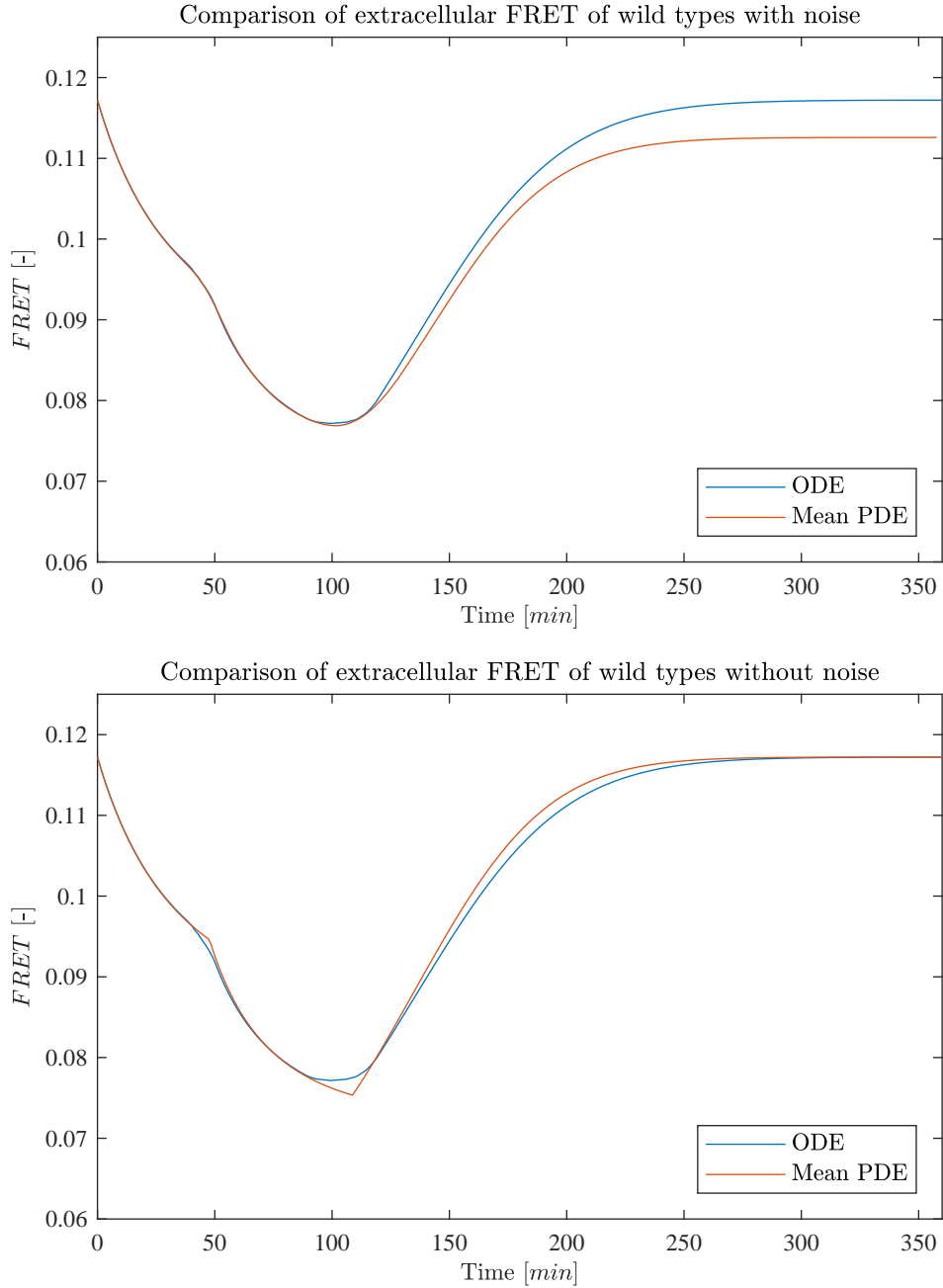

Figure 7.3.: *Comparison of wild type FRET kinetics for shake flask experiments, that is the ODE, and PDE model, using ODE setting; (a) There is a noise regarding the thresholds ξ_p and ξ_n; (b): There is no noise regarding the thresholds;*

7.1.2. **Variation of model parameters**

In the beginning of this chapter, we assumed an educated guess of the diffusion rate $D = 24.6 \cdot 10^{-9}$. However, we don't know for sure if this is really true. Additionally, we assumed no extracellular degradation rate since this was one conclusion of the ODE results. However, there is no hint yet, that this also holds for the PDE respectively for the pad experiments. Therefore, we vary on the one hand the order of the diffusion parameter D, that is,

$$D \in \left\{ D_0 \cdot 10^{-15}, D_0 \cdot 10^{-12}, D_0 \cdot 10^{-9}, D_0 \cdot 10^{-6}, D_0 \cdot 10^{-3} \right\}$$

with $D_0 = 24.6 \frac{m^2}{min}$ and on the other hand the extracellular degradation rate γ_e with $[\gamma_e] = \frac{1}{min}$ as following:

$$\gamma_e \in \left\{ 0, 10^{-3}, 10^{-2}, 10^{-1}, 1 \right\}.$$

All other parameters of the mutant and wild type simulations are chosen as in subsection 7.1.1. The results of the mutant simulations are given in figure 7.4 and 7.5, the changes in the solutions for the wild type can be found in figure 7.6 and 7.7.

As usual we consider first the result of the mutant population and start with the intracellular kinetics, see figure 7.4. For the moment we consider the first column, that means the diffusion rate varies and $\gamma_e = 0$ is the standard value from the previous setting. The third row corresponds to the standard diffusion rate. Starting from that point, we see that if we increase the diffusion rate, we there are no changes. But decreasing the diffusion has the effect that FRET dos decrease slower and also dos not reach the level of the ODE FRET coloured as blue line. This is reasonable since it takes more time until signalling molecules from the surrounding area of the colony reach the bacteria. If we consider the third row, then we change the degradation rate and the diffusion rate is the standard one. Increasing the degradation leads to a similar result. It seems that the FRET still decreases with the same magnitude but does not reach the same low level. This just means that at the end, we run out of signalling molecules. All other plots are a combination of both effects.

Variation of intracellular FRET of mutants

Figure 7.4.: *We use the parameter setting of subsection 7.1.1 with varying diffusion rate D and extracellular degradation rate γ_e. The red graphs corresponds to the intracellular FRET of the PDE model, the blue graphs of the ODE model.*

The plots of the extracellular FRET, figure 7.5 are also reasonable using the same arguments. At a first glance, we consider the first column whereas the third row corresponds to the standard diffusion. Increasing the diffusion from that state, it has no effect to the FRET. But as soon as we decrease the diffusion, we see that the *y*-intercept increases. Furthermore, the curve increases slower respectively the curve is almost a straight line in the last row. Both observations have the same reason: Due to the smaller diffusion the bacteria have less to almost no signalling molecule to absorb. Increasing the extracellular degradation rate leads to the effect that we run out of signalling molecules earlier. That means for the FRET that the *y*-intercept increases as well and we always tend to the same end level as the standard FRET coloured in blue which means there are no signalling molecules left.
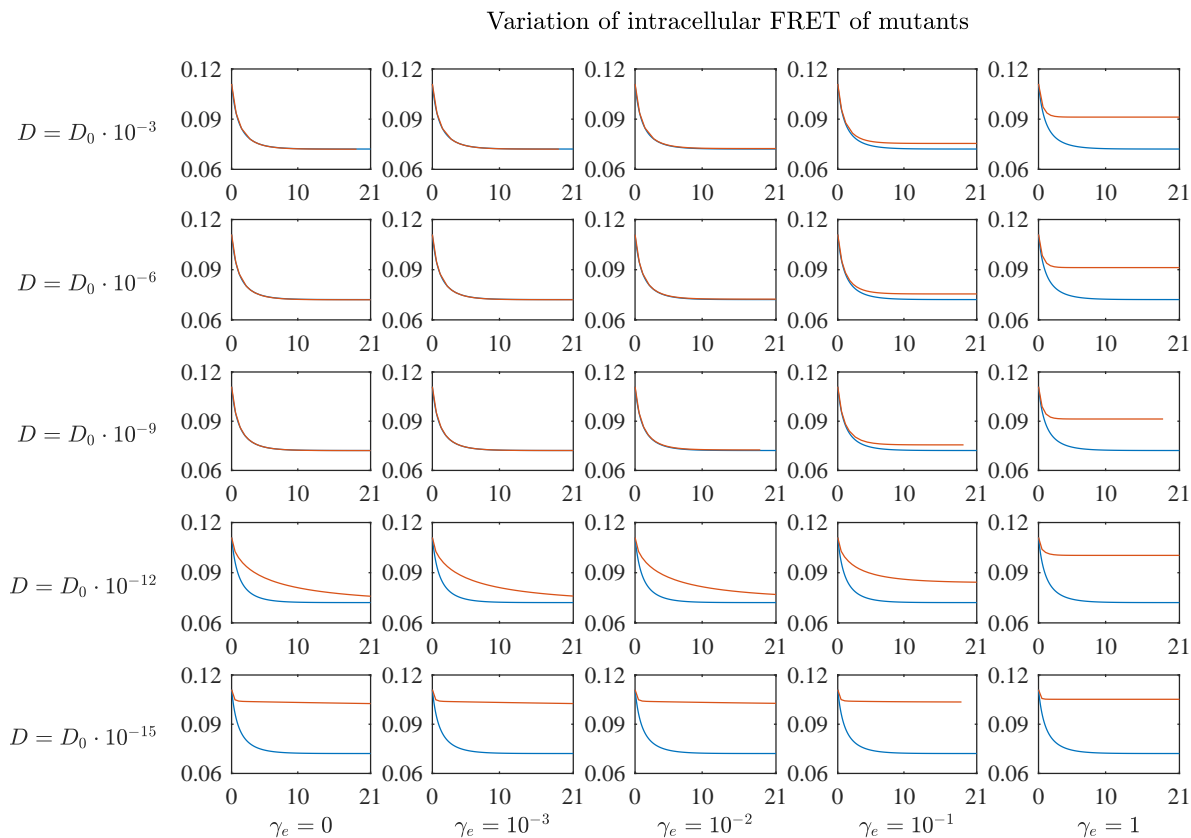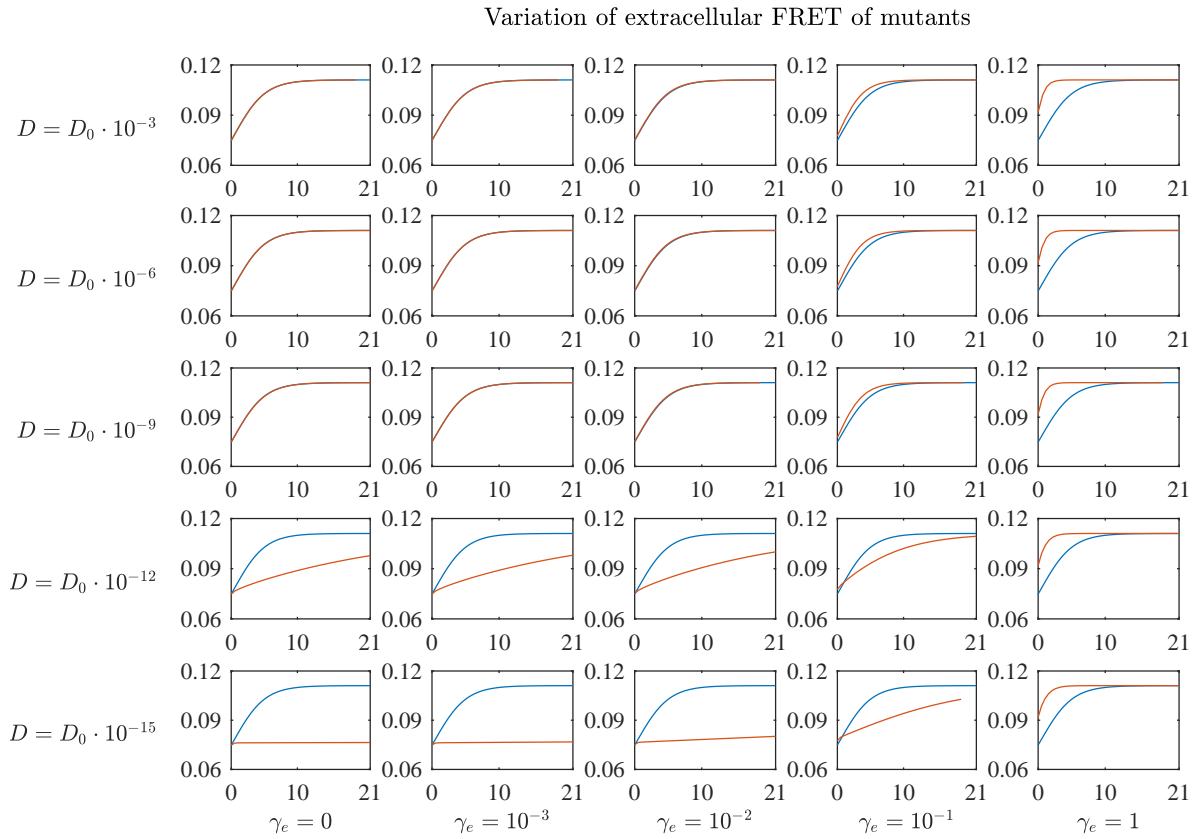
Variation of extracellular FRET of mutants

Figure 7.5.: *We use the parameter setting of subsection 7.1.1 with varying diffusion rate D and extracellular degradation rate γ_e. The red graphs corresponds to the extracellular FRET of the PDE model, the blue graphs of the ODE model.*

We start to discuss the results of the wild type with noise in figure 7.6 at first and consider the first column. As usual, increasing the diffusion rate starting with the standard diffusion shows no further effects. When we decrease the diffusion to $D = D_0 \cdot 10^{-12}$, there is hardly an effect notable, which is surprising, since we could see changes for the mutant type quite clear. Decreasing the diffusion further to $D = D_0 \cdot 10^{-15}$, there is only a small minimum notable and we have almost a straight line. But here, it has different reasons as for the extracellular FRET of the mutant type. For the mutant type, we had an almost straight line because there were hardly signalling molecules available to absorb. But the wild types produce their own signalling molecules. So because of the small diffusion, the wild type has the chance to absorb almost immediately its recently produced signalling molecules. Thus, the extracellular signalling molecule concentration barely increases which means we only have an extremely small decrease of FRET. Note that the wild type reaches both feedback thresholds. Otherwise the FRET would not reach the end level of the blue curve. Increasing the degradation rate, we see in the first four rows that the minimum of FRET increases and moves to the right which just means that the negative feedback regarding the production process is reached at later time points. Note that in the last row, we can not say any longer that we have reached

all feedbacks for all variation of γ_e's, because now, a strong extracellular degradation could be responsible that we run out of signalling molecules.

Figure 7.6.: *We use the parameter setting of subsection 7.1.1 with varying diffusion rate D and extracellular degradation rate γ_e. Here we find the solutions of the extracellular FRET of a wild type population with noise of the thresholds ξ_p and ξ_n. The red graphs corresponds to the PDE model, the blue graphs to the ODE.*

The explanations for wild type kinetics without noise in the threshold, see figure 7.7, is analogous. The FRET curve is only not so smooth which means we can see better when the thresholds were reached. That means the noise smooths the curve which was the reason to introduce it in the ODE model in section 3.9.

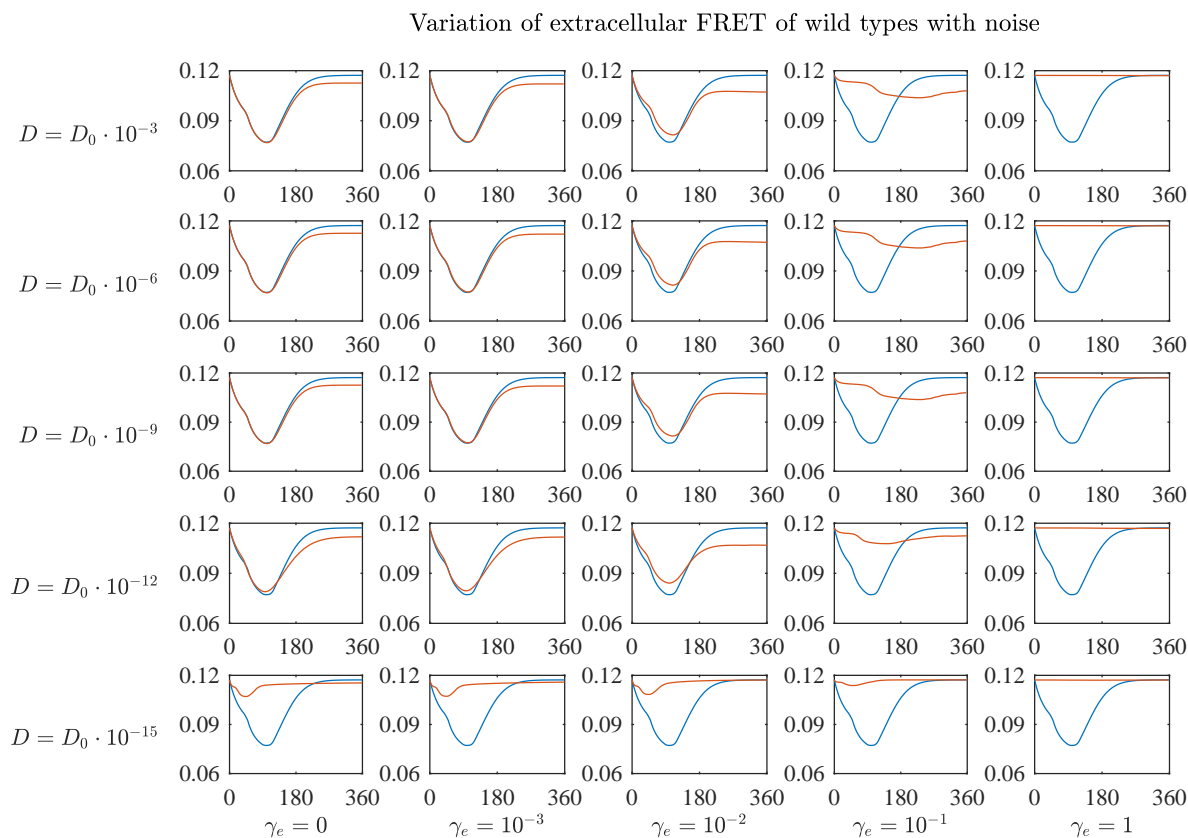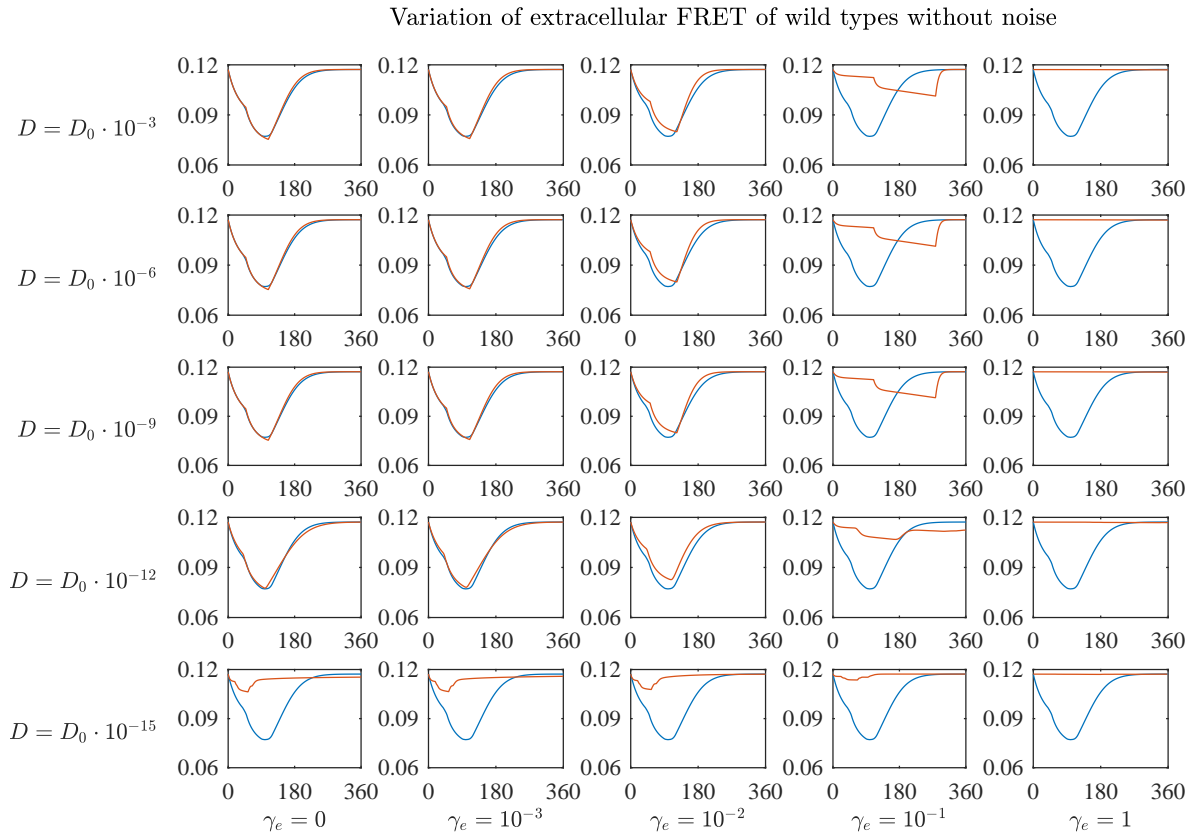Variation of extracellular FRET of wild types without noise

Figure 7.7.: *We use the parameter setting of subsection 7.1.1 with varying diffusion rate D and extracellular degradation rate γ_e. Here we have no noise regarding the thresholds. The red graphs corresponds to the PDE model, the blue graphs to the ODE.*

7.1.3. Variation of geometrical parameters

In the beginning of this chapter, we derived the geometrical parameters such as the radius of the pad r_p and the radius of a colony r_{col}. For the last one, we assumed that the boundary of the colony does not change in time. Naturally, that is not true. If bacteria grow, then of course they also grow spatially in x and y direction. So before we start to model a free boundary problem which is difficult solve, we vary the colony radius r_{col} and keep the number of bacteria equally to figure out if this change has a relevant effect. After that, we increase the radius of the pad r_p and of the colony r_{col} such that we obtain so called "macrocolonies" and wonder if this leads to new phenomena.

Variation of colony size

The radius of the simulated pad is still $r_p = 71\mu m$, but the radius of the colony size r_{col} varies now with the dimensionless factor $v = \{0.5, 0.8, 1.3, 1.7\}$ such that the adjusted colony size $r_{col,new}$ lies in the set $\{0.5 \cdot r_{col}, 0.8 \cdot r_{col}, 1.3 \cdot r_{col}, 1.7 \cdot r_{col}\}$ for each

simulation run. Note that we distinguish between a constant number of bacteria for each radii (case 1) and a changing number of bacteria according to the change of the colony radius (case 2). For the simulation, we use the models and parameter values of section 7.1.1.

Case 1: Let's consider a constant number of bacteria for each colony having different radii in each run. As always, we start with the mutant type to investigate if these changes have any effects to the uptake kinetics. Since the model equations work with a bacterial surface density, we need to adjust the density b_{m0} for each radii which reads then

$$b_{m0} = \frac{b_{col}}{r_{col,new}^2 \pi}.$$

Note that we assumed no population growth within this simulation, thus the concentration of bacteria is constant in time. The result for the uptake kinetic is given in figure 7.8. We see that the FRET curves, neither intracellular nor extracellular, are equally for all radii. So for the moment, the change of the geometrical colony size has no effect to the uptake process.
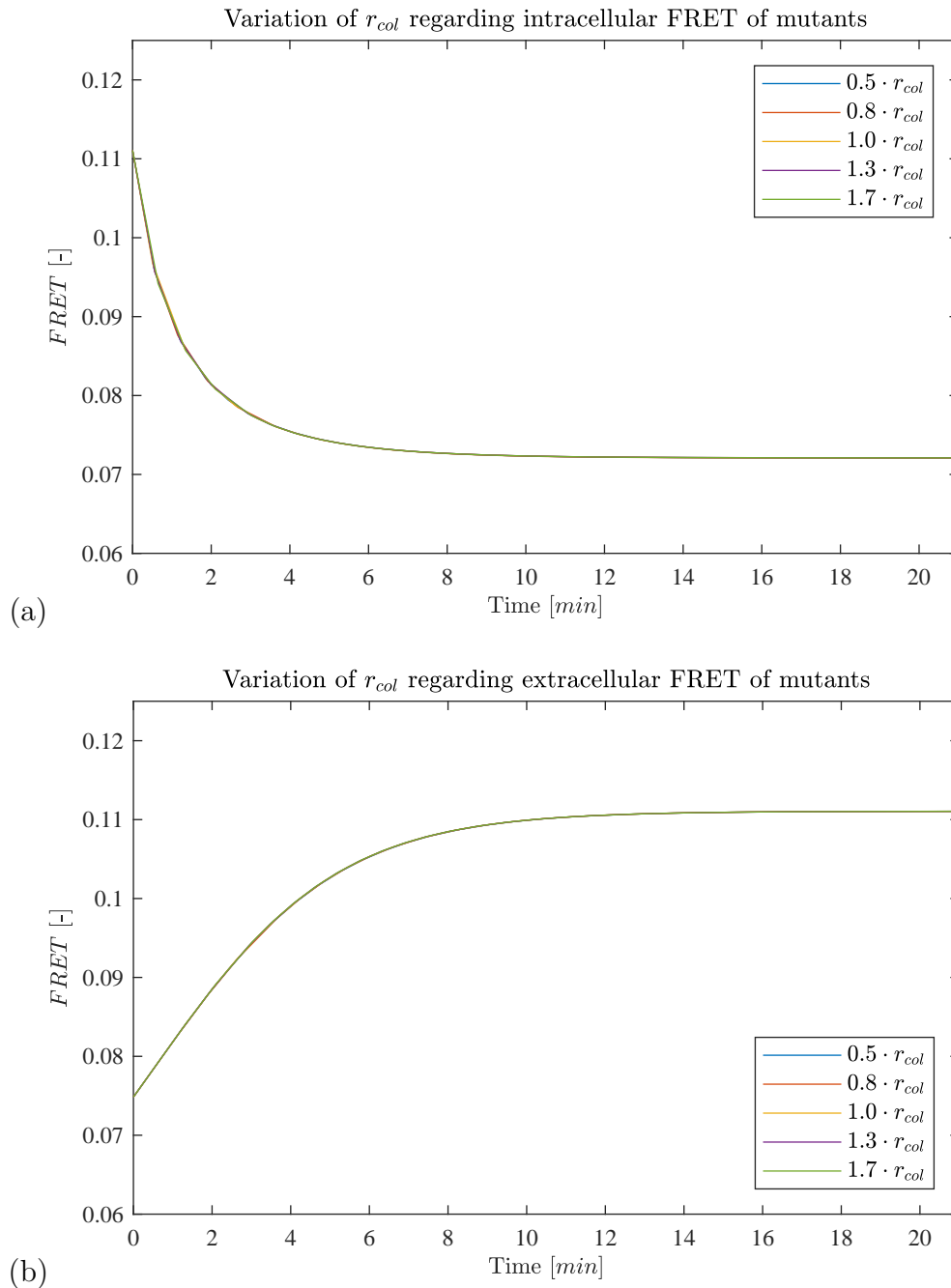
Figure 7.8.: *We use the parameter setting of subsection 7.1.1 with the same number of bacteria for each radii; (a): Intracellular FRET kinetics of mutant types with different radii; (b): Extracellular FRET kinetics of mutant types with different radii;*

We do the same approach for the wild type colonies and thus have to adjust for each radius the initial number and the carrying capacity to

$$b_{w0} = \frac{b_{col}}{r_{col,new}^2 \pi}$$

$$\kappa = \kappa_{ode} \frac{A \cdot h}{V_{ode} r_{col,new}^2 \cdot \pi \cdot h}.$$

As for the uptake kinetics, the FRET curves of the wild type are equal when we have no noise with respect to the thresholds, see figure 7.9(b). Figure 7.9(a) contains the noise and we see that they are not equal in the end any more because of that noise. However they behave altogether equally. That means the change of the colony radius has no significant effect to the production process of the wild type.

(a)

(b)
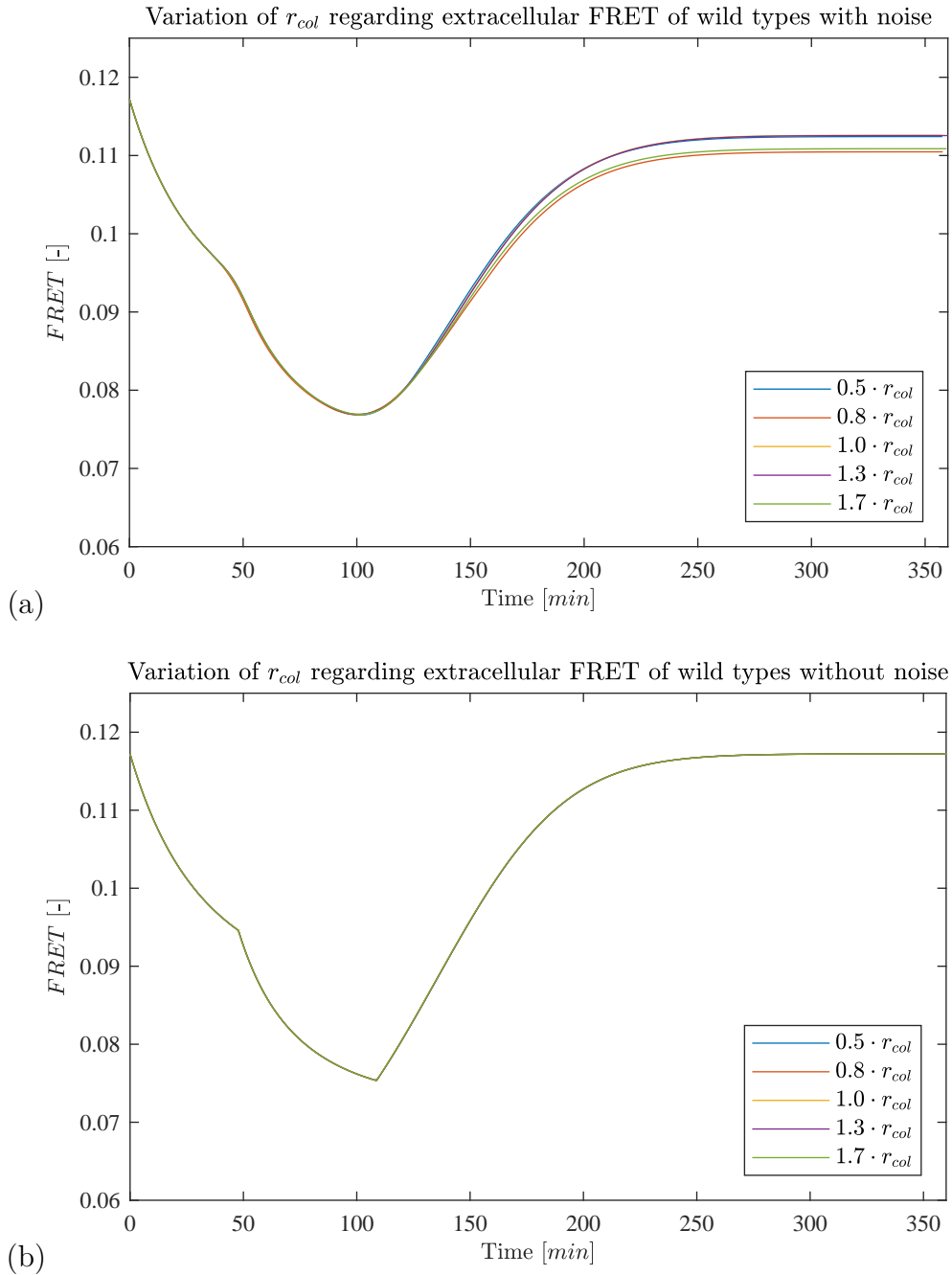
Figure 7.9.: *We use the parameter setting of subsection 7.1.1 with the same number of bacteria and an adjusted carrying capacity κ for each radius to plot the extracellular FRET kinetics; (a) There is a noise regarding the thresholds ξ_p and ξ_n; (b): There is no noise regarding the thresholds;*

Henceforth, we can conclude that both processes, uptake and production, are invariant regarding the change of the geometrical colony size. That means that a model with a free boundary problem would not yield further insights of the kinetics, at least not

for the current experimental setting.

Case 2: Now we adjust the number of mutants according to the factor of the colony radius r_{col} such that the density of bacteria for varying colony sizes is the same. Starting with the mutant type, we see when we adjust the colony size b_{col} according to the corresponding factor v, this factor cancels and thus, the density is the same for all simulation runs:

$$b_{m0} = \frac{v^2 b_{col}}{r_{col,new}^2 \pi} = \frac{b_{col}}{r_{col}^2 \pi}.$$

The results for all runs can be seen in figure 7.10. Let's consider the intracellular FRET kinetics results first. The bigger the colonies become and thus the total number of bacteria, the bigger is the end level of FRET. That is reasonable since each bacterium of a in total number bigger mutant colony has absorbed finally less signalling molecules. That means by implication that the extracellular FRET curve increases faster for bigger colonies since we have less signalling molecules in the environment.

Variation of r_{col} and same mutant colony densities regarding intracellular FRET

(a)

Variation of r_{col} and same mutant colony densities regarding extracellular FRET

(b)
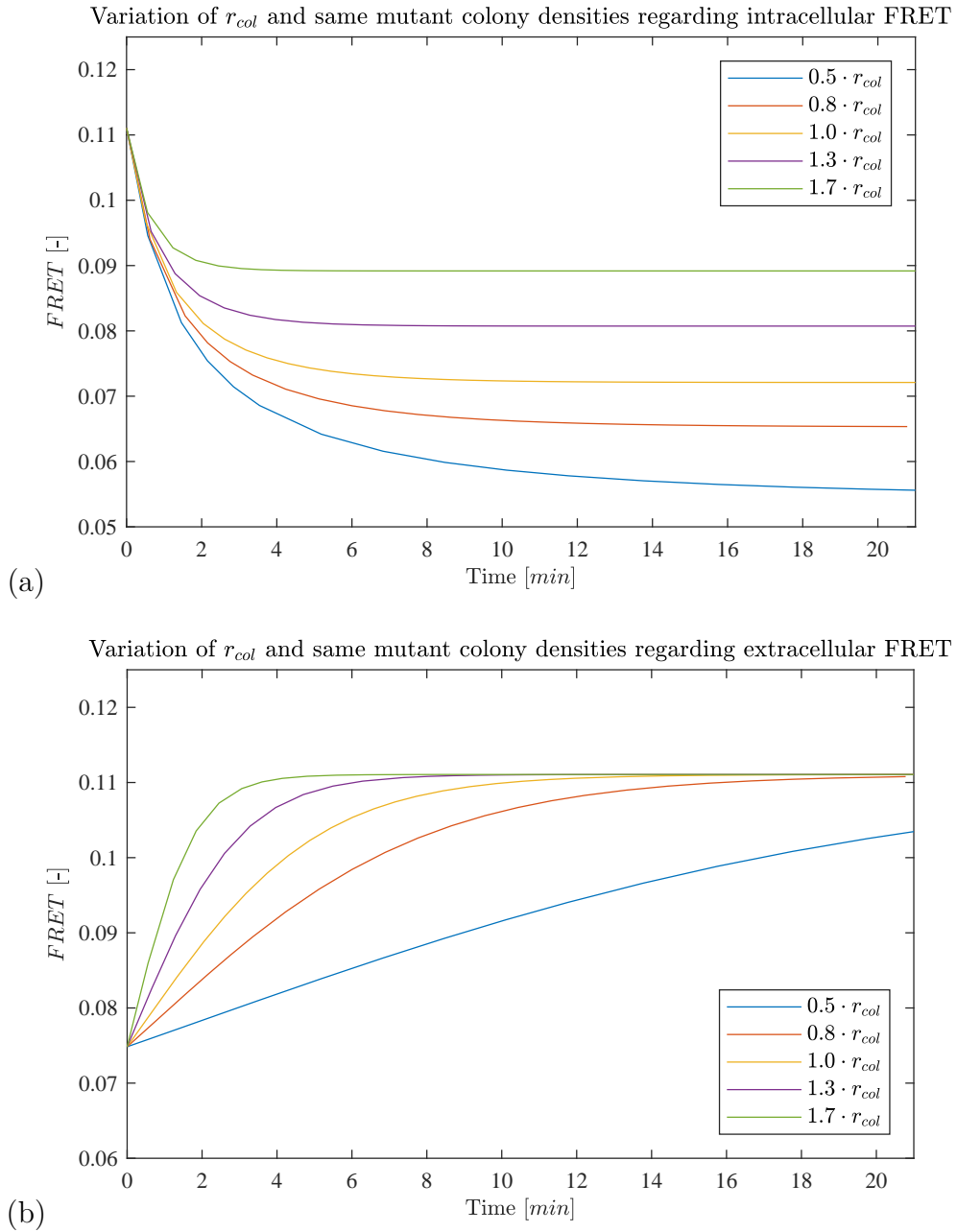
Figure 7.10.: *We use the parameter setting of subsection 7.1.1 with a growing number of bacteria according to each radii; (a): Intracellular FRET kinetics of mutant types with different radii; (a): Extracellular FRET kinetics of mutant types with different radii;*

We do the same approach for the wild type colonies, but have to adjust for each radius the initial number and the carrying capacity to

$$b_{w0} = \frac{b_{col}}{r_{col}^2 \pi}$$

$$\kappa = \kappa_{ode} \frac{A \cdot h}{V_{ode} r_{col,new}^2 \cdot \pi \cdot h}.$$

The simulation results are given in figure 7.11 whereas the plot in (a) contains the noise, plot (b) the results without noise. As usual, the FRET curves with noise reach different levels caused by the threshold noise. But for both cases, we can see the same behaviour as for the extracellular FRET of the mutant colonies, that is, the bigger the colony radius becomes, the steeper is the FRET curve. The explanation for that is the same as for the mutants. Additionally, by increasing the colony size, the minimum becomes smaller and is reached earlier.

Variation of r_{col} and same wild type colony densities regarding extracellular FRET with noise

(a)

Variation of r_{col} and same wild type colony densities regarding extracellular FRET without noise

(b)
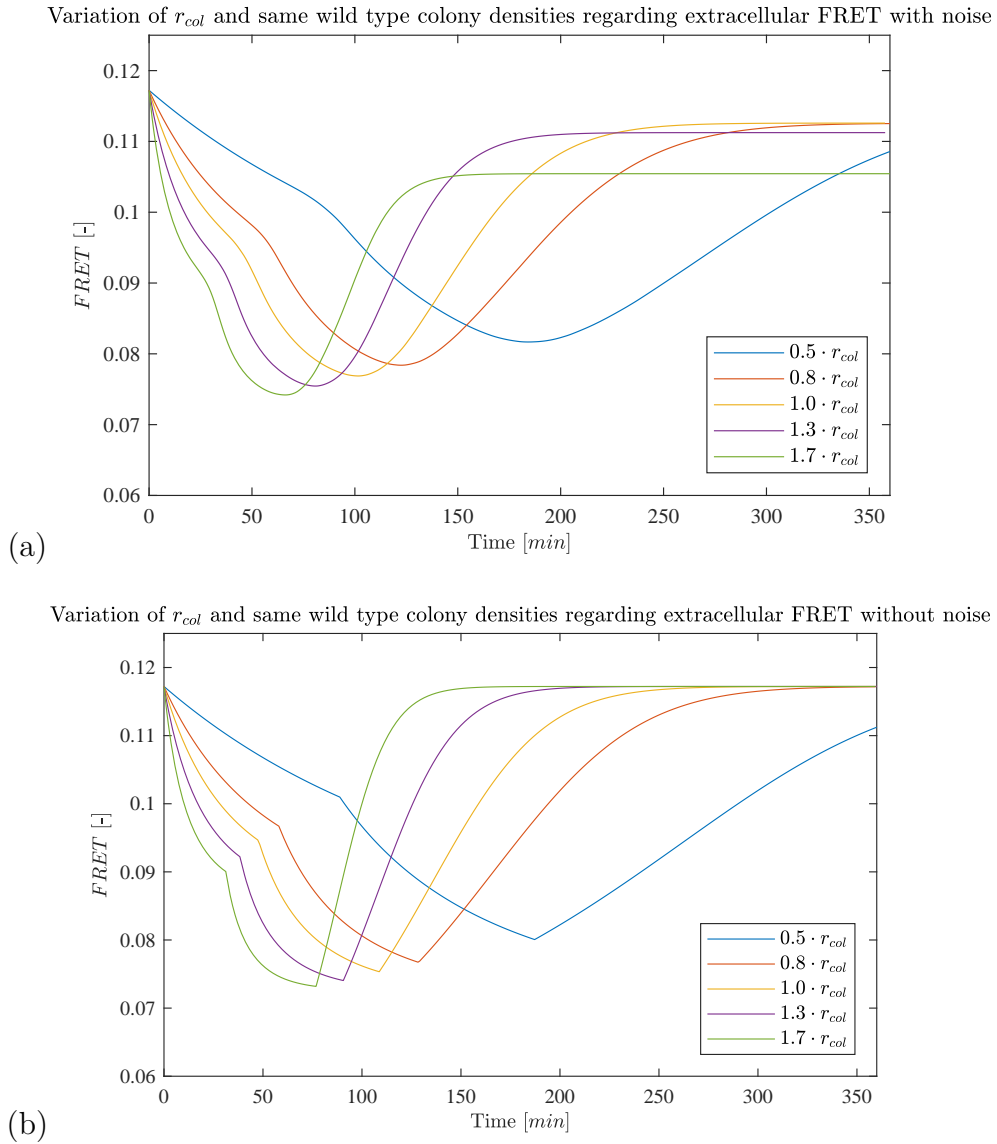
Figure 7.11.: *We use the parameter setting of subsection 7.1.1 with an adjusted carrying capacity κ and a growing initial number of bacteria according to each radii to plot the extracellular FRET kinetics; (a) There is a noise regarding the thresholds ξ_p and ξ_n; (b): There is no noise regarding the thresholds;*

Henceforth, we can conclude that the model behaves as expected.

Macrocolonies

So far, we considered relatively small colony sizes. Let's check if the results changes if we consider macrocolonies. Therefore, we increase the radius of the simulated pad by a factor of 5 which leads to a size of $r_{p,macro} = r_p \cdot 5 = 353\mu m$. In paragraph "Variation of colony size", the colony radius was varied by a factor set v. We enlarge this set also by

factor 5, leading to new radii $r_{col,macro} \in \{2.5 \cdot r_{col}, 4.0 \cdot r_{col}, 5.0 \cdot r_{col}, 6.5 \cdot r_{col}, 8.5 \cdot r_{col}\}$. Note that the ratio of the simulated pad and colony size is the same for macro- and microcolonies.

In figure 7.12, we see that the mutant macrocolonies behave like the microcolonies. There is only a very small difference which can only be caused by the spatial difference, that is, in the macrocolony case, the signalling molecule has to cover bigger paths. That means it takes a bit longer until neighbouring signalling molecules reach the colonies resulting in steeper FRET slopes for microcolonies. This hypothesis can be supported by the wild type macrocolony simulation, see figure 7.13. We detect no significant difference of macro- and microcolonies. Since wild types produce their own signalling molecules, the concentration of signalling molecules is higher there and they are not that dependent on neighbouring signalling molecules than the mutant colonies.

(a)

(b)

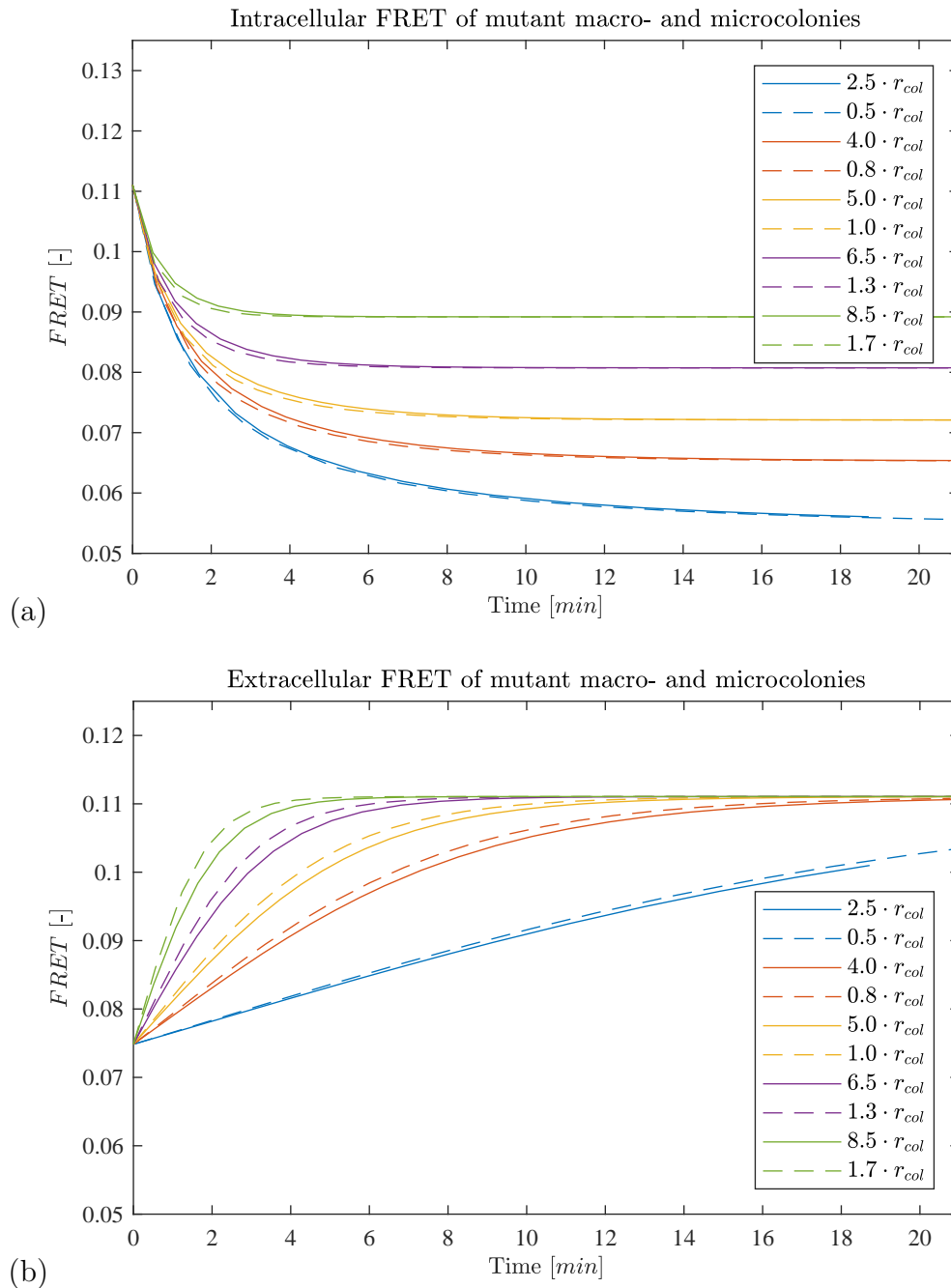Figure 7.12.: *We use the parameter setting of subsection 7.1.1 with a growing number of bacteria according to each radius. The dashed lines correspond to microcolonies of a same simulated pad - colony size ratio; (a): Intracellular FRET kinetics of mutant types with different radii depicted in a solid line; (b): Extracellular FRET kinetics of mutant types with different radii depicted in a solid line.*
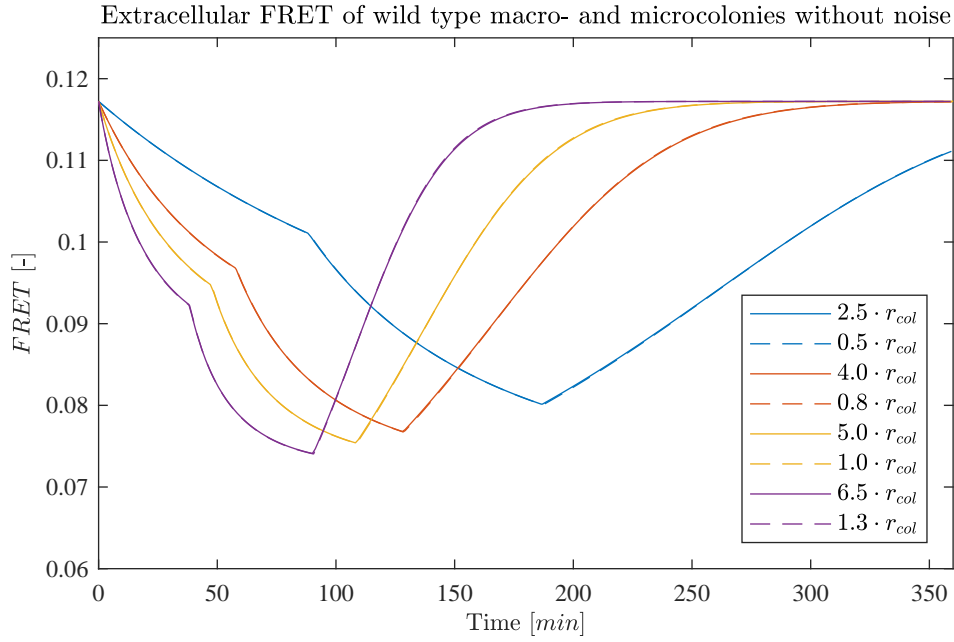
Figure 7.13.: *We use the parameter setting of subsection 7.1.1 with an adjusted carrying capacity κ and a growing initial number of bacteria according to each radii. We see the solutions of the extracellular FRET of a wild type population without noise regarding the thresholds. The solid curves correspond to the macrocolonies, whereas the dashed lines correspond to microcolonies of a same simulated pad - colony size ratio.*

Finally, macrocolonies do not yield significantly different solutions. Moreover, it seems that the FRET curve depends on the ratio of colony size and pad size as the comparison of macro- and microcolonies in figure 7.13 represents.

7.2. Reproduction of pad experiments results

In this chapter we solve the PDE-ODE system (4.7)-(4.12) with the recalculated parameter values from table 3.9 and compare experimental and simulated results. Yet, we don't know when the cell comes to the decision to initiate the sporulation process. It might be the threshold $\xi_n(\vec{x})$ or maybe some other trigger. In order to compare the results, we introduce a feedback ratio which can be compared to the experimentally observed sporulation ratios, see figure 4.1.

Definition 7.2.1 (Feedback ratios). *The **feedback ratio** λ_i of colony i at time t is given by*

$$\lambda_i(t) := \frac{\text{\# of cells achieving threshold within colony i at time t}}{\text{\# of cells of colony i at time } t_0}$$

with t_0 being the initial time point.

The **general feedback ratio λ** is given by

$$\lambda(t) := \frac{\text{\# of cells achieving threshold at time } t}{\text{\# of all cells at time } t_0}.$$

Remark 7.2.2. *The general feedback ratio can also consider exclusively wild type respectively mutant colonies. Then we will refer to this as $\lambda_W(t)$ **wild type** respectively $\lambda_M(t)$ **mutant**.*

In figure 4.2, there is some bacterial growth data of one colony given. We see that it starts with one bacterium, that is, $b(t_0) = 1$. The bacteria was counted regardless of its location. So we fit the data to the solution of ODE logistic growth function, see (3.28). The best fit solution is given in figure 7.14 and the corresponding parameters read

$$\alpha_{ode} = 13.5 \cdot 10^{-3} \frac{1}{min}$$

$$\kappa_{ode} = 44.8.$$
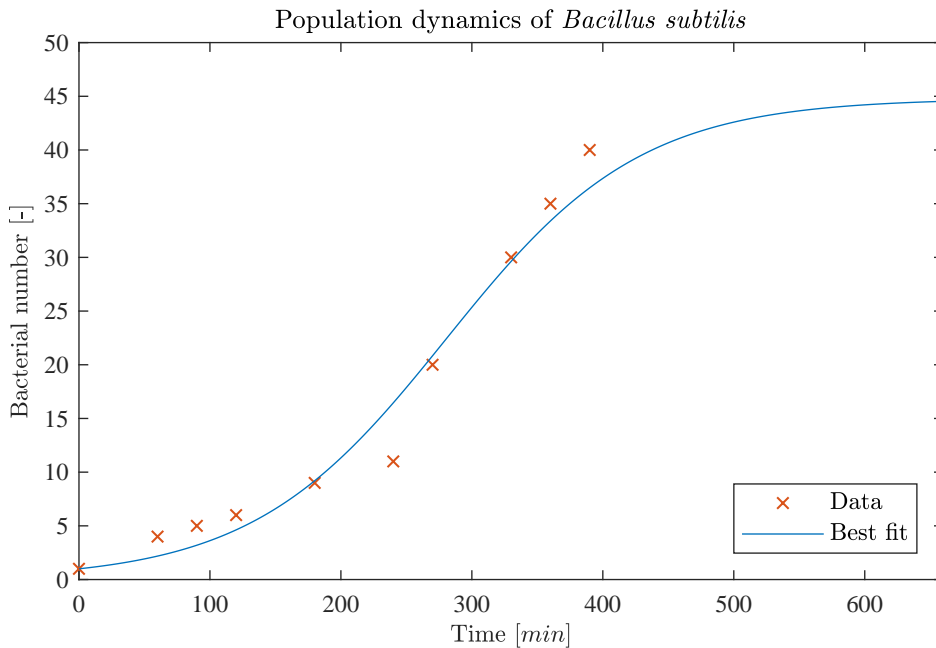
Figure 7.14.: *The data is given in figure 4.2. Assuming logistic growth of the bacteria, the best fit is depicted as a solid blue line.*

The exponential reproduction rate α_{ode} can be used for the PDE equation (4.9) without any changes, that is $\alpha = \alpha_{ode}$. But the carrying capacity κ_{ode} has to be divided by the reaction volume of one colony to use it for the PDE setting, that is $\kappa = \frac{\kappa_{ode}}{A_{col} \cdot h}$.

7.2.1. Wild type experiment

We assume that hypothesis HW 4 holds and use the corresponding parameter set in table 3.9. These were recalculated with the approach in section 6.4. In this section, we use the negative feedback that is, production of signalling molecules stops, as a trigger for sporulation and calculate the feedback ratio with respect to that threshold. The result of this simulation is given in figure 7.15(c). For the moment, this seems to be a good result since the curve is similar to the black depicted solid curve in the top plot of figure 4.1. Additionally, we can see in figure 7.15(a) that the mean extracellular signalling molecule concentration is at most approximately $10\frac{nmol}{m^2}$ meaning that the exponential absorption of signalling molecules in the PDE model is justified. Furthermore, all colonies have the same feedback ratio characteristic such that it seems there is no spatial effect among wild types recognizable. In figure 7.16, we see the distribution of the signalling molecule concentration and bacteria which has reached the negative feedback threshold. Let's start with (a). On the left, we see the signalling molecule concentration and it seems, that it is spatially constant. However, if the C_e axis is rescaled, that is the plot in the middle, we can see peaks arising due to the production of signalling molecules by the bacteria. On the right, we see that in each colony some bacteria has reached the negative threshold. It seems there is no structure which bacteria in the colony reaches the threshold first. The plots in (b) shows the state 30 minutes later. More bacteria has reached the threshold meaning that less bacteria produce signalling molecules and the peaks become smaller. After further 15 minutes, that is (c), there is hardly bacteria left producing signalling molecules. Since they still absorb them, we can see sinks at the distribution of signalling molecule concentration.
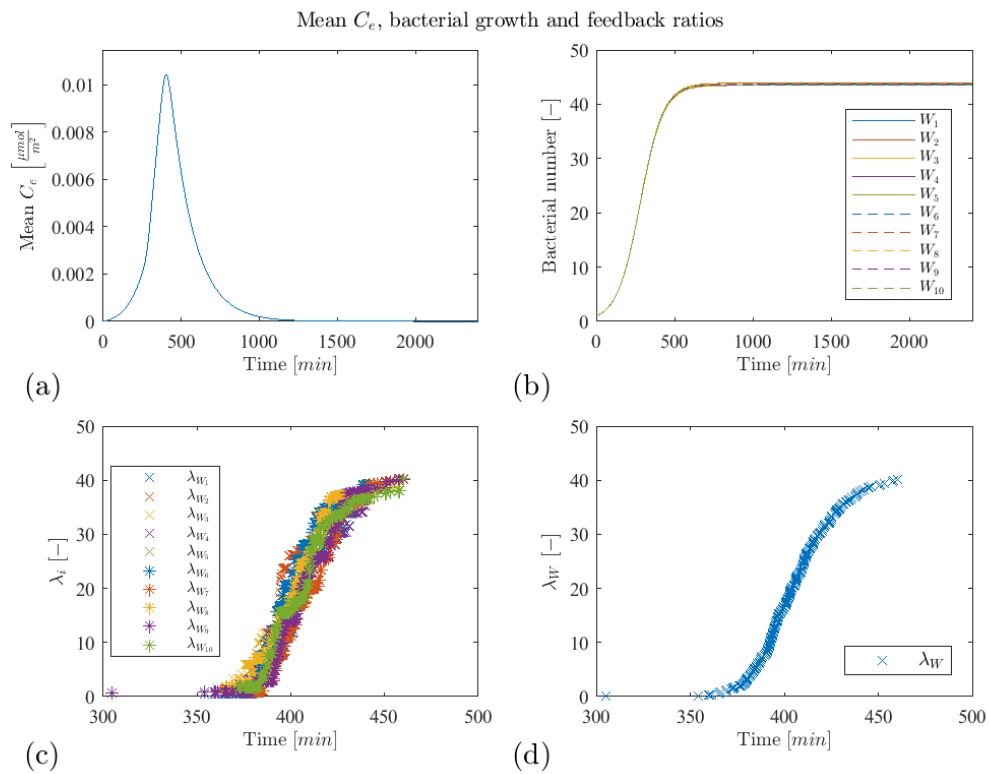
Figure 7.15.: *Simulation results of a wild type population with noise; (a): Mean extracellular signalling molecule concentration in the pad; (b): Bacterial growth of each colony; (c): Feedback ratio for each colony using the negative feedback; (d): General feedback ratio regarding wild types using the negative feedback.*
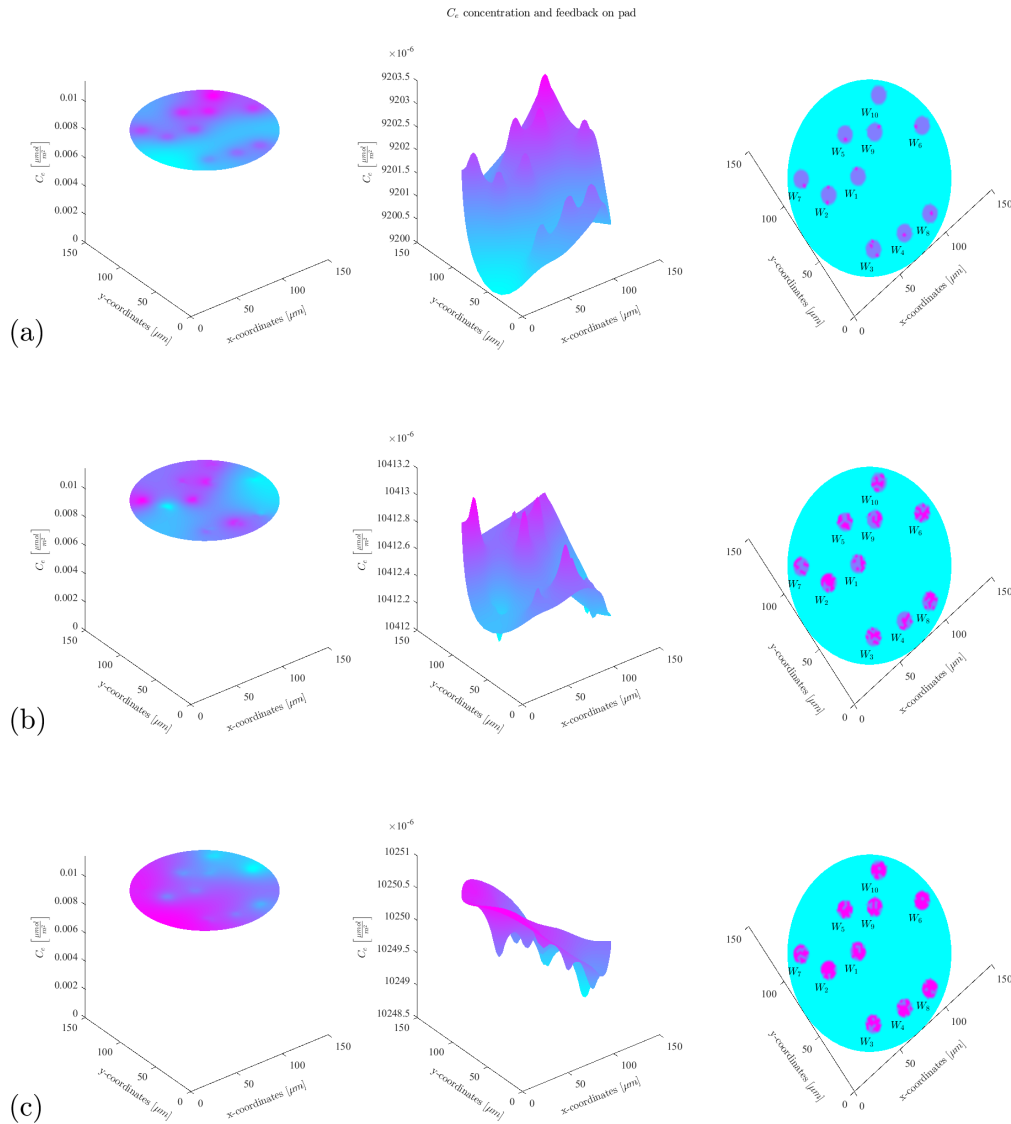
Figure 7.16.: *On the left and middle column, the distribution of the signalling molecule concentration is given. On the right, we see the pad with the colonies. A pink marked dot on the colony means that bacteria has reached there the negative feedback; Plots correspond to (a) $t \approx 370$ minutes, (b) $t \approx 400$ minutes and (c) $t \approx 415$ minutes;*

We stated, that there are not really spatial effects noticeable. However, the noise of the threshold somehow hides the spatial effects. Removing the noise, one can observe on the one hand that the feedback thresholds of the colonies are separated, see figure 7.17(c). On the other hand, considering a colony, e.g. W_1 in figure 7.18, the bacteria in the middle reaches the threshold first evolving then to the outer bacteria. We also note, that all bacteria reach the threshold in some seconds.
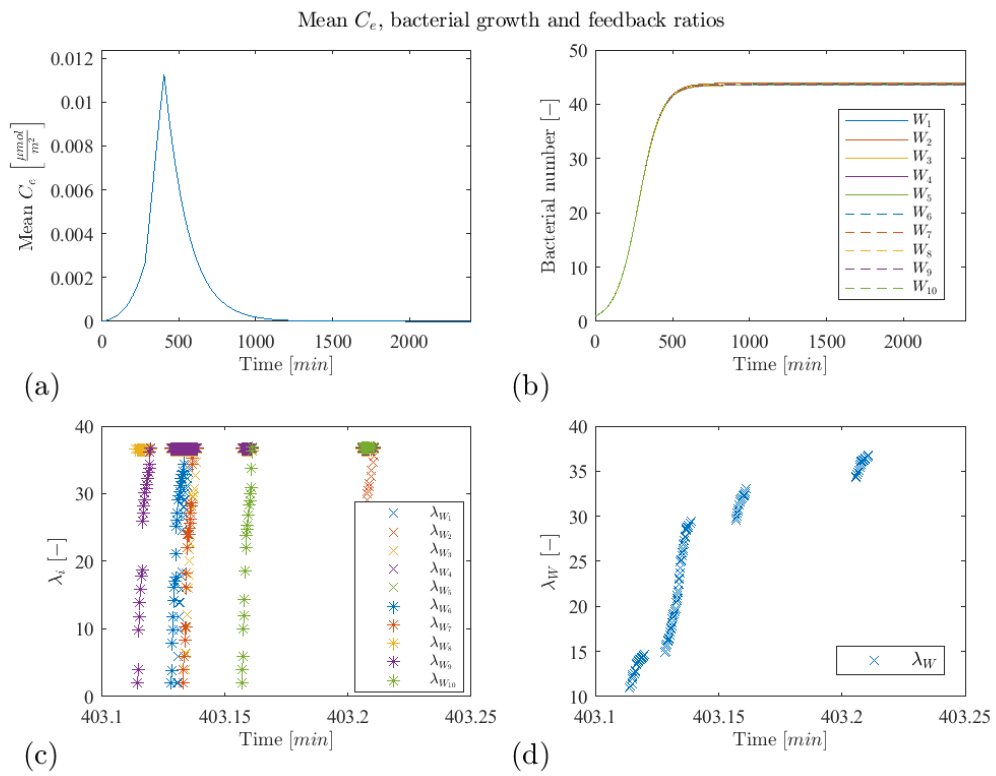
Figure 7.17.: *Same description as in figure 7.15, but now with no noise in the thresholds.*
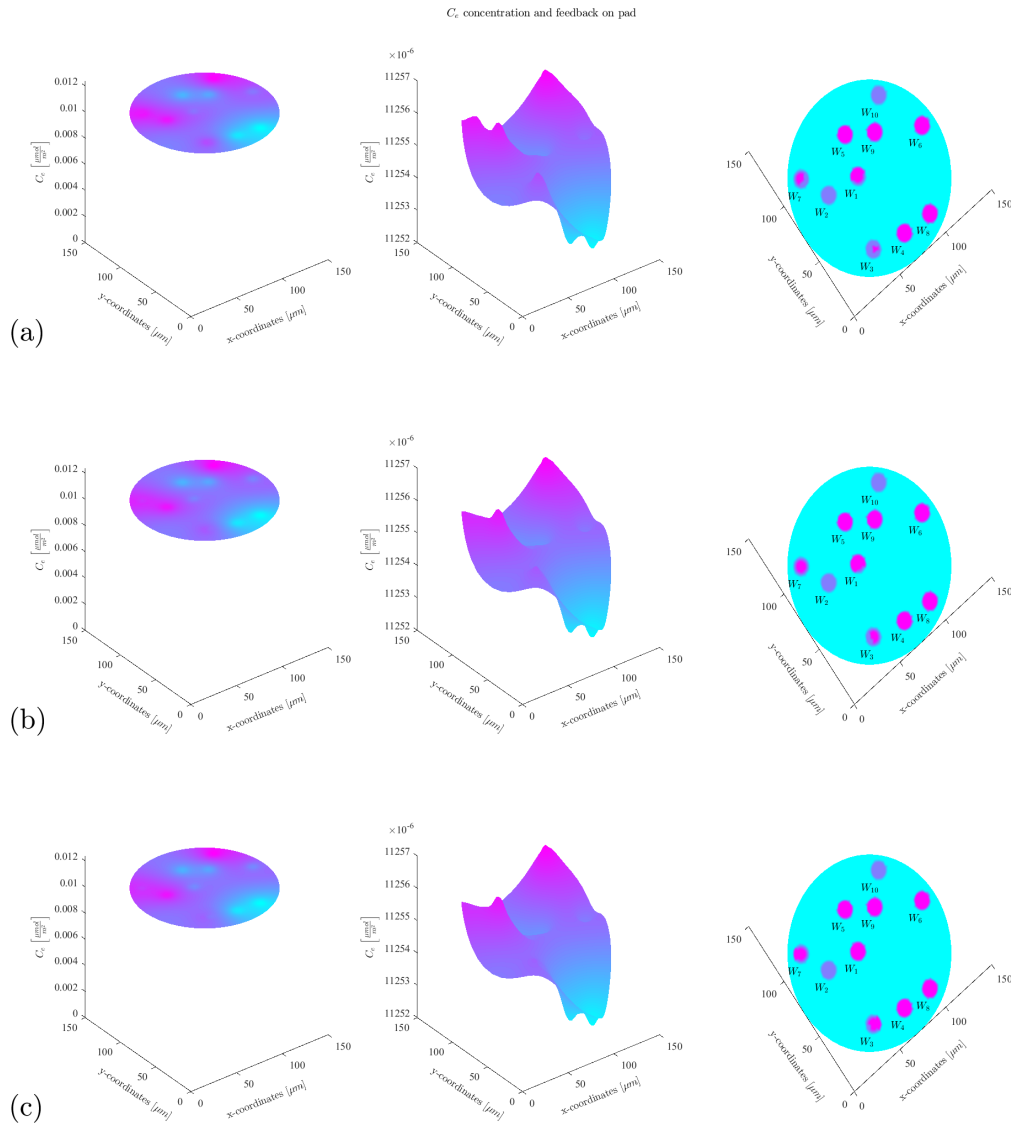
Figure 7.18.: *Same description as in figure 7.16but now without noise in the thresholds; Plots correspond to (a) $t \approx 403.135$ minutes, (b) $t \approx 403.136$ minutes and (c) $t \approx 403.137$ minutes;*

7.2.2. Mutant experiment

In this chapter, we concentrate on the experimental stimulus of $10\frac{\mu mol}{l}$ only. The mutant's parameter set is given in table 3.3 and we assume hypothesis HM 2 which regards to a continuous absorption of signalling molecules. We recalculate the parameters as described in section 6.4. For the wild types, we used the negative feedback of the production term as indicator to calculate the feedback ratio. We know that mutants were characterised as bacteria producing no signalling molecules. However, we can still eval-

uate when the intracellular concentration of the mutants reach in this case an imaginary negative feedback. The plot of the feedback ratio is given in figure 7.19(d). One can see that it starts way too early! A reason could be the exponential absorption of signalling molecules since one restriction to the model approach was that it works only for small extracellular concentrations in the range of $\frac{nmol}{l}$. In a personally received manuscript of the μCats laboratory, one can find an approach to model the uptake of the ODE model with a sigmoidal function. We use their best fit values to find the parameter for a linear absorption which reads finally $\sigma_c = 0.2 \cdot 10^{-12} \frac{l}{min \cdot cells}$. We do not go here into further details how the model equations and numerical approach changes. Instead, we consider immediately the result which is given in figure 7.20. One can see that the extracellular concentration in (a) is more or less constant. That's because of the linear absorption. Again, the feedback ratio in (d) increases way too early meaning that the absorption term is not the crucial factor of the phenomenon.
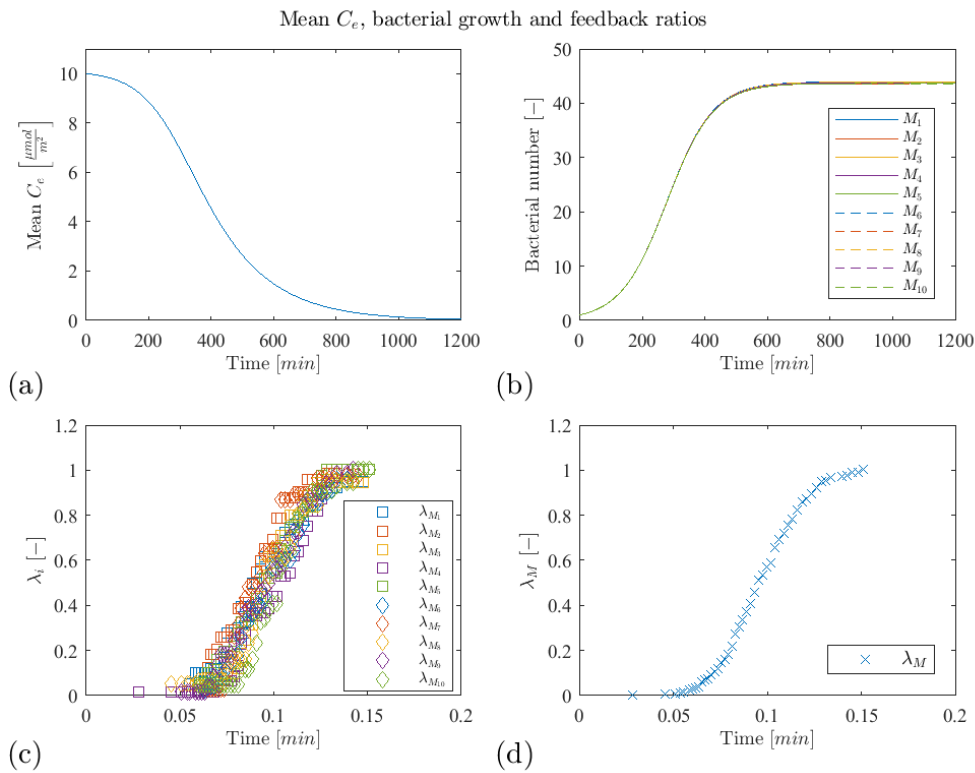
Figure 7.19.: *Same description as in figure 7.15 but now for mutants.*
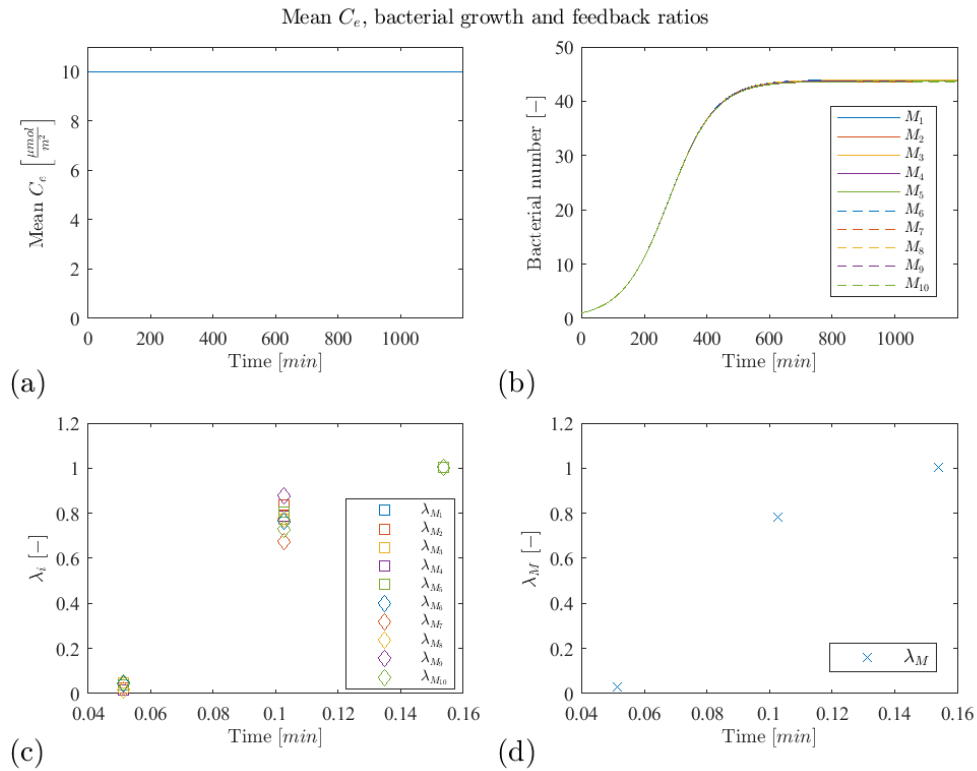
Figure 7.20.: *Same description as in figure 7.19 but now with a linear absorption.*

So far, we assumed no extracellular degradation rate γ_e. But the environmental situation in the PDE is different as for the ODE experiments. Thus, the signalling molecule might be degraded by extracellular peptidases. We run the simulation with a linear absorption as above and a high extracellular degradation rate of $\gamma_e = 1\frac{1}{min}$. The simulation results can be found in figure 7.21. Although the extracellular signalling molecule concentration in (a) decreases very fast, there is still enough left such that the feedback is reached very fast.

163
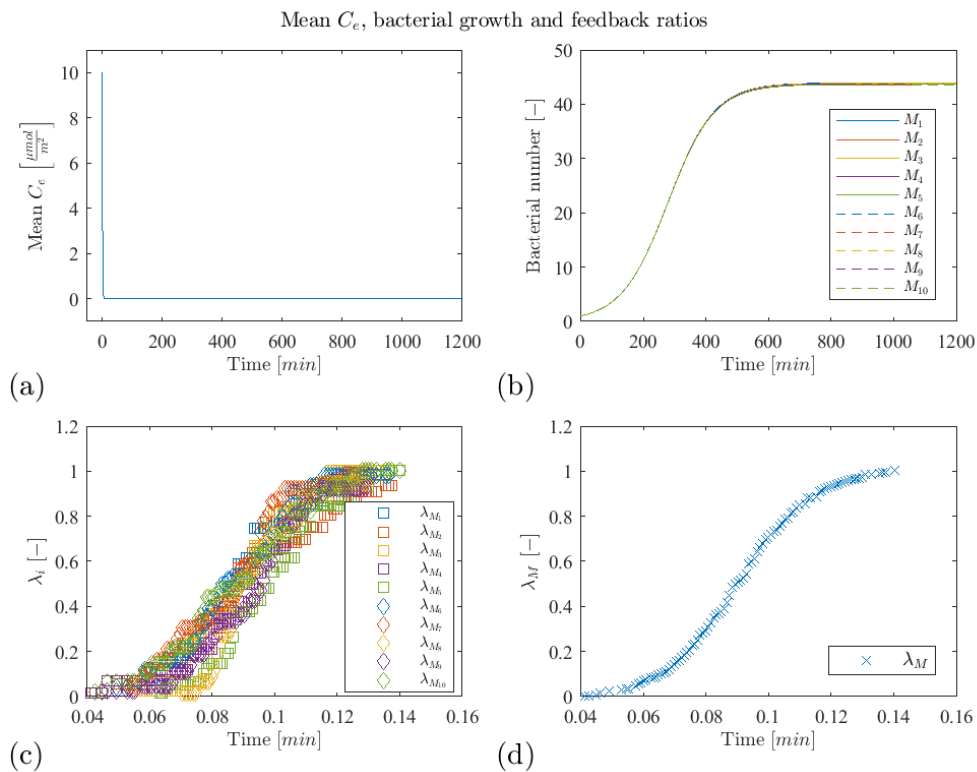
Figure 7.21.: *Same description as in figure 7.20, but now with a high extracellular degradation rate $\gamma_e = 1\frac{1}{min}$.*

However, we can detect a similar phenomenon as for the wild types. Assuming also no noise in the threshold, we can see in figure 7.22, right column, that the bacteria on the outside of the colony reaches the threshold first, evolving then to the inner bacteria. So the feedback behaviour is, considered in a spatial way, vice versa compared to the wild types.
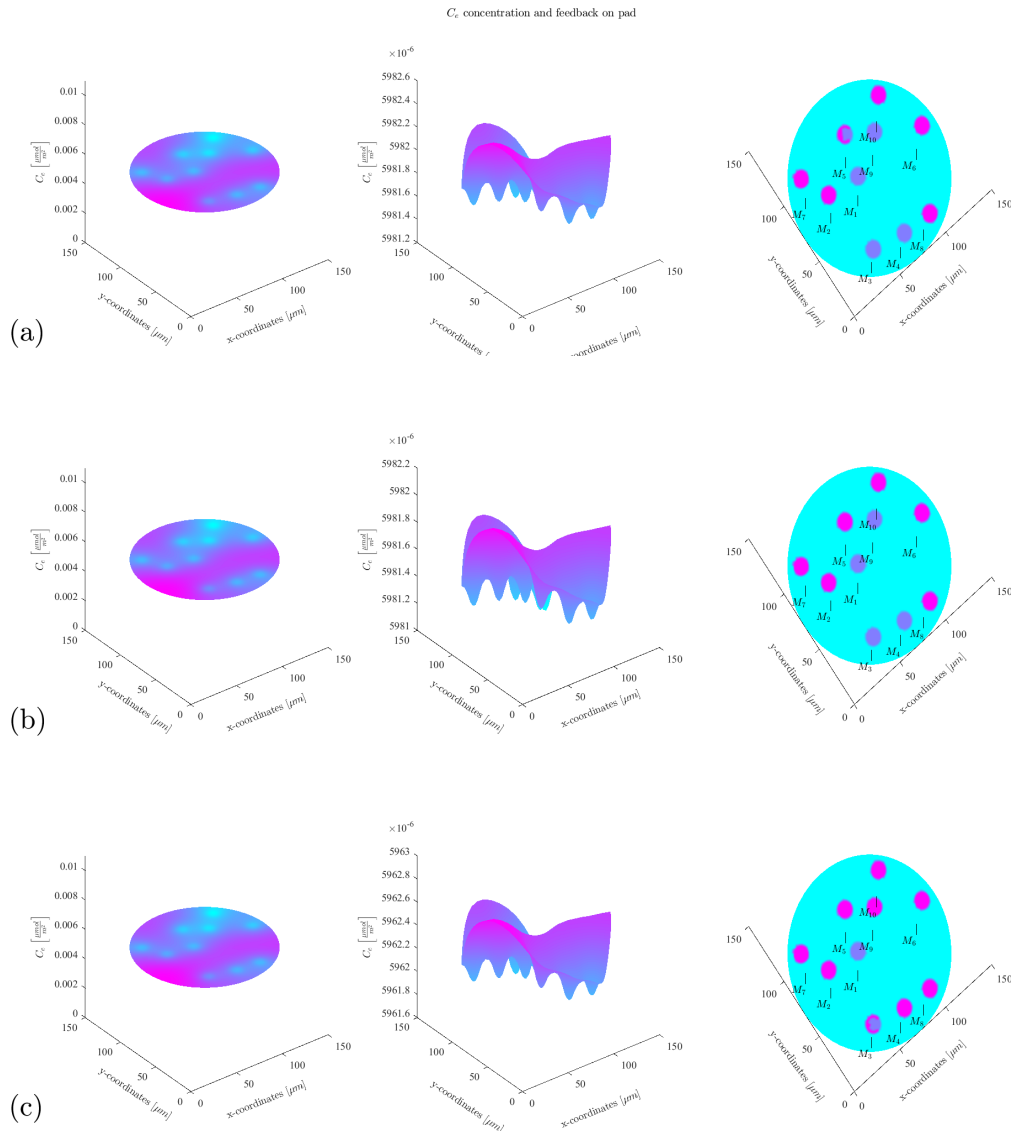
Figure 7.22.: *Same description as in figure 7.16, but now for mutant colonies; Plots correspond to (a) $t \approx 339.77$ minutes, (b) $t \approx 339.78$ minutes and (c) $t \approx 340.5$ minutes;*

7.2.3. Wild type - mutant ratio experiment

Although the evaluation of the stimulation experiments of the mutant yields no satisfying results, we still test the setting of different wild type - mutant ratios. We use the parameter set of table 3.9 which corresponds to the wild type assuming hypothesis HW 4 and table 3.3 with hypothesis HM 2 for the mutants. The results are given in figure 7.23. There we see, that if we increase the number of mutants, the feedback ratio starts to rise later. Also the slope of the feedback ratio decreases. Compared to the

experimental result which is given in the second plot of figure 4.1, it is very different. On the one hand, in the experiments, all ratios start to rise approximately at the same time. On the other hand, the feedback ratios tend to different levels whereas in our plot, all reach approximately the same level.
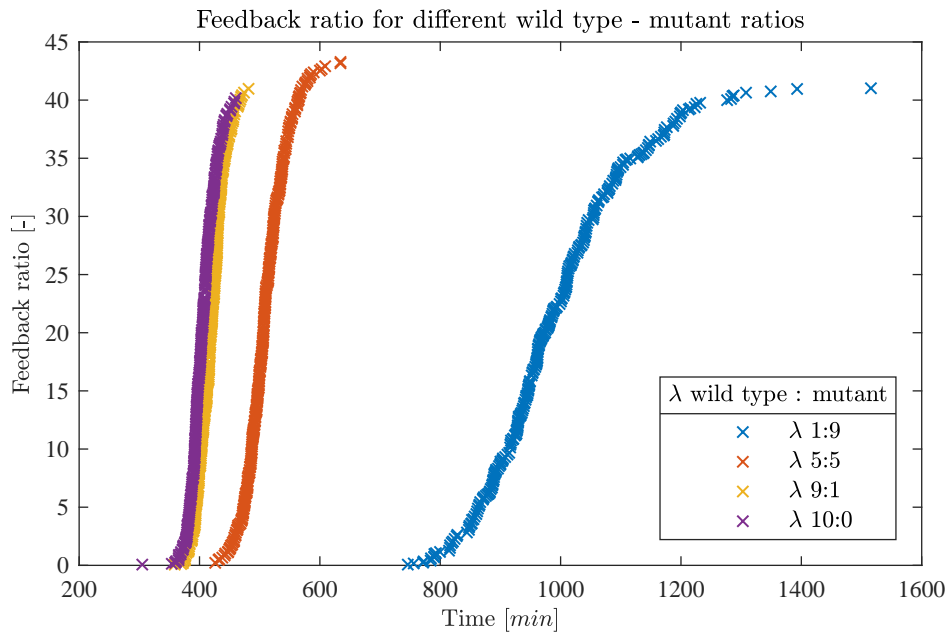
Figure 7.23.: *One can see the feedback ratios for different ratios of wild type - mutant colonies.*

Let's consider anyway the 5 : 5 ratio experiment in figure 7.24 in more detail. We can consider that the mutants do reach the threshold later than the wild types since the slope of the general feedback ratio regarding the wild type is bigger than the one of the mutant. This can be explained by the fact that the mutants have to wait until signalling molecules diffuses to them. So we can detect a spatial effect here which coincides with the observations of the μCats laboratory.
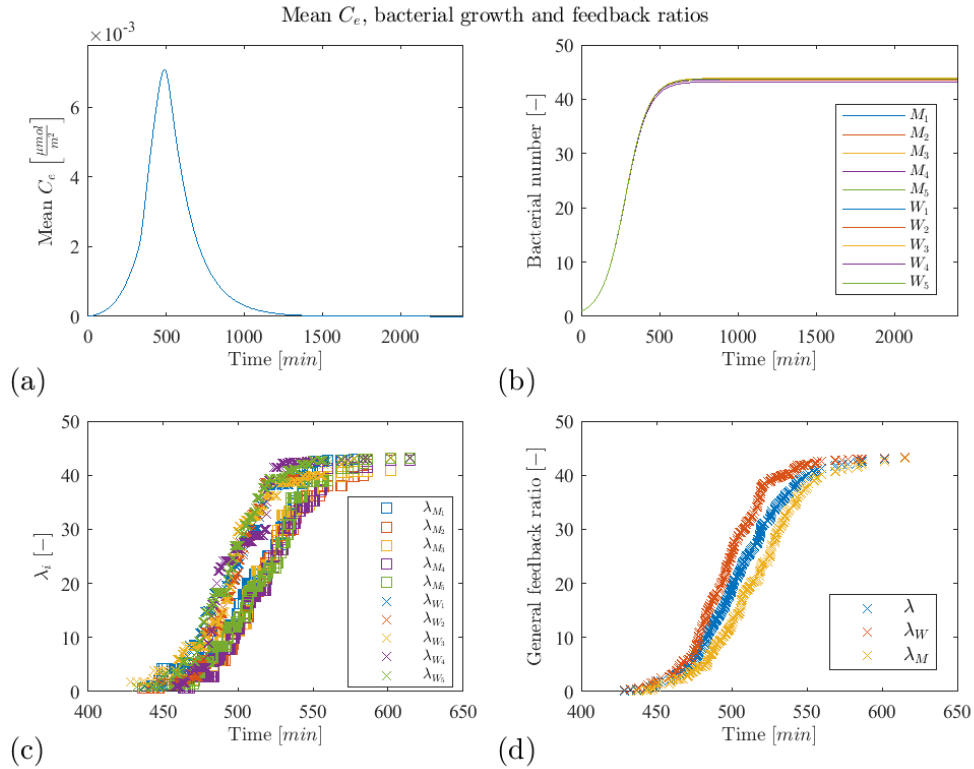
Figure 7.24.: *Same description as in figure 7.15 for a* 5 : 5 *ratio experiment.*

7.3. Conclusion for the PDE model

After we have evaluated the PDE model, we checked the influence of the FRET kinetics by varying the diffusion rate D and extracellular degradation rate γ_e. If we increase the degradation rate, then we obtain a slower decrease of intracellular FRET with a higher end level. The end level of the extracellular FRET increases as well and so do the intercept. If we increase the diffusion rate, there is no significant change of the results. Decreasing the diffusion though, the spatial effects become more significant. The intracellular FRET decreases slower and the end level increases, whereas the intercept of the extracellular FRET increases and the end level decreases a bit.

Changing the geometrical colony size assuming the same number of bacteria leads surprisingly to no change, neither for the absorption process nor for the production process. Adjusting then the bacterial number to the corresponding colony size, the intracellular FRET level increases by increasing the mutant colony size. For the extracellular FRET, the slope is steeper if the colony size is increased and all variations tend to the same level. The results of the wild type macrocolonies is similar. The slope of the extracellular FRET becomes steeper by increasing the colony size. Furthermore, an increased bacteria size leads to a higher concentration of signalling molecules and thus, the minimum becomes smaller. Additionally, both threshold feedbacks were reached

earlier for the same reason.

The reproduction of the wild type experiments yield reasonable results. We see that spatial effects are small since the feedback ratio starts to increase for (almost) all colonies simultaneously after almost 6 hours. After 2 hours, all bacteria in each colony have reached the negative feedback, see figure 7.25. That means, from initially 1 bacterium we obtain at the end approximately 40 spores. Compared to the experimental results, see the black curve of the second plot in figure 4.1, the result is acceptable, but not so good. There it took at least 8 hours until we are nearby reach the maximum number of spores.
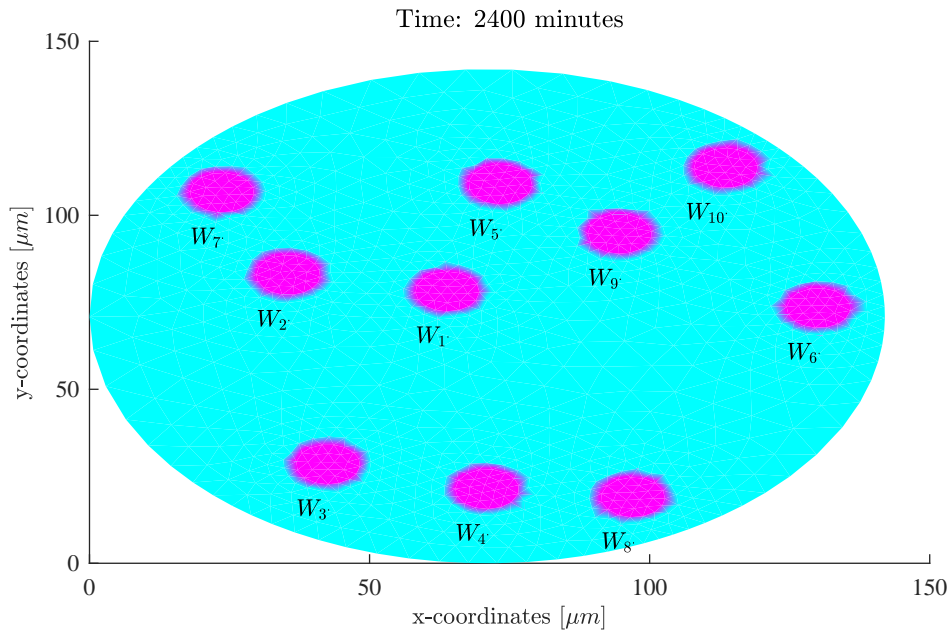
Figure 7.25.: *If a point in the grid has reached the negative feedback, it is marked in pink. Since each colony is fully pink, each bacterium has reached the negative feedback.*

The stimulation of the mutants completely failed since the negative feedback is reached too early. The absorption rate σ is just to high and neither depend on the exponential approach nor on the linear approach. Even a high extracellular degradation rate γ_e yields no significant improvement. Also the simulation of the ratio experiment generates no acceptable results. Instead of starting to increase at the same time and reaching different levels, the different ratios start to increase later the more mutants we have in the pad and all ratios have the same level. The one and only similarity is the slope of the ratios: The more mutants we have, the lower is the slope of the ratios. That is reasonable since mutants do not produce signalling molecules and therefore, they have to wait until signalling molecules reaches them.

We were also not able to reproduce quantitatively the experimental results of the ratio experiments. However, we found a spatial effect considering the 5 : 5 ratio experiment

in more detail, that is, mutants reach the feedback later than wild types.

Nevertheless, it seems that the parameter values of the ODE models regarding to the shake flask experiments can not be used for the PDE model regarding the pad experiments. There is even the possibility to change the model equation which is discussed in the conclusion chapter 8 in more detail.

Chapter 8

Conclusion/Prospects

In the beginning of this thesis, we wonder if spatial effects regarding the initialisation of sporulation in bacterial colonies can be explained by mathematical models. Before we deal with PDEs, we consider first ODEs to obtain more informations of the production and absorption processes of signalling molecules. After that, we imply the obtained results into the PDE model.

As stated, the first approach was to model the signalling molecule kinetics with an ODE model in chapter 3 to evaluate experimental results and obtain some insights in the production and absorption process of signalling molecules. We stated various hypotheses regarding those processes leading to diverse models. For each model, we were able to state existence and uniqueness of solutions and performed after that a best fit simulation. Let's start to recite the results of the absorption process of mutants. On the one hand, we saw in section 3.5 that the absorption of signalling molecules with a constant rate is maintained over the experimental time and yields very good FRET fits for a stimulus of $10\frac{nmol}{l}$. On the other hand, the data of a higher stimulus of $100\frac{nmol}{l}$ can not be fitted with the model given in section 3.5. Furthermore, changing the absorption process from a linear function to a sigmoidal function yields better results for the first four data points, but then it failed, too. At a first glance, it seemed that the absorption stops. However, a slower absorption of the signalling molecules by the mutants could be also the reason for the slower increase of extracellular FRET. Thus, we could gain further insights of the absorption kinetics if we have data points for a wider time range and more data points at later time points. A side result while testing the hypotheses with respect to the absorption process yields that there are neither an intracellular degradation nor an extracellular degradation on a relevant level. The production process of signalling molecules by wild types yields very good results if we include two switches, see section 3.11 respectively section 3.10. First, there is a switch from an initially low, constant production rate to a higher, constant produc-

tion rate. After a certain length of time, the production process stops. Both switches are controlled by the intracellular signalling molecule concentration, reaching certain thresholds. However, there is the open question of competition effects regarding the absorption of signalling molecules since the wild type produces further molecules which are absorbed by the same pump. Assuming a competition effect, we obtain still a very good FRET, only the production rates and feedback threshold change. That means the data is not consistent in order to determine the parameters. A different experiment is required to decide if the competition effect can be rejected or not. Note that the μCats laboratory rather supports the idea of a competition effect.

Then we stated a PDE-ODE model in chapter 4 using the informations from above. Unfortunately, we were only able to prove uniqueness for a special case of the PDE-ODE system (4.7) - (4.12), that is, for a time constant bacteria population. So far, uniqueness of the full system can be shown only for a certain time interval whereas it is not possible to state the range of this interval since it depends on the value θ in (5.23) and for this value, we have no concrete estimation. The results in section 7.2 regarding the absorption process of the mutants were quite bad. As we already concluded, it might be wrong to use the parameter values from the ODE experiment. Thus, one could vary the absorption rate σ and degradation rates γ_e and γ_i but also the production rates Π and $\Delta\Pi$ of the wild type bacteria. However, this costs quite much computation time to test. A further attempt to improve the results is to change the model equations and/or conditions. So far, we assumed homogeneous Neumann boundary condition, which means nothing else that we do not lose any signalling molecules at the boundary. However, the signalling molecules could "glue" on the boundary and bottom of the pad, which means we "loose" these signalling molecules for the quorum sensing process. Due to the fast diffusion, this would be a not negligible amount. Furthermore, we could implement an absorption term which depends on the extracellular signalling molecule concentration as discussed above. Such a dependency may be the case for the production term, too. To prove this, one would need further special experiments. A further adjustment to the model could be the change in the population dynamic of the bacteria regarding the PDE case. We assumed a logistic growth motivated by the data. However, we never took into account that the growth could be influenced by the signalling molecules. We saw from data sets of the μCats that higher stimulated mutants grow faster and the number of cells within a colony was higher. Moreover, it seems to be natural, that after some certain signalling molecule concentration, the bacterium stops to reproduce itself and initiate instead the sporulation process. That means we would add an indicator function to the right hand side of the bacteria. Purely hypothetical, the threshold for the absorption stop might be the same as the indicator for the bacterium to proliferate. For all this, more data is required. Additionally, the μCats concluded from the experiments that sometimes, not the entire colony sporulates. Our present PDE-ODE model can reproduce such a behaviour. Recall the wild type results in section 7.1.1. There, we saw that the *FRET* curve with noise in the thresholds did not reach the end level and we argued that some bacteria did not reach the threshold. The plots of

the right column in figure 7.16 shows how a possible end state could look like. We just have the "problem" that there are to much signalling molecules in the pad such that each bacterium reaches the threshold.

A further reason for a mismatch of experimental data and simulation results might be the fact that we neglected in all models the influence of nutrients. Especially in pad experiments this could be a additional influencing factor for the initialisation of sporulation.

Last but not least, we can conclude that the production process definitely depends on the intracellular signalling molecule concentration and spatial effects can be detected by the model. However, there are many open questions which require more experimental data and new model assumptions to answer them.

Appendix A

Theorems

A.1. Fixed point theorems

Theorem A.1.1 (Banach's Fixed Point Theorem). *Assume*

$$A : X \to X$$

is a nonlinear mapping, and suppose that

$$\|A\langle u \rangle - A\langle \tilde{u} \rangle\| \leq \gamma \|u + \tilde{u}\| \quad (u, \tilde{u} \in X)$$

for some constant $\gamma < 1$. Then A has a unique fixed point.

Theorem and proof can be found in [9], Chapter 9.2.1, Theorem 1.

Theorem A.1.2 (Schauder's Fixed Point Theorem). *Let X be a real Banach space. Suppose $K \subset X$ is compact and convex, and assume also*

$$A : K \to K$$

is continuous. Then A has a fixed point in K.

This theorem and its proof is stated in [9], chapter 9.2.2, Theorem 3. There's also a second version of Theorem A.1.2 which is given in [4], chapter 21.3, inclusively the proof in the appendix, chapter 26.8.

Theorem A.1.3 (Schauder's Fixed Point Theorem Second Version). *A continuous operator A in a Banach space X shall map a convex, closed set X into itself. Assume that the image set AX is relatively compact, then A has at least one fixed point in M.*

We will use only the second version of Schauder's Fixed Point Theorem, the first version is only given for reasons of completion.

A.2. Inequalities

Theorem A.2.1 (Young's Inequality with ϵ). *Let $1 < p, q < \infty$, $\dfrac{1}{p} + \dfrac{1}{q} = 1$. Then with $a, b, \epsilon > 0$*

$$ab \leq \epsilon a^p + \frac{(p\epsilon)^{1-q}}{q} b^q.$$

Young's Inequality Theorem and its proof can be found in [9], Appendix B.2.d.

Theorem A.2.2 (Gronwall's inequality differential form). *Let $x(\cdot)$ be a non-negative, absolutely continuous function on $[0, T]$, which satisfies for a.e. t the differential inequality*

$$\frac{\mathrm{d}}{\mathrm{d}t} x(t) \leq h(t)x(t) + g(t),$$

where $h(t)$ and $g(t)$ are non-negative, summable functions on $[0, T]$. Then

$$x(t) \leq e^{\int_0^t h(\tau)d\tau} \left[x(0) + \int_0^t g(\tau)d\tau \right]$$

for all $0 \leq t \leq T$.

Theorem A.2.3 (Generalized Gronwall's inequality). *Suppose $x(t)$ satisfies*

$$x(t) \leq g(t) + \int_0^t h(\tau)x(\tau)d\tau, \quad \tau \in [0, T]$$

with $g(t) \in \mathbb{R}$ and $h(t) \geq 0$. Then

$$x(t) \leq g(t) + \int_0^t g(\tau)h(\tau)e^{\int_\tau^t h(s)ds} d\tau, \quad \tau \in [0, T].$$

Moreover, if in addition $g(\tau) \leq g(t)$ for $\tau \leq t$, then

$$x(t) \leq g(t)e^{\int_0^t h(\tau)d\tau}, \quad \tau \in [0, T].$$

Theorem A.2.2 is cited form [9], Appendix B.2.j., and Theorem A.2.3 is cited from [32], Lemma 2.7. We just change the names of the variables to obtain a consistent and comparable statement. The proofs can also be checked there, except for the last statement of Theorem A.2.3. This will be proved here.

Proof. We assume $g(\tau) \leq g(t)$ for $\tau \leq t$. Then it holds

$$
\begin{aligned}
x(t) &\leq g(t) + \int_0^t g(\tau)h(\tau)e^{\int_\tau^t h(s)ds}\,d\tau \\
&\leq g(t) + g(t)\int_0^t h(\tau)e^{-\int_t^\tau h(s)ds}\,d\tau \\
&= g(t) + g(t)\int_0^t \frac{\mathrm{d}}{\mathrm{d}\tau} - e^{-\int_t^\tau h(s)ds}\,d\tau \\
&= g(t) + g(t)\left(-e^0 + e^{\int_0^t h(s)ds}\right) \\
&= g(t)e^{\int_0^t h(\tau)d\tau}.
\end{aligned}
$$

$\square$

A.3. ODE solutions

Theorem A.3.1 (Picard-Lindelöf). *Suppose $f \in C(U, \mathbb{R}^n)$, where U is an open subset of $\mathbb{R}^{n+1}$, and $(t_0, x_0) \in U$. If $f(t,x) \in C(U, \mathbb{R}^n)$ is locally Lipschitz continuous in the second argument, uniformly with respect to the first, then there exists a unique local solution $\bar{x}(t) \in \mathcal{C}^1(I)$ of $\dot{x} = f(t,x)$, $x(t_0) = x_0$, where I is some interval around t_0. More specific, if $V = [t_0, t_0 + T] \times \overline{B_\delta(x_0)} \subset U$ and M denotes the maximum of $|f|$ on V. Then the solution exists at least for $t \in [t_0, t_0 + T_0]$ and remains in $\overline{B_\delta(x_0)}$, where $T_0 = \min T, \frac{\delta}{M}$. The analogous result holds for the interval $[t_0 - T, t_0]$*

Proof and theorem is given in [32], chapter 2, p. 36.

Theorem A.3.2 (Non-negativity of ODE solutions). *Suppose that f in $\dot{x}(t) = f(t,x)$ has the property that solutions of initial value problems $x(t_0) = x_0 \geq 0$ are unique and, for all i, $f_i(t,x) \geq 0$ whenever $x \geq 0$ satisfies $x_i = 0$. Then $x(t) \geq 0$ for all $t \geq t_0$ for which it is defined, provided $x(t_0) \geq 0$.*

The Theorem as well a proof can be found in [29], Proposition B.7.

A.4. Measure theory

Theorem A.4.1 (Fubini-Tonelli Theorem for Lebesgue and Riemann integrable functions). *Let $(X, \mathcal{A}, \mu)$ be a measure space, and let $f : X \times [a,b] \to \mathbb{C}$. Assume that $R\int_a^b f(x,y)\,dy$ exists μ-a.e., f is μ-measurable for all $y \in [a,b]$, and that there is $F \in \mathcal{L}_\mu^1(X)$ for which*

$$
\forall (x,y) \in X \times [a,b], \quad |f(x,y)| \leq F(x).
$$

Then $\int_X f(x,t)\, d\mu(x)$ is Riemann integrable and

$$\int_X \left(R\int_a^b f(x,y)\, dy \right) d\mu(x) = R\int_a^b \left(\int_X f(x,y)\, d\mu(x) \right) dy.$$

The Theorem and the corresponding proof is stated in [1], chapter 3.7, Theorem 3.7.12.

Theorem A.4.2 (Rellich-Kondrachov Compactness Theorem). *Assume U is a bounded open subset of $\mathbb{R}^n$, and ∂U is $\mathcal{C}^1$. Suppose $1 \le p < n$ and $p^* = \dfrac{pn}{n-p}$. Then $\mathcal{W}^{1,p}(U)$ is compactly embedded in $\mathcal{L}^q(U)$ for each $1 \le q < p^*$, written*

$$\mathcal{W}^{1,p}(U) \subset\subset \mathcal{L}^q(U), \quad 1 \le q < p^*.$$

Rellich-Kondrachov's Compactness Theorem and the corresponding proof can be found in [9], chapter 5.7, Theorem 1.

Theorem A.4.3 (Dominated convergence theorem). *Assume the functions $\{f_k\}_{k=1}^{\infty}$ are integrable and*

$$f_k \to f \quad a.e..$$

Suppose also

$$|f_k| \le g \quad a.e.,$$

for some measurable function g with $\int_{\mathbb{R}^n} |g|\, d\vec{x} < \infty$. Then

$$\int_{\mathbb{R}^n} f_k\, d\vec{x} \to \int_{\mathbb{R}^n} f\, d\vec{x}.$$

This is cited from *Evans* [9], Appendix E.3., Theorem 5.

A.5. Maximum principles

Theorem A.5.1 (Strong maximum principle). *Assume $u \in \mathcal{C}_1^2((0,T] \times U) \cap C(\overline{(0,T] \times U})$ and*

$$c \equiv 0 \qquad in\ (0,T] \times U$$

with $Lu := -\sum_{i,j=1}^n a^{i,j} u_{x_i x_j} + \sum_{i=1}^n b^i u_{x_i} + cu$. Suppose also U is connected.

(i) If

$$u_t + Lu \le 0 \qquad in\ (0,T] \times U$$

and u attains its maximum over $\overline{(0, T] \times U}$ at a point $(t_0, x_0) \in (0, T] \times U$, then

$$u \text{ is constant on } (0, t_0] \times U.$$

(ii) Likewise, if

$$u_t + Lu \geq 0 \qquad in \ (0, T] \times U$$

and u attains its minimum over $\overline{(0, T] \times U}$ at a point $(t_0, x_0) \in (0, T] \times U$, then

$$u \text{ is constant on } (0, t_0] \times U.$$

This result and its proof can be found in [9], chapter 7.1.4, Theorem 11.

Appendix A. Theorems

Appendix B

Background regarding best fit simulations in chapter 3

In this chapter a brief summary is given of finding the best fit parameters and deriving the confidence interval of the fitted curves in chapter 3.

B.1. ODE solver

First of all, one has to solve the ODE systems in chapter 3 in order to determine the best parameters fitting the data best. If we have a continuous right hand side, we use the MATLAB solver *ode15s*. It is a quasi-constant step size implementation of the numerical differentiation formulas, briefly NDFs, in terms of backward differences. Additionally, *ode15s* can solve stiff problems which often arises after the space discretization of parabolic problems. For more information see [27]. If we have a discontinuous right hand side, the system can be solved by applying the so called "event driven method". The discontinuities will be located, in our case the time when we fulfil the necessary condition, and the solver restart at this point. For more details see [7]. Such a method can be implemented into the *ode15s* solver. Briefly described, after the *ode15s* solver executed a successful step, we ask if the intracellular concentration has reached the threshold. In case this holds, we change the right hand side and the solver restart to solve the system with this adjusted right hand side. Note that one has to do further adjustments regarding the solver such that we obtain no error message, e.g. rewrite the output function.

B.2. Best fit parameter

We want to fit the FRET data points with our computed solution as good as possible. That means after we have solved the ODE systems and derived the numerical solution of the intracellular signalling molecule concentration, we can evaluate the FRET function (3.1). The resulting curve should be as close as possible to the sampled FRET data points. One possibility to realize this is to use the *fsolve* function of MATLAB. This MATLAB function starts at a self-chosen point and tries to find the root of the object function. One can choose between three different algorithms: the "trust-region-dogleg" (default), the "trust-region" and "levenberg-marquardt" algorithm. More informations can be found in the MATLAB documentation. As object function, we choose the difference of the mean and the evaluated function with the parameters being the argument. However, the *fsolve* function admits also negative parameter solutions which contradicts with the assumption biological feasible parameters, that means non-negativity. Indeed this happens for the degradation rates γ_e and γ_i. Unfortunately, we can not set lower bounds for the arguments using the *fsolve* function. Therefore we use the *fmincon* function which has the option to set upper and lower bounds for the arguments. The MATLAB function *fmincon* needs a starting point and attempts to find a minimizer of the object function subjected to a constraint. Our problem can be realized by setting the previous object function as a nonlinear constraint and minimizing a constant function, e.g. zero. That means *fmincon* tries to find a parameter set such that the nonlinear constraint is fulfilled. The interior-point optimization uses first a "Newton step" and if this fails it attempts a "conjugated gradient step" at each iteration. More details to this topic are in the MATLAB documentation. The *fmincon* algorithm is used to find the parameter set of our best fit solution. We denote this best fit parameter set as $\hat{\theta}$.

Next we want to estimate the parameter confidence intervals based on F distribution. That means we assume for the confidence region that the error terms are jointly normally distributed. The goal of nonlinear regression is to find the optimal parameter set θ to minimize the sum of squared residuals SSR defined by

$$SSR(\theta) = \sum_{i=1}^{n} (y_i - f(\theta))^2 \tag{B.2.1}$$

whereas n denotes the number of fitted values, y_i is the ith value of the variable to be predicted, x_i is the ith value of the explanatory variable, and $f(x_i)$ is the predicted value of y_i.
The confidence region for the parameter set is a set of points for which $SSR(\theta)$ is less than or equal to a constant which reads

$$\frac{SSR(\theta) - SSR\left(\hat{\theta}\right)}{SSR\left(\hat{\theta}\right)} \leq \frac{p}{n-p} F_{p,n-p}^{\alpha}. \tag{B.2.2}$$

The number of parameters is given as p and the confidence level as α. The formula and more information are given in [26], [33]. For the approach to estimate the confidence interval we proceed as follows: We minimize and maximize each parameter separately whereas the other best fit parameters are fixed. This is the object function for the *fmincon* solver. As nonlinear constraint, the inequality (B.2.2) has to be fulfilled. We use again the interior-point optimization as algorithm.

B.3. Confidence interval of the fitted curves

Since we do not have so many data points to estimate the confidence interval of the fitted curves, we perform a bootstrapping procedure of the raw data to enlarge the data set. The raw data points contained were sampled at random to generate 10^4 data sets. For each random data set, we want to find a best fit solution by using the approach described above. Then we calculate the limits of the 95% percent fits by the 0.025 and 0.975 quantiles of the best fits of each random data set.

Appendix B. Background regarding best fit simulations in chapter 3

Appendix C

Some MATLAB code for solving ODE systems

This code presents the implementation of the event driven method and is copied from a solver solving the wild type ODE system derived by the finite element method.

```matlab
x_interp=[t,t_new];
y_interp=[Ce';Ce_new'];

if t_new-t<10^(-3)
    xq=linspace(t,t_new,4);
    nq=4;
else
    xq=linspace(t,t_new,40);
    nq=40;
end

% Solve the ODE Ci';
[t2_new,Ci_new]= ode45(@(t,y) ...
    myodeabsorp(t,y,x_interp,y_interp,n,sigma,bac(t)), xq,y);

% Calculate the thresholds
Bacteria=bac(t2_new);

etan_new_all=xi_n.*Bacteria(Bacindex,:);
etan_new=repmat(etan,1,nq);
etan_new(¬logical(Sn_index_old(end,Bacindex)),:)= ...
    etan_new_all(¬logical(Sn_index_old(end,Bacindex)),:);
etan_new=etan_new';

etap_new_all=xi_p.*Bacteria(Bacindex,:);
```

```
24      etap_new=repmat(etap,1,nq);
25      etap_new(¬logical(Sp_index_old(end,Bacindex)),:)= ...
            etap_new_all(¬logical(Sp_index_old(end,Bacindex)),:);
26      etap_new=etap_new';
27
28      % Find new nodes where feedback is reached
29      Sn_index_new=[];
30      Sp_index_new=[];
31
32      Sn_index_new(1:length(t2_new),Bacindex)= ...
            Ci_new(:,Bacindex)≥etan_new(:,:);
33      Sn_diff=Sn_index_new(:,Bacindex) ...
            -repmat(Snr_index_old(Bacindex),length(xq),1);
34
35      Sp_index_new(1:length(t2new),Bacindex)= ...
            Ci_new(:,Bacindex)≥etap_new(:,:);
36      Sp_diff=Sp_index_new(:,Bacindex) ...
            -repmat(Sp_index_old(Bacindex),length(xq),1);
37
38      Sn_diff_2=any(any(Sn_diff==1,2),1);
39      Sp_diff_2=any(any(Sp_diff==1,2),1);
40
41      % Check if feedback is reached and adjust equations as the case ...
            may be
42      if   Sn_diff_2 || Sp_ediff_2
43
44          Feedback=true;
45
46          if Sn_diff_2 && ¬Sp_diff_2
47              [r1,c1]=find(Sn_diff≠0);
48              [r2,¬]=find(min(r1)==r1);
49
50              t_new=t2_new(r1(r2(1)));
51              Ce_new=interp1(x_interp,y_interp,t_new)';
52              Ci_new=Ci_new(r1(r2(1)),:);
53
54              etan=etan_new(r1(r2(1)),:)';
55              etan(c1(r2))=Ci_new(Bacindex(c1(r2)));
56
57              Sn_index_old([Bacindex(c1(r2))])=1;
58
59              tF_n=[tF_n,t_new];
60
61          elseif ¬Sn_diff_2 && Sp_diff_2
62
63              [r1,c1]=find(Sp_diff≠0);
64              [r2,¬]=find(min(r1)==r1);
65
66              t_new=t2_new(r1(r2(1)));
67
68              Ce_new=interp1(x_interp,y_interp,t_new)';
69              Ci_new=Ci_new(r1(r2(1)),:);
```

```matlab
70
71             etap=etap_new(r1(r2(1)),:)';
72             etap(c1(r2))=Ci_new(Bacindex(c1(r2)));
73
74             Sp_index_old([Bacindex(c1(r2))])=1;
75
76             tF_p=[tF_p,tnew];
77
78
79      else
80
81             [ri1,ci1]=find(Sn_diff≠0);
82             [ri2,¬]=find(min(ri1)==ri1);
83
84
85             [rp1,cp1]=find(Sp_diff≠0);
86             [rp2,¬]=find(min(rp1)==rp1);
87
88
89         if ri1(ri2)<rp1(rp2)
90
91                 t_new=t2_new(ri1(ri2(1)));
92
93                 Ce_new=interp1(x_interp,y_interp,t_new)';
94                 Ci_new=Ci_new(ri1(ri2(1)),:);
95
96                 etan=etan_new(ri1(ri2(1)),:)';
97                 etan(ci1(ri2))=Ci_new(Bacindex(ci1(ri2)));
98
99                 Sp_index_old([Bacindex(ci1(ri2))])=1;
100
101                 tF_n=[tF_n,tnew];
102
103         elseif rp1(rp2)<ri1(ri2)
104
105                 t_new=t2_new(rp1(rp2(1)));
106
107                 Ce_new=interp1(x_interp,y_interp,t_new)';
108                 Ci_new=Ci_new(rp1(rp2(1)),:);
109
110                 etap=etap_new(rp1(rp2(1)),:)';
111                 etap(cp1(rp2))=Ci_new(Bacindex(cp1(rp2)));
112
113                 Sp_index_old([Bacindex(cp1(rp2))])=1;
114
115                 tF_p=[tF_p,tnew];
116         else
117
118                 t_new=t2_new(rp1(rp2(1)));
119
120                 Ce_new=interp1(x_interp,y_interp,t_new)';
121                 y2new=y2new(rp1(rp2(1)),:);
```

```matlab
122
123                 etap=etap_new(rp1(rp2(1)),:)';
124                 etap(cp1(rp2))=Ci_new(Bacindex(cp1(rp2)));
125                 etan=etan_new(ri1(ri2(1)),:)';
126                 etan(ci1(ri2))=Ci_new(Bacindex(ci1(ri2)));
127
128
129                 Sn_index_old([Bacindex(ci1(ri2))])=1;
130                 Sp_index_old([Bacindex(cp1(rp2))])=1;
131
132                 tF_n=[tF_n,tnew];
133                 tF_p=[tF_p,tnew];
134
135             end
136         end
137
138         Load_new = @(t,y)Load_F(Points,Triang_bac_w,Sn_index_old, ...
                Sp_index_old,bac(t),Pi_min,Pi_Δ);
139
140         ode = @(t,y) Stiff(t,y)*y+Load_new(t,y);
141         tspan=[t_new,tspan(end)];
142         Ce_0=Ce_new;
143         Ci_0=Ci_new;
144         etan_0=etan;
145         etap_0=etap;
146         done=true;
147         done2=false;
148
149     end
150
151     % Calculate bacterial density and thresholds
152     bac_new= bac(tnew);
153
154     if ¬Spore
155        etan=etan_new(end,:)';
156        etap=etap_new(end,:)';
157     end
```

Bibliography

[1] J. J. Benedetto and W. Czaja. *Integration and Modern Analysis*. Springer Science & Business Media, 2009.

[2] I. B. Bischofs, J. A. Hug, A. W. Liu, D. M. Wolf, and A. P. Arkin. Complexity in bacterial cell–cell communication: quorum signal integration and subpopulation signaling in the *Bacillus subtilis* phosphorelay. *Proceedings of the National Academy of Sciences*, 106(16):6459–6464, 2009.

[3] R. M. Clegg. The history of FRET. In *Reviews in Fluorescence 2006*, pages 1–45. Springer, 2006.

[4] L. Collatz. *Functional Analysis and Numerical Mathematics*. Academic Press Inc., 1966.

[5] H. De Jong, J. Geiselmann, G. Batt, C. Hernandez, and M. Page. Qualitative simulation of the initiation of sporulation in *Bacillus*. *Bulletin of mathematical biology*, 66(2):261–299, 2004.

[6] A. R. Diaz, L. J. Core, M. Jiang, M. Morelli, C. H. Chiang, H. Szurmant, and M. Perego. *Bacillus subtilis* rapa phosphatase domain interaction with its substrate, phosphorylated spo0f, and its inhibitor, the *PhrA* peptide. *Journal of bacteriology*, 194(6):1378–1388, 2012.

[7] L. Dieci and L. Lopez. A survey of numerical methods for IVPs of ODEs with discontinuous right-hand side. *Journal of Computational and Applied Mathematics*, 236(16):3967–3991, 2012.

[8] P. Eichenberger et al. The program of gene transcription for a single differentiating cell type during sporulation in *Bacillus subtilis*. *PLoS biology*, 2(10):1664–1683, 2004.

[9] L. C. Evans. *Partial differential Equations*. Graduate Studies in Mathematics, V. 19. American Mathematical Society, 2002.

[10] W. C. Fuqua, S.C. Winans, and E. P. Greenberg. Quorum sensing in bacteria - the LuxR–LuxI family of cell density- responsive transcriptional regulators. *Journal of bacteriology*, 176(2):269–275, 1994.

[11] G. Gerhardt and R. N. Adams. Determination of diffusion coefficients by flow injection analysis. *Analytical chemistry*, 54(14):2618–2620, 1982.

[12] S. Jabbari, J. T. Heap, and J. R. King. Mathematical Modelling of the Sporulation-Initiation Network in *Bacillus Subtilis* Revealing the Dual Role of the Putative Quorum-Sensing Signal Molecule *PhrA* . *Bulletin of mathematical biology*, 73(1):181–211, 2011.

[13] D. T. Jones and D. R. Woods. Acetone-butanol fermentation revisited. *Microbiological reviews*, 50(4):484–524, 1986.

[14] M. Kilian, U. Steiner, B. Krebs, H. Junge, G. Schmiedeknecht, R. Hain, et al. FZB24® *Bacillus subtilis*–mode of action of a microbial agent enhancing plant vitality. *Pflanzenschutz-Nachrichten Bayer*, 1(00):1, 2000.

[15] P. Knabner and L. Angermann. *Numerical methods for elliptic and parabolic partial differential equations*, volume 44. Springer Verlag, 2003.

[16] A. L. Koch. Turbidity measurements of bacterial cultures in some available commercial instruments. *Analytical biochemistry*, 38(1):252–259, 1970.

[17] J. Müller and Ch. Kuttler. *Methods and Models in Mathematical Biology*. Springer, 2015.

[18] C. J. Paredes, K. V. Alsaker, and E. T. Papoutsakis. A comparative genomic view of clostridial sporulation and physiology. *Nature reviews. Microbiology*, 3(12):969–978, 2005.

[19] M. Perego and J. A. Hoch. Cell-cell communication regulates the effects of protein aspartate phosphatases on the phosphorelay controlling development in *Bacillus subtilis*. *Proceedings of the National Academy of Sciences*, 93:1549–1559, 1996.

[20] P. O. Persson and G. Strang. A Simple Mesh Generator in Matlab. *SIAM Review*, 46(2):329–345, 2004.

[21] P. J. Piggot and J. G. Coote. Genetic aspects of bacterial endospore formation. *Bacteriological reviews*, 40(4):908–962, 1976.

[22] P. J. Piggot and D. W. Hilbert. Sporulation of *Bacillus subtilis*. *Current opinion in microbiology*, 7(6):579–586, 2004.

[23] S. K. Rai and A. K. Mukherjee. Statistical optimization of production, purification and industrial application of a laundry detergent and organic solvent-stable subtilisin-like serine protease (Alzwiprase) from *Bacillus subtilis* DM-04. *Biochemical Engineering Journal*, 48(2):173–180, 2010.

[24] R. Redfield. Is quorum sensing a side effect of diffusion sensing? *Trends in microbiology*, 10(8):365–370, 2002.

[25] M. Schallmey, A. Singh, and O. P. Ward. Developments in the use of Bacillus species for industrial production. *Canadian journal of microbiology*, 50(1):1–17, 2004.

[26] G. A. F. Seber and C. J. Wild. *Nonlinear regression.* John Wiley & Sons, 2003.

[27] L. F. Shampine and M. W. Reichelt. The Matlab ODE suite. *SIAM journal on scientific computing*, 18(1):1–22, 1997.

[28] R. E. Showalter. Hilbert Space Methods for Partial Differential Equations. *Electronic Journal of Differential Equations*, Monograph 01, 1994.

[29] H. L. Smith and P. Waltman. *The Theory of the Chemostat.* Cambridge University Press, 1995.

[30] V. A. Solonnikov. Proceedings of the Steklov Institute of Mathematics. In O. A. Ladyzenskaja, editor, *Boundary value problems of mathematical physics. V*, volume 102, pages 157–165. American mathematical society, 1967.

[31] A. L. Sonenshein. Control of sporulation initiation in *Bacillus subtilis*. *Current opinion in microbiology*, 3(6):561–566, 2000.

[32] G. Teschl. *Ordinary Differential Equations and Dynamical System*, volume 140. American Mathematical Society Providence, 2012.

[33] K. Vugrin, L. Swiler, R. Roberts, N. Stucky-Mack, and S. Sullivan. Confidence region estimation techniques for nonlinear regression in groundwater flow: Three case studies. *Water Resources Research*, 43(3), 2007.

[34] J.r Wadsworth and Ch. S. Cockell. Perchlorates on Mars enhance the bacteriocidal effects of UV light. *Scientific reports*, 7(1):4662, 2017.

[35] W. Walter. *Gewöhnliche Differentialgleichungen.* Springer Verlag, 2000.

[36] Ch. M. Waters and B. L. Bassler. Quorum sensing: Cell-to-Cell communication in Bacteria. *Annual Review of Cell and Developmental Biology*, 21:319–346, 2005.

[37] L. Westers, H. Westers, and W. J. Quax. *Bacillus subtilis* as cell factory for pharmaceutical proteins: a biotechnological approach to optimize the host organism. *Biochimica et Biophysica Acta (BBA)-Molecular Cell Research*, 1694(1-3):299–310, 2004.

[38] P. Williams, K. Winzer, W. C. Chan, and M. Cámara. Look who's talking: communication and quorum sensing in the bacterial world. *Philosophical Transactions of the Royal Society of London B: Biological Sciences*, 362:1119–1134, 2007.

[39] K. Winzer et al. Bacterial cell-to-cell communication: sorry can't talk now - out to lunch! *Current opinion in microbiology*, 5(2):216–222, 2002.

[40] H. Withers, S. Swift, and P. Williams. Quorum sensing as an integral component of gene regulatory networks in Gram-negative bacteria. *Current opinion in microbiology*, 4(2):186–193, 2001.

[41] O. C. Zienkiewicz, R. L. Taylor, and J. Z. Zhu. *The Finite Element Method - Its Basis & Fundamentals*. Elsevier Ltd., 7 edition, 2013.